Assessment of DNA Damage and DNA Damage Response and Repair in Dormancy-enriched Leukemia Cells

Sahar ALdosari, MSc, BMed Sci (Hons)

Department of Academic Haematology
Division of Cancer and Stem Cells

School of Medicine
University of Nottingham

Thesis submitted to the University of Nottingham for the degree of Doctor of Philosophy

October 2017

Abstract

Acute myeloid leukaemia (AML) is a heterogeneous myeloid malignancy characterized by clonal expansion of abnormal/immature hematopoietic precursor cells in the bone marrow. A side compartment in the BM niche consists of abnormal, quiescent cells, which are called dormant leukemic initiating cells (DLICs). Patients with AML tend to respond well to remission induction chemotherapy, but relapse is common because current therapies cannot completely eradicate leukemic cells. It is widely accepted that $CD34^{+}CD38^{-}$ DLICs are more resistant to chemotherapy and that they contribute to drug resistance and relapse of AML to a greater extent than progenitor $CD34^{+}CD38^{+}$ cells. DLICs have been extensively characterised, but they remain a critical area of investigation for clinical research because of the low prevalence of DLICs and similarity to normal HSCs. A model of dormancy *in vitro* that shows most of the features of DLICs had previously been established in the Nottingham Haematology Group. This study used this model and aimed to investigate whether the response to DNA damage was different in dormancy-enriched cells compared to cycling leukemic cells following chemotherapy. The amount of DNA damage was assessed up to 24 hours pre- and post- drug treatment using the neutral Comet assay. Lower levels of damage were observed in dormancy-enriched cells following etoposide (ETO) treatment at 4 hours ($p = 0.04$), although this switched at the 24 hour time point where accumulated DNA double-stranded breaks (DSBs), in dormancy-enriched KG1a cells were associated with a higher percentage of viable cells. DNA damage response cascade markers in both dormancy-enriched and cycling cells showed phosphorylation by flow cytometry (phospho-H2AX139, pATM-S1981, H2AX142, and pChk-Thr68) in response to conventional AML chemotherapy. Significantly lower levels of cleaved PARP-Asp214 and active caspase 3 were observed in dormancy-enriched cells

treated with ara-c (p = 0.0001) or ETO (p = 0.0001) at 24 hours, strongly indicating that survival responses are activated in dormancy-enriched cells. Induction of 53BP1 foci, the hallmark of non-homologous end joining (NHEJ) was observed following treatment with ara-c (p = 0.038) and ETO (p = 0.049) in dormancy-enriched cells, indicating the NHEJ repair pathway is the preferred mechanism for DSB repair. At the molecular level, BTG2 expression was involved in the DNA damage response. Significant induction of BTG2 was detected in cycling treated cells with ETO for 24 hours. In conclusion, this study provides evidence that phosphorylation of H2AX139 and H2AX142 is a key response marker that may explain the mechanism underlying the drug resistance of DLICs and induction of repair. Therefore, results of this study may help in devising novel treatment strategies for AML that target H2AX142 of DLICs to permanently eradicate all leukemic cells and improve overall survival.

Acknowledgments

This is the realization of a dream, but I can describe my feelings at this point in the journey. I have always wanted to learn (and learn to learn); I am not just asking for a degree. Here, I am a few steps away from my dream. I have been at the University of Nottingham for higher education (masters and PhD degree) for 5 years. I have gone through beautiful and happy days, filled with success and achievement, as well as hard days of loneliness, loss, and difficulty away from my family. I am grateful for all of these moments, with their sweetness and bitterness that made me write these lines now for my PhD thesis. In these few lines, I would like to thank my family who has been with me the longest in this journey. I dedicate this thesis to the soul of my mum. Mammy, I wish you could be with me now to see your tears, smiles, and pride in me. I know you fought against cancer a long time. It was too early to find the appropriate treatment for you, but I know you feel each moment I was thinking about you. I thank my father who has trusted me from the very beginning. I thank my dearest sisters Huda and Anood for standing by me for these past years. I thank my beloved elder brother Khaled who has long supported me, with his mercy, his calls, and the love in his eyes. I thank Shatha, my lovely niece who has not stopped saying she misses me. Thank you to all of my beloved family, thank you, and I am eager to return to you.

I thank my excellent supervisors Dr. Claire Seedhous and Dr. Monica Pallis for their unlimited support. I thank them for their knowledge, humanity, and passion, the extent of which I have never seen before. Thank you. I learned a lot about research and skills to be a good scientist in the future from each of you. I thank my colleagues, Dr. Martin, Dr. Mazen, Dr. Nancy, and Dr. Huda for all of the beautiful days that we have spent in the department. I am very grateful for

everything. I am glad that I enjoyed it, that I challenged myself and kept striving, that I stayed, and that I am still learning. Thanks to all of those on my way who helped push me forward. Thanks to Saber, the man who prepared my coffee each morning and asked how I was doing. Thank you to the bus driver who stopped for me when I came late to the bus stop. Thanks to the cells I cultured for many days; they gave me promising data and helped me continue this research. Thanks to the University of Nottingham. I enjoyed the journey and, today, my dream has come true.

List of Publications

Poster abstract

S Aldosari; M Pallis; N Russell; C Seedhouse. Assessment of DNA damage and DNA damage response and repair in dormant leukaemic cells: 281. British Journal of Haematology. 173:116, April 2016. Poster presentation at 36th World Congress International Society of Haematology, Glasgow, Scotland, 2016

S Aldosari; M Pallis; N Russell; C Seedhouse. DNA Damage Response in Dormant AML cells: 288. British Journal of Haematology. 173:118, 18-21 April 2016. Poster presentation at 36th World Congress International Society of Haematology, Glasgow, Scotland.

https://insights.ovid.com/britishhaematology/bjha/2016/04/001/assessment-dna-damage-response-repair-dormant/281/00002328

S Aldosari; M Pallis; N Russell; C Seedhouse. H2AX-tyrosine 142 phosphorylation plays a role in determining cell fate in conjunction with phosphorylated H2AXserine 139 in the dormancy enriched leukaemic cell line (KG1a) post DNA damage. The 9th Saudi student conference on 13 -14 February 2016. Birmingham, UK.

http://uksacb.org/sites/default/files/user/SSC9-Proceedings.pdf

List of Conferences and Meetings attended

1-Division of Cancer and Stem Cells Spring Meeting 2nd May 2017. Poster presentation. The University of Nottingham. Nottingham, UK.

2- The British Society for Haematology Annual Scientific Meeting 27-29 March 2017. Brighton, UK.

3- The Cancer Research Nottingham Annual Symposium programme, the 26th May 2016. Oral presentation. Nottingham, UK.

4- XXXVI World Congress of the International Society of Haematology Hosted By: British Society for Haematology SECC Glasgow, 18th - 21st April 2016. Poster presentation.

5- The 9th Saudi Students Conference 2016 Hosted by the Scientific Society for Saudi Students in the United Kingdom (SSSSUK). Birmingham, UK. Poster presentation.

6- M5 Universities Flow Cytometry Meeting 15th December 2015. Poster presentation.

7. BD Introduction to Flow Cytometry Course on 13th May 2015, Oxford, UK.

8- The 8th Saudi Students Conference 2015 Hosted by the Scientific Society for Saudi Students in the United Kingdom (SSSSUK) 31 JAN-1 FEB 2015. London, UK. Poster presentation.

9- Postgraduate Research students Oral Presentation on 25th February 2015, Royal Derby Hospital. Derby, UK.

10 - The 7th Saudi students Conference 2014 hosted by the Scientific Society for Saudi Students in the United Kingdom (SSSSUK) on 1-2 Febrauary 2014. Edinburgh, Scotland.

11- 16th Molecular Haemopoiesis hosted by Leukaemia and lymphoma research foundation on 16th October 2013. London, UK.

List of abbreviations

7-AAD	7-amino-actinomycin D
AML	acute myeloid leukaemia
ATM	ataxia telangiectasia mutated
ATR	ataxia- and Rad-related
ATRA	all trans-retinoic acid
ANGPT1	angiopoietin 1
ASXL1	additional sex combs-like 1
Ara-c	cytosine arabinoside
ABC	ATP binding cassette
BER	base excision repair
BRCA1	breast cancer type 1 susceptibility protein
BRCA2	breast cancer type 2 susceptibility protein
BSA	bovine serum albumin
BM	bone marrow
βTrCP	β-transducin repeat-containing protein
BFU-E	erythroid burst forming units
Bmi1	ring finger oncogene 1
cDNA	complementary DNA
CEBPA	CCAAT/enhancer binding protein α
CXCR4	chemokine receptor type 4
CLP	common lymphoid progenitors
CMP	common myeloid progenitors
CFU-E	erythroblast colony forming units

CBP	CREB binding protein
Cbl	casitas B-lineage lymphoma
Chk2	checkpoint kinase 2
Cdk2-cyclin	cyclin dependent kinase 2/cyclin complex
CB	cord blood
CM	complete medium
ChIP	chromatin immunoprecipitation
CLO	clofarabine
DLICs	dormant leukemic initiating cells
DDR	DNA damage response
DSBs	double-stranded breaks
IDH1	isocitrate dehydrogenase 1
DNMT3A	DNA methyltransferase 3A
DAXX	death domain-associated protein
DAPK	death-associated protein kinase
DMC1	disrupted meiotic cDNA1
ECs	endothelial cells
EPO	erythropoietin
EZH2	enhancer of zeste homologue 2
Egr1	early growth response protein 1
ETO	etoposide
FSC	fixed stained cells
FoxOs	forkhead box O
Fbw7	F-box and WD repeat domain-containing 7
FAB	the French-American-British
FISH	fluorescence in situ hybridization
FCM	flow cytometry

FACS	fluorescence activated cell sorter
GMP	granulocyte-macrophage progenitor
G-CSF	granulocyte-colony stimulating factor
GML	glycosylphosphatidylinositol anchored molecule like
HSCs	haematopoietic stem cells
HOX	Hox-cluster
HR	homologous recombination
HSPCs	hematopoietic stem and progenitor cells
ITD	internal tandem duplications
IL-7	interleukin7
IDH1	isocitrate dehydrogenase 1
IRF-1	interferon regulatory factor 1
IR	ionizing radiation
JAK1	Janus kinases 1
JNK	c-Jun N-terminal kinases
LIC	leukaemia-initiated
LSC	leukaemia stem cells
LT-HSCs	long-term reinitiation of HSCs
LMPPs	lymphoid-primed multipotential progenitors
MAP	mitogen-activated protein
MCL-1	myeloid cell leukaemia 1
MDC1	mediator of DNA damage checkpoint 1
MDS	myelodysplastic syndrome
MMR	mismatch repair
MMS	methyl methanesulfonate

mRNA	messenger RNA
MAP	mitogen-activated protein
MSCs	mesenchymal stem cells
Megs	megakaryocytes
MEP	megakaryocyte erythrocyte progenitors
MPPs	multipotential progenitors
MkE	megakaryocyte-erythroid
MLL	mixed lineage leukaemia
mTORC1	mammalian target of rapamycin complex 1
Myc	myelocytomatosis proto-oncogene
MRN	Mre11-Rad50-Nbs1
mTOR	mammalian target of rapamycin
NER	nucleotide excision repair
NHEJ	non-homologous end joining
NK-AML	normal karyotype–AML
NER	nucleotide excision repair
NF-κB	nuclear factor-κB
NGS	normal goat serum
OS	overall survival
OPN	osteopontin
γ-H2AX	phosphorylation of Ser139 of histone variant H2AX
PBS	phosphate-buffered saline
PBS-AA	phosphate-buffered saline albumin azide
PCR	polymerase chain reaction
PE	phycoerythrin
PF4	platelet factor 4

Pbx1	pre-B-cell leukaemia transcription factor 1
pRb	retinoblastoma protein
PIKK	phosphatidylinositol3 kinase-like kinase
PTIP	Pax transactivation domain-interacting protein
PB	peripheral blood
PS	phosphatidylserine
Pgp	p-glycoprotein
PKC	protein kinase C
PTM	post-translational modification
qPCR	quantitative polymerase chain reaction
ROS	reactive oxygen species
RT-PCR	reverse transcriptase–polymerase chain reaction
RIF1	RAP1-interacting factor 1
SCF	stem cell factor
SCGE	single gel electrophoresis assay
SD	standard deviation
SDS–PAGE	sodium dodecyl sulfate - polyacrylamide gel electrophoresis
SSB	single-strand break
ssDNA	single-strand DNA
SDF1α	stromal-derived factor 1
ST-HSCs	short term hematopoietic stem cells
SMC3	structural maintenance of chromosome 3
SSA	single-strand annealing
STR	short tandem repeat
TBE	tris/borate/EDTA
TBST	tris buffered saline Tween 20

TKD	tyrosine kinase domain
TPO	thrombopoietin
TGFβ1	transforming growth factor beta1
TLS	translation DNA synthesis
TPA	tetradecanoylphorbol-13-acetate
TNF	tumour necrosis factor
UV	ultraviolet light
VCAM1	vascular cell adhesion protein 1
WHO	World Health Organization
WT	wild-type
WAC	WW domain-containing adaptor with coiled-coil
XRCC1	x-ray repair cross-complementing 1
XRCC3	x-ray repair complementing defective repair in Chinese hamster cells 3

Table of Content

List of Table

List of Figure

Chapter1:
Introduction

1. Introduction

1.1 Human haematopoietic stem and progenitor cell expansion in the bone marrow (BM) microenvironment

Haematopoietic stem cells (HSCs) are clonogenic cells that reside in the bone marrow (BM) and can produce multiple lineages representing all blood cells (Estey and Dohner 2006; Wilson and Trumpp 2006; Yahata, Muguruma *et al.* 2008; Morrison and Scadden 2014). The BM niche serves as a microenvironment harbouring stem cells in a strictly protected cavity. The BM niche maintains a system of balanced output by controlling stem cell proliferation, lineage commitment, and differentiation (Pietras, Warr *et al.* 2011; Copley and Eaves 2013; Morrison and Scadden 2014). The BM cavity is composed of the stroma, endosteum (endosteal niche), and blood vessels called the sinusoidal endothelium (perivascular niche) (Estey and Dohner 2006; Crisan, Yap *et al.* 2008; Cordeiro-Spinetti, Taichman *et al.* 2015). Numerous studies have attempted to determine the location of HSCs, which reside in the endosteal or in the perivascular area, or both, depending on cellular responses to injury and increased demand for blood cell production. Sixty percent of HSCs are located at surface of tubercular and endosteal bone, close to a dense network of small arterioles and sinusoids (Cho, Kim *et al.* 2004; Crisan, Yap *et al.* 2008; Hao and Baltimore 2009; Reagan and Rosen 2016). Arterioles are composed of thin-walled endothelial cells (ECs) and are derived from large arteries in the endosteal niche, where they connect sinusoids to central veins (Hermitte, Brunet de la Grange *et al.* 2006; Wilson and Trumpp 2006; Crisan, Yap *et al.* 2008). Both arteries and sinusoids control nutrient delivery to the BM niche and regulate gas exchange to provide a hypoxic microenvironment (Shalem, Dahan *et al.* 2008; Ehninger and Trumpp 2011). Other important cellular components of the BM include mesenchymal stem cells (MSCs), osteoblasts, osteoclasts,

chondrocytes, myocytes, fibroblasts, and megakaryocytes (Megs), which provide proximity signals to HSCs, adipocytes, and endothelial cells (Stier, Ko *et al.* 2005; Wilson and Trumpp 2006). These cells support short- and long-term haematopoiesis via secreted hematopoietic factors that operate on HSCs and progenitor cells. BM MSCs surround arteriolar and sinusoidal vessels that provide a direct connection with the non-luminal side of ECs (Crisan, Yap *et al.* 2008). By secreating growth factors, ECs play a role in regulating the activity of, and preserving HSCs in the BM cavity. MSCs, the main players in the niche and other cellular components also release the growth factors, chemokines, and cytokines that maintain HSC stemness (Ehninger and Trumpp 2011). These signalling molecules can be classified into three groups according to their critical influence on HSC activity. Stem cell factor (SCF), interleukin 7 (IL-7), thrombopoietin (TPO) (de Graaf and Metcalf 2011), osteopontin (OPN) (Stier, Ko *et al.* 2005), transforming growth factor beta 1 (TGFβ1) (Yamazaki, Iwama *et al.* 2009), platelet factor 4 (PF4 or CXCL4), and angiopoietin 1 (ANGPT1) (Zhang, Lu *et al.* 2004) are the enforcers of HSC dormancy. These work together with adhesion factors, such as vascular cell adhesion protein 1 (VCAM1), stromal-derived factor 1 (SDF1α), C-X-C chemokine receptor type 4 (CXCR4) (Sugiyama, Kohara *et al.* 2006), and extracellular matrix (ECM) proteins, including fibronectin, hyaluronic acid, various selectins (e.g., CD62), and N-cadherin and β-catenin, which belong to the cadherin family of cell adhesion molecules (Zhang, Niu *et al.* 2003); these molecules are involved in homing and sheltering HSCs in the niche. The third group includes notch ligand, IL-7, and erythropoietin (EPO), which regulate cell proliferation and promote differentiation of HSCs (Nakamura-Ishizu and Suda 2013). These categories are not entirely discrete, as most of these molecules, such as those in the mTOR complex, can be classified into more than one group and perform multiple functions (Hoshii, Matsuda *et al.* 2014). Dormancy facilitates long-term

reinitiation of HSCs (LT-HSCs) and protects cells from acquiring mutations. Dormant HSCs, in the endosteal niche, are likely situated near to osteoblast/nestin+ MSCs. Active progenitor HSCs are more abundant than are dormant HSCs, are situated farther from from the endosteum, and are surrounded by sinusoidal ECs in the perivascular niche, which promote self-renewal, maintenance, and proliferation (Wilson, Oser *et al.* 2007; Kunisaki, Bruns *et al.* 2013). The sympathetic nervous system regulates the HSC niche via nerve fibres that expand from perivascular cells located around sinusoids in the BM. The different components, of the BM niche, work in harmony to regulate haematopoiesis (Morrison and Scadden 2014).

1.1.1 Normal haematopoiesis

Haematopoiesis is a process which undifferentiated progenitor cells undergo multiple cell divisions and lose their multilineage potential to form mature cells of different lineages. HSCs are the only haematopoietic cells that retain the potential for multi-potency and self-renewal. The cellular and molecular microenvironment of the BM maintains HSC balance (haemostasis) to generate billions of mature blood cells while maintaining an adequate pool of HSCs for the continual production of cells (Wilson and Trumpp 2006; Morrison and Scadden 2014).

HSCs in humans develop in the yolk sac, resulting in the initial production of macrophages and mature red blood cells; after maturation, more primitive hematopoietic and lymphoid cells types emerge (Wang and Wagers 2011; Woolthuis and Park 2016). In the next stage of development, HSCs translocate to the liver and spleen, where they divide and proliferate. Thereafter, HSCs migrate to niches in the BM, where HSCs reside throughout adulthood (Morrison and Scadden 2014). The hierarchical structure of normal haematopoietic cells allows the maintenance of a distinct set of stem cells which divide asymmetrically to produce identical self-renewing progeny

(Drake, Khoury *et al.* 2011). Concurrently, HSCs produce progenitor cells that differentiate into cells that are responsible for blood functions. Two subpopulations of HSCs can be distinguished based on their behaviour under laboratory conditions: (1) long-term quiescent HSCs and (2) active or short-term HSCs (ST-HSCs). ST-HSCs can to differentiate, proliferate, and self-renew for a defined interval. Once ST-HSCs have lost their capacity for self-renewal, they are no longer termed stem cells and are considered progenitors that generate mature functional blood cells (Chao, Seita *et al.* 2008; Yahata, Muguruma *et al.* 2008; Seita and Weissman 2010; Bianco 2011; Morrison and Scadden 2014).

ST-HSCs develop into two types of oligolineage-restricted progenitors: common lymphoid progenitors (CLPs) and common myeloid progenitors (CMPs). Eventually, oligopotent progenitors, unipotent progenitors, and differentiated cells are formed. The CMP can produce granulocyte-macrophage progenitors (GMPs), whereas megakaryocyte erythrocyte progenitors (MEPs) generate megakaryocytes and erythrocytes. CLPs give rise to pre-B and pre-T cells that develop into B and T lymphocytes. Erythroid burst-forming units (BFU-E) generate pro-erythroblast colony forming units (CFU-E) before erythrocytes are formed (Copley and Eaves 2013; Morrison and Scadden 2014). These cells frequently express lineage-affiliated genes consistent with their differentiation potential (Kopp, Avecilla *et al.* 2005; Bianco 2011). However, a recent model of haematopoietic hierarchy suggests that multipotential progenitors (MPPs) initially differentiate from LT-HSCs into lymphoid-primed multipotential progenitors (LMPPs), having lymphoid and granulocyte-macrophage, but not megakaryocyte-erythroid [MkE], potential (Figure 1.1.1) (Lai and Kondo 2006; Arinobu, Mizuno *et al.* 2007; Moignard, Macaulay *et al.* 2013; Manz and Boettcher 2014; Döhner, Weisdorf *et al.* 2015).

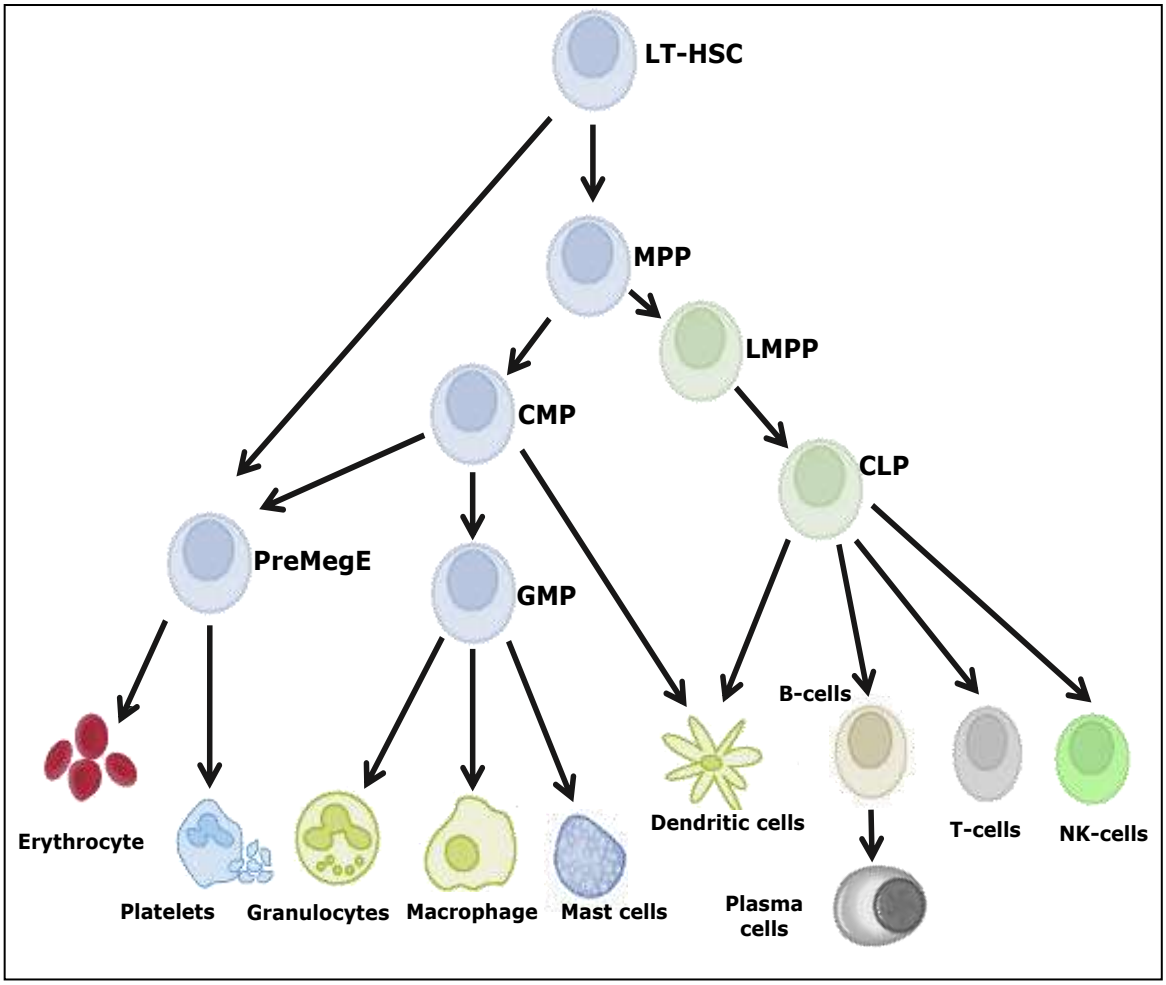

Figure 1.1.1: Haematopoietic hierarchy. Multipotent progenitor (MPP) subsets of long-term haematopoietic stem cells differ in their ability to generate myeloid lineages, the megakaryocyte–erythroid lineage, and the lymphoid lineage. Lymphoid-primed multipotent progenitors differentiate to lymphoid- and granulocyte-macrophages but do not show megakaryocyte-erythroid potential. More committed myeloid and lymphoid progenitors can be found downstream.

1.1.2 Leukemogenesis and myeloid malignancy

Frequent exposure of HSCs to internal and external agents, during haematopoiesis, can lead to damage, which results in haematological transformation and malignancy. Growing evidence indicates that malignant clones of HSCs are generated by the transformation of normal stem cells by genetic mutations, chromosomal changes, and/or epigenetic alterations, leading to the disruption in normal mechanisms that control stem cell growth and proliferation (Bonnet and Dick 1997; Gilliland, Jordan *et al.* 2004; Mawad and Estey 2012;

Welch, Ley *et al.* 2012). The multistep transformation of HSCs may include an initial event that creates a population of pre-leukemic leukaemia stem cells (LSC), followed by subsequent mutations at either the stem or progenitor cell level giving rise to leukemic blast cells. This is the two-hit hypothesis (Jerez, Sugimoto *et al.* 2012; Schmitt-Graeff, Nitschke *et al.* 2015). This project specifically focuses on AML, which originates from at least two classic mutations in a myeloid precursor cell, causing uncontrolled cellular proliferation, a halt in differentiation, and escape from apoptosis. Class I mutations cause constitutive activation of tyrosine kinases, or impairment of downstream signalling molecules, resulting in proliferation (Jerez, Sugimoto *et al.* 2012; Schmitt-Graeff, Nitschke *et al.* 2015). Class II mutations result in dysfunction of transcription factors involved in cellular differentiation, such as acute myeloid leukaemia 1/eight-twenty-one oncoprotein fusion protein (AML1/ETO), core binding factor ß/smooth muscle myosin heavy chain (CBFß/SMMHC), promyelocytic leukaemia/retinoic acid receptor alpha (PML/ RARα), nucleoporin 98kDa/homeobox protein Hox-A9 (NUP98/HOXA9), and mixed lineage leukaemia (MLL) gene fusions (Walter, Othus *et al.* 2013). Additionally, non-fusion mutations may occur in haematopoietic transcription factors and transcriptional coactivators, involved in the regulation of transcription, such as histone acetyltransferase P300, CREB binding protein (CBP), members of the extended Hox-cluster (HOX), and transcriptional mediators/intermediary factor 2 (TIF2) (Takahashi 2011; Brecqueville, Rey *et al.* 2012). A review by Bernasconi *et al.* provides insight into the specific chromosomal fusions, which generate LSCs from progenitors via activation of self-renewal, without widespread reprogramming of gene expression (Bernasconi 2008).

Additional mutations are detected in genome-wide and candidate-gene studies and are associated with somatic alterations in

epigenetics-related genes in AML patients. These genes are required to for regulation of histone post-translational modification of chromatin and/or DNA methylation states in haematopoietic progenitors (Figueroa, Lugthart *et al.* 2010). Many of these mutations are not classified as either Class I or Class II, suggesting that the "two-hit model" is insufficient (Jankowska and Szpurka 2012). These include mutations in tet methylcytosine dioxygenase 2 (TET2) (Figueroa, Abdel-Wahab *et al*. 2010), isocitrate dehydrogenase 1 (IDH1), IDH2 (Figueroa, Abdel-Wahab *et al.* 2010), additional sex combs-like 1 (ASXL1), enhancer of zeste homologue 2 (EZH2), and DNA methyltransferase 3A (DNMT3A) (Ley, Ding *et al.* 2010; Yan, Xu *et al.* 2011; Challen, Sun et al. 2012; Garg, Nagata *et al.* 2015).

Additionally, mutations occur in genes involved in DNA methylation, chromatin remodelling, histone methylation, myeloid transcription factors, signalling, adhesion, cohesin complexes, and the spliceosome (Garg, Nagata *et al*. 2015). For example, the WW domain-containing adaptor with coiled-coil (WAC) mediates protein-protein interactions and binds proteins containing short linear peptide motifs, which are proline-rich or contain at least one proline. Furthermore, structural maintenance of chromosomes 3 (SMC3) is required to encircle sister chromatids to mediate sister chromatid cohesion. In addition to its role in the cohesion of sister chromatids, SMC3 is associated with the RC-1 complex, a mammalian protein complex that promotes repair of DNA gaps and deletions via recombination (Ding, Ley *et al.* 2012). The DIS3 homologue, exosome endoribonuclease, and 3'-5' exoribonuclease (DIS3) are indispensable for survival and participate in a multitude of events involved in cellular RNA processing and degradation (Tomecki, Drazkowska *et al.* 2014). Additionally, DEAD-box helicase 41 (DDX41) acts as a tumour suppressor gene (Lewinsohn, Brown *et al.* 2016), and death domain-associated protein (DAXX) is a transcriptional coregulator involved in multiple cellular

functions, including apoptotic and non-apoptotic AML cell (Chang, Naik *et al.* 2011; Ding, Ley *et al.* 2012).

1.1.3 Characterization and regulation of LSCs and HSCs

Most primitive HSCs are dormant (Pelicci 2012). Therefore, LT-HSCs divide infrequently and only enter and exit the cell cycle in response to BM injury or hematopoietic stress. These dormant cells contain low levels of RNA transcripts and exhibit a low rate of metabolism and low level generation of reactive oxygen species (ROS) (Blagosklonny 2006; Wilson, Laurenti *et al.* 2009; Pallis, Burrows *et al.* 2013). Similar to normal adult HSCs, LSCs maintain at least some of the genotypic, phenotypic, and morphological characteristics of cells in the original population. Gal *et al.* showed that 34% of expressed genes are shared by both LSCs and HSCs (Gal, Amariglio *et al.* 2006). The rare populations of dormant LSCs are characterised by their ability to self-renew and undergo uncontrolled proliferation with no or little differentiation, producing immature myeloid blast cells in the BM and peripheral blood (Guan and Hogge 2000; Jordan and Guzman 2004; Jan and Majeti 2013). Most of this research has been conducted in mice, where serial transplantation serves as the gold standard for determining self-renewal capacity. Studies have identified LSC markers, generally assumed to be the same surface markers as those found on normal HSCs, including CD34+, CD38−, and CD71−; however, LSCs are also identified by the antigens CD90−, CD117−, CD123+, CD33+, and CD44+ (Geller, Zahurak *et al.* 1990; Jin, Hope *et al.* 2006). Further research on LSC phenotypes has shown a more mature CD34+ CD38+ progenitor cell population in some samples of AML (Aguirre-Ghiso 2007; Taussig, Miraki-Moud *et al.* 2008). In contrast, dormant HSCs in mice are identified by CD150+, CD48−, and CD135− (Wilson, Oser *et al.* 2007). A more detailed survey of the LSC phenotypes indicates that the vast majority of cells are CD34+ AML cells. In some LSCs, including those

with nucleophosmin (NPM1) mutations, CD34+ cells are infrequent or absent, whereas in other LSCs, both CD34+ and CD34− populations were present (Aguirre-Ghiso 2007; Taussig, Miraki-Moud *et al.* 2008). AML occurs at the progenitor stage of maturation, after HSC markers are lost and the cells reacquire capacity for self-renewal.

Regulation of dormant stem cells is classified based on the use of intrinsic and extrinsic pathways (Bianco 2011). A series of intracellular regulatory molecules, including forkhead box O (FoxOs), mammalian target of rapamycin complex 1 (mTORC1), F-box and WD repeat domain-containing 7 (Fbw7), early growth response protein 1(Egr1), pre-B-cell leukaemia transcription factor 1 (Pbx1), retinoblastoma protein (pRb), casitas B-lineage lymphoma (Cbl), myelocytomatosis proto-oncogene (Myc), and polycomb ring finger oncogene 1 (Bmi1), have been shown to modulate dormancy, cycling, self-renewal, and capacity of HSCs/LSCs (Bockamp, Antunes *et al.* 2009; Wilson, Laurenti *et al.* 2009). Thrombopoietin (TPO) and KIT play crucial roles in sustaining the dormancy of HSCs, with inhibition of these molecules leading to a reduced number of cells in the G0 phase (Qian, Buza-Vidas *et al.* 2007; Thorén, Liuba *et al.* 2008). LSCs have unique molecular features identified by studying studies examining primary AML cells. For instance, interferon regulatory factor 1 (IRF-1) and death-associated protein kinase (DAPK) are tumour suppressor genes that are consistently overexpressed in LSCs (Guzman, Upchurch *et al.* 2001). Additionally, high expression of nuclear factor-κB (NF-κB) is a marker for malignant progenitor cells (Guzman, Neering *et al.* 2001).

1.2 AML

AML refers to a neoplasm of immature myeloid progenitors. AML is a heterogeneous malignancy characterized by clonal expansion of abnormal haematopoietic precursor cells. The overproduction of

malignant myeloid cells prevents the BM from producing functional blood cells, resulting in anaemia, bleeding, and an increased risk of infection (O'Donnell, Abboud *et al.* 2012). The incidence of leukaemia varies across the world. In the UK, approximately 7,600 people are diagnosed annually with leukaemia. Of those, about 2,300 people have AML. AML can occur at any age, but is most common in adults; the incidence increases with age, with a median age of 70 years old at onset (Blagosklonny 2006; Estey and Dohner 2006; Shah, Andersson *et al.* 2013). The number of men, diagnosed with AML is estimated to be 33 % higher than that of women, according to a report published in 2013 by the Leukaemia and Lymphoma Society. A possible reason for differences between the genders, in the percentage of AML occurrence, may be linked to the ABO blood group genes (Jackson, Menon *et al.* 1999; Bianco, Farmer *et al.* 2001; Tavasolian, Abdollahi *et al.* 2014). Significantly more group O males are diagnosed with AML than group O females. This is related to the presence of sex responsive gene near to the ABO gene locus on chromosome 9; this gene may protect against AML in-group O women (Jackson ,1999).

1.2.1 Diagnosis and classification of AML

BM morphology remains the diagnostic cornerstone for the identification of various subtypes of myeloid neoplasms. Two main systems, used to divide AML into subtypes, are the French-American-British (FAB) and the newer World Health Organization (WHO) classification systems. The FAB system, classification of AML, for the classification of AML, was established in the 1970s. It divides AML into subtypes M0 to M7, based on the origin of the cell from which the leukaemia developed, assessment of how mature the cells appear under a microscope, and cytochemical staining of the blasts (Bennett, Catovsky *et al.* 1976; Guan, Gerhard *et al.* 2003; van Rhenen, van Dongen *et al.* 2007; Grimwade, Hills *et al.* 2010; Estcourt and Bain 2013; Walter, Othus *et al.* 2013). In 1999,

Duchayne and colleagues suggested a ninth morphologic subtype called acute basophilic leukaemia (M8). The FAB classification system, however, does not take into account many of the factors that affect disease outcomes (Duchayne, Demur *et al.* 1999). The WHO has developed a newer system that includes additional factors; nonetheless, it still does not take into account the many factors affecting prognosis. The WHO system divides AML into several groups, based on certain genetic, immunophenotypic, biological, and clinical features (Table 1.2.1) (Estcourt and Bain 2013; Walter, Othus *et al.* 2013). The classification system includes all the cases diagnosed, with blasts representing 20 % or more of cells in the BM; this is a lower percentage of blasts than those used in previous systems, leading to the inclusion of many types of AML with myelodysplasia-related changes (Döhner, Estey *et al.* 2010).

A determination of the blast percentage should be assessed by flow cytometry, and further prognostic information can be gained by immunohistochemical detection of stemness markers (Döhner, Estey *et al.* 2010). Additionally, a complete cytogenetic profile is required to establish karyotypes before and after response to therapy; specific karyotypes are strongly associated with prognosis. Other tests include reverse transcriptase–polymerase chain reaction (RT-PCR) and/or fluorescence in situ hybridization (FISH) to detect cytogenetic or sub-microscopic abnormalities not detected by routine karyotyping (Mrozek 2008; Mawad and Estey 2012). Additionally, detection of genetic mutations can aid in diagnosis and determining prognosis (Takahashi 2011; Nardi and Hasserjian 2016).

Acute myeloid leukemia classification(WHO 2008)	
Categories	
1	**Acute myeloid leukemia with recurrent genetic abnormalities**
	AML with t(8;21)(q22;q22); RUNX1-RUNX1T1
	AML with inv(16)(p13.1q22) or t(16;16)(p13.1;q22); CBFB-MYH11
	APL with t(15;17)(q22;q12); PML-RARA
	AML with t(9;11)(p22;q23); MLLT3-MLL
	AML with t(6;9)(p23;q34); DEK-NUP214
	AML with inv(3)(q21q26.2) or t(3;3)(q21;q26.2); RPN1-EVI1
	AML (megakaryoblastic) with t(1;22)(p13;q13); RBM15-MKL1
	Provisional entity: AML with mutated NPM1
	Provisional entity: AML with mutated CEBPA
2	**Acute myeloid leukemia with myelodysplasia-related changes**
3	**Therapy-related myeloid neoplasms**
4	**Acute myeloid leukemia, not otherwise specified (NOS)**
	Acute myeloid leukemia with minimal differentiation
	Acute myeloid leukemia without maturation
	Acute myeloid leukemia with maturation
	Acute myelomonocytic leukemia
	Acute monoblastic/monocytic leukemia
	Acute erythroid leukemia
	Pure erythroid leukemia
	Erythroleukemia, erythroid/myeloid
	Acute megakaryoblastic leukemia
	Acute basophilic leukemia
	Acute panmyelosis with myelofibrosis (syn.: acute myelofibrosis; acute myelosclerosis)
5	**Myeloid sarcoma (syn.: extramedullary myeloid tumor; granulocytic sarcoma; chloroma)**
6	**Myeloid proliferations related to Down syndrome**
	Transient abnormal myelopoiesis (syn.: transient myeloproliferative disorder)
	Myeloid leukemia associated with Down syndrome
7	**Blastic plasmacytoid dendritic cell neoplasm**
8	**Acute leukemias of ambiguous lineage**
	Acute undifferentiated leukemia
	Mixed phenotype acute leukemia with t(9;22)(q34;q11.2); BCR-ABL1
	Mixed phenotype acute leukemia with t(v;11q23); MLL rearranged
	Mixed phenotype acute leukemia, B/myeloid, NOS
	Mixed phenotype acute leukemia, T/myeloid, NOS
	Provisional entity: Natural killer (NK)–cell lymphoblastic leukemia/lymphoma

Table 1.2.1: Acute myeloid leukaemia and related precursor neoplasms (WHO 2008), taken from (Döhner, Estey et al. 2010)

1.2.2 Treatment of AML

The optimal strategies for AML treatment remain largely undetermined, and treatment outcomes are heterogeneous. Treatment of AML is based on several factors such as the age of the patient, performance status, cytogenetic findings, molecular profile, and patient preference. Typical treatment of most types of AML, except for acute promyelocytic M3, consists of two phases of chemotherapy: remission induction and consolidation. The remission induction phase is required to clear the BM of leukemic blasts and reduce the number of blasts in the BM to a normal level. This is usually associated with normal BM functioning and normal numbers of healthy blood cells in circulation. The consolidation phase, which begins after the patient has recovered from the induction phase, aims to eradicate residual LSCs to prevent the relapse of AML (Jordan and Guzman 2004). The length of the consolidation phase depends on the aggressiveness of the AML and is often determined by the presence of chromosomal abnormalities, which are grouped into categories of favourable, intermediate, and adverse. Patients in the favourable risk group are usually advised to continue with chemotherapy, whereas those in the unfavourable risk group are subjected to allogeneic stem cell transplantation, if appropriate. However, the majority of AML patients are at intermediate cytogenetic risk; research, to further stratify these patients via genomics, and determine the best courses of treatment, is underway (Döhner, Estey *et al.* 2010; Burnett, Wetzler *et al.* 2011). An analysis of 5876 young adult patients, who were classified into 54 cytogenetic subgroups and treated in the United Kingdom Medical Research Council clinical trials, provides a more reliable indicator of outcomes for patients with rare abnormalities. This report showed that t(15;17), t(8;21), and inv(16)/t(16;16) variants are the only abnormalities conferring a relatively favourable prognosis (Grimwade, Hills . 2010)

1.2.2.1 Standard AML chemotherapy

The nucleoside analogue cytosine arabinoside (ara-c), is a cornerstone chemotherapeutic agent for the treatment of AML, and is incorporated into DNA during the S phase. Ara-c enters the cell mainly via equilibrative nucleoside transporter 1 (hENT1) and is phosphorylated to Ara-CMP by 2-deoxycytidine kinase (dCK). Subsequently, two additional phosphorylation steps, to form ara-CTP, are mediated by (deoxy) cytidylate kinase (UMP-CMPK) and nucleoside diphosphate kinases (NDKs), respectively. In the nucleus, ara-CTP acts similarly to human cytosine deoxyribose; ara-CTP is incorporated into DNA during DNA synthesis, leading to termination of DNA replication and stalling of replication forks, accumulation of DNA strand breaks, and apoptosis (Wolff, Herzig *et al.* 1989; Staib, Lathan *et al.* 1998). For most patients with AML, the primary treatment regime still involves high doses of ara-c combined with an anthracycline, which is most often daunorubicin (DNR), and can be substituted with doxorubicin, idarubicin or mitoxantrone (Faderl, Verstovsek *et al.* 2006; Tefferi and Letendre 2012). The activity of anthracyclines includes inhibition of DNA and RNA synthesis occurring via intercalation between the base pairs of DNA and RNA strands, which subsequently prevents the replication of rapidly dividing leukemic cells. Additionally, anthcyclines inhibite topoisomerase enzyme II (Gewirtz 1999; Fernandez, Sun *et al*. 2009). Normally, topoisomerase II cuts both strands of a double-stranded DNA; introducing another portion of the duplex through the cut, and resealing the cut during replication, utilizes ATP and enhances DNA integrity and survival of the cycling cell (Gewirtz 1999). Inhibition of topoisomerase enzyme II activity by drugs divited into two classes known as topoisomerase enzyme II poisons and topoisomerase enzyme II catalytic inhibitors (Burden and Osheroff 1998; Hande 2008). Topoisomerase enzyme II poisons prevents topoisomerase II from re-ligating cleaved DNA, which introduces numerous DNA breaks

and lesion in the proteins covalently bound to DNA (Nitiss 2009). Topoisomerase II catalytic inhibitors are potent chelating agents that block the activity of topoisomerase II in the catalytic cycle before the hydrolysis of ATP (Andoh and Ishida 1998).

DNR appears to act by inhibiting DNA, and DNA-dependent RNA synthesis, by forming a complex with DNA, intercalating between base pairs and uncoiling the helix (Löwenberg, Ossenkoppele *et al.* 2009). The cytotoxic activity of DNR leads to the formation of complexes between DNA and nuclear topoisomerase II, and stabilization of the complex, which prevents re-ligation (Di Marco, Arcamone *et al.* 1975; Gewirtz 1999; Löwenberg , Ossenkoppele *et al.* 2009). Topoisomerase II can be targeted by etoposide (ETO), which inhibits enzyme-mediated DNA ligation manly in G2 and S phases of the cell cycle, and leads to the accumulation of double-stranded breaks. Consequently, preventing entry into the mitotic phase of cell division, formation of free radicals, alkylation of DNA, and interaction with cellular components cause cell death (Burden and Osheroff 1998; Baldwin EL 2005; Hande 2008).

The regimen "7 + 3" indicates continuous intravenous infusion of a chemotherapeutic agent for 7 days (ara-c at 100 mg/m^2 per day, combined with 3 days of DNR at 45 mg/m^2 per day, idarubicin at 10–12 mg/m^2, or mitoxantrone at 10–12 mg/m^2), administrated on days 1, 2, and 3 to patients eligible for intensive induction therapy (Fernandez, Sun *et al.* 2009). The addition of a topoisomerase II inhibitor, ETO, to the standard "7 + 3" regimen is effective against AML, either alone or in combination with, other treatments (Staib, Lathan *et al.* 1998).

Multidrug resistance is frequently observed in patients with AML who fail to enter remission after chemotherapy. A variety of ATP-binding cassette (ABC) transporters, localized in the cell membrane, induce multidrug resistance by effluxing a variety of chemotherapeutic

agents from malignant cells (Bodó, Bakos *et al.* 2003). Moreover, a study by Cheng *et al.* revealed that overexpression of p53 promotes resistance to anti-leukemic agents by maintaining cell cycle arrest and activating p21 (Cheng, Rodrigues *et al.* 2000). Preneoplastic damage may also activate the DNA damage response (DDR) signalling pathways that may contribute to drug resistance (Gorgoulis, Vassiliou *et al.* 2005; Saito, Uchida *et al.* 2010). A limited number of reports indicate that LSCs may contribute to chemo/radio resistance via activation of DDR checkpoints, causing increased DNA repair capacity (Yan, Qin *et al.* 2009; Rosen, Putta *et al.* 2010).

Conversely, although ara-c is one of the typical treatments for most types of AML, except M3, a number of side effects have been reported. Ara-c may cause myelosuppression, anorexia, nausea, vomiting, diarrhoea, oral inflammation, hepatic dysfunction, fever, rash, and bleeding (Burnett, Wetzler *et al.* 2011; Löwenberg , Pabst *et al.* 2011). Additionally, via interactions with iron, anthracyclines contributealtered Ca^{+2} dynamics in cardiomyocytes, and can cause an irreversible increase in mitochondrial Ca^{+2} loading and ATP content; this can lead to mitochondrial impairment caused by increased generation of reactive oxygen species in cardiac mitochondria (Jain 2000; Fernandez, Sun *et al.* 2009; Octavia, Tocchetti *et al.* 2012; Zorov, Juhaszova *et al.* 2014; Görlach, Bertram *et al.* 2015).

1.2.2.2 Targeted therapy for cycling and dormant LSCs

Clofarabine (CLO; 2-chloro-2’-arabino-fluoro-2’-deoxyadenosine, CAFdA, Cl-F-ara-A) is a a recently developed chemotherapeutic agent, available for the treatment of AML. CLO is a second-generation purine nucleoside analogue and has been established as an efficient chemotherapeutic to treat relapsed AML, particularly in elderly patients who are not candidates for intensive therapy (Zhenchuk, Lotfi *et al.* 2009; Burnett, Russell *et al.* 2010). CLO is toxic to actively dividing leukemic cells; it inhibits DNA polymerase and prevents

ribonucleotide reductase from building new molecules of DNA. Consequently, the amount of intracellular deoxynucleoside triphosphates, required for DNA replication, is reduced, and apoptosis is triggered (Ghanem, Jabbour *et al.* 2010; Xie, Edwards *et al.* 2012). In primary AML samples, only cells in the S phase were damaged by CLO (Seedhouse, Grundy *et al.* 2009). CLO has favourable properties such as stability in acidic environments, which allows it to be administered in an oral formulation; it is also resistance to phosphorylitic cleavage and deamination (Kantarjian, Jeha *et al.* 2007; Zhenchuk, Lotfi *et al.* 2009). Clinical trials show that CLO is effective as a single antileukemic agent, or in combination with ara-c, in elderly patients, and it results in high rates of complete remission (CR), but no significant improvement in survival rates (Faderl, Verstovsek *et al.* 2006).

TG02 is one of the most recent anti-cancer agents in development; it is a multikinase inhibitor that affects vital protein kinases in the cell cycle and transcription molecules involved in cell division, proliferation, differentiation, and apoptosis (Pallis, Abdul-Aziz *et al.* 2012). TG02 inhibits the cell cycle regulators CDK1 and CDK2, and transcription regulators CDK7 and CDK9; it is also a potent inhibitor of MAPK-ERK, Janus kinases (JAK1, 2, and 3), FLT3, and STAT, a molecule in the central signal transduction pathway that controlling haematopoiesis and immune system functions (Aguirre-Ghiso 2007; Pallis, Abdul-Aziz *et al.* 2012). Furthermore, TG02 targets CDK9-dependent survival proteins, myeloid cell leukemia-1 (Mcl-1) and X-linked inhibitor of apoptosis protein (XIAP). Mcl-1 is a member of antiapoptotic B cell lymphoma-2 (Bcl-2) family, regulated via the MAPK-ERK signalling pathway. Mcl-1 normally promotes cell survival by inactivating its proapoptotic counterpart and preserving the integrity of the outer mitochondrial membrane (Fukuda and Pelus 2001). Overexpression of Mcl-1, reported in AML, caused by

mutations in the promoter of the *Mcl-1* gene or increase expression to cytokines such as interleukin-6 (Carter, Mak *et al.* 2005; Thomas, Lam *et al.* 2010; Pallis, Abdul-Aziz *et al.* 2012). XIAP is a potent inhibitor of caspase activity; it inhibits caspases-9 and -3 and blocks cell death (Carter, Mak *et al.* 2005). In patients with AML, high levels of XIAP correlate with poor overall survival and resistance to treatment (Tamm, Kornblau *et al.* 2000; Tamm, Richter *et al.* 2004). TG02 increases the apoptosis of CD34+CD38-CD123+ AML cells via inhibition of Mcl-1 and XIAP (Goh, Novotny-Diermayr *et al.* 2012; Pallis, Abdul-Aziz *et al.* 2012; Pallis, Burrows *et al.* 2013). TG02 is currently in clinical trials in the US as an oral drug for patients with relapsed leukaemia and myeloid malignancies (Goh, Novotny-Diermayr *et al.* 2012).

Furthermore, to target dormant LSCs, a two-step therapy has been proposed: first, dormant LSCs would be activated, mobilized, and enter the cell cycle in response to factors such as granulocyte-colony stimulating factor (G-CSF). Chemotherapy could then be administered, possibly including drugs that target certain molecules or pathways of LSCs but not HSCs (e.g., CD33 with Mylotarg) to eliminate the majority of leukaemic cells, as well as activated LSCs (Cortes, O'Brien *et al.* 2004; Viale and Pelicci 2009; Essers and Trumpp 2010). Awakening leukaemia stem cells from dormancy by administration of G-CSF and chemotherapy, has yielded conflicting results. For eradication of leukaemia, targeting the leukemic stem cells, by interrupting their dormancy, has shown adequate outcomes in favourable and intermediate risk patients with AML (Löwenberg , van Putten *et al*. 2003; Viale and Pelicci 2009; Essers and Trumpp 2010; Pabst, Vellenga *et al.* 2012; Nomdedeu, Lara-Castillo *et al.* 2015). Others have failed to show a beneficial effect of this strategy in AML patients with unfavourable-risk cytogenetic abnormalities (Dombret , Chastang *et al.* 1995; Heil, Hoelzer *et al.* 1997; Relling,

Boyett *et al.* 2003). Pushing LSCs out of the BM niche leads to sensitization of cells, and reduction of their clonogenic capacity, by disruption of the CXCR4-CXCL12 axis. Additionally, G-CSF induces growth factor independent 1 transcriptional repressor (GFI-1), which renders them susceptible to CXCL12 (Souza 1986; De La Luz Sierra, Gasperini *et al.* 2007). However, interrupting dormancy of LSCs raises the risk of secondary myeloid malignancy, or rapid relapse with undetectable molecular genetic abnormality, although such cases are rare (Relling, Boyett *et al.* 2003; Cortes, O'Brien *et al.* 2004).

1.2.2.3 Relapsed AML

Relapses occur because of re-expansion of residual leukemic cells that escape the cytotoxic effects of chemotherapy; this LSC population may reside mainly within the stem cell CD34+CD38− compartment. Approximately 20 to 40 % of patients are chemoresistant and do not enter remission, whereas 50 to 70 % of patients, who achieve remission, relapse within 3 years (Ferrara, Palmieri *et al.* 2004). Major patterns of clonal evolution, during AML relapse, have been identified and show that relapse may result from any of the following: 1) LSCs that were only partially eradicated; 2) de novo AML, presumably caused by toxicity from treatment, that is misidentified as a relapse; and 3) a subclone of a clone that survived the initial therapy, acquired additional mutations, and expanded (Figure 1.2.2.3) (Ding, Ley *et al.* 2012; Welch, Ley *et al.* 2012; Ramos, Mo *et al.* 2015).

Advances in the treatment of AML have resulted in improved CR rates. Remission rates, in adult patients with AML, are inversely related to age; 60 to 80 % of young adults, and 40 to 60 % of older patients with AML attain CR status following the appropriate induction therapy (Rowe 2009; Burnett, Wetzler *et al.* 2011). Accumulating evidence suggests that cases of relapse and drug resistance may result from the quiescent state of LSCs (Ferrara, Palmieri *et al.* 2004;

Hope, Jin *et al.* 2004; Rowe 2009; Essers and Trumpp 2010; Horton and Huntly 2012; Ramos, Mo *et al.* 2015). Special events, such as multiple of mutations or epigenetic changes in LSCs, may cause relapse of AML. Some acquired mutations may alter the growth properties of AML cells or confer resistance to additional chemotherapy. Most commonly, hematologic relapse is characterized by the reappearance of circulating blasts and cytopenias, which are identified by molecular or cytogenetic markers (Buccisano, Maurillo *et al.* 2012).

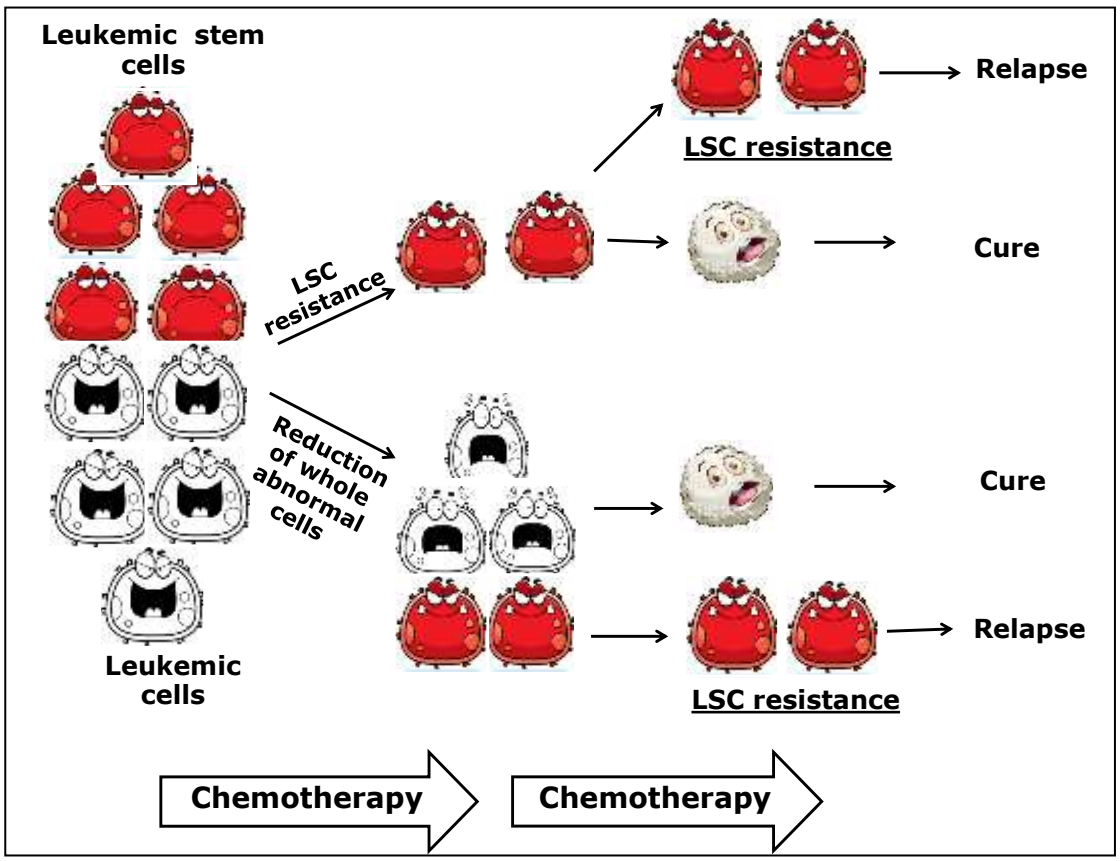

Figure 1.2.2.3: Incomplete elimination of leukaemic stem cells leads to relapse of acute myeloid leukaemia. Standard chemotherapy eradicates active leukaemic cells, but leukaemia stem cells (LSCs) in dormant state can resist chemotherapy.

1.3 DNA Damage Response (DDR)

1.3.1 Types of DNA damage

The structure of DNA is vulnerable to DNA-damaging agents that induce DNA lesions in all organisms (Fedor, Vignard *et al.* 2013). The human DNA undergoes several thousand to a million damaging events per day, resulting from various exogenous and endogenous sources *in vivo* (Jackson and Bartek 2009). Endogenous damage such as spontaneous or enzymatic conversions, lead to base loss and destabilize the N-glycosidic bond that links nucleobases and a sugars unite (Lindahl 1993; Jackson and Loeb 2001). Some endogenous metabolic damage occurring during hydrolysis reactions, can partially or completely cleave the nucleotide base from the DNA strand, leading to nucleotide substitutions, insertions, and deletions (Lord and Ashworth 2012). Additionally, up to 10,000 depurination events can occur per day (Nakamura and Swenberg 1999; Dahlmann, Vaidyanathan *et al.* 2009). Depurination is a spontaneous breakage of the chemical bond that links between a purine base and deoxyribosyl phosphate chain; this can lead to mutations and create sequence diversity (Fresco and Amosova 2017). Loss of pyrimidine bases, also known as depyrimidination can occur at a rate 20 to 100-fold per day (Dahlmann, Vaidyanathan *et al.* 2009). Furthermore, the loss of amine groups from adenine, guanine, and cytosine rings, called depyrimidination, generates unnatural bases such as hypoxanthine and xanthine; these are undetected by DNA repair enzymes, causing genome instability (Friedberg 2003; Dahlmann, Vaidyanathan *et al*. 2009). Endogenous DNA lesions can occur as simple breaks of one strand (SSBs), or both strands of DNA (DSBs) by predominant reactive oxygen species (ROS); free radicals and chemical species with one unpaired electron) produced after replication and transcription (Jackson and Loeb 2001; Dalle-Donne, Rossi *et al.* 2006; Woodbine, Brunton *et al.* 2011).

Exposure to exogenous mutagens, such as ionizing radiation (IR), ultraviolet (UV) light, and chemical agents, generate DNA strand breaks (SSB and DSBs) and cross-linking of DNA (Besaratinia, Synold *et al.* 2005; Rübe, Fricke *et al.* 2011; Esposito and So 2014). DSBs create discontinuities in DNA strands and are lethal lesions, because they can lead to the loss of genetic information. DSBs can cause sequence changes, translocations, alterations in chromosome numbers, and chromosomal rearrangements, all of which occur in myeloid malignancies (Besaratinia, Synold *et al.* 2005; Murray, Stiff *et al.* 2012). Moreover, DNA cross-links are induced upon exposures to various endogenous or exogenous agents, such as alkyting agents. Covalent linkage, resulting in DNA cross-links, can occur in either the same strand (called intrastrand crosslink), or in the opposite strand of the DNA (known as interstrand crosslink) (Price, Johnson *et al.* 2014; Talhaoui, Shafirovich *et al.* 2015). Cross-links can also occur between DNA and protein, thus interfering with the progression of replication and transcription machineries and contributing to carcinogenesis (Deans and West 2011; Tretyakova, Groehler *et al.* 2015).

1.3.2 DDR signalling cascade

DDR is comprised of an extensive signalling network of collaborative mechanisms that are triggered in cells by DNA damage (Figure 1.3.3.1) (Bartkova, Horejsi *et al.* 2005; Kastan 2008). A number of molecules are involved in checkpoint signalling, cell cycle arrest, DNA repair, and apoptosis and can be classified as sensors, transducers, and effectors. These molecules ensure that DNA damage is repaired or that the cell undergoes apoptosis; different molecules are at play at different stages in the cell cycle. At the site of DNA damage, phosphatidylinositol 3 kinase-like kinase (PIKK)-associated proteins, which are a family of serine-threonine kinases characterized by the presence of a C-terminal catalytic motif domain, are required to promote DDR (Bartkova, Horejsi *et al.* 2005; Rai, Peng *et al.* 2007).

The Mre11-Rad50-Nbs1 (MRN) complex (sensor) plays important roles in detection and signalling in response to DSBs, followed by the recruitment of ATM, which phosphorylates H2AX (Tomimatsu, Tahimic *et al.* 2007). The PIKK–complex is phosphorylated, and DNA damage sensors are activated by key regulators of checkpoint pathways, including ATM (ataxia telangiectasia, mutated), ATR (ATM and Rad3-related), and DNA-PK protein kinases (Bakkenist and Kastan 2003). DSBs activate these molecules, which in turn phosphorylate histone H2AX, at serine 139, and checkpoint kinase 2 (ChK2), with subsequent activation of the p53 protein (Polo and Jackson 2011). Accumulation of p53 in the nucleus inhibits the transition to S phase via cyclin dependant kinase 2/cyclin complex (cdk2-cyclin E or A) inhibitor p21 (Meek 2004). Thus, the cell cycle is blocked at the G1/S phase to repair the lesion and prevent damage from being transmitted to daughter cells, or to promote apoptosis if the DNA damage is unsuccessfully repaired (Shibata, Conrad *et al.* 2011). Alternatively, direct phosphorylation of cdc25a allows for rapid activation of the G2/M checkpoint, which can arrest the cell cycle or cause apoptosis. Figure 1.3.3.1 shows the main sensor, transducer, and effector molecules of interest in this project.

The H2AX142 phosphorylation marker is associated with the cells, chosen to undergo apoptosis, or activate repair responses following genotoxic stress (Cook, Ju *et al.* 2009); this was important for this study. The persistence of H2AX142 phosphorylation, following DNA damage, promote apoptosis and disrupts the DNA repair process (Cook, Ju *et al.* 2009; Brown, Eykelenboom *et al.* 2012; Jacobs, Misri *et al.* 2016). Tyr142, of histone H2AX, is phosphorylated by Williams-Beuren syndrome transcription factor kinase WSTF kinase (pH2AX-Tyr142) at its C terminus, but dephosphorylation occurs via EYA phosphatase in response to DNA damage, which is required for the recruitment of the mediator of DNA damage checkpoint protein 1

(MDC1) to γH2AX and downstream DDR signalling. Failure to dephosphorylate H2AX142 blocks DDR signalling and promotes apoptosis via activation/recruitment of c-Jun N-terminal kinase (JNK) (Cook, Ju *et al.* 2009; Zhang, Lu *et al.* 2012). Phosphorylation of H2AX, in the absence of DNA damage, may explain the involvement of H2AX in maintaining fidelity of the mitotic process and the faithful transmission of genetic information (Brown, Eykelenboom *et al.* 2012; Tu, Li *et al.* 2013). Imatinib induces of H2AX142 phosphorylation and apoptosis in chronic myelogenous leukaemia cells *in vitro* via the caspase-3/Mst1 pathway (Cook, Ju *et al.* 2009; Zhang, Lu *et al.* 2012).

1.3.3 DSB repair pathways

The harmful impacts of DNA DSBs are mediated by multi-component macromolecular protein complexes, which detect the damage, and intricate protein signalling cascades that ensure genomic integrity. In mammalian cells, there are at least six major DNA repair pathways, some of which are activated in order to correct base errors, such as translation DNA synthesis (TLS), base excision repair (BER), nucleotide excision repair (NER), and mismatch repair (MMR). DSBs stimulate collaborative mechanisms to repair breaks in the DNA by homologous recombination (HR) and non-homologous end-joining (NHEJ) (Friedberg 2003). A specific DNA repair pathway corrects the majority of DNA damage or DNA replication errors; however, there is functional redundancy between pathways, and often a lesion can be repaired by more than one pathway (Takata, Sasaki *et al.* 1998; Kunkel 2004). Single-strand annealing (SSA) is another type of homology-directed repair mechanism that uses shorter homologous sequences than homologous recombination (HR) (Frankenberg-Schwager, Gebauer *et al.* 2009).

The MRE11-RAD50-NBS1 protein complex (MRN) plays an essential role during the early steps of DNA double-strand break (DSB) repair

(Dinkelmann, Spehalski *et al.* 2009). The MRE11 protein composed of an N-terminal Mn2+/Mg2+-dependent phosphoesterase domain, and two distinct C-terminal DNA-binding domains (Williams, Williams et al. 2007; Giunta, Belotserkovskaya *et al.* 2010). The biochemical activities of MRE11 include intrinsic DNA binding activity to reseal DSB ends, and endo- and exonuclease activities to counteract single- and double-stranded DNA substrates, in order to facilitate recombination, repair, and genomic stability (Buis, Wu *et al.* 2008; Dinkelmann, Spehalski *et al.* 2009; Shibata, Moiani *et al.* 2014). Each MRE11 molecule binds a single RAD50, forming an MRE11-RAD50 complex (Cahill and Carney 2007). RAD50 exhibits both sequence and structural homology to structural maintenance of chromosome (SMC) family members, which control the higher-order structure and function of chromatin (van der Linden, Sanchez *et al.* 2009). The N-terminal Walker A and C-terminal Walker B nucleotide binding motifs embed to form the ATP-binding cassette (ABC)-type ATPase domain, which joins and disassembles the end of dsDNA. Additionally, the NBS1 protein binds this complex, via interactions with MRE11, to produce an overall MRE11-RAD50-NBS1 complex stability and function (van der Linden, Sanchez *et al.* 2009). NBS1 is composed of the forkhead-associated (FHA) domain and two adjacent BRCA1 C Terminus (BRCT) domain at its N-terminus. The FHA domain binds phosphorylated threonine residues in Ser/Thr motifs present in DNA damage response proteins. The BRCT domains in NBS1 bind Ser/Thr motifs when the serine residue is phosphorylated. The serial phosphorylation, caused by protein interactions, is crucial for recruiting DNA repair and checkpoint proteins in response to SSBs and DSBs (Giunta, Belotserkovskaya *et al.* 2010; Lee and Dunphy 2013). NBS1 is responsible for translocation of the MRN complex into the nucleus while the MRE11-RAD50- core complex remains cytoplasmic (Lamarche, Orazio *et al.* 2010). Because DSBs are present, the MRE11-RAD50-NBS1 (MRN) complex a sensor of DSBs

and induced cell-cycle checkpoint signalling, as well as a DSB repair effector in the NHEJ and HR pathways (Figure 1.3.3.1) (Williams, Williams *et al.* 2007; Giunta, Belotserkovskaya *et al.* 2010). Additionally, the MRN complex associates with telomeres (caps at the end of each chromosome) to protect the chromosomes from deterioration (Giunta, Belotserkovskaya *et al.* 2010; Lamarche, Orazio *et al.* 2010).

The lack of MRN complex function is implicated in many genetic disorders and predisposition to cancer. Mutations in MRE11 cause ataxia-telangiectasia-like disease (ATLD) and mutations of NBS1 cause Nijmegen breakage syndrome (NBS) (Tsubouchi and Ogawa 1998; Heikkinen, Karppinen *et al.* 2003; Chrzanowska, Gregorek *et al.* 2012; Krenzlin, Demuth et al. 2012). Furthermore, mutations in RAD50 are involved in susceptibility to breast and ovarian cancer, and sensitivity to ionizing radiation, and alters the configuration of chromatin at meiotic DNA double-stranded break sites in premeiotic and meiotic cells (Ohta, Nicolas *et al.* 1998; Luo, Yao *et al.* 1999; Heikkinen, Karppinen *et al.* 2003).

1.3.3.1 HR and NHEJ

HR repair faithfully restores genetic information lost at the site of a DSB. HR requires direct physical contact between homologous sequences to enable base pairing of a single DNA strand, at one end of a broken chromosome, with complementary DNA of an undamaged sister chromatid or homologous chromosome sequence. A template for accurate repair is only available when DNA has been replicated in the S or G2 phases of cycling cells (Chapman, Taylor *et al.* 2012). The initial step in HR processing of DSBs, is the formation of a pre-synapsis. Two recombinases, Rad51 and disrupted meiotic cDNA1 (DMC1), catalyse the pairing and shuffling of homologous sequences in eukaryotic cells. During the presynaptic phase, assembly of Rad51 and DMC1 helical filaments, bound to ssDNA, is enhanced by

recombination mediators such as BRCA1 and breast cancer type 2 (BRCA2) (Zhao, Vaithiyalingam *et al.* 2015; Martinez, von Nicolai *et al.* 2016). Each helical turn comprises six Rad51 molecules and 18 nucleotides in the Rad51–ssDNA filament. This ssDNA in the filament is stretched to a length that is half that of B-form dsDNA. During the synapse, Rad51 facilitates the formation of a physical connection between the damaged DNA strand and homologous duplex DNA template, to create heteroduplex DNA called a D-loop. Post-synapse, Rad51 dissociates from dsDNA to expose the 3'-OH required for DNA synthesis (Takata, Sasaki *et al.* 1998; Li and Heyer 2008). Additionally, the partner and localizer of *BRCA2 (PALB2)* gene is one of the many genes involved in regulation of the HR repair pathway (Figure 1.3.3.1A) (Heyer, Ehmsen *et al.* 2010). Mutations in HR genes lead to repair failure (Cerbinskaite, Mukhopadhyay *et al.* 2012). The risk of developing AML may increase in cases involving genetic defects in the core protein components of HR, such as x-ray repair complementing defective repair in Chinese hamster cells 3 (XRCC3), which is required for biological activity and governs the formation of the Rad51C-XRCC3 complex (Cerbinskaite, Mukhopadhyay *et al.* 2012).

Unlike HR, NHEJ, which is straightforward ligation of broken ends, does not need a homologous chromatid and, therefore, occurs throughout the cell cycle. NHEJ is the dominant repair pathway of the G0/G1 phase, repairing up to 85 % of DSBs (Mahaney, Meek *et al.* 2009). However, NHEJ is an error-prone pathway, because it does not rely on homology at the site of repair and may create micro-deletions or mutations of DNA sequences. In mammals, the key components of NHEJ include: DNA ligase IV (LIGIV), X-ray repair cross-complementing protein (XRCC4), DNA-dependent protein kinase transducer (DNA-PKcs), Ku heterodimer (Ku70 and Ku80), DNA polymerases (polμ and polλ), and possibly Artemis (Moon, Garcia-

Diaz *et al.* 2007; Hill and Lee 2010). During NHEJ, the MRN complex is required for DSBs detection, checkpoint signalling, and resection of DNA ends. Additionally, the MRN complex is important for chromatin remodelling at DSBs and activating the DNA-PK kinases. The DNA-PK function, in stabilizing DNA ends, directly facilitates break ligation, and the LIGIV/XRCC4 complex is recruited to the DNA ends via interaction with Ku (Tomimatsu, Tahimic *et al.* 2007). The kinase activity of DNA-PK is essential for NHEJ (Kurimasa, Kumano *et al.* 1999; Hill and Lee 2010). It may act as scaffold for recruiting DNA repair factors to DNA strand breaks (Murray, Stiff *et al.* 2012). The dissociation of DNA-PK from the DNA-Ku70/80 complex, caused by its ability to autophosphorylate, results in kinase inactivation, which is not completely understood (Kurimasa, Kumano *et al.* 1999). DNA-PK can also phosphorylate other factors implicated in NHEJ, including: Artemis, polynucleotide kinase/phosphatase (PNKP), H2AX, and p53 (Tomimatsu, Tahimic *et al.* 2007; Mahaney, Meek *et al.* 2009). Additionally, 53BP1 is a key positive regulator of NHEJ-mediated DSB repair. It acts as a scaffold protein for recruiting two downstream effectors, RAP1-interacting factor 1 (RIF1) and Pax transactivation domain-interacting protein (PTIP), at the DSBs sites to direct NHEJ DNA repair by pATM (Bothmer, Robbiani *et al.* 2011). ATM phosphorylates 53BP1 in different stages of the cell cycle; however, 53BP1 foci are observed predominantly in G1 cells (Feng, Li *et al.* 2015).

DNA DSB repair by NHEJ occurs in three steps: DNA end-binding and bridging, terminal end processing, and ligation. During the DNA end-binding and bridging step, a Ku heterodimer (Ku70 and Ku80) forms a ring that encircles duplex DNA (Tomimatsu, Tahimic *et al.* 2007; Pardo, Gómez-González *et al.* 2009). A bridge between the broken DNA ends is formed, and Ku protects these ends from degradation. Consequently, Ku aligns the DNA to enhance polymerase, nuclease,

and ligase accessibility to the broken DNA ends. DNA-PK is recruited, leading to phosphorylation of several nuclear proteins, including DNA ligase IV and XRCC4 (Davis and Chen 2013). The phosphorylation of DNA ligase IV, and/or XRCC4 may affect their interactions with Ku and other proteins. Terminal processing of the DNA ends is required prior to gaps being filled by DNA polymerase, which creates blunt ends that must be ligated. The nuclease Artemis opens the closed blunt ends where two strands of a DSB have been linked. Then, the nuclease activity of the DNA-PKcs complex cleaves the 5' and 3' DNA overhangs. Finally, ligation occurs, once the blunt ends recruit the XRCC4/DNA ligase IV ligation complex to join the DNA ends (Figure 1.3.3.1B) (Pardo, Gómez-González *et al.* 2009; Davis and Chen 2013).

Mutation in any one of these NHEJ genes leads to cell death, profound immune deficiencies, ionizing radiation sensitivity, and/or cancer predisposition in human patients (Fattah, Ruis *et al.* 2008; Gavande, VanderVere-Carozza *et al.* 2016). Ku80 deficiency in mouse cells results in a marked increase in chromosomal aberrations, including breakages and translocations (Difilippantonio, Zhu *et al.* 2000); an earlier study on human somatic cells revealed that the biological consequences of mutated XRCC4 primarily involve impaired activity of LIGIV (Grawunder, Wilm *et al.* 1997). Moreover, DNA-PKcs null (Ferguson, Sekiguchi *et al.* 2000) or Artemis-deficient fibroblasts (Rooney, Sekiguchi *et al.* 2002) increase genomic instability in mice and demonstrate a higher frequency of spontaneous chromosomal aberrations, compared with those of wild-type mice. Furthermore, NHEJ failure has been documented in mice having that have mutations in the tyrosine kinase receptor FLT3; inhibitors components of the NHEJ pathway confer enhanced sensitivity to topoisomerase II inhibitors in leukaemia cells (Tallman, Gilliland *et al.* 2005; Willmore, Sunter *et al.* 2005; Peng and Lin 2011).

1.4 The role of B-cell translocation gene 2 (BTG2) in dormant leukemic cells

BTG2, an anti-proliferative gene, encodes a conserved protein belonging to a family of transcription co-factors, which includes BTG1, BTG3, BTG4, TOB, and TOB2 (Yang, Morita *et al.* 2008; Horiuchi, Takeuchi et al. 2009; Winkler 2010). The members of the BTG/TOB protein family have high sequence similarity. For example, BTG1 and BTG1 and BTG2 show 70 % identity, whereas the TOB protein possesses the largest C-terminal containing a PABP-interacting motif (PAM motif), which allows it to bind with the poly(A)-binding protein (PABP)(Duriez, Moyret-Lalle *et al.* 2004; Yang, Morita *et al.* 2008; Horiuchi, Takeuchi *et al.* 2009). BTG2 has three distinct regions, Box A, B, and C, which are conserved in other homologues (Duriez, Falette *et al.* 2002; Winkler 2010). The BTG/TOB family is involved in cell cycle arrest and cell differentiation during development (Tirone 2001; Duriez, Moyret-Lalle *et al.* 2004; Mollerstrom, Kovacs *et al.* 2010; Winkler 2010). BTG1 has been used as a potential treatment-related biomarker to monitor the remission status of patients with AML-M2 and M3 (Lin, Gary *et al.* 1996; Cho, Kim *et al.* 2004). A possible role for BTG2 in DSB repair has been proposed recently (Choi, Kim *et al.* 2012; Imran and Lim 2013); one study showed that induction was of BTG2 is more dependent on p53 than is BTG1 and TOB expression, which occurs in the absence of p53 activity (Cortes, Moyret-Lalle *et al.* 2000). Furthermore, a study, published recently, suggested that oxidative stress up-regulates the expression of BTG2 via the ROS–PKC–NF-κB cascade; this may occur independently of p53 and may be associated with various biological phenotypes that are dependent on the cellular context (Ryu, Lee *et al*. 2004; Imran and Lim 2013).

TOB proteins contribute to the negative control of cell growth and act as tumour suppressors (Horiuchi, Takeuchi *et al.* 2009). Moreover,

TOB, highly expressed in T-cells, maintains cell quiescence via modulation of transcription (Tzachanis, Freeman *et al*. 2001; Yusuf and Fruman 2003), and modulates deadenylation, a key step in mRNA turnover (Ezzeddine, Chang *et al.* 2007; Doidge, Mittal *et al.* 2012).

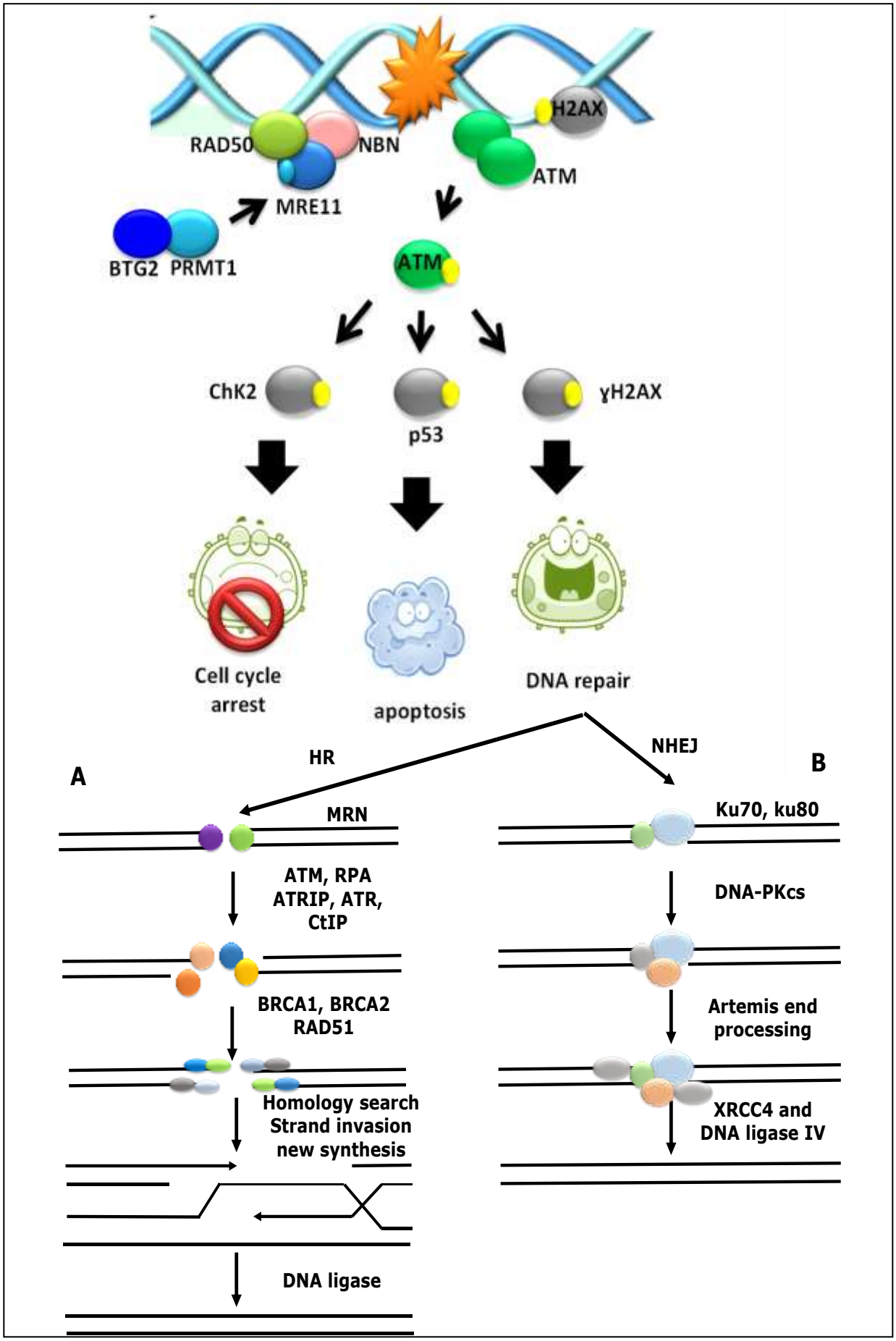
RAD50
NBN
H2AX
ATM
MRE11
BTG2 PRMT1
ATM
ChK2
p53
γH2AX
Cell cycle arrest
apoptosis
DNA repair
HR
NHEJ
A
B
MRN
Ku70, ku80
ATM, RPA ATRIP, ATR, CtIP
DNA-PKcs
BRCA1, BRCA2 RAD51
Artemis end processing
Homology search Strand invasion new synthesis
XRCC4 and DNA ligase IV
DNA ligase

Figure 1.3.3.1: DNA damage and signalling cascade of DNA response (DDR). The upper flow chart represents the cellular response to damage, which may involve activation of a cell cycle checkpoint, execution of DNA repair, or, when the damage is severe, initiation of apoptosis. A network of protein kinases is activated by DNA double-stranded breaks (DSBs). ATM is the primary kinase that phosphorylates downstream kinases by phosphorylation in a cell cycle-specific manner. Activated ATM directly phosphorylates three protein effectors: p53, γH2AX, and ChK2. In addition, the proposed action of BTG2 in response to DSBs is illustrated. In the lower flow chart DNA DSB repair pathways are shown. (A) Homologous recombination (HR) repair. After the MRN complex recognizes a DSB and activates the ATM kinase, single-strand DNA (ssDNA) is formed. The exposed ssDNA is coated with RPA to facilitate HR repair. Then, during synapse, a RAD51 nucleoprotein filament is assembled that replaces the RPA-coated ssDNA, performs homology sequence searching, and mediates strand invasion. Post-synapse DSBs are restored by joining the ends of DNA molecules, DNA synthesis, ligation, and resolution of gaps. (B) DNA DSB repair is mediated by NHEJ through three steps: DNA end-binding and bridging, terminal end processing, and ligation directly by the action of the KU70/80 complex and DNA-PKcs, followed by XRCC4-ligase4.

1.5 DNA damage and response in HSCs, LSCs, and progenitors

DDR is essential for maintaining normal HSC function and preventing leukemogenesis (Lord and Ashworth 2012). How LSCs respond to DNA damage remains largely unexplored because of the dormancy of stem cells, their low numbers, and their sensitivity to isolation procedures. Recent findings suggest that mammalian HSCs respond to DNA damage in different ways in order to maintain quiescence and repair the damage. Two published studies addressed the mechanism of DSB repair in HSCs and progenitors after IR. In human cord blood, Milyavsky *et al.* found that haematopoietic stem and progenitor cells (HSPCs) exhibit slower DNA damage repair kinetics and are more radiosensitive than progenitor cells. Delays in DSB repair in HSPCs, relative to that in progenitors, have been associated with persistent phosphorylation of ɣH2AX foci and inactivation of p53 or Bcl-2

expression that mediates the apoptotic response (Milyavsky, Gan *et al.* 2010).

However, HSPCs and myeloid progenitors, isolated from young mice revealed that HSPCs exhibit faster repair kinetics and are more resistant to 2 Gy of IR than are myeloid progenitors. HSPCs are less likely to undergo apoptosis compared with downstream myeloid progenitor cells. To repair DSBs, dormant HSPCs may use the NHEJ pathway, which is error prone and may contribute to mutagenesis at the stem cell level (Rossi, Bryder *et al.* 2007; Mohrin, Bourke *et al.* 2010). Hence, HPSCs and progenitor compartments respond to DNA damage in different ways. Additionally, the capacity of HSCs to repair DNA lesions diminishes with aging, which may lead to DNA damage accumulation and the development of leukaemia (Rossi, Seita *et al.* 2007; Rübe, Fricke *et al.* 2011). Rossi *et al.* revealed that HSCs from young mice are free of γH2AX foci, compared with 82 % of stem cells from old mice showing multiple foci. This group also reported that HSCs, in the old mice, process DNA damage by three genomic maintenance mechanisms involving nucleotide excision repair (NER), telomere maintenance, and NHEJ pathways (Rossi, Bryder *et al.* 2007). Others have reported that HSCs in elderly people tend to repair DNA lesions via the error-prone NHEJ repair pathway, which more often results in mutations causing radio-resistance, and resistance to apoptosis, than does repair via other pathways (Rübe, Fricke *et al.* 2011). Another study evidenced that HSCs lose their self-renewal capacity, and ability to respond to DNA damage, with age (Niida and Nakanishi 2006). Numerous DNA injuries can be recognized and corrected in the HSCs; however, damage may block the ability of a cell to self-correct, allowing a mutation to become established. This may lead to uncontrolled proliferation and the induction of additional mutations, resulting in leukaemogenesis. Taken together, numerous discrepancies are present in these

findings; these may be due to the differences between species and replicative ages of the cells.

The early work by our group demonstrated that a dormancy-enriched cell line displays unrepaired damage after drug treatment, indicating the vulnerability of dormant cells (Jawad, Seedhouse *et al.* 2010). A study of the CD34+ CD38− subset of primary cells, treated with specific drugs, showed that they are primed for apoptosis rather than for damage repair (Jawad, Yu *et al.* 2012). Recently, Xiao *et al.* found that accumulation of DNA damage in dormant LSCs, weakens the induction of DDR and enhances the resistance of leukemic cells to apoptosis (Xiao, Zou *et al.* 2012). Earlier studies showed that the DNA repair system contributes to LSC survival and drug resistance (Mony, Jawad *et al.* 2008; She, Niu *et al.* 2012).

Deficiencies in the DNA damage and response pathways may affect the ability of HSCs to proliferate, self-renew, and initiate apoptosis. Although a defect in a single pathway may be compensated by other DDR pathways (Takata, Sasaki *et al.* 1998), impairment can drive malignant cells to be either more sensitive or more resistant to chemotherapeutics (Curtin 2012). Current studies are assessing the feasibility of inhibiting these pathways in order to enhance the efficiency of chemotherapies; these studies often use a synthetic lethal approach, which is a strategy based on disrupting key regulatory genes, involved in DDR cascades and/or in DNA repair pathways, to destroy non-dividing LSCs) (Chan and Giaccia 2011; Leung, Rosen *et al.* 2011; Shaheen, Allen *et al.* 2011). In clinical trials, several inhibitors and novel compounds have been used to induce synthetic lethality as one of the most recent concepts reflecting advances in the understanding of DNA damage and repair pathways (Leung, Rosen *et al.* 2011), and contributing to the development of targeted therapeutics for blood malignancies.

1.6 An in vitro model of dormancy

Relapse is related to a sub-compartment of LSCs escaping chemotherapy by exiting the cell cycle and resting in the G0 phase (Jordan and Guzman 2004; Saito, Kitamura *et al.* 2010). This chemotherapy-resistant population of LSCs is present at a very low level in the BM; therefore, it is difficult to isolate and characterize these cells (Dick 2005; Horton and Huntly 2012; Pallis, Burrows *et al.* 2013). Some AML cell lines have AML stem cell characteristics and, therefore, serve as valuable tools for *in vitro* and *in vivo* studies of LSCs. We need model systems, to enable us to focus on the properties of dormant cells and investigate DNA damage and DDR. An isogenic model is would help obtain reliable, reproducible, and informative data on basal DNA damage and DDR in cells in cell cycle arrest and/or with different growth rates.

Previously, our group had established an *in vitro* system, based on mammalian target of rapamycin (mTOR) inhibition, designed to enrich dormant cells in the KG1a cell line following culture with 100 nM rapamycin (Pallis, Burrows *et al.* 2013). mTOR, a conserved kinase in eukaryotes, plays a crucial role in coordinating different cellular processes, including proliferation, survival, protein synthesis, and transcription, in response to the presence of nutrients, energy, stress, hormones, and growth factors (Estey and Dohner 2006; Chen, Liu *et al.* 2008; Cully and Downward 2012). In the BM, mTOR activity of dormant HSCs is restricted to conserving their HSC potential (Chen, Liu *et al.* 2008; Hoshii, Tadokoro *et al.* 2012; Yang, Rudge *et al*. 2013). There are two distinct mTOR signalling complexes known as rapamycin-sensitive mTOR signalling complex 1 (mTORC1) and rapamycin-insensitive mTOR signalling complex 2 (mTORC2). Inactivated mTOR has been detected in a subset of AML stem cells exhibiting HSC properties and long-term survival (Hoshii, Tadokoro *et al.* 2012; Yang, Rudge *et al.* 2013). The tuberous sclerosis complex

(TSC) has emerged as a major negative regulator of mTOR. TSC1 deletion, in HSCs, drives them out of dormancy and into rapid proliferation (Chen, Liu *et al.* 2008; Hoshii, Tadokoro *et al.* 2012).

Conversely, rapamycin inhibits the mechanistic mTOR, which is a serine/threonine-specific protein kinase belonging to the family of phosphatidylinositol-3 kinase (PI3K) related kinases (PIKKs). Rapamycin, one of the first generation mTOR inhibitors, is moderately successful in the treatment of cancer (Shang, Seedhouse *et al.* 2008). Modest responses to rapamycin therapy have been reported in renal cell carcinoma, neuroendocrine tumours of the pancreas, and mental cell lymphoma, that is associated with TSC1 and TSC2 mutations (Récher, Beyne-Rauzy *et al.* 2005; Benjamin, Colombi *et al.* 2011). This may be because rapamycin is an allosteric inhibitor and partially inhibits mTOR activity (Osmulski and Gaczynska 2013). (Osmulski and Gaczynska 2013). Rapamycin binds outside the kinase domain and prevents mTORC1-dependent S6K1 phosphorylation, causing minor suppression of 4E-EBP1 activity and other mTORC1 substrates (Sparks and Guertin 2010). Additionally, rapamycin recovers the negative feedback inhibition via S6K1 and Grb10 and promotes PI3K-AKT survival signalling (Wang, Hawk *et al.* 2008). Grb10 negatively regulates the insulin and insulin-like growth fator receptors (Hsu, Kang *et al.* 2011). Indeed, phosphorylation of Grb10 promotes the stability of mTOR1 and activates the MAPK pathway, providing another potential avenue for resistance and promoting cancer cell survival (Yu, Shen *et al.* 2008; Hsu, Kang *et al.* 2011; Hung, Garcia-Haro *et al.* 2012). Inhibition of mTORC1 by rapamycin activates human stem cell-like memory T (TSCM) cells and switches their metabolism to fatty acid oxidation required for TSCM generation. Rapamycin increases a long-term repopulation capacity and confers stemness to human naive T cells (Scholz, Jandus *et al.* 2016). TSC-mTOR pathway is a key regulator of HSC quiescence; the

pathway functions by repressing ROS production (Chen, Liu *et al.* 2008; Mohrin, Bourke *et al.* 2010; Rübe, Fricke *et al.* 2011). The binding of TANK binding kinase 1 (TBK1), in the BM niche, induces cell cycle arrest and enhances chemotherapeutic resistance of prostate cancer cells *in vitro* and *in vivo*. Rapamycin inhibits the interaction of TBK1 with mTOR, which plays an important role in the dormancy induction and drug resistance of prostate cancer (Kim, Jung *et al.* 2013).

Inhibition of cellular growth was successfully induced in mTOR-inhibited KG1a cells that were phenotypically dormant. The dormancy-enriched cells were characterised by low levels of RNA synthesis following continuous culture in 100 nM rapamycin for 11 days (Pallis, Burrows *et al.* 2013). Dormancy enrichment of an AML cell line by serum withdrawal, serum starvation, heparin, L-glutamine, nutrient withdrawal, mitogens, or growth factor withdrawal leads to induced apoptosis in a statistically significant percentage of cells. In addition, hypoxia is known to regulate several cellular processes and signal transductions in the bone marrow with the oxygen tension approximately 1 to 7 % (Hermitte, Brunet de la Grange *et al.* 2006). The α regulatory subunits of hypoxia inducible factors, HIF-1α and HIF-2α, play a role in tumour-suppressor-mediated ubiquitylation and proteasomal degradation, as do numerous hypoxia-inducible mRNAs that contribute to energy metabolism, angiogenesis, and apoptosis. However, culturing AML cells under hypoxic condition *in vitro* is difficult, unless the culturing is conducted in a hypoxic laminar flow hood combined with a hypoxic incubator. Maintaining the cultured cells under hypoxic conditions is also difficult during experimental processing, cell counting, labelling cells with fluorescent markers, and at room temparture or 37 ^{o}C. Furthermore, studies have shown significant induction of apoptotsis and sensitisation in cells cultured under hypoxic environment *in vitro*

(Lee, McClintock *et al.* 2002; Steinbach, Wolburg *et al.* 2003; Steinbach, Wolburg *et al.* 2005); this interferes with examining damage and repair in a stable dormant population.

In contrast, inhibition of the mTOR pathway by rapamycin resultes in no detectable apoptosis, as examined by annexin V, or sublethal damage, which is determined by foci of phospho-γH2AX139 damage. Furthermore, low ROS generation, decreased cell size, and reduction in mitochondrial metabolism are detected by the XTT assay in dormancy-enriched cells (Pallis, Burrows *et al.* 2013). Therefore, the dormancy-enriched KG1a cell model was deemed a suitable model for studying quiescent or non-cycling cellular population; the model mimics the behaviour of these cells in the BM, and was used as the standard model in this study.

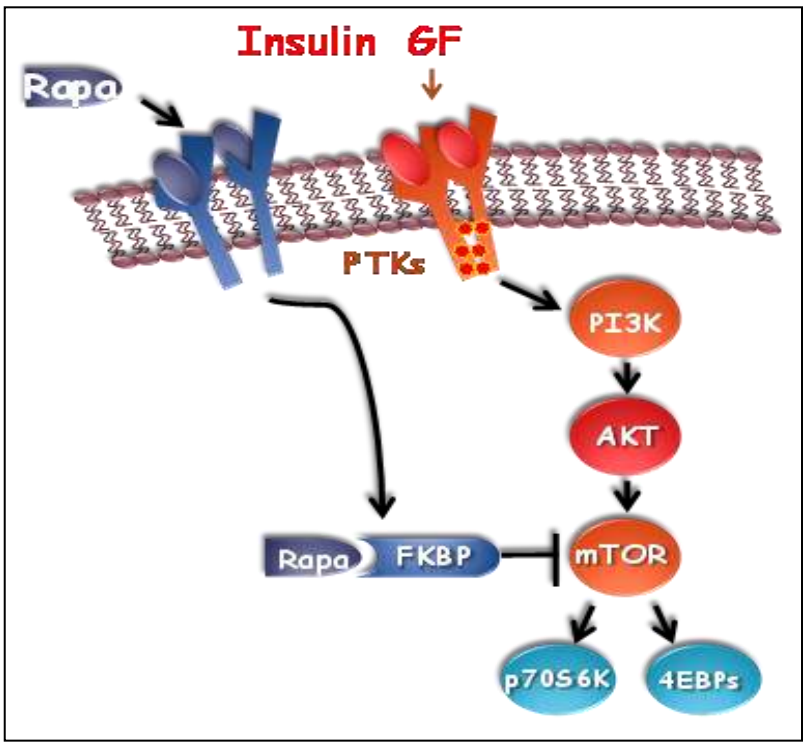

Figure 1.6: Diagram illustrating the mechanism of mammalian target of rapamycin inhibition by rapamycin. Rapamycin (mTOR) inhibitor rapamycin inhibits mTOR complex by associating with FK506-binding protein 12 (FKBP12), which then directly binds to mTORC1, suppressing downstream phosphorylation of (p70S6K1) and eukaryotic translation initiation factor 4E binding protein-1 (4EBPs).

Enrichment of dormancy in TF1a and M091 cell lines, using TGFβ, has shown promise as an *in vitro* model of dormancy established by Dr. Mazin ALasadi. This model has shown significant reduction in cell proliferation, and these cells were found to possess features of dormancy, including low nuclear ki-67 and P57 and translocation of FOXO3a. Additionally, cell morphology, assessed by immunohistochemistry, showed stem cells in periarteriolar niches, which exhibit less nutrient perfusion than that of their perisinusoidal counterparts. Furthermore, complete gene profiling suggested that TF1a-TGFβ cells acquire features of dormancy *in vitro* and mimic quiescent LSCs in the BM. Therefore, in our project, dormancy-enriched TF1a-TGFβ cell model was used to compare and contrast with KG1a-Rapa cell model findings (Chapter 5).

1.7 DNA damage and apoptosis detection strategies

Several methods have been used to detect different types of DNA damage in leukemic cells. A review of literature yielded a number of reports on standard and modified approaches to detect DNA damage. The next part of this chapter focuses on methods devised to identify DNA strand breaks, repair, and apoptosis.

1.7.1 Comet assay

Over a decade ago, the comet assay was considered a standard technique for detecting DNA damage (either SSBs or DSBs) or products resulting from oxidative damage and alkaline-labile sites. The comet assay is sensitive, quantitative, simple to perform, economical, and versatile in its application (Liao, McNutt *et al.* 2009). Importantly, the comet assay can be used to detect damage at the level of individual cells in either cell lines or primary cells (Collins 2004; Olive and Banath 2006). Cells embedded in agarose on a slide are lysed and then electrophoresed at a neutral or alkaline pH. DNA breaks are indicated by DNA moving from the head and forming a tail, which is visualized by fluorescence microscopy after staining with

a DNA-binding dye (Olive and Banath 2006). Several studies, undertaken to improve the lysis of cell membranes, have monitored cells post lysis from 5 hours to overnight (Tice, Agurell *et al.* 2000; Nickson and Parsons 2014). Various temperatures of lysis solutions have also been studied to determine the optimal temperature for preventing extraneous damage (Azqueta, Gutzkow *et al.* 2011; Ersson and Moller 2011). The most common parameters for precise comet tail measurement, using available software are tail length and tail moments. Tail moments are used to assess the relative fluorescence intensity of the head and tail because of their specificity for the background or threshold in image analysis (Collins 2004). The comet assay has a range of common variant techniques that can be modified to precisely assess different types of DNA damage and repair. The most common approach is the use of alkaline conditions to assess overall DNA damage, whereas a neutral comet assay is more specific for DSBs (Wojewódzka, Buraczewska *et al.* 2002). In addition, a number of other less common variants have been studied, such as the FISH comet (Escobar, Smith *et al.* 2007; Spivak 2010), bromodeoxyuridine labelling (Dolbeare 1995), and detection of DNA repair intermediates (Shaposhnikov, Salenko *et al.* 2008; Spivak, Cox *et al.* 2009).

1.7.2 Flow cytometry (FCM)

By the mid-1970s, flow cytometers, or fluorescence activated cell sorters (FACS), developed by Leonard Herzenberg (Stanford), were beginning to emerge. FCM is simple, cost-efficient, fast, objective, and provides a quantitative recording of fluorescent signals from individual cells; it also facilitates the physical separation of cells of interest (Otsuki, Li *et al.* 2003). FACS assays can be used to rapidly analyse large cell populations, assess the heterogeneity of cell populations, detect/sort cell subpopulations with different properties, identify/sort rare cells by correlating multiple parameters with the

expression of particular cell attributes in the same cells, and determine the number of cells in each cell cycle phase. FACS applications have been developed to detect apoptosis and differentiate between several types of cell death using chemical dyes and immunostaining (Otsuki, Li *et al.* 2003).

1.7.2.1 Detection of DDR events

Immunocytochemical analysis of the activation of DDR proteins ATM, DNA-PKc, and Chk2, and the phosphorylation of p53 and histone H2AX, can identify biomarkers of DNA damage including DSBs. Additionally, DDR proteins have been proposed as *in vitro* or *in vivo* prognostic reporters following the events of DNA damage (Halicka, Ozkaynak et al. 2009). Using phospho-specific antibodies, conjugated to different colour fluorochromes (e.g., FITC with propidium iodide [PI] or 7-aminoactinomycin D [7-AAD] used to detect DNA content), followed by multivariate flow-cytometric analysis, can detect phosphorylated proteins responding to DNA damage. The most common biomarker, used to study DDR, is phosphorylation of H2AX on serine 139 (γH2AX) (Rogakou, Pilch et al. 1998; Banáth and Olive 2003).

1.7.2.2 Apoptosis markers

Annexin V allows the identification of cell surface changes that develop in the early stages of apoptosis. Cell populations can be evaluated by microscopy or flow cytometric analysis. In dying cells, the inner lipid bilayer of a membrane is exposed to cell surfaces through the action of an amino phospholipid translocase (Logue, Elgendy *et al.* 2009). This property of apoptotic cells enables annexin V to bind with high affinity to phosphatidylserine in the presence of Ca^{2+}. Non-viable cells will strongly stain with annexin V. In contrast, in living cells, annexin V cannot bind the lipid bilayer (inner layer) of the cell membrane. This approach is rapid, precise, unbiased, and reliable, and requires minimal sample volume. Annexin V, therefore,

offers a quantitative method for assessing cell viability. Additionally, it allows more efficient discrimination between apoptotic and necrotic cells using dyes such as PI (Logue, Elgendy *et al.* 2009).

PARP is involved in DNA repair, where it functions as an important player in SSB via the BER pathway (Langelier, Riccio *et al.* 2014). Additionally, PARP-1 participates in DBS via the NHEJ pathway (De Vos, Schreiber *et al.* 2012). In response to mild cell stress, the PARP enzyme can activate repair and survival machinery. However, in cases of severe, irreparable DNA damage, this protein can be cleaved at one of the main cleavage targets of caspase-3 *in vivo* to prime apoptosis or cell necrosis through consumption of NAD+ and ATP. Cleavage of PARP occurs between Asp214 and Gly215, which separates the PARP amino-terminal DNA-binding domain (24 kDa) from the carboxy-terminal catalytic domain (89 kDa). PARP helps cells maintain viability; cleavage of PARP facilitates cellular disassembly and serves as a marker of apoptosis (Igney and Krammer 2002; Krishnakumar and Kraus 2010).

1.8 Subnuclear foci to detect and characterize alterations in DDR molecules via immunofluorescence microscopy

This is the traditional approach for visualizing and quantifying foci within a single nucleus. Nuclear foci are analysed by manual counting using immunofluorescence microscopy. The formation of protein aggregates (foci), at sites of DNA DSBs, is visualized by immunostaining with selective labelling antibodies conjugated to fluorescence dyes such as FITC. This approach allows the direct detection of protein and chromatin dynamics, at the site of a break, using a 100× lens under an epifluorescence microscope (Polo and Jackson 2011). The formation of discrete foci, following IR or chemotherapy, is characteristic of several proteins involved in DDR, as well as DNA repair genes such as phospho-γH2AX139, 53BP1, and RAD51, and can be visualized by immunofluorescence microscopy.

Over the past decade, laser scanning confocal microscopy (LSCM) has been used to obtain high-resolution images, enhancing the detection and accuracy of scoring the nuclear foci indicative of proteins active in different stages of the DDR pathway (Baer, Stewart *et al.* 2001).

1.9 Project objective

Leukaemia cells can lie dormant for days or weeks before dividing, which may explain why patients with AML respond to remission induction chemotherapy, but relapse later. We investigated the hypothesis stating that dormancy supress cellular sensitivity to chemotherapeutic drugs and DLICs possess unique strategies for handling DSBs compared with the strategies of cycling leukemic cells (CLCs). This project was aimed at evaluating the response of dormancy-enriched cells to chemotherapeutic agents with a focus on DNA damage and DDR. The project objectives were:

1- To examine the levels of DNA damage incurred by cycling cells, and dormancy-enriched cells, after subtoxic doses of chemotherapeutic agents.

2- To identify potential differences in upstream DDR markers such as ATM-Ser1981 and H2AX139, between dormancy-enriched cells and cycling cells in their response to DNA damage.

3- To determine the cell fate of dormancy-enriched and cycling cells; to assess whether these cell types tend to trigger DNA repair and/or apoptosis machinery after DNA damaging treatment.

Chapter 2:

Materials and Methods

2.1 Materials

Table 2.1 shows the chemical products used in this experimental work.

Name	Provided by
Paraformaldehyde	Fisher Scientific Ltd (Loughborough, UK)
Sodium azide	
Tris-base	
Glycine	
Roswell Park Memorial Institute (RPMI-1640)	Sigma (Poole, Dorset, UK)
Foetal calf serum	First Link (UK)
Recombinant human granulocyte-macrophages colony stimulating factor (GM-CSF)	Novartis (Basel, Switzerland)
Thrombopoietin (TPO)	Peprotech (Rocky Hill,USA
Glutamine	Sigma (Poole, Dorset, UK)
Streptomycin/penicillin	Sigma (Poole, Dorset, UK)
Fibronectin	Sigma-Aldrich, UK
Rapamycin	Sigma-Aldrich, UK
Trypan blue	Sigma-Aldrich, UK

Table 2.1: List of materials used in this study

2.2 Cell lines and routine maintenance

The KG1a cell line was purchased from the European Collection of Animal Cell Cultures (Salisbury, UK), and maintained in complete medium (CM) comprising: 80 % Roswell Park Memorial Institute (RPMI)-1640 supplemented with 20 % heat inactivated foetal calf serum (FCS), 2mM L-glutamine, 100 U/mL penicillin, and 10 µg/mL streptomycin. M07e, an IL-3- or GM-CSF-dependent human megakaryoblastic leukaemia cell line, was obtained from the German Collection of Microorganisms and Cell Cultures (DSMZ, Braunschweig, Germany). It was maintained in a 10 ml culture flask in complete medium comprising: 78 % Rosewell Park Memorial Institute RPMI-1640 (Sigma) supplemented with 20 % fatal calf serum (FCS, First Link UK), 2mmol/L L-glutamine (Sigma), 100 U/mL penicillin, 10

µg/mL streptomycin (Sigma), and 10ng/mL recombinant human granulocyte-macrophage colony stimulating factor (GM-CSF) (Novartis).

All cells were cultured at 37 °C and 5 % CO_2 in a humidified incubator, and all experiments were performed with cells in the log phase between 5-30 passage numbers. Cells were routinely tested for mycoplasma and subjected to short tandem repeat (STR) fingerprinting to confirm that there was no contamination or genetic drift in the AML cell line. cDNAs, (provided by Dr. Alasadi), were used to confirm the dormancy marker in the TF1a (Salisbury, UK) and M0-91 (Sloan-Kettering Institute, USA) cell lines, and dormancy TGFβ-models, recently established by our group. Characteristics of this cell line are shown in Table 2.2.

Cell lines	Cell type	Phenotype	Origin
M07e	Human acute megakaryoblastic leukaemia	CD33+,CD13+, CD34-,CD38+, Pgp-,CD42+	Established from the peripheral blood of a 6-month-old girl with acute megakaryoblastic leukaemia (AML M7) at diagnosis; subline of the growth factor-independent M-07
KG1a	Human acute myeloid leukaemia	CD33+,CD13+,CD34+,CD38-, Pgp+,CD42-	Established from the bone marrow of a 59-year-old man with erythroleukaemia that developed into AML; KG-1a is a subclone of the AML cell line KG1
TF1a	Human acute myeloid leukaemia	CD33+,CD13+,CD34+,CD38-, Pgp+	Established from the bone marrow of 35 years Japanese male with erythroleukaemia, a factor-independent variant isolated from the factor-dependent TF1 cell line
M0-91	Human acute myeloid leukaemia	CD34- CD38+	Established from a Japanese patient with undifferentiated AML (AML-M0).

Table 2.2: Human leukemic cell lines used in this study

(Information taken from: http:www.dsmz.de)

2.2.1 AML cell lines enriched for dormancy

In preliminary studies, KG1a cells were grown in the presence of rapamycin to induce acquisition of key features of dormant cells. This cell line was selected specifically because of its primitive status; it is the less differentiated variant of the KG1a cell line, having high expression of CD34+ and being the most resistant to standard chemotherapy. The KG1a cell line, enriched for dormancy shows additional features of dormancy characterised by small size and low levels of RNA and protein synthesis, and reversible exit from the cell cycle into the quiescence; these features are similar to those of quiescent DLICs in the BM. Enrichement of dormancy *in vitro,* using rapamycin maintains cell survival for up to 14 days with insignificant levels of apoptosis, rendering this a useful model for establishing how to target such cells. However, an efficient and informative model of dormancy is still needed for studying the properties and behaviour of DLICs in response to chemotherapy. Therefore, this project aimed to establish a new model of dormancy, using the M07e (acute megakaryoblastic leukaemia) cell line, grown with thrombopoietin (TPO).

2.2.1.1 M07e culture for dormancy enrichment using TPO and GM-CSF

M07e was cultured for 11-21 days, initially with different TPO concentrations, in order to establish cell lines with different rates of growth and proliferation. Three separate 10 mL flasks for were established, with appropriate volumes of complete medium to maintain cell concentration of 10^5 cells/mL. At day 0 (baseline), cells were cytokine-starved overnight, then treated with GM-CSF (0, 10 or 17 ng/mL) or with TPO (0, 1 or 10 ng/mL). All cell cultures were incubated under conditions of 5 % CO_2 at 37 °C. Proliferation was monitored, and fresh culture medium was added every 3 days or as needed to avoid the overcrowding. Cell densities were kept at 2 x 10^5

- 8 x 10^5/mL to maintain growing phase, and cell count were estimated at days 4, 6, 8, 11, 14, and 21, using Trypan blue dye (Sigma Aldrich) in a haemocytometer counting chamber.

2.2.1.2 Culture with an mTOR pathway inhibitor (the rapamycin model)

KG1a cells at a density of 2 × 10^5/mL were seeded in a cell culture flask with 100 nM rapamycin diluted in CM and cultured for 48 hours. Cells were grown in two conditions: one with rapamycin to produce dormancy-enriched KG1a cells and another without rapamycin to produce cycling KG1a cells. After 48 hours of growth with or without rapamycin, the total number of cells in each flask was calculated using the cell counting method described below. The required numbers of proliferating untreated and dormancy-enriched rapamycin-treated cells were then resuspended in fresh CM with rapamycin. Then, they were either treated with the appropriate drugs and inhibitors or left as untreated controls. The same drugs and inhibitors were used in proliferating cells and dormancy-enriched cells. Each experiment was repeated at least three times, with culture in each condition performed in triplicate in each experiment with each repetition.

2.3 AML primary patient cell characteristics

An analysis of 12 cDNA samples from primary cells from patient with AML was performed (Table 2.3) to identify dormancy features. Peripheral blood (PB) or BM samples were obtained during diagnosis of patients with AML (excluding M3 subtype) in preservative-free heparin or EDTA tubes. All samples were diagnostic samples collected pre-treatment, and only samples received within 48 hours of collection were analysed. The Nottingham 1 Research Ethics Committee (reference number 06/Q2403/16) approved use of these samples.

ID	Cytogenetics	Age	FAB	% CD34+	% CD34+ CD38-	% ki67+ blasts	% ki-67+ CD34+ CD38-
151701	add5q, add 11q	41	unknown	21.4	<1	42	NA
151363	11q23	56	M5	<1	<1	7	NA
668	normal	61	M4	11.9	6.0	37	12
150428	inv(16)	43	M4	37.4	7.1	81	94
661	normal	50	M5	54	<1	41	NA
149223	Normal	67	unknown	31.9	<1	51	NA
608	normal	20	M5	72.5	2.6	69	27
672	normal	80	M1	97	8	37	31
148549	failed	75	M0	50	10	72	78
151283	t(8;21)	54	M2	74	7.8	38	42
663	abn(17 p)	59	M2	1.5	<1	41	NA
665	normal	43	M1	28	1.4	34	11

Table 2.3: Characteristics of AML primary samples

2.4 Drug preparation and treatment

Differences in DDR between dormancy-enriched and cycling cells were determined. Different drug concentrations were initially used to establish correct doses, as described in detail below. The concentrations to induce DNA damage for each drug were: ara-c (dissolved in d-H2O), 2.0, 4.1, and 8.2 μM; ETO (dissolved in DMSO), 10, 20, and 40 μM; DNR (dissolved in d-H2O), 1.5, 3, and 6 μM; and TG02 (dissolved in DMSO), 50, 100, and 200 nM. To establish the concentrations of chemotherapeutic agents that would induce a low level (10 – 20 %) of apoptotic cells, drug dilutions were prepared in CM on the day of each experiment. Two sets of FACS tubes were prepared to treat cells with four different chemotherapeutic agents. The first set was used for cycling cells, and the second set was used for dormancy-enriched KG1a cells. Approximately 1×10^5 cells/mL were collected and rinsed with RPMI-1640, pelleted, and then resuspended in fresh medium for the comet assay. Then, 5×10^5/mL

cells were placed into FACS tubes (1 mL each) for DDR assays, and up to 1–2 × 10^6 cells were placed in FACS tubes for the molecular analysis. In each set, one tube was left untreated, with the drug omitted but the diluent (e.g., DMSO) included. Treated cells were vortexed and then incubated for the required time points at 37°C in 5% CO_2. Additionally, in order to investigate the link between NF-κB inhibition and BTG2 expression and survival of dormancy-enriched cells and chemotherapy resistance, three flasks of cells were incubated with parthenolide at concentrations of 1-1000 μM (diluted in methanol) for 24 hours, in advance of experiments with both cycling and dormancy-enriched KG1a cells. Table 2.4 shows the anti-neoplastic chemotherapeutic agents and inhibitors used and their mechanisms of action.

Agents	Mechanism of Action
Cytosine arabinoside (ara-c) (Cat# C1768) Sigma-Aldrich	Inhibits DNA synthesis with cell phase specificity, killing cells undergoing DNA synthesis (S phase) and blocking the progression of cells from the G1 phase to the S phase through the inhibition of DNA polymerase
Etoposide (ETO) (Cat# 1226) Tocris Bioscience (Bristol, UK)	Binds to and inhibits topoisomerase II and its function in ligating cleaved DNA molecules, resulting in the accumulation of single- or double-strand DNA breaks, the inhibition of DNA replication and transcription, and apoptotic cell death; acts primarily in the G2 and S phases of the cell cycle.
Daunorubicin hydrochloride (DNR) (Cat# D8809) Sigma-Aldrich	Inhibits DNA and RNA synthesis and stabilises complexes between DNA and nuclear enzyme topoisomerase II after the DNA has been separated for replication, thereby preventing the formation of DNA helices and causing the accumulation of double-stranded breaks
TG02 (Cat# SB1317) Tragara Pharmaceuticals	A multikinase inhibitor that inhibits signalling pathways downstream of CDKs 1, 2, and 3 and inhibits initiation of transcription (CDK9) and neuronal development (CDK5); also targets mutant

(Carlsbad, CA, USA)	FLT3, signal transducer and activator of transcription-5 (STAT5), and JAK2
Parthenolide (Cat# P0667) Sigma-Aldrich	Parthenolide, a sesquiterpene lactone isolated from the herb feverfew (Tanacetum parthenium). Parthenolide prevente degradation of IκB-α and IκB-β without interfere with DNA binding activity of activated NF-κB by inhibition of IkB kinase and/or direct modification of the p65 protein resulting in stabilization of cytoplasmic IκBα, which in turn inhibits NF-κB translocation
B02 (Cat# SML0364) Sigma-Aldrich	A specific RAD51 small molecule inhibitor
MG132, **Z-Leu-Leu-Leu-al** (Cat# C2211) Sigma-Aldrich	An inhibitor of proteasome activity

Table 2.4: Anti-neoplastic and inhibitor agents

2.5 Cell counting and cell viability assays

2.5.1 Manual cell counting using the Trypan Blue exclusion test

The principle of the Trypan Blue technique is that living cells have intact cell membranes that can exclude Trypan Blue, whereas those with damaged cell membranes take up the dye and become visually blue. Cells were resuspended in a known volume of medium, mixed thoroughly, and then 10 µL of the suspension was transferred to an Eppendorf tube and mixed with 10 µL of filtered Trypan Blue (1:1 volume). Ten microliters of the mix was introduced into the V-shaped wells of a haemocytometer to cover the area with the cell suspension. The counting chamber was then placed under a microscope. Viable cells in the four corners of the chamber were counted. Finally, the number of cells/mL was calculated by multiplying the average count per square by the dilution factor and 10^4 (Strober 2001).

2.5.2 Alamar blue assay

KG1a cells at a density of 5 × 10^5/mL were prepared in medium, and then 100 µL of the suspension was transferred to each well in 96-well plates. Thereafter, the cells were treated with ETO, ara-c, DNR, or TG02 at various concentrations and incubated at 37 °C in a humidified 5 % CO_2 incubator for up to 24 hours. After 2, 4, 6, and 24 hours, 10 µL of Alamar Blue reagent was added to the wells, and the plates were incubated for another 4 hours. The resulting fluorescence was then read at 560/590 nm using a plate reader (FluoStar-Optima, BMG Lab Technology, Germany). A standard curve was generated according to the manufacturer's instructions. The fold change in the number of cells based on metabolic activity was calculated for each time point after subtracting the fluorescence of heat-treated cells that were used as a negative control. The percentage of metabolically active viable cells was calculated by dividing the number of treated cells by the number of untreated ones. In addition, cells were treated with DMSO at the highest concentration used as a drug diluent in the experiment to ensure that DMSO did not affect cell viability.

2.5.3 Fixed stained cell (FSC) assay

2.5.3.1 Preparation of fixed stained cells

A previously established in-house method that allows rapid evaluation of viable cells by flow cytometric counting was used (Pallis, Syan *et al.* 1999). Peripheral blood mononuclear cells from healthy volunteers were prepared using a standard density gradient technique. Cells in PBSAA (phosphate-buffered saline [PBS], 1 % BSA, and 0.1 sodium azetide, Sigma) were incubated with 20 µL FITC-conjugated CD45 antibody (Becton Dickinson Bioscience, UK) for 20 minutes, washed twice in PBSAA, and re-suspended in fresh 2 % paraformaldehyde. The final cell concentration was determined using haemocytometer and Trypan Blue exclusion.

2.5.3.2 FSC/7-AAD cell viability assay by flow cytometry

A flow cytometric technique that incorporated an internal standard for counting cells and 7-amino actimomycin D (7-AAD) was used to assess cell viability at intervals of 2, 4, and 24 hours. This method allowed the actual number of cells to be calculated rather than the proportion of cells that were viable following culture. Twenty-five microliters of well-mixed cultured cells were added to 250 µL of (10 µg/mL 7-AAD) and 25 µL of fixed stained CD45+ normal mononuclear cells (FSCs) of known concentration as an internal standard. Cells were incubated for 15 minutes on ice, and then the cells were analysed by flow cytometry using BD FACSCanto software. The number of viable cells was determined by excluding dead cells and multiplying by the number of FSCs (Figure 2.5.3.2). The FSC/7-AAD flow cytometric method for counting viable cells was performed with the following calculation:

Viable cell count (cells/mL) = (%$P2$ AND $P4$) / (%$P3$) X FSC

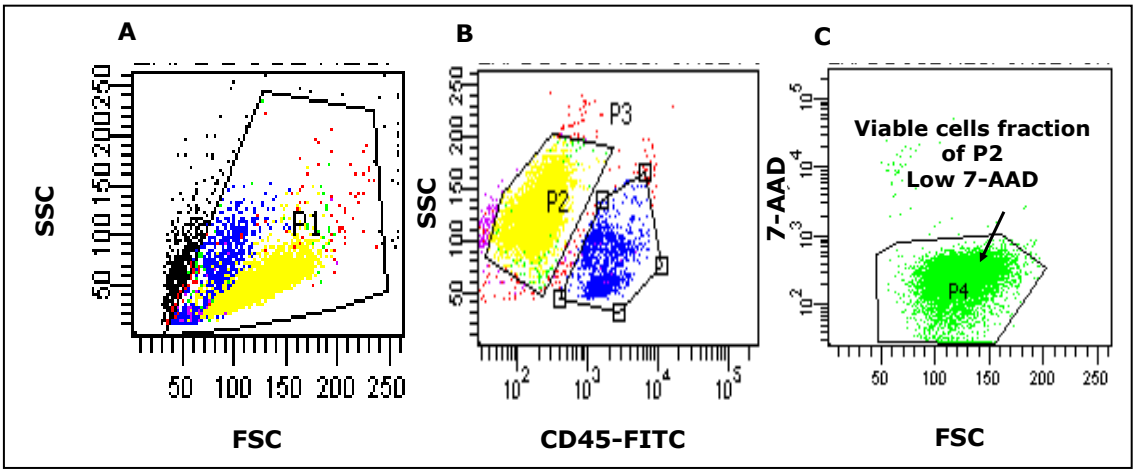

Figure 2.5.3.2: FSC/7-AAD Cell Viability assay by flow-cytometry. (A)FSC/SSC plot, P1. (B)The fixed CD45 pre-labelled normal mononuclear cells (FSC), P3 and the unlabelled AML sample cells P2. (C)P4 is set around 7AADlow/FSC high event (viable cells) derived from P2. The number of viable cells was quantified by excluding dead cells and multiplying by the number of FSC.

2.5.4 Annexin V assay

Apoptotic cells were detected using an annexin V kit (Trevigen) according to the manufacturer's instructions. Annexin V-FITC apoptosis detection is based on the observation that soon after initiating apoptosis, cells translocate membrane phosphatidylserine (PS) from the inner face of the plasma membrane to the cell surface. Once on the cell surface, PS is easily detected by staining with a fluorescent conjugate of annexin V, a protein that has a high affinity for PS. PI was used as a counterstain to discriminate necrotic/ dead cells from viable cells (Figure 2.5.4). One hundred microliters of an annexin-V mixture (84.5 µL dH2O, 0.5 µL annexin-V, 5 µL PI, and 10 µL 10× binding buffer) was added to 4 × 10^5 cells and incubated for 15 minutes at room temperature in the dark. Thereafter, 400 µL of 1× binding buffer was added to each tube. Data on annexin V positivity of the cells were collected on a FACSCanto II analyser using FACSDiva software.

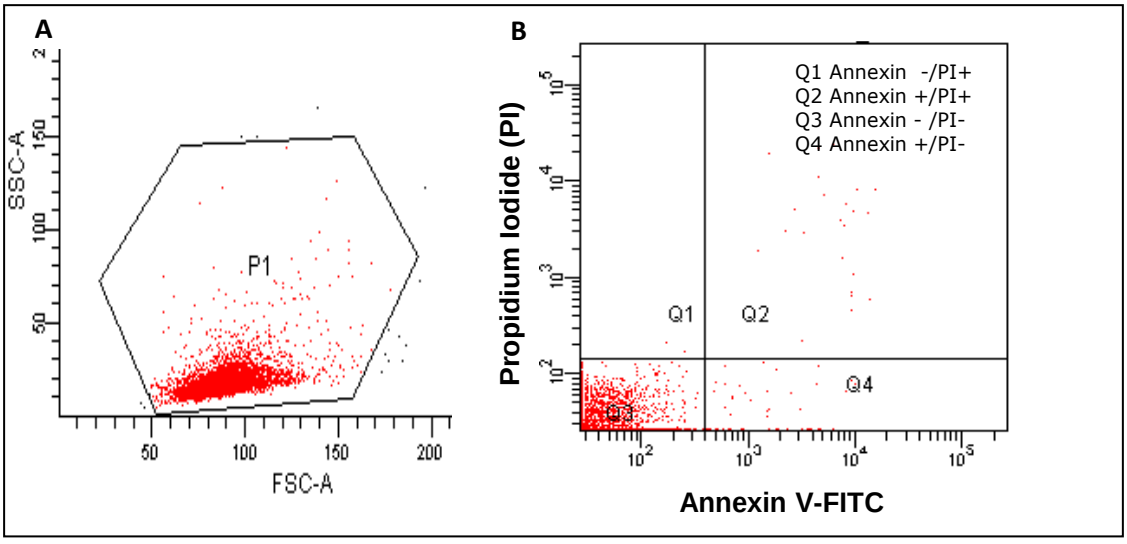

Figure 2.5.4: Annexin V FITC-A vs PI-A contour plots with quadrant gates showing four populations. (A) SSC/FSC plots showed the cell population in untreated cells (B) Apoptosis analysis using Annexin V assay shows accumulating viable population of cells that are negative for both Annexin V and propidium iodide (PI) in lower-left quadrant of dot plot shows high percentage in the untreated control cells viable and non-apoptotic (Q3, Annexin–PI–population) compared with few early apoptotic (Q4, Annexin V+PI–) or necrotic in cells (Q2, Annexin V+PI+).

2.6. DNA damage detection by comet assay

2.6.1 Controls

A preliminary analysis was conducted using commercial control cells (NC0-NC3) for neutral comet testing (Trevigen) to standardize methods between different runs. The control cells were treated with certain drugs under various conditions to generate increasing amounts of damage in the control series, and then aliquots were cryopreserved in liquid nitrogen. Control cells were thawed rapidly and resuspended in ice-cold PBS at a concentration of 5×10^4 cells for use in each experimental condition. A sample of untreated cells was always used as an internal control of assay variability, endogenous levels of damage within cells, and detection of additional damage that might occur during sample preparation. Control cells and treated cells were handled in an identical manner (Collins 2004; Olive and Banath 2006).

2.6.2 Sample and slide preparation

Cell samples were prepared immediately before starting the assay, with gentle handling and out of the light to the extent possible to prevent DNA damage from UV light. Buffers were cooled to 4 °C to minimise endogenous damage and inhibit repair during sample preparation. PBS free of calcium and magnesium was used to inhibit endonuclease activities. Cells (1×10^5) were washed twice with CM, pelleted at 400 × *g* for 5 minutes, and re-suspended in 50 µL of PBS. The cells were then mixed with 450 µL of melted LMAgarose (Trevigen), initially at 85–90 °C and then cooled to 42 °C before mixing with the cells. Then, 50–75 µL of the mixture was immediately pipetted onto a CometSlide (Trevigen) and the agarose/cell mixture was spread with a pipette tip to ensure complete coverage of the sample area. Thereafter, the comet slides were placed in the dark at 4 °C for 10 minutes to increase adherence of the samples in agarose. The slides were immersed for two hours or for overnight in pre-chilled

lysis solution (Trevigen) at 4 °C to remove membranes from cells and histones from DNA.

2.6.3 Neutral buffer preparation

To prepare 1× Tris borate-EDTA (1× TBE; 89 mM Tris-base, 89 mM boric acid, and 2 mM EDTA, pH 8.0), neutral electrophoresis buffer from 10× TBE stock buffer was diluted in d-H2O to prepare 2 litres of working buffer that was cooled to 4 °C the day prior to the experiment. Freshly made solution was utilized.

2.6.4 Slide electrophoresis

After overnight incubation of slides in the lysis solution, the buffer was drained, and the slides were placed in a horizontal electrophoresis tank. A specialised black comet electrophoresis tank was used to allow processing of a large number of slides in the dark. Neutral buffer was added until it just covered samples, and then the slides were incubated for 30 minutes to remove the lysis solution and facilitate DNA unwinding. Electrophoresis was conducted for 20, 30 or 40 minutes at 22V (1 V/cm, 400 mA). Negatively charged, damaged DNA fragments migrate toward the anode during electrophoresis. After removing excess electrophoresis buffer, slides were rinsed three times in distilled water, and then the cells were fixed by immersion in 70 % ethanol for 5 minutes and air dried at room temperature in the dark overnight for neutral comet testing. Drying allowed all cells to collect in a single plane to facilitate scoring.

2.6.5 Fluorescent staining

SYBR Green was purchased from (Sigma-Aldrich, cat# S9430) diluted to 1:75,000 in 1× TBE buffer (Fisher Bioreagents) (10 mM Tris-HCL and 1 mM EDTA, pH 7.5), and then 75–100 µL SYBR green solution was pipetted onto each circle of dried agarose and stained for 5–15 minutes at room temperature in the dark. Slides were turned on their

sides and gently tapped to remove excess SYBR green solution prior to scoring.

2.6.6 Epifluorescence microscopy

The migrated DNA (comet) was observed under an epifluorescence microscope at 20X magnification (BX61, Olympus Tokyo, Japan). The steps of the comet assay are summarised in Figure 2.6.

2.6.7 Comet assay analysis

DNA damage was assessed using an automatic image analysis system (CometAssay IV software, Perceptive Instruments, UK) to measure the olive tail moment. This is defined as the amount of DNA in the tail, and the displacement between the centre of mass of the comet head and the centre of mass of the tail describes the tail length. FOR each condition, 200 cells were scored from two slides. Duplicate agarose spots in each slide were scored randomly (50 cells in each spot).

1. Untreated or cells treated with DNA damaging agents

Treated cells

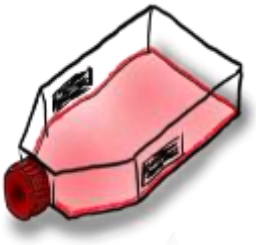

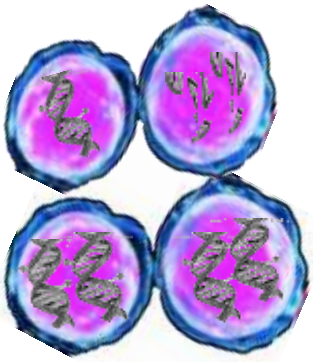

Untreated cells

2. Cells embedded in LMAgaros and adhered to comet slides

3. Cells incubated with lysis buffer 2 hours or overnight

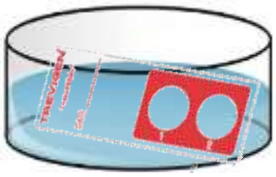

4. Electrophoresis to separate damaged and undamaged DNA

5. Analysis of comets

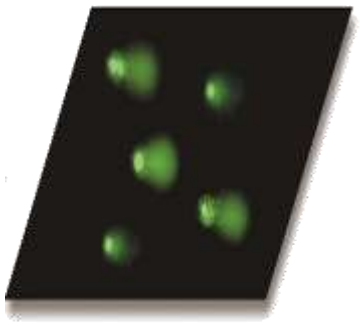

Figure 2.6: The comet "single cell gel electrophoresis" (SCGE) steps. 1-Treated and untreated populations of cells were exposed to genotoxic agents for 4 or 24 hours. 2-Cells were harvested, washed twice, and re-suspended and embedded in a thin layer of agarose gel on comet slides. 3-Cellular proteins were then lysed in detergent solution. 4-The DNA was electrophoresed stained with a DNA-specific fluorescent dye (SYBR green). 5-Measurement of the DNA segregated into a "head" (composed largely of intact genomic DNA) and a "tail" (comprising damaged SSBs and DSBs) or fragmented DNA, with the fluorescence intensity and length of the tail being directly proportional to the extent of DNA damage.

2.7 FACS

All FACS were performed on a FACSCanto II (BD Biosciences), using an excitation source with up to three lasers to detect eight colours. Each experiment included a compensation set-up to avoid fluorescence overlap.

2.7.1 Cell fixation and permeabilization

2.7.1.1 Fixation with 4 % paraformaldehyde and 100% methanol

Cells (2.5–5 × 10^5/mL), either untreated or treated with chemotherapeutic agents, were fixed with 4 % paraformaldehyde in PBS (1:1 volume), incubated at 37 °C for 15 minutes, and then rinsed twice with PBS and pelleted. Cells were then resuspended in 500 µL of PBS, and 450 µL of the suspension was added to each tube before permeabilization in ice-cold 100 % methanol for 10 minutes on ice. Samples were stored at −20 °C for at least 30 minutes.

2.7.1.2 Fixation with 4% paraformaldehyde and 0.1% Titon x100

Cells (5 × 10^5/mL), either untreated or treated with chemotherapeutic agents, were fixed with 4 % paraformaldehyde,

incubated at 37 °C for 15 minutes, and then rinsed twice with PBS and pelleted. Thereafter, cells were permeabilized in PBS with 0.1 % 100× Triton and 2 % normal goat serum (NGS) for 5 minutes. Cells were washed twice in cold PBS, resuspended in 100 µL PBS, and labelled with the appropriate antibody.

2.7.1.3 Fixation with 4 % paraformaldehyde and 0.1 % Tween 20

Cells (5×10^5/mL), either untreated or treated with chemotherapeutic agents, were fixed with 4 % paraformaldehyde, incubated at 37°C for 15 minutes, and then rinsed twice with PBS with 0.1 % Tween 20 and pelleted. Thereafter, cells were permeabilized and blocked using 10 % BSA in PBS with 0.1 % Tween 20 for 1 hour at room temperature and then pelleted and washed twice before subsequent experimentation.

2.7.1.4 Assessment of DDR markers by FACS

Treated and untreated cells (5×10^5 of cycling /dormancy-enriched KG1a cells) were fixed and permeabilized as described in section 2.7.1.1. Cells were then rinsed twice with PBSAA and resuspended in 100 µL of the first antibody for 1 hour at room temperature in the dark: 5 µg/mL mouse monoclonal IgG anti-phospho-H2AX Ser139 (Millipore cat# JBW301), 5 µg/mL mouse IgG1 isotype control for H2AX, 2.5 µg/mL mouse monoclonal pATM antibody (Chemicon cat# MAB3806), and 100 µg/mL IgG1 isotope control for pATM (Dako cat# abX0931). In addition, 2 µL/mL Chk2-Thr68 rabbit polyclonal antibody (Cell Signalling Technology cat# 2661) was either added or not (negative control). Cells were washed twice with PBSAA to remove excess antibodies. Eighty microliters of 20 % NGS or normal rabbit serum (NRS, Sigma-Aldrich, UK) was added to the corresponding tube as a blocking agent and incubated for 30 minutes on ice, followed by the addition of secondary FITC-conjugated antibodies and incubation for 30 minutes at room temperature in the

dark. Cells were washed twice in PBSAA, pelleted, resuspended in 300 µL of 7-AAD (25 µg/mL), and counterstained for 20 to 30 minutes to estimate the amount of intracellular DNA. For quantitative analysis, fluorescence values were obtained using BD FACSDiva 6.1.2 software.

2.7.1.5 Assessment of apoptosis markers by FACS

2.7.1.5.1 Activated caspase 3 assay

Cells (2.5×10^5) were harvested from culture in each condition. Cell pellets were washed twice with 2 mL of PBS and resuspended in 0.5 mL of PBS for fixation and permeabilization as described in section 2.7.1.1. Tubes were subsequently incubated at −20 °C. Five microliters of anti-activated caspase 3-PE AB (BD, cat# 561011) was added to test tubes with untreated or negative control cells (see Table 2.7.2).

2.7.1.5.2 Cleaved PARP assay

The events of apoptotic cell death were measured by cleaved-poly (ADP-ribose) polymerase on cell lines either treated with drugs or left untreated. One hundred microliters of fixed cells (as in section 2.7.1.1) were incubated for 30 minutes with 1 µL of mouse anti-cleaved PARP-Asp214 antibody (Alexa Fluor 647 Conjugate, BD, cat# 558710) at room temperature in the dark (see Table 2.7.2). Cells were washed twice with PBSAA, pelleted, resuspended in 300 µL PBSAA, and analysed by flow cytometry.

2.7.2 Determination of phospho-H2AX142

Test and control cells (5×10^5)/mL were fixed and permeabilized as in section 2.7.1.3, with the addition of 1 % BSA/10 % NGS to block non-specific protein-protein interactions. The cells were then incubated with an antibody recognising the phosphorylated H2AX142 epitope (cat# ab94602, 5 µL/mL) overnight at 4 °C. Cells were washed to remove excess primary antibody and then incubated with

the secondary antibody (goat anti-rabbit IgG-FITC conjugated diluted 1:250) for 1 hour (see Table 2.7.2). Cells were rinsed twice with PBSAA and resuspended in 300 µL PBSAA prior to FACS analysis (see Table 2.5). A portion of treated and untreated control cells were spread on glass slides after a second wash with PBSAA to remove excess unbound antibodies prior to immunofluorescence staining. Cellular DNA was counterstained with Vectashield mounting medium for DAPI fluorescence, and then a coverslip was placed over the cells. One hundred cells and foci were visualized for each slide and scored using CellSens Standard software under a 100X objective on an Olympus epiflourescence microscope. Because the numbers of foci varied in cells, H-scores were estimated, and cells were divided into groups according to the number of foci present. The number of foci present were divided into five groups: N (no damage, no foci), L (low, 1–6 foci), M (medium, 7–12 foci), H (high, >13), and C (completely damaged) as previously described (Figure 2.7.2) (Seedhouse, *Grundy et al.* 2009). The H score was calculated using the following formula:

H-score= N + 2L + 3M + 4H + 5C.

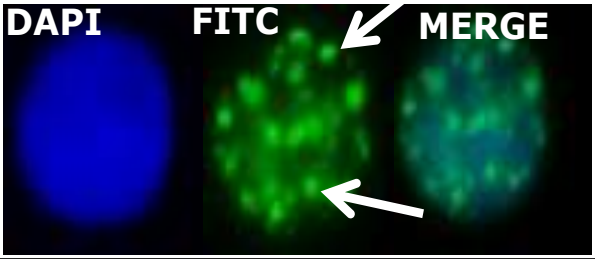

Figure 2.7.2: Foci appearance under the immunofluorescence microscopy are indicated by FITC conjugated AB. 100 cells were scored, number of cells is calssified according to the number of foci (indicated by arrows); N (no damage, no foci), L (low, 1–6 foci), M (medium, 7–12 foci), H (high, >13), and C (completely damaged). H-score calculated by N + 2L + 3M + 4H + 5C formula.

Primary antibody (1st layer)	**Supplier**	**Secondary antibody (2nd layer)**	**Supplier**
DNA damage response (DDR) markers			
Mouse monoclonal IgG anti-phosphoH2AX Ser139 (1: 200 dilution)	Millipore cat#JBW301	Polyclonal goat anti-mouse IgG–FITC conjugated	Dako (cat# F0479)
Isotype mouse IgG1, (1: 50 dilution)	Dako (cat# X0931)		
Mouse monoclonal anti-phospho ATM(1: 100 dilution)	Chemicon (cat# MAB3806)	Rabbit anti-mouse IgG (ab)2 FITC-conjugated	Dako (cat# F0313)
Isotope mouse IgG1, control (1: 200 dilution)	Dako(cat# X0931)		
Rabbit polyclonal phosphChk2 Thr68 (1 in 25 dilution)	BD Technologies (cat# 2661)	Goat anti-rabbit IgG FITC-conjugated (1:11 dilution)	Sigma-Aldrich (cat# F1262)
Rabbit polyclonal anti-phosphoH2AXY142 antibody (1 in 50 dilution)	Abcam (cat#94602)	Goat anti-rabbit IgG FITC-conjugated (1:11 dilution)	Sigma-Aldrich (cat# F1262)
Apoptosis markers			
Rabbit polyclonal anti-active caspase3-PE conjugate (1: 20 dilution)	BD Technologies (cat# 2215734)	_____	_____
Mouse monoclonal anti-PARP1 antibody-Alexa Fluor 647 (1: 10 dilution)	BD Technologies (cat# 558710)	_____	_____

Table 2.7.2: List of markers used to examine features of dormant leukemic cells, DDR and apoptosis.

2.8 Immunofluorescence Staining and Foci Counting

2.8.1 Preparation of slides

2.8.1.1 Fibronectin coating technique

Fibronectin (Sigma Aldrich, cat# F0556) was prepared at 20 µg/mL in PBS. Four hundred microliters of solution used to coat each slide (Vfm CellPath, UK), and then slides were incubated overnight at 4 °C. The next day, the slides were washed twice with PBS and then incubated for 2 hours at 37 °C in a closed box to allow cell attachment. After this, the slides were left to air dry for 1 hour in a biological safety cabinet to prevent contamination. Subsequently, 5×10^5 cells/mL were fixed and processed as described in sections 2.7.1.1 and 2.7.1.2 or 2.7.1.3.

2.8.1.2 Immunofluorescence method for detection of foci

Phospho-H2AX139 foci were evaluated by immunofluorescence, with 4–5 × 10^5/mL treated and untreated cycling and dormancy-enriched cells fixed as described in section 2.7.1.1 and then incubated with primary phosph-H2AX139 antibody (1:500) or 53BP1 rabbit polyclonal antibody (H-300 IgG, Santa Cruz Biotechnology, cat# 22760, 1:50 dilution) at room temperature in the dark for 2 hours. Negative control mouse IgG (1:50) was added to the control tube. After two washes with PBSAA, the cells were incubated with 3 µL of appropriate secondary antibodies, anti-mouse IgG-FITC or goat anti-rabbit IgG $(ab)^2$ FITC (cat# F1262, 1:11 dilution) for 1 hour in the dark at room temperature, followed by an additional wash with PBSAA.

To assess RAD51, 5×10^5 cells/mL were treated with chemotherapeutic agents with or without 10 µM B02 (RAD51 inhibitor) for 2 hours prior to damage induction. Then, cells were fixed and permeabilized as described in section 2.7.1.2. The slides were blocked by incubation overnight at 4 °C in 2 % BSA in PBS. Rabbit polyclonal anti-RAD51 (H-92, Santa Cruz Biotechnology, cat#

8349, 1:500 dilution) was incubated with cells for 1 hour at room temperature. The cells were incubated with goat anti-rabbit IgG (ab) [2] FITC (F1262, 1:11 dilution) for 1 hour in the dark at room temperature after blocking NGS) to avoid non-specific binding.

All cells were washed twice with PBSAA, pelleted, and resuspended in 100 µL of PBSAA. Then, 20 µL of cells was spread on glass slides (VFM Cell Path, UK) after two washes with PBSAA. Cellular DNA was counterstained with DAPI-fluorescent Vectashield mounting medium, and then a coverslip was placed over the cells. Foci were counted by visualizing 100 cells for each condition and scored using CellSens Standard software under a 100× objective of an Olympus epiflourescence microscope. Because the number of foci varied in cells, H scores were estimated. The number of foci present were divided into five groups: N (no damage, no foci), L (low, 1–6 foci), M (medium, 7–12 foci), H (high, >13), and C (completely damaged) as previously described (Seedhouse, Grundy *et al.* 2009). The H score was calculated as follows: N + 2L + 3M + 4H + 5C.

2.9 Assessment of NF-κB (p65) translocation

Cycling or dormant cells (4×10^5, treated/untreated)/mL were rinsed in cold PBS, pelted, fixed in 100 % cold methanol for 5 minutes, and then pelleted again. To permeabilize cells, 2 mL of 0.5 % saponin was incubated with cells for 2 hours in a cold room on a mixer. Cells were pelleted, and then 5 µL of anti-NF-κB antibody (NF-κB P65 mouse monoclonal IgG1, Santa Cruz Biotechnology, cat# 8008, 1:500 dilution in 0.2 % saponin) was incubated with cells overnight in a cold room. After the cells were rinsed with PBSAA, non-specific binding was blocked with NGS (Sigma) for 30 minutes, and a FITC-conjugated secondary goat anti-mouse IgG (Dako, cat# F0479) was incubated with cells for 2 hours at 4 °C. The cells were rinsed with PBSAA, and then 20–50 µL of cells was spotted onto each glass slide

and left to dry at room temperature in the dark. DAPI-containing Vectashield was added, coverslips were placed over the cells, and slides were left to dry overnight in the dark at 4 °C. Cellular localisation of NF-κB was assessed using an Olympus epifluorescence microscope.

2.10 Molecular Methods

2.10.1 RNA extraction

RNA was extracted from 2 × 10^6 cells/mL from each condition using a QIAamp blood RNA isolation kit (cat# 52304; Qiagen) according to the manufacturer's protocol, with the addition of a DNase (cat# 79254, Qiagen) digestion step. RNA was stored at −80 °C or processed immediately for cDNA synthesis.

2.10.2 RNA quantitation

A NanoDrop 2000 Spectrophotometer (Thermo Fisher Scientific, USA) was used to determine the RNA concentration and purity by the optical absorbance at 260/280 nm.

2.10.3 cDNA synthesis

cDNA was prepared from 2 µg of RNA, denatured at 65 °C and then placed on ice for 5 minutes. Subsequently, the RNA was mixed with 21.5 µL of reverse transcription master mix, containing 200 µL of 5× first strand buffer (Invitrogen, Life Technologies Ltd., UK, Y02321), 40 µL of 25 mM dNTPs (Invitrogen, 10297-018), 100 µL of 0.1 M DTT (Invitrogen, Y00147), 33 µL of random primer at a concentration of 3 µg/µL (Invitrogen, 12097-018), 65 µL of DEPC-treated water, 1 µL of 40 U/µL RNasin (Promega, UK, N251B), and 1.5 µL of MMLV reverse transcriptase at a concentration of 200 U/µL (28025-013; Invitrogen). The cycling program consisted of 37 °C for 60 minutes, 95 °C for 10 minutes, and then a hold at 4 °C. Finally, cDNAs were stored at −20 °C.

2.10.4 Polymerase chain reaction (PCR) optimisation

The primer sequences for amplification of the coding region (474 bases) of BTG2 were designed using Primer3 Input version 4.0 (http://primer3.sourceforge.net; sequences are shown in Table 2.10.4). The optimal conditions for amplification were determined by assessing different annealing temperatures and $MgCl_2$ concentrations. The annealing temperature was set between 55–65 °C at temperatures of 55.0, 55.2, 55.9, 57.0, 58.2, 59.4, 60.6, 61.8, 63.0, 64.1, 64.8 and 65.0 °C. The $MgCl_2$ concentrations tested were 1.0, 1.5, and 2.0 mM (Applied Biosystems), Taq polymerase (Amplitaq Gold, Applied Biosystems), 10 × PCR Buffer (Applied Biosystems, Warrington, UK), 1.25 µL of 20 pmol/µL BTG2 forward and reverse primers (Invitrogen) (Table 2.10.4), 200 µM dNTPs (Amersham Pharmacia Biotech), and 1 µL of DNA, with a 25 µL volume completed with water. PCR amplification was performed using a T-gradient thermoblock (Biometra, Germany) according to the following parameters: Amplitaq Gold activation at 95 °C for 10 minutes, followed by 35 cycles consisting of 1 minute at 95 °C for DNA denaturation, 1 minute at the primer annealing temperature, and 1 minute at 72 °C for primer extension. This was followed by 10 minutes at 72°C to ensure final extension. PCR products were loaded onto a 2 % agarose gel in 1× TBE with 0.5 µg/100 mL ethidium bromide and run at 200 volts for 30 minutes, after which time products were visualised under a UV light and compared to a DNA ladder with known sizes.

Primer	Sequence (5'->3')	Str END	Length	Temp	GC %
BTG2_Forward	GGTAACGCTGTCTTGTGGA	4-47	19	57.40	52.63
BTG2_Reverse	GACAACAGGCCACCACATAC	594 -613	20	58.83	55.00

Table 2.10.4: Primers used in amplification and sequencing reactions.

2.10.5 Sequencing reactions

PCR products from KG1a cells were purified using a QIAquick PCR Purification Kit (Qiagen). Each sample was sequenced with the forward primer and reverse primer. One microliter of PCR product was mixed with 3.2 pmol of forward or reverse primer, 3 μL of sequence mix (BigDye Terminator V3.1–Cycle Sequencing Kit, cat# 4337455, Applied Biosystems), and 5 μL of 2.5 × buffer a 20 μL volume completed with water. The following sequencing cycles were repeated 25 times: 96 °C for 1 minute, 96 °C for 10 seconds, 50 °C for 5 seconds, and 60 °C for 4 minutes using a T-Gradient Thermocycler (Whatman Biometra). Thereafter, 20 μL of the sequenced products was purified using 2 μL of sodium acetate (3 M, pH 5.2) and 50 μL of 100 % ethanol, and then incubated on ice for 20 minutes. After centrifugation for 20 minutes at 13,000 rpm, supernatants were discarded, and 150 μL of 70 % ethanol was added to wash the pellets. Tubes were spun again for 5 minutes at 13,000 rpm, and supernatants were removed. Thereafter, the pellets were left to air dry for 5 minutes and then stored at −20 °C until analysis. The sequencing products were resuspended in HiDye (Applied Biosystems) and run on an ABI Prism 3130 Genetic Analyser (Applied Biosystems). Sequences were analysed using Applied Biosystems Sequencing Analysis software 5.2.

2.11 Real-time PCR

The real-time PCR master mix contained 0.8 μL of diluted cDNA (1:15), 5 μL of Sybr Green PCR Master Mix (4309159; Applied Biosystems), and 1 pmol specific primers for the relevant gene. Primers were purchased from Qiagen (Table 2.11). Negative controls (no template) were included in each experiment, and all reactions were run in triplicate. Quantitative PCR was performed on an ABI Prism 7500 (Applied Biosystems) using standard cycling conditions. After 40 cycles, the products were heated from 60 °C to 95 °C over a

20-minute period for a melting curve analysis. This allowed the specificity (single melting peak) of the products to be determined and the absence of primer-dimers to be confirmed. The housekeeping gene β2-microglobulin (β2M) was used to standardize cDNA quantities in the samples. Standard curves were generated using serial dilutions of KG1a cDNA, and the relative expression levels of transcripts were determined by calculating the ratio of target gene expression to that of β2M.

Name	Product code	Sequence 5' to 3'
B2M	(Pallisgaard, Clausen *et al.* 1999)	Fw GAGTATGCCTGCCGTGTG Rv AATCCAAATGCGGCATCT
BTG2	QT-00240247	Fw GCGAGCAGAGGCTTAAGGT Rv GGGAAACCAGTGGTGTTTGTA
NBN	QT-00075775	Fw CCATCGATGGTGTGCACTCATTTGTGGACG RvCCGCTCGAGCGGGGTTCATCAATGGGTGGG TA
RAD50	QT-00037170	Fw CTTATACAGGACCAGCAGGAAC Rv CCTTTCTGTCGCCCTAATGC
RAD1	QT-00091287	Fw ATGGCAATGCAGATGCAGCT Rv TCAGTCTTTGGCATCTCCCA
FANCG	QT-00064967	Fw TAATACGACTCACTATAGGG) Rv TAGAAGGCACAGTCGAGG)
XRCC3	QT-00095921	Fw GCT GTC TCG GGG CAT GGC TC Rv GCT TCC GCA TCC TGG CTA AA

Table 2.11: Primers for real-time PCR

2.12 Western Blotting and Immune-Detection

2.12.1 Preparation of cell lysates

Cells (1×10^7)/mL were washed with ice-cold PBS and resuspended in lysis buffer (50 nM Tris [pH 7.4], 150 mM NaCl [Fisher Scientific, Loughborough, UK], 1 % NP-40 [BDH Laboratory Supplies, Lutterworth, UK], 0.25 % Na-deoxycholate, 1 mM EDTA, 2 μg/mL leupeptin, 5 μg/mL aprotinin, 1 μg/mL pepstatin, 20 mM NaF, 1 mM phenylmethylsulfonyl fluoride (PMSF), and 3 mM sodium orthovanadate) for 30 minutes. Samples were then sonicated before the addition of 200 mM PMSF and incubated for 30 minutes on ice.

The samples were clarified by centrifugation at 10,000 × *g*, and supernatants were assayed for protein content using a Bio-Rad dye reagent. Protein lysates were denatured by boiling for 5 minutes in 4× lamellae buffer immediately prior to loading.

2.12.2 Sodium dodecyl sulphate polyacrylamide gel electrophoresis (SDS-PAGE)

Samples were separated using SDS-PAGE in a Mini-PROTEAN Tetra cell combined system. Gels were prepared at the appropriate concentration based on the molecular weight of the target protein (Table 2.12.2). A separating gel was cast in a gel cassette, leaving 1.5 cm at the top for a stacking gel to be cast. The separating gel was allowed to set for at least 30 minutes before the stacking gel was applied. Gels were run in 1× running buffer (25 mM Tris-base, 190 mM glycine, 0.1 % SDS, pH 8.3) at 200 V for 1 hour.

15 % Separating gel	**Volume**	**4 % Stacking gel**	**Volume**
d.H_2O	5.0 mL	d.H_2O	6.1 mL
30 % Acrylamide/bis	2.30 mL	30 % Acrylamide/bis	1.3 mL
Lower buffer	2.50 mL	Upper buffer	2.5 mL
10 % APS	0.10 mL	10 % APS	50 µL
TEMED	10.00 µL	TEMED	10 µL

Table 2.12.2: Constitution of SDS-PAGE electrophoresis gels

2.12.3 Transfer and immunodetection

Proteins were transferred to nitrocellulose membranes (Whatman Protran). Immunoblotting was performed using a BIO-RAD Mini Trans-Blot Electrophoresis system for 45 minutes at 100 V in 1 % transfer buffer (25 mM Tris base, 190 mM glycine, and 20 % methanol). Membranes were blocked for 30 minutes at room temperature with 5 % milk powder (Blotting-Grade Blocker, cat# 170-6404, USA) and then incubated with primary antibody diluted in 1 % milk powder overnight at 4 °C on a shaker. Membranes were then washed three time for 10 minutes each with 1 % Tris-buffered

saline with Tween 20 in 1 % TBST, (10× TBST buffer: 24.2 g Tris base, 87.6 g NaCl, 1000 mL dH2O, and 10 ml Tween 20, pH 7.4–7.6). Membranes were then incubated with the corresponding secondary antibody diluted in 1 % milk powder to detect bands corresponding to the proteins of interest (Table 2.12.3). Proteins were visualized by chemiluminescence (Hyperfilm ECL; Amersham) using a 1 in 5 developer and fixation system. The density of bands was determined using ImageJ analysis software (NIH) (Schneider, *et al* 2012).

Antibody		Dilution	Supplier
Primary antibody	Anti-BTG2 mouse monoclonal (ab58219)	1:5000	Abcam
	Anti-actin(C-2) β-actin (sc-8432)	3:1000	Santa Cruz
	Anti-H2AX-Y142 rabbit polyclonal (ab94602)	1:2000	Abcam
Secondary antibody	Goat anti-mouse HRP IgG (sc-2055)	1:5000	Santa Cruz
	Anti-rabbit monoclonal (cat# 12812)	1:11	Cell Signaling Technology

Table 2.12.3: List of antibodies used in immunoblotting.

2.12.4 Statistical analysis

GraphPad Prism software (Statmate) version 2.0 and SPSS version 19.0 were used for the statistical analyses. The significance of differences was determine using paired Student's t-test and one-way analysis of variance (ANOVA) for parametric data or Wilcoxon signed rank and Kruskal-Wallis test for non-parametric data. Spearman's rank correlation coefficient (rho) was calculated to determine the correlation between dormancy and proliferation markers. P values less than 0.05 were considered significant.

Chapter 3: Assessment of DNA Damage and DDR

3.1 Background

Assessment of DNA damage, in the KG1a rapamycin cell line model, was conducted to determine baseline and induced damage under different conditions. The comet assay was applied to measure DNA strand breaks, because it directly assesses DNA damage, rather than the cellular response to damage. Damage in individual cells was also determined. Under an electrical current, fragmented DNA migrates creating a tail 'comet' that can be measured; therefore, DNA strand breaks were estimated by the neutral comet assay (Olive and Banath 2006; Zhang, Chen *et al.* 2011). DNA lesions are generated in numerous ways, such as by exposure to IR, UV light, and chemotherapeutic agents, by errors during cell replication, or in response to ROS, which can be by-products of metabolism. DNA damage activates the DDR system (Polo and Jackson 2011). In brief, cellular responses to damaged DNA are mediated by distinct kinase signalling cascades, with components that belong to the phosphatidylinositol 3-kinase-related kinase (PIKK) family, ataxia-telangiectasia mutated (ATM), ataxia-telangiectasia rad3-related (ATR), and DNA-PK kinases. DSBs are the most lethal types of DNA damage, recognized by MRN protein complexes or sensors; this results in phosphorylation of ATM and activation of downstream proteins required for cell cycle arrest, repair, or apoptosis in cases where the damage is deemed irreversible (Jazayeri, Falck *et al.* 2006).

Various molecules are involved in the signalling and adhesive interaction between HSCs and the BM niche (Ehninger and Trumpp 2011; Louria-Hayon 2014; Morrison and Scadden 2014). In this chapter, we aimed to establish a cell model of dormancy enrichment using thrombopoietin (TPO) and the M07e cell line (Qian, Buza-Vidas *et al.* 2007). HSCs long-term expressing the thrombopoietin receptor (MPL), are a quiescent cells associated with TPO-producing

osteoblastic cell population in the adult BM nishe. The binding of TPO molecules to MPL stimulates signalling that lead to the upregulation of β1-integrin and cyclin-dependent kinase inhibitors in the HSCs. Inhibition of the TPO/MPL signalling pathway reduces the number of quiescent LT-HSCs (Yoshihara, Arai *et al.* 2007).

The standard model of KG1a, enriched for dormancy by the mTOR inhibitor (rapamycin), was established previously in our laboratory, and was used in this project for further analysis, as described in later chapters. This chapter describes preliminary studies on chemosensitivity and selecting appropriate chemotherapeutic agents, doses, and time points. This allowed us to address the main aim of this project, which was assessing the differences in induction of DNA damage, and/or response to DNA damage, in cycling cells compared with those in dormancy-enriched cells. Flow-cytometry and immunofluorescence assays were used to detect the DDR markers pATM-Ser1981, phosph-H2AX139, and pChk2-Thr68.

3.2 Model of dormancy

3.2.1 M07e with GM-CSF and TPO

M07e is a cell line dependent on human GM-CSF, having surface markers characteristic of both myeloid progenitors and megakaryocytes. TPO is a critical thrombopoietic and megakaryocytopoietic regulator and plays a role in maintaining of quiescence of HSCs in the niche (Qian, Buza-Vidas *et al.* 2007; Yoshihara, Arai *et al.* 2007; de Graaf and Metcalf 2011). To produce a slowly proliferating subset of cells, with acquired dormancy features of BM LSCs, we investigated the effects of TPO (0, 1 or 10 ng/mL) on the proliferation and survival of M07e cells. It was hypothesised that low concentrations of TPO would push cells out of the cell cycle into G0 and/or slow the proliferation rate of M07e over long-term cell culture.

The survival of M07e cells, following 72 hours of GM-CSF starvation, may be due to the presence of residual growth factor that feeds the cells culture before apoptotic cells are noticed. Culturing cells with increasing concentrations of TPO can supress cellular apoptosis for up to 14 days of culture, but does not promote proliferation (Table 3.2.1). When enriching cells for dormancy *in vitro*, it is important to select agents are that not toxic and do not stimulate apoptosis. Growing M07e cells with a combined dose of TPO + GM-CSF (1 ng/Ml TPO + 10 ng/ml GM-CSF) or (1 ng/ml TPO + 17 ng/mL GM-CSF) for 7 to 21 days results in unexpectedly inconsistent rates of cell proliferations. Thus, our attempts to generate an *in vitro* model of the M07e cell line, using TPO in the presence or absence of GM-CSF to produce cell populations with different rates of proliferation (slow, standard, and rapid) have shown largely inconsistent results, and the hypothesis was rejected.

Growth factors	**Days of culture**	**Growth**	**Percentage of non-viable cells**
0 ng/mLTPO	14	No growth	56 %
1 ng/mLTPO	14	No growth	7 %
10 ng/mL TPO	14	No growth	3 %
10 ng/mL GM-CSF (Control)	21	Consistent growth	0.4 %
0ng/mL GM-CSF (Control)	21	No growth	45 %
10 ng/mL GM-	21	Inconsistent	1-2 %

CSF+1 ng/mL TPO		growth	
17 ng/mL GM-CSF+ 1 ng/mL TPO	21	Inconsistent growth	0.1 - 0.8 %

Table 3.2.1: The M07e AML cell line, cultured with TPO in the presence or absence of GM-CSF. Trypan blue was used to estimate cell viability and for manual cell counts. Each condition was assessed in triplicate over three independent experiments.

3.2.2 KG1a cells cultured with mTOR inhibitor

A model of dormancy-enriched KG1a cells was established using the inhibitor of the mTOR pathway, rapamycin. KG1a cells were cultured at 2 × 10^5/ml on days 0, 2, and 4, in a medium containing 100 nM rapamycin. A significant inhibition of growth was successfully induced in the immature KG1a cell line at day 2 ($p = 0.0009$) and at day 4 ($p = 0.0001$) (grey line), compared with that in the cycling cells (black line; Figure 3.2.2A, n=15), confirming our previous findings (Pallis, Burrows *et al.* 2013). Apoptosis was assessed by annexin V labelling at day 2 and 4, showing that 99 % of cells were viable with and without rapamycin (Figure 3.2.2B; n=1). The total RNA content of lysed cells, measured by NanoDrop for cycling cells and cells enriched for dormancy by rapamycin, showed a reduction in the RNA content of dormancy-enriched KG1a cells compared with that of the cycling KG1a cells (Figure 3.2.2C, n=15).

Mitogen-activated protein kinase (MAPK)/extracellular signal-regulated protein kinase (ERK) is a key signal transducing pathway that transports extracellular stimuli from the cell surface to the nuclei (Chambard, Lefloch *et al.* 2007; Shaul and Seger 2007). Studies have shown that inhibition of mTOR by rapamycin activates the MAPK/ERK

signalling pathway (Carracedo, Ma *et al.* 2008; Rastogi, Jiang *et al.* 2013). To assess whether the MAPK pathway is activated after inhibition of mTOR, treated cycling and dormancy-enriched KG1a cells with the MEK inhibitor, U0126, with or without rapamycin. The levels of the ribosomal protein S6 (RPS6), which mediates mTORC1 S6 phosphorylation, were used as a control to measure mTOR inhibition by rapamycin. The combination of an mTOR inhibitor (rapamycin) and an MEK inhibitor (U0126) inhibited cell proliferation and decreased the phosphorylation of the mTOR pathway in the KG1a cells. Two-houres incubation with U0126 induced complete suppression of RNA translation via inhibition of RPS6, in dormancy-enriched KG1a (Figure 3.2.2D; n=1). Enriching dormancy by rapamycin inhibits the mTOR pathway by blocking proteins involved in cell-cycle progression, as well as ribosomal proteins and elongation factors necessary for translation.

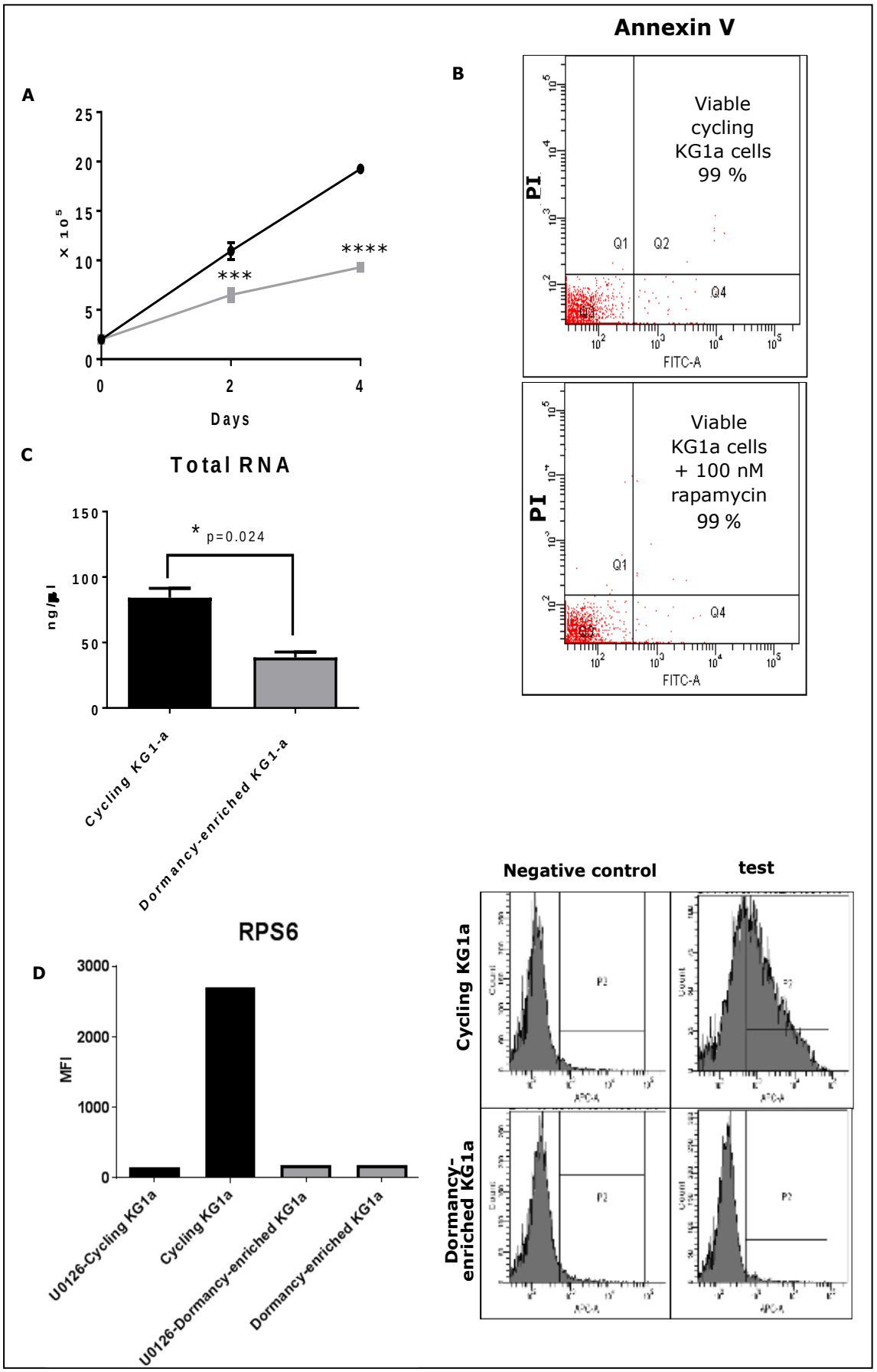
A
25
20
15
10
5
0
x 10^5
***
****
0
2
4
Days
B
Annexin V
Viable cycling KG1a cells 99 %
PI
Q1
Q2
Q4
FITC-A
Viable KG1a cells + 100 nM rapamycin 99 %
C
Total RNA
150
100
50
0
ng/µl
* p=0.024
Cycling KG1-a
Dormancy-enriched KG1-a
D
RPS6
3000
2000
1000
0
MFI
U0126-Cycling KG1a
Cycling KG1a
U0126-Dormancy-enriched KG1a
Dormancy-enriched KG1a
Negative control
test
Cycling KG1a
Dormancy-enriched KG1a

Figure 3.2.2: A model of dormancy-enriched KG1a cells established using an inhibitor of the mTOR pathway (rapamycin). (A) Significant growth inhibition, induced in KG1a cells at day 2 and 4 (grey line), compared with that of the cycling cells (black line) (n=15). (B) Apoptosis, assessed by annexin V labelling at day 2 and 4, shows that 99 % of cells were viable with and without rapamycin. (C) The total RNA content of lysed cells, measured by nanodrop for cycling cells and cells enriched for dormancy by rapamycin. (D) Phosphorylation of the S6 ribosomal protein increases during translation of RNA in cycling KG1a (black bars, left graph); representative histogram shows the shift in the fluorescence intensity of RPS6 phosphorylation in cycling and dormancy-enriched cells (right panel); n=1. Each condition conducted in triplicate and the data points are indicated by the mean ± SD. * represents a P value of <0.05 compared with untreated cells; ** represents P <0.01; ***P <0.001; ****P <0.0001.

3.3 Chemosensitivity of KG1a cells to AML chemotherapeutic agents

In studies preceding the work in this thesis, KG1a cells were grown in the presence of 100 nM rapamycin to enrich for dormant cells. A number of key features of dormancy were identified, such as low levels of RNA, slow proliferation, low levels of induced ROS, and low metabolic activity with no detectable apoptotic cells (Pallis, Burrows *et al.* 2013). The dormancy-enriched KG1a cell model was used to assess the response to four different anti-leukemic compounds in order to establish the concentrations of DNA-damaging agents that would produce an IC_{10}–IC_{20} response. A dose, causing just 10–20 % cell death, is important to ensure that the cells are damaged sufficiently, but not enough to trigger the process of dying, which masks survival processes and results in dead and decaying cells whose products can interfere with assays.

A nucleoside analogue (ara-c), topoisomerase II inhibitors (DNR and ETO), and a transcriptional CDK/RP2 inhibitor (TG02) were used to treat cycling and dormancy-enriched KG1a cells. These drugs were chosen because they are all relevant to AML treatment regimens, used in standard and clinical trials. Cells were seeded in triplicate in

96 well plates, at 4.5-5.0 X 10^5/mL cells, and treated for 2, 4, 6, and 24 hours with: an increasing dose of ara-c at the final concentrations of 2.0, 4.1, and 8.2 μM; ETO (10, 20, and 40 μM), TG02 (50, 100, and 200 μM); and DNR (1.5, 3, and 6 μM). Untreated cycling and dormancy-enriched cells were used as controls. Cell viability was assessed by Alamar Blue assay after prolonged incubation times (6 and 24 hours) or FSC/7AAD after short incubation times (2 and 4 hours); results were confirmed by manual cell counting using Trypan blue. Both untreated cycling and dormancy-enriched KG1a control cells were confirmed surviving cells appeared healthy, negative for Trypan blue-staining, proliferative and metabolically active, with small round nuclei and intact cell membrane, assessed by the Alamar Blue assay; the 7-AAD negative status was confirmed by the FSC/7-AAD assay.

Cycling cells, treated with increasing doses of 4.1 μM ara-c for 2 hours, showed an insignificant decline in cell viability at 5.56 X 10^5/mL compared with 5.7 X 10^5/mL of untreated cells. Similarly, treatment with 4.1 μM ara-c for 2 hours produced an in insignificant reduction in dormancy-enriched cells, from 4.7 x 10^5/mL of untreated cells to 3.8 X 10^5/mL after treatment. Further reduction in the viability of cycling and dormancy-enriched cells was detected following 4 hours of with 4.1 μM ara-c; viability decreased to 1.8 X 10^5/mL and 2.1 X 10^5/mL respectively. Incubation of cells with 4.1 μM ara-c, for up to 24 hours, resulted in the viability of 1.6 and 2.7 x 10^5/mL in cycling and dormancy-enriched cells, respectively (Figure 3.3i).

Treatment with 20 μM ETO produced unclear reduction in the cellular viability at the 2 hour time point. Compared with 5.45 X 10^5/mL untreated cycling cells, the number of cycling cells, treated with 20 μM ETO, was reduced to 5.09 X 10^5/mL. Additionally, incubating dormancy-enriched cells with 20 μM ETO for 2 hours produced no

clear decline in the cell count 4.83 x 10^5/mL untreated cells vs. 4.51 x 10^5/mL treated cells. After 4 hours of treatment with ETO, the viable cell count was reduced to 2.2 x 10^5/mL in cycling, and 2.3 x 10^5/mL in dormancy-enriched cells, compared with analogous untreated cells. Following 24 hours of treatment with ETO, viability significantly declined in cycling cells (1.9 x 10^5/mL) and in dormancy-enriched cells (1.8 x 10^5/mL) (Figure 3.3ii).

In response to 100 nM TG02 for 2 hours, the viability of cycling cells was reduced from 4.7 X 10^5/mL to 4.5 X 10^5/mL. Similarly, the dormancy-enriched cells reduced from 4.9 X 10^5/mL to 4.0 X 10^5/mL. At the 4 hour time point, viable cycling and dormancy-enriched cells were reduced to 2.03 x 10^5/mL. Further incubation of cells, up to 24 hours, showed a clear dose-dependent decline in response to TG02 (Figure 3.3iii).

In response to 1.5 μM DNR, both cycling and dormancy-enriched cells showed an insignificant reduction in viability after 2 hours of treatment. Small, but significant, differences in viability were observed in cycling cells after 4 hours of incubation with 1.5 μM DNR; compared with 5 x 10^5/mL of untreated cells, viability was reduced to 2.1 x 10^5/mL after treatment in cycling cells, and to 3.6 X 10^5/mL in dormancy-enriched cells. Further incubation of cells, for up to 24 hours, showed singnificantly reduced viability of 1.8 X 10^5/mL and 2.6 X 10^5/mL in cycling and dormancy-enriched cells, respectively (Figure 3.3iv).

Our findings indicate that the 2 hour time point induced minimal or no cell sensitivity afer treatment with ara-c, ETO, TG02, or DNR in cycling or dormancy-enriched KG1a cells; thus this time point was exluded from further studies. The 4 and 6 hour time points in cycling and dormancy-enriched KG1a cells, induced chemosensitivity to all the drugs used, between IC_{10}-$IC_{20;}$ therefore, the 4 hour time point was selected to try and establishe an even earlier time at which

biological changes begin to appear within the cells. The 24 hour time point was included to compare and track the consistency of drug-triggered induction of DNA damage and repair mechanisms over short and prolonged times of incubation.

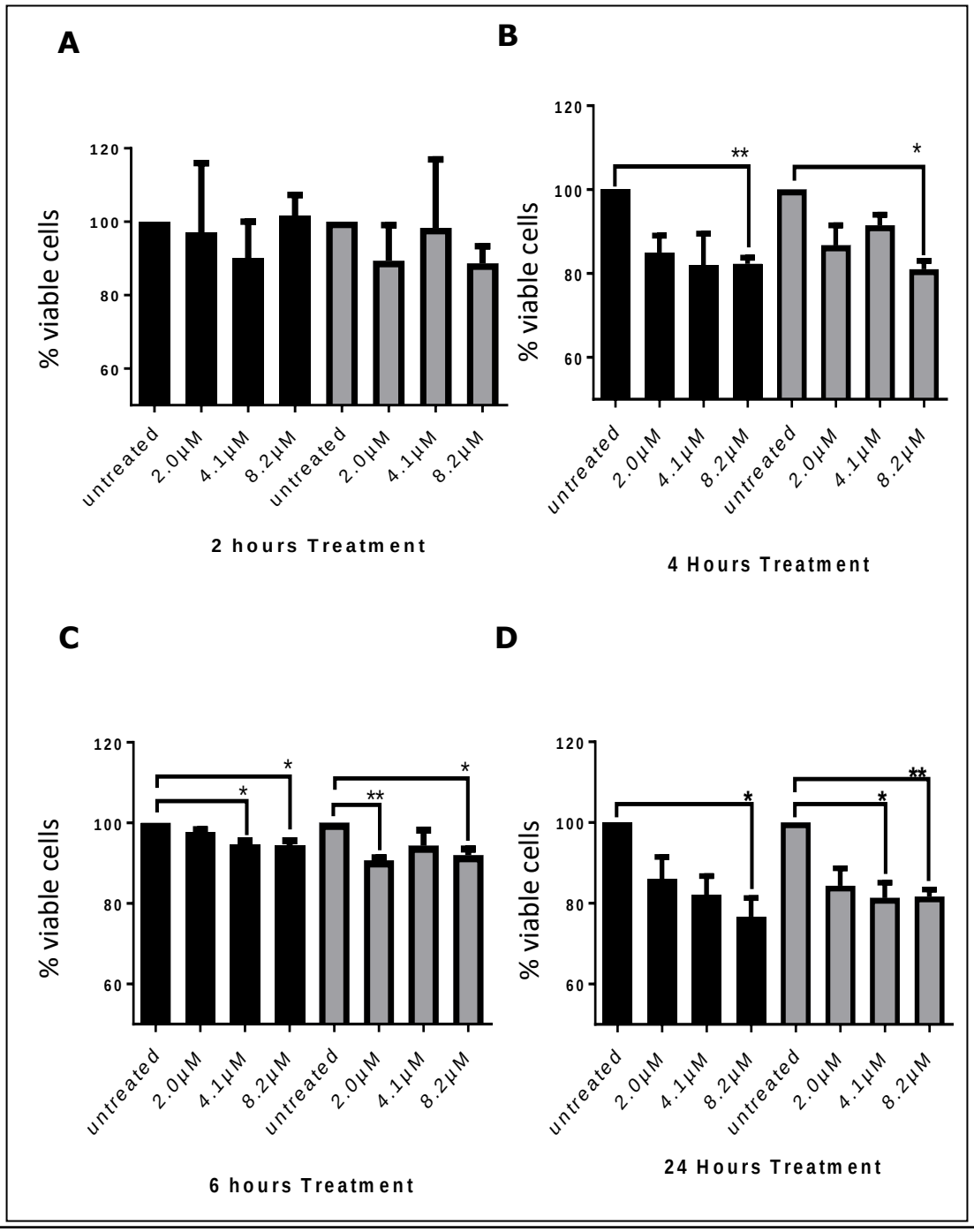

Figure 3.3i: Chemosensitivity of cycling and dormancy-enriched KG1a responses to ara-c, used to establish the 24-hour IC_{10}-IC_{20}. Cycling cells are depicted by black bars and dormancy-enriched cells by grey bars; untreated cycling cells are compared to treated cycling cells, and untreated dormancy-enriched cells are compared to treated dormancy-enriched cells (at the doses of 2.0, 4.1, and 8.2 μM) at: (A) 2, (B) 4, (C) 6, (D) 24 hours. IC_{10} and IC_{20} are shown using GraphPad Prism-7 software. Each condition conducted in triplicate, and data points indicate the mean **+** SD of n = 3 independent assays. * represents a P value of <0.05 compared with untreated cells; ** represents P < 0.01."

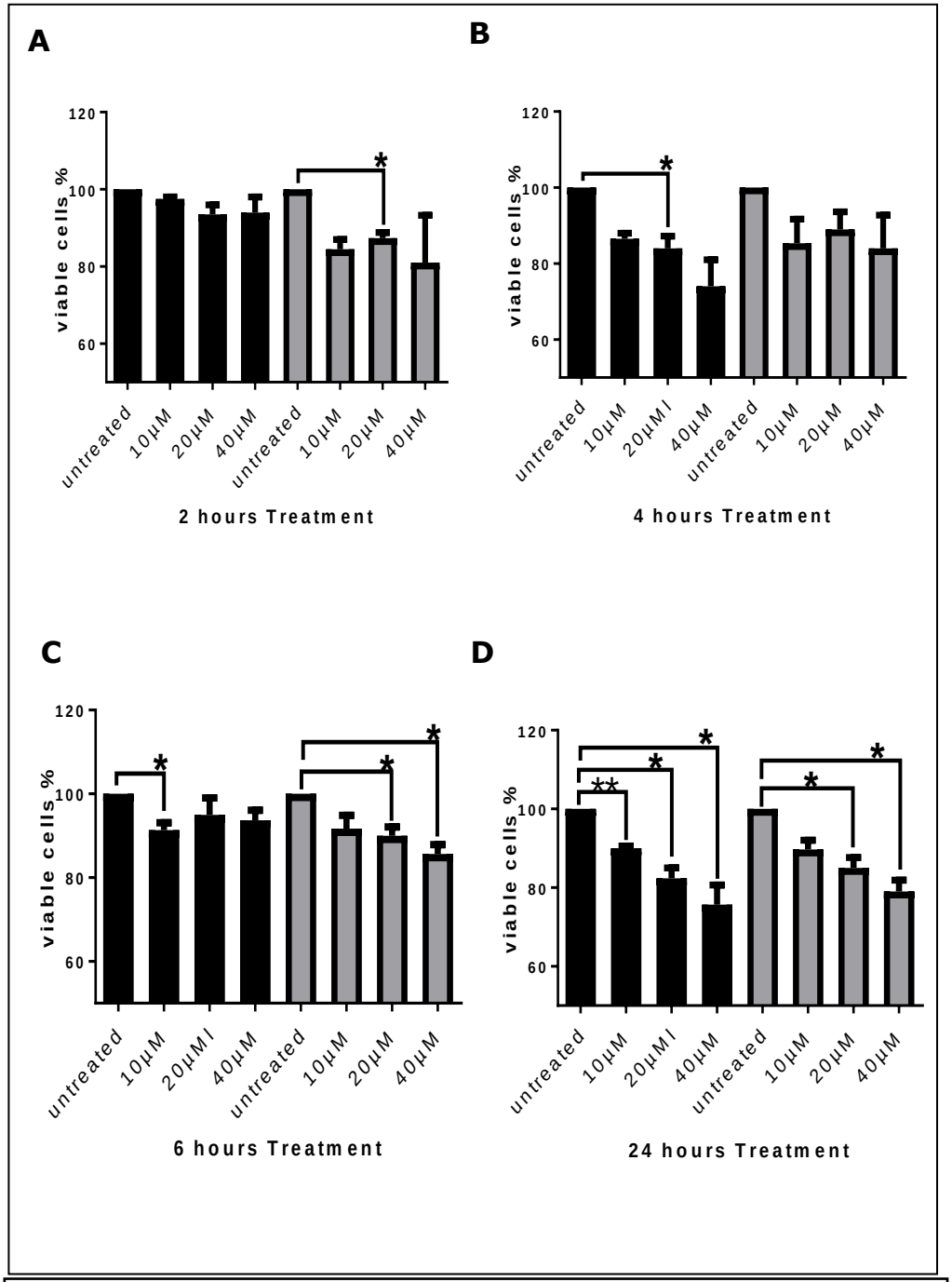

Figure 3.3ii: Chemosensitivity of cycling and dormancy-enriched KG1a responses to ETO to establish the 24-hour IC_{10}-IC_{20}. Cycling cells are depicted by black bars and dormancy-enriched by grey bars, untreated cycling cells compared to treated cycling cells and untreated dormancy-enriched cells compared to treated dormancy-enriched cells with (10, 20, 40μM) at: (A) 2, (B) 4, (C) 6, (D) 24 hours. Both IC_{10} and IC_{20} using GraphPad Prism-7 software for future experiments. Each condition conducted in triplicate, and data points indicate the mean + SD of n = 3 independent assays. * represents a P value compared with untreated cells of <0.05, ** represents P < 0.01.

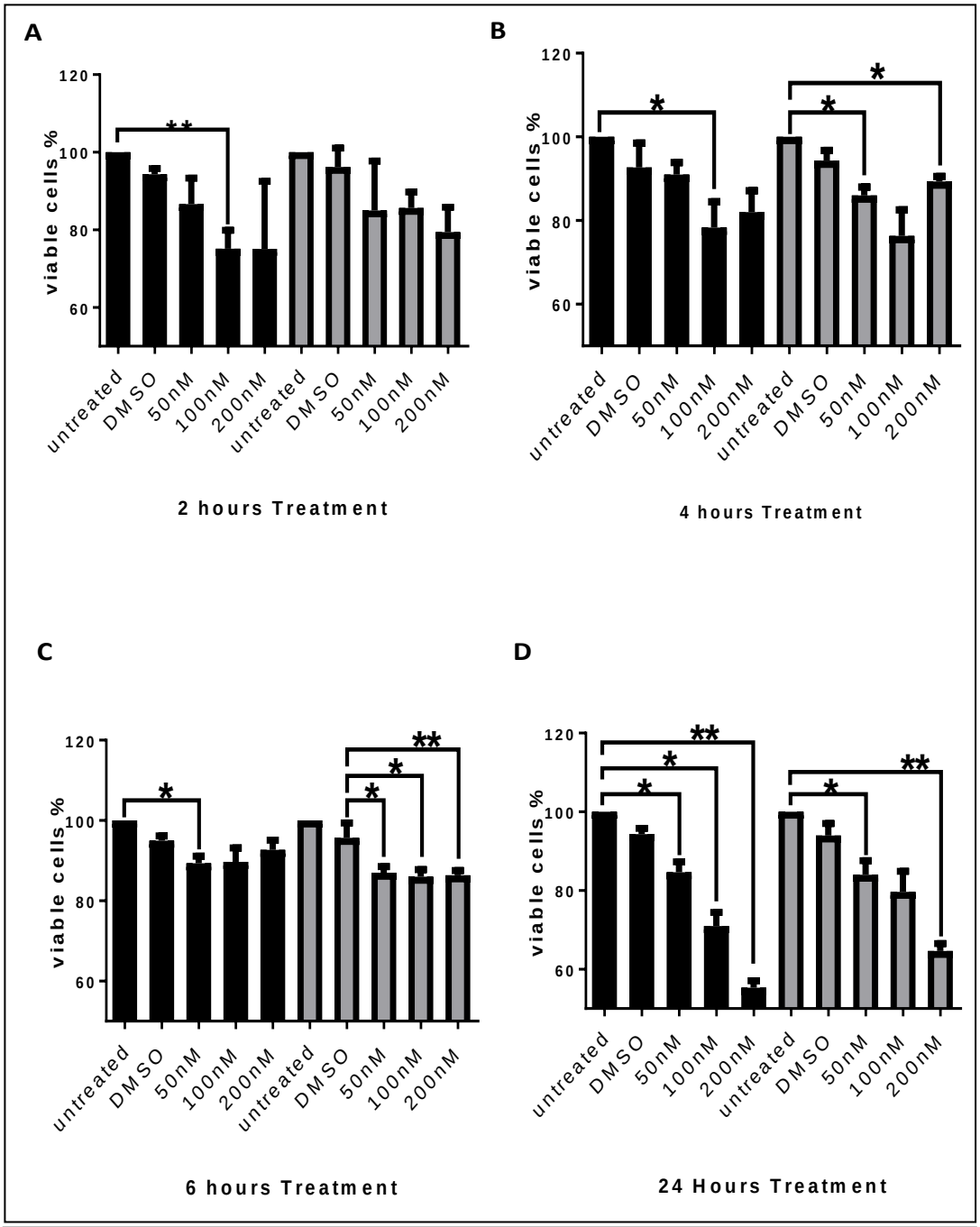

Figure 3.3iii: Chemosensitivity of cycling and dormancy-enriched KG1a responses to TG02 to establish the 24-hour IC_{10}-IC_{20}. Cycling cells are depicted by black bars and dormancy-enriched by grey bars, untreated cycling cells compared to treated cycling cells and untreated dormancy-enriched cells compared to treated dormancy-enriched cells with (50, 100, 200 nM) at: (A) 2, (B) 4, (C) 6, (D) 24 hours. Both IC_{10} and IC_{20} using GraphPad Prism-7 software for future experiments. Each condition conducted in triplicate, and data points indicate the mean and SD of n = 3 independent assays. * represents a P value compared with untreated cells of <0.05, ** represents P < 0.01.

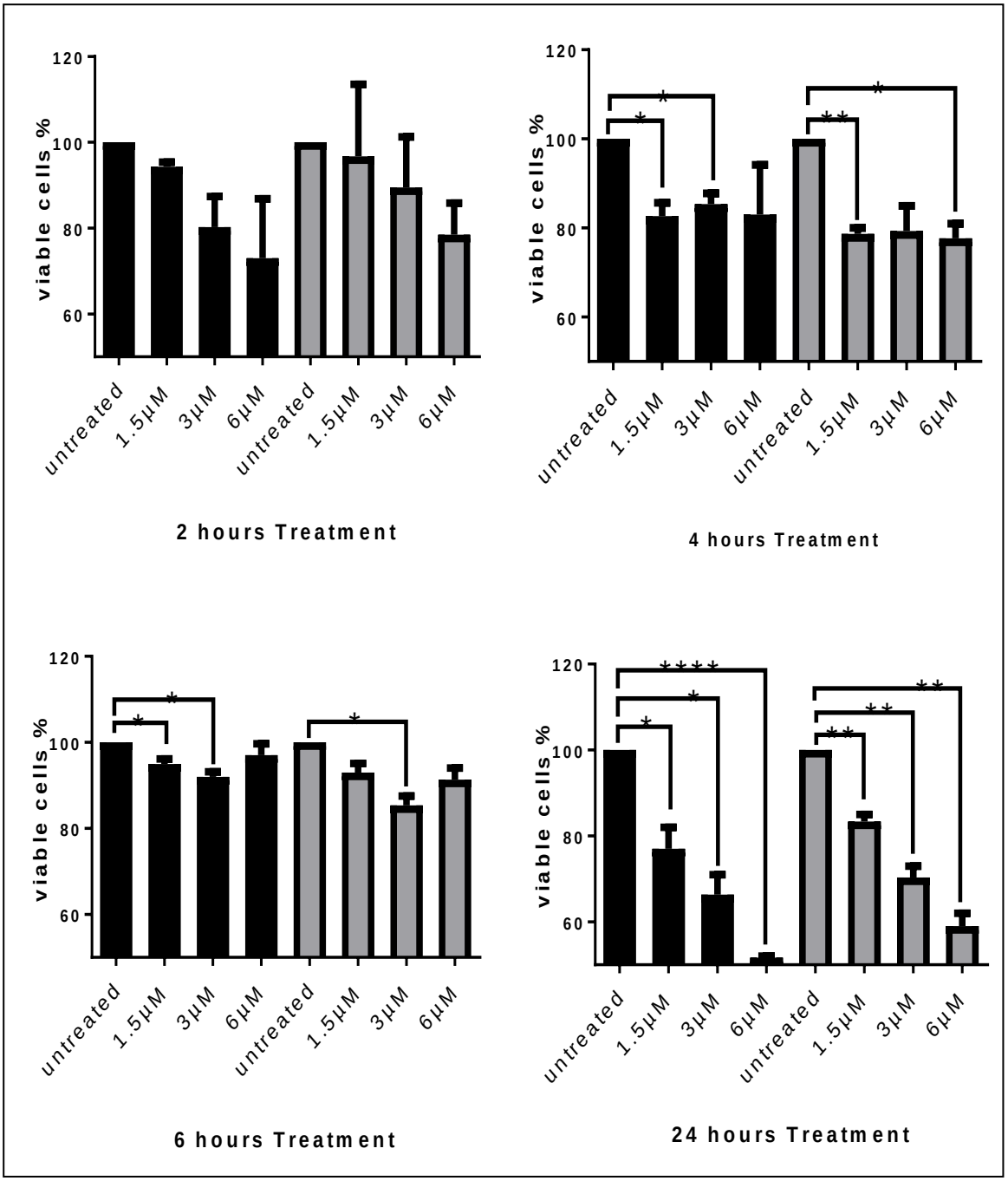

Figure 3.3iv: Chemosensitivity of cycling and dormancy-enriched KG1a responses to DNR to establish the 24-hour IC_{10}-IC_{20}. Cycling cells are depicted by black bars and dormancy-enriched by grey bars, untreated cycling cells compared to treated cycling cells and untreated dormancy-enriched cells compared to treated dormancy-enriched cells with (1.5, 3, 6 µM) at: (A) 2, (B) 4, (C) 6, (D) 24 hours. Both IC_{10} and IC_{20} using GraphPad Prism-7 software for future experiments. Each condition conducted in triplicate, and data points indicate the mean + SD of n = 3 independent assays. * represents a P value compared with untreated cells of <0.05, ** represents P < 0.01, ***P <0.001.

3.4 Assessment of DNA damage in dormancy-enriched cells by comet assay

3.4.1 Preliminary analysis of DNA damage using comet assay control cells

The comet assay is associated with high variability. In order to optimise assay conditions, minimise variability, and verify reproducibility between runs of neutral comet assays, preliminary optimization tests of lysis and electrophoresis times were conducted with comet control cells (Trevigen). The neutral version of the comet assay was used to estimate DNA strand breaks (Olive and Banath 2006). Three of four commercial control cell populations were treated with increasing concentrations of ETO, resulting in increases in tail moment values following electrophoresis under neutral conditions (NC0, untreated control; NC1-3, increasing ETO concentrations). Cells were embedded in agarose on a slide, lysed, and electrophoresed in neutral buffer. Tail moment measurements reflect both the amount of damaged DNA in the tail and the distance of migration. It is expected that NC0 is cell with undamaged DNA (supercoiled), and thus does not migrate very far from the nucleoid under the influence of an electric current. Wherease NC1, NC2 and NC3 are dose-dependent cells and the amount of DNA damage increased with increasing the concentration of ETO. Figure 3.4.1A shows that NC0 fluorescence was confined to the nucleoid, which is suggestive of undamaged DNA; an increasing tail moment was seen in the treated NC1– NC3 cells. Various lysis (2 hours and overnight) (Figure 3.4.1B & C) and electrophoresis times (15, 20, 30, and 40 minutes) were assessed (Figure 3.4.1D, E & F). Overnight lysis with 30 to 40 minutes of electrophoresis time showed the expected results, indicating the appropriate assay conditions for low inter-run variation (Figure 3.4.1E, n = 10). Because the comet assay is subject to variability as a result of different temperatures, depths of electrophoresis buffer, and amounts of agarose, efforts were made to hold these variable

constant using a specially designed electrophoresis tank that enabled cooling during electrophoresis, working in an air-conditioned laboratory, and using exactly the same volume of ice-cold electrophoresis buffer and agarose. In addition, the comet assays were repeated multiple times and for each condition 200 cells were scored (2 slides per condition) to enhance result reliability.

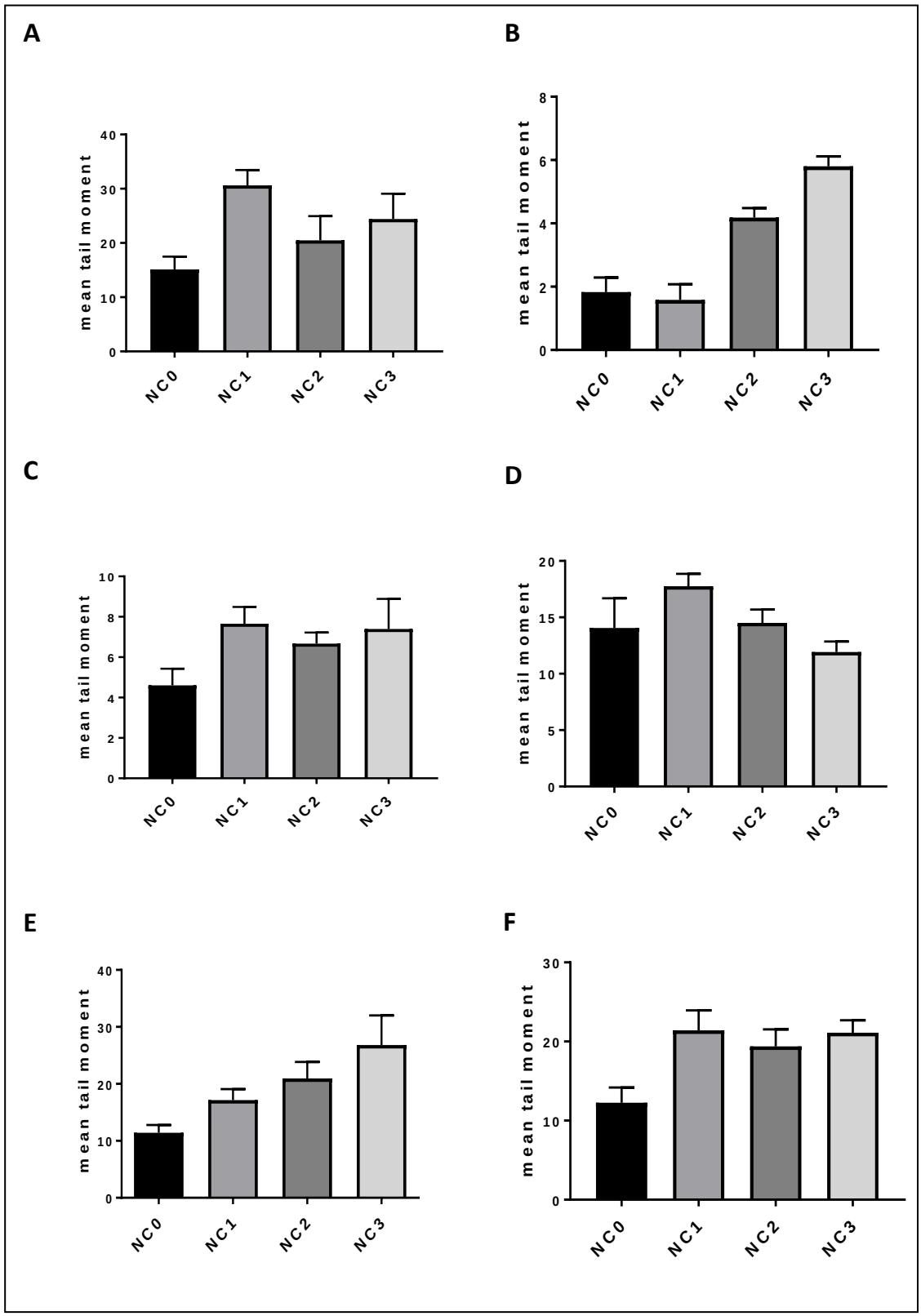
A
mean tail moment
0
10
20
30
40
NC0
NC1
NC2
NC3
B
mean tail moment
0
2
4
6
8
NC0
NC1
NC2
NC3
C
mean tail moment
0
2
4
6
8
10
NC0
NC1
NC2
NC3
D
mean tail moment
0
5
10
15
20
NC0
NC1
NC2
NC3
E
mean tail moment
0
10
20
30
40
NC0
NC1
NC2
NC3
F
mean tail moment
0
10
20
30
NC0
NC1
NC2
NC3

Figure 3.4.1: Neutral comet assay lysis and electrophoresis time optimisation experiments using commercial control cells. Mean tail moments were calculated for control cell populations NC0-NC3. (A) Two hours of lysis with 20 minutes of electrophoresis. (B) Two hours of lysis with 40 minutes electrophoresis. (C) Overnight lysis with 15 minutes of electrophoresis. (D) Overnight lysis with 20 minutes of electrophoresis. (E) Overnight lysis with 30 minutes electrophoresis, (F) Overnight lysis with 40 minutes of electrophoresis. In each experiment, data points indicate the mean and SD of n = 3 independent assays.

3.4.2 Dormancy-enriched KG1a cells show no difference in the basal level of DNA strand breaks when compared to that of cycling cells as determined by the comet assay

The neutral comet assay was conducted on dormancy-enriched KG1a cells to determine the baseline damage that occurs during cell growth and metabolism, in comparison cycling KG1a cells. Dormancy-enriched KG1a cells showed no difference in the basal level of DNA strand breaks compared to that of cycling KG1a cells in the neutral comet assay ($p = 0.305$, $n = 12$) (Figure 3.4.2).

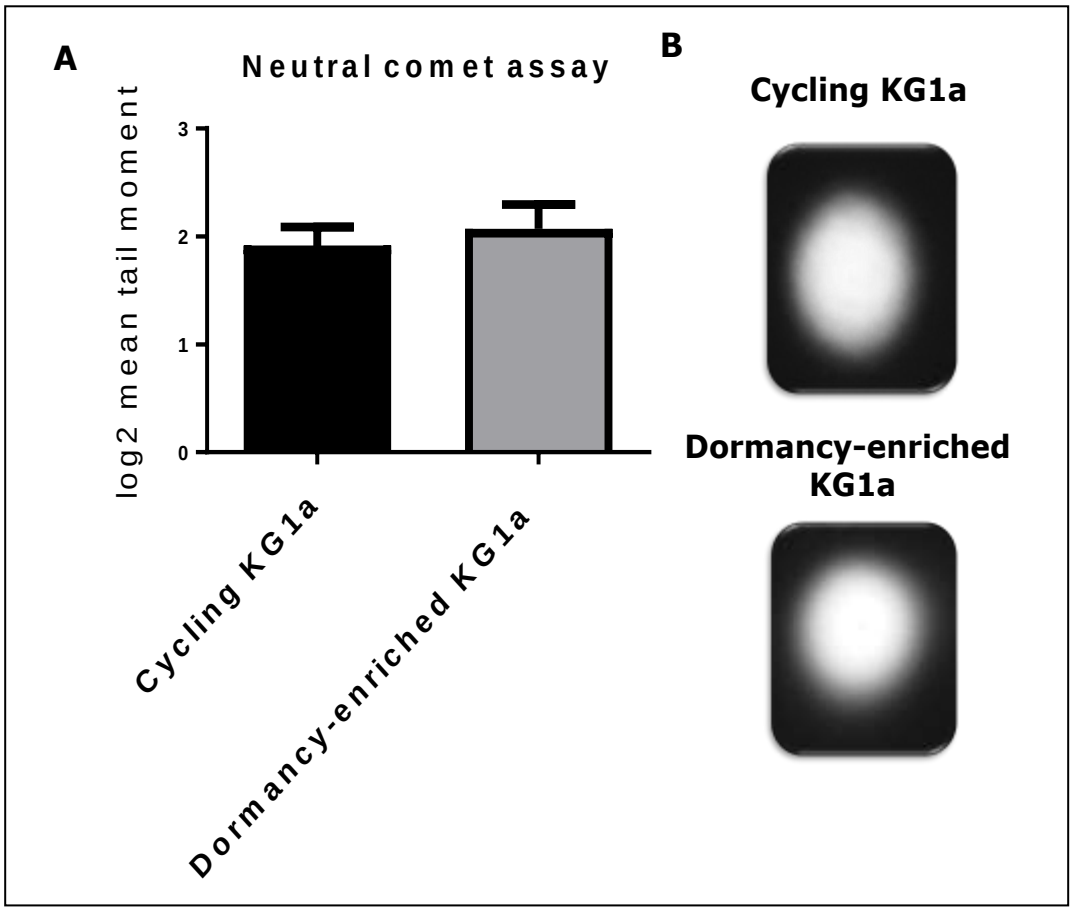

Figure 3.4.2: Basal DNA damage assessment of dormancy-enriched KG1a cells. Mean tail moment for cycling and dormancy-enriched KG1a cells. (A) SSB/DSBs were assessed by the neutral comet assay. 200 cells were scored per condition, and data points indicate the mean and SD of n = 12 independent assays. (B) Representative images of neutral comet tails are shown for both cycling and dormancy-enriched KG1a cells.

3.4.3 Assessment of drug-induced DNA damage in cycling KG1a cells and the dormancy-enriched KG1a cell model

In order to assess DNA damage in cycling and dormancy-enriched KG1a cells, treated with ara-c, TG02, DNR, and ETO, the neutral comet assay was performed following 4 and 24 hours of incubation with each drug. The establishment of IC_{10-20} concentrations for the drugs, used in these experiments, is described in section 3.2. Figure 3.4.3 shows data for tail moments following treatment. The results of the untreated controls confirm the results in section 3.4.2: there was no difference between the basal levels of damage in cycling and dormancy-enriched cell populations.

All the drugs induced significant damage at both time points, when we compared the cycling and dormancy-enriched cells before and after drug treatment; the exception was treatment with ara-c, at 4 hours, in dormancy-enriched cells (Table 3.4.3). Cycling cells showed significant damage in response to ara-c, compared with that shown by dormancy-enriched cells, at the 4-hour time point ($p = 0.0420$, $n = 6$, Figure 3.4.3i). In contrast, the dormancy-enriched cells became more sensitive to induction of DNA damage when treated with ara-c for 24 hours. Notably, dormancy-enriched KG1a cells showed more damage at 24 hours than did in cycling KG1a cells exposed to ara-c for the same time ($p = 0.0416$, $n = 11$).

Furthermore, significantly more damage was detected in cycling cells after 4 hours of incubation with ETO compared with that in dormancy-enriched cells ($p = 0.0495$, $n = 8$) (Figure 3.4.3iv). At 24 hours, however, the dormancy-enriched cells showed higher levels of damaged DNA following ETO treatment compared with that of cycling cells at 24 hours, this is a reversal of the pattern seen at 4 hours ($p = 0.0131$, $n = 8$) (Figure 3.4.3v).

There was no difference in the levels of TG02-induced DNA damage when comparing dormancy-enriched cells and cycling cells at either 4

hours (p = 0.8265, n = 3) (Figure 3.4.3vii) or 24 hours (p = 0.4583, n = 3) (Figure 3.4.3viii). This was also the case when cells were incubated with DNR; there were no differences when comparing treated dormancy-enriched cells and cycling cells at 4 hours (p = 0.3565, n = 3) (Figure 3.4.3x) or at 24 hours (p = 0.7807, n = 6) (Figure 3.3.3xi). It is important to note that cells were screened for the presence of apoptotic cells after damage was induced under in each condition; in each independent experiment, we confirmed that the treatment was killing no more than 20 % of cells. Therefore, the appropriateness of the $IC_{10\text{-}20}$ doses was confirmed in each assay.

	Untreated cycling KG1a		**Untreated dormancy-enriched KG1a**	
	4 hours	24 hours	4 hours	24 hours
Ara-c	p = 0.0004, n = 6	p = 0.0030, n = 11	p = 0.5312, n = 6	p = 0.0001, n = 11
ETO	p = 0.0001, n = 8	p = 0.0001, n = 8	p = 0.0051, n = 8	p = 0.0010, n = 8
TG02	p = 0.0001, n = 3	p = 0.0172, n = 3	p = 0.0004, n = 3	p = 0.0025, n = 3
DNR	p = 0.0001, n = 3	p = 0.0113, n = 6	p = 0.0001, n = 3	p = 0.0014, n = 6

Table 3.4.3: P values (p) comparing the amount of DNA damage, measured by comet assays, in untreated cycling cells and treated cycling cells or untreated dormancy-enriched and treated dormancy-enriched cells. Treatment was using ara-c, ETO, TG02, or DNR for 4 and 24 hours.

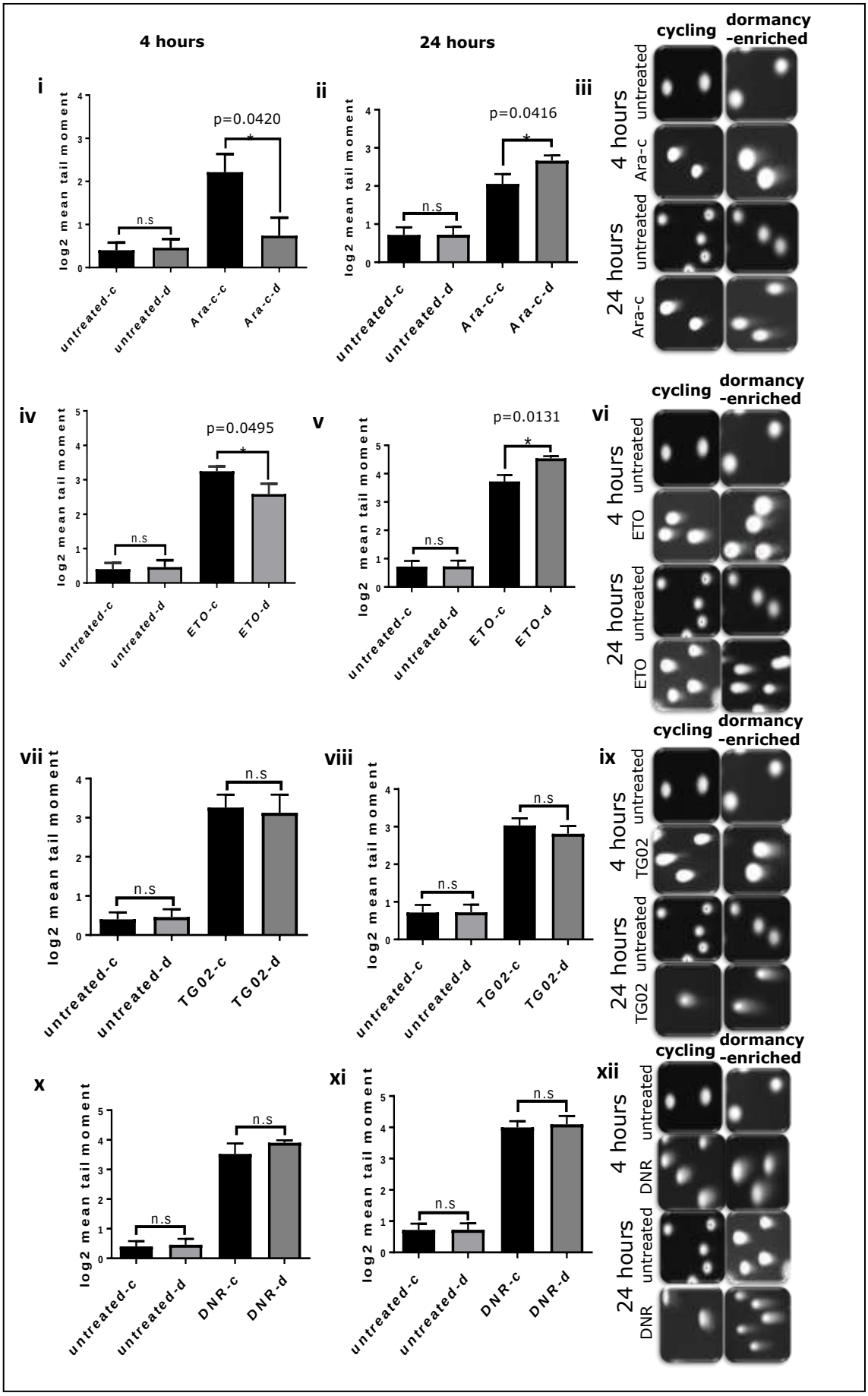
4 hours
24 hours
i
ii
iii
log2 mean tail moment
p=0.0420
p=0.0416
n.s
*
untreated-c
untreated-d
Ara-c-c
Ara-c-d
cycling
dormancy -enriched
4 hours
24 hours
untreated
Ara-c
iv
v
vi
p=0.0495
p=0.0131
ETO-c
ETO-d
ETO
vii
viii
ix
TG02-c
TG02-d
TG02
x
xi
xii
DNR-c
DNR-d
DNR

Figure 3.4.3: DNA damage, assessed in dormancy-enriched KG1a after incubation with DNA-damaging agents, by neutral comet assay. Graphs show comet assay mean tail moments for cycling/dormant KG1a following 4 and 24 hours of treatment with: (i/ii) 4.1 μM ara-c, (iv/v) 20 μM ETO, and (vii/viii) 100 nM TG02. (x/xi) Treatment with DNR (1.5 μM) for 4 and 24 hours. Representative images of the comet tails are shown (iii, vi, ix, xii). *P <0.05 and n.s = not significant. In each experiment, 200 cells were scored per condition, and data points indicate the mean and the SD calculated using GraphPad Prism-7 software.

3.5 Cellular response to drug-generated DNA damage in dormancy-enriched and cycling KG1a cells

3.5.1 Phosphorylation of ATM-Ser1981

In response to DSBs, eukaryotic cells activate a DDR cascade and cell cycle checkpoints, which prevent further progression through the cell cycle following DNA damage. This response involves the participation of a multitude of proteins and post-translational events to ensure the maintenance of genome integrity. ATM is normally present in the nucleus as an inactive dimer that monomerizes in response to DNA DSBs. This monomerization is associated with autophosphorylation at Ser1981, which further activates ATM (Bakkenist and Kastan 2003; Jazayeri, Falck *et al.* 2006; Huang da, Sherman *et al.* 2009). In order to assess this DDR event in dormancy-enriched cells and cycling KG1a cells treated with ara-c, ETO, and TG02, a phospho-ATM assessment was performed using a flow cytometric technique after cells were incubated with each drug for 4 and 24 hours. Fold changes in phosphorylation are presented in Figure 3.5.1 A & B, with both cycling and dormancy-enriched KG1a cells showing an increase in p-ATM after damage induction with ara-c and ETO compared to that in untreated cycling and untreated dormancy-enriched cells. This, however, was not the case for cells treated with TG02. Because the focus of this project was to find differences in cellular responses between cycling and dormancy-enriched cells after damage induction,

and because TG02 did not elicit a damage response, no further work was performed with this drug.

Both ara-c and ETO trigger ATM phosphorylation at both time points compared to untreated cells, except TG02 (Table 3.5.1). Figure 3.4.1 A demonstrates an increase in phosphorylated ATM-Ser1981 in response to ara-c at 4 and 24 hours; however, there was no significant difference in the p-ATM response when comparing the cycling and dormancy-enriched cells at 4 hours (p = 0.1747, n = 8) or 24 hours (p = 0.1017, n = 8). The same was also true for cells treated with ETO (p = 0.4859 and p = 0.5262, n = 8) (Figure 3.5.1B). As mentioned above, no phosphorylated ATM was detected in cells treated with TG02 (p = 0.6915 and 0.7661, n = 3) (Figure 3.5.1C). Flow cytometric analysis of cells treated with DNR was not possible because it was highly fluorescent, which interfered with the fluorescence of labelled antibodies which used in this study.

ATM-Ser1981	**Untreated cycling KG1a**		**Untreated dormancy-enriched KG1a**	
	4 hours	24 hours	4 hours	24 hours
Ara-c	p = 0.0011, n = 8	p = 0.0001, n = 8	p = 0.0004, n = 8	p =, 0.0003 n = 8
ETO	p = 0.0044, n = 8	p = 0.0001, n = 8	p = 0.0004, n = 8	p = 0.0003, n = 8
TG02	p = 0.0174 n = 3	p = 0.6369 n = 3	p = 0.5341, n = 3	p = 0.4567 n = 3

Table 3.5.1: P values (p) comparing p-ATM levels measured by flow cytometry comparing untreated cycling cells and treated cycling cells or untreated dormancy-enriched and treated dormancy-enriched cells. Treatment was using ara-c, ETO or TG02 for 4 and 24 hours.

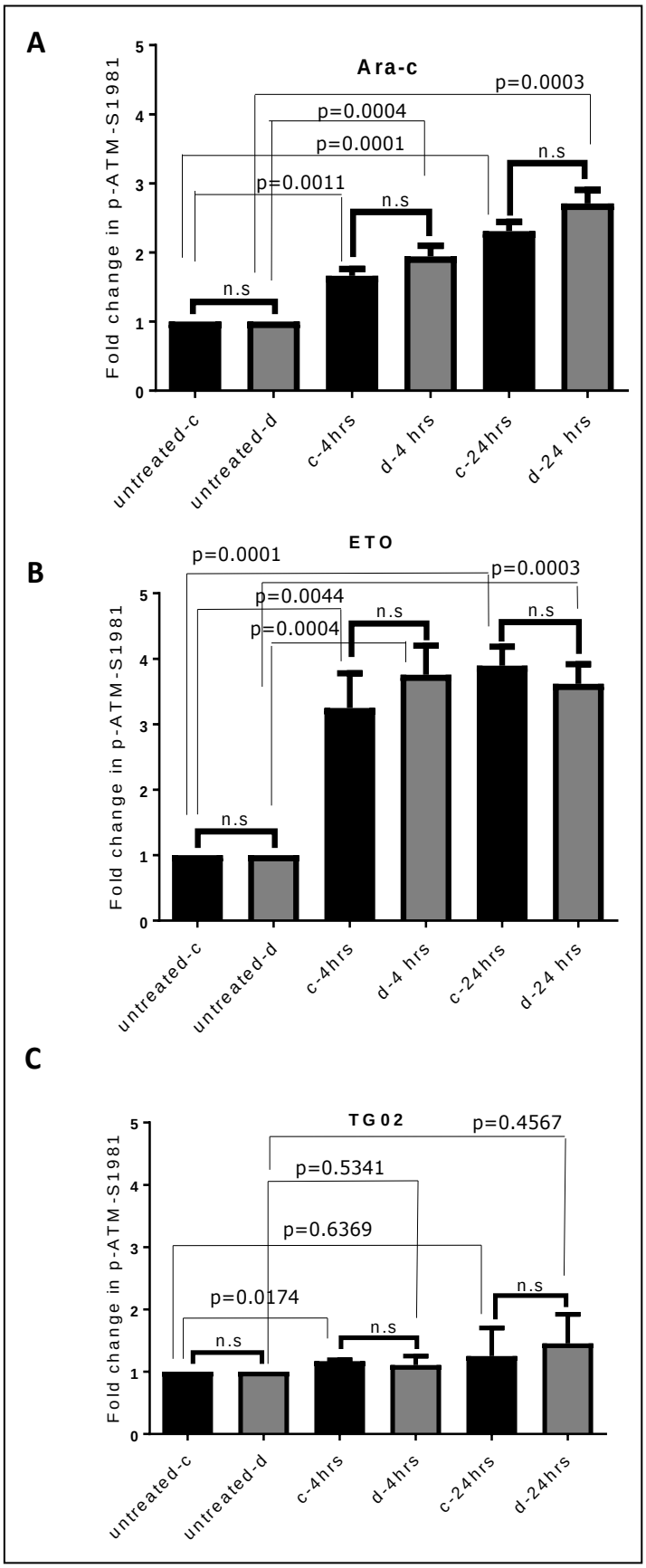
A
Ara-c
Fold change in p-ATM-S1981
p=0.0003
p=0.0004
p=0.0001
n.s
p=0.0011
n.s
n.s
untreated-c
untreated-d
c-4hrs
d-4 hrs
c-24hrs
d-24 hrs
B
ETO
Fold change in p-ATM-S1981
p=0.0001
p=0.0003
p=0.0044
n.s
n.s
p=0.0004
n.s
untreated-c
untreated-d
c-4hrs
d-4 hrs
c-24hrs
d-24 hrs
C
TG02
Fold change in p-ATM-S1981
p=0.4567
p=0.5341
p=0.6369
n.s
p=0.0174
n.s
n.s
untreated-c
untreated-d
c-4hrs
d-4hrs
c-24hrs
d-24hrs

Figure 3.5.1: Assessment of p-ATM levels in cycling and dormancy-enriched KG1a cells following drug treatment. Graphs show changes in p-ATM levels following treatment with (A) 4.1 μM ara-c (n = 8), (B) 20 μM ETO (n = 8), or (C) 100 nM TG02 (n = 3) at 4 and 24 hour time points. Data are expressed as fold change in fluorescence intensity of cycling (black bars) or dormancy-enriched KG1a cells (grey bars). Each condition conducted in triplicate, and the data points indicate the mean and SD using GraphPad Prism-7 software , n.s= not significant..

3.6 DNA damage induces significantly greater levels of phospho-H2AX139 in cycling cells than in dormancy-enriched cells

3.6.1. Flow-cytometric analysis of phospho-H2AX139

Levels of phospho-H2AX139 were measured in both dormancy-enriched and cycling KG1a cells following DSBs induction by DNA-damaging agents. Figure 3.6.1A & B shows representative flow cytometry dot plots of phospho-H2AX139 in both cycling KG1a and dormancy-enriched KG1a cells treated with ara-c or ETO compared to those in untreated cells. Figure 3.6.1 C & D show the summary charts of the mean fluorescence intensities. All drugs induced phospho-H2AX139 at both time points in cycling and dormancy-enriched cells compared to untreated cells (Table 3.6.1).

After damage induction, phospho-H2AX139 was measured in cycling cells following 4 hours of ara-c treatment; however, no increase in phospho-H2AX139 was seen in dormancy-enriched cells at this time point, which agrees with the finding that no detectable DNA damage was induced in these cells after 4 hours of ara-c treatment (Figure 3.4.3). The difference in phospho-H2AX139 at 4 hours was statistically significant when comparing cycling and dormancy-enriched cells (52 % positive versus 11 %; p = 0.0055, n = 8)

(Figure 3.6.1C). Twenty-four hours of treatment with ara-c resulted in large increases in γH2AX in both cycling and dormancy-enriched cells; however, the level in cycling cells (42.4 %) was significantly higher than that (36.7 %) in dormancy-enriched cells (p = 0.0182, n = 12) (Figure 3.6.1B). ETO treatment resulted in large increases in phospho-H2AX139 in both cell populations at 4 and 24 hours; however, once again, levels were significantly higher in cycling cells; at 4 hours, 85.5 % of cycling cells compared to 43.5 % of dormant cells showed an increase in phospho-H2AX139 expression (p = 0.0188, n = 8) (Figure 3.6.1A & C), and at 24 hours, 72.7 % of cycling cells and 60.5 % of dormancy-enriched cells showed an increase in phospho-H2AX139 expression (p = 0.0273, n = 12) (Figure 3.6.1B & D).

phosph-H2AX139	**Untreated dycling KG1a**		**Untreated dormancy-enriched KG1a**	
	4 hours	24 hours	4 hours	24 hours
Ara-c	p = 0.0239, n = 8	p = 0.0001, n = 12	p = 0.7910, n = 8	p = 0.0021, n = 12
ETO	p = 0.0091, n = 8	p = 0.0001, n = 12	p = 0.0859, n = 8	p = 0.0082, n = 12

Table 3.6.1: P values (p) comparing phosph-H2AX139 levels measured by flow cytometry comparing untreated cycling cells and treated cycling cells or untreated dormancy-enriched and treated dormancy-enriched cells. Treatment was using ara-c, ETO orTG02 for 4 and 24 hours.

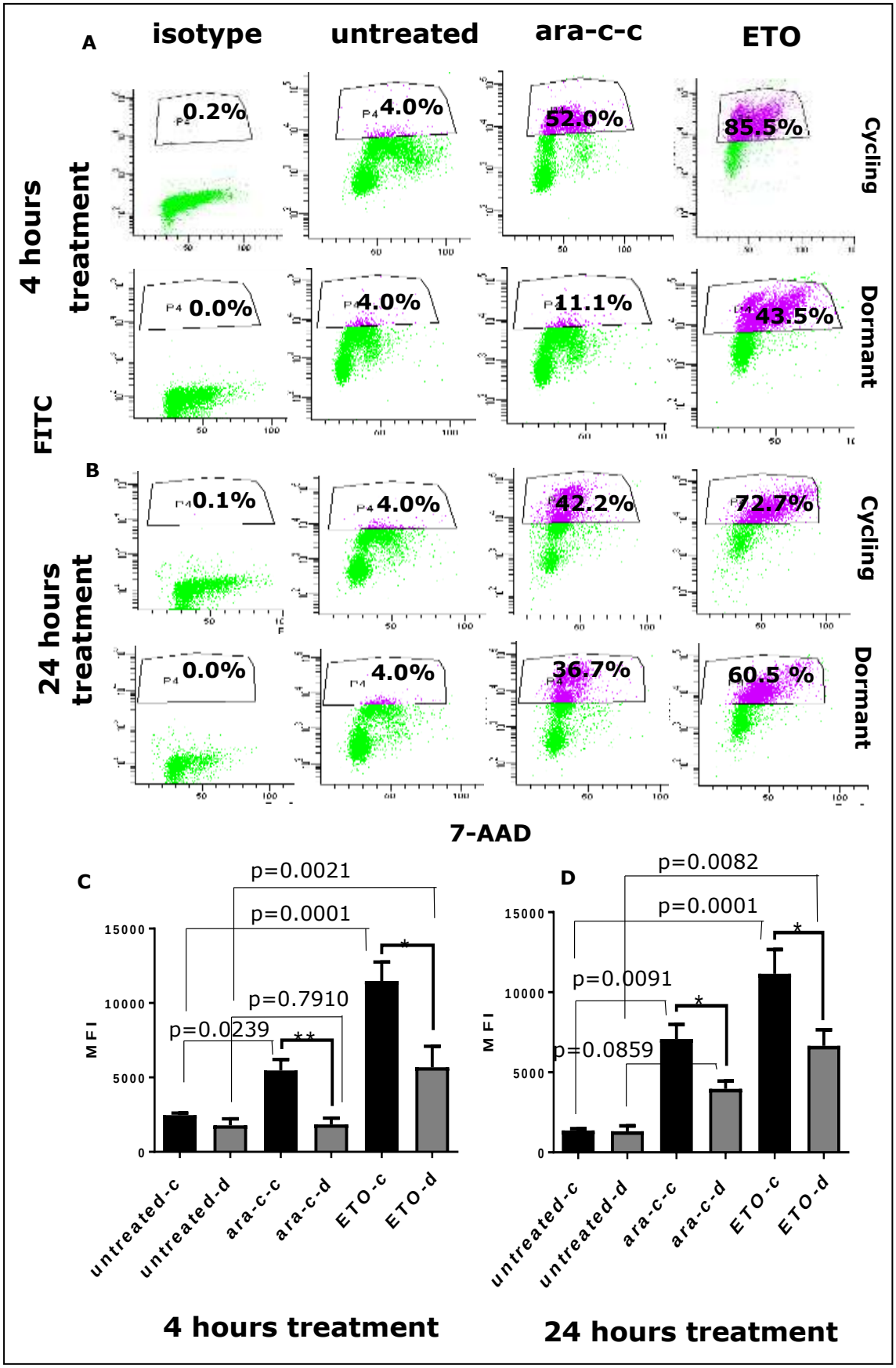
A
isotype
untreated
ara-c-c
ETO
4 hours treatment
0.2%
4.0%
52.0%
85.5%
Cycling
0.0%
4.0%
11.1%
43.5%
Dormant
FITC
B
24 hours treatment
0.1%
4.0%
42.2%
72.7%
Cycling
0.0%
4.0%
36.7%
60.5 %
Dormant
7-AAD
C
p=0.0021
p=0.0001
p=0.7910
p=0.0239
MFI
untreated-c
untreated-d
ara-c-c
ara-c-d
ETO-c
ETO-d
4 hours treatment
D
p=0.0082
p=0.0001
p=0.0091
p=0.0859
MFI
24 hours treatment

Figure 3.6.1: Assessment of phospho-H2AX139 levels in cycling and dormancy-enriched KG1a cells following drug treatment. (A) Representative flow cytometry plots show levels of phospho-H2AX139 following DNA-damaging drug treatment in both cycling KG1a (top panel) and dormancy-enriched KG1a (bottom panel) after 4 hours and (B) 24 hours of treatment with 4.1 μM ara-c or 20 μM etoposide (ETO). (C) Summary of the change in phospho-H2AX139 at 4 hours and (D) 24 hours of treatment in cycling KG1a (black bars) and dormancy-induced KG1a (grey bars) cells. Each condition conducted in triplicate, and data points indicate the mean and SD. * represents a P value compared with untreated cells of <0.05, ** represents P < 0.01.

3.6.2. Immunofluorescence analysis of phospho-H2AX139 foci

Immunofluorescence staining was performed as a more sensitive technique to indicate phospho-H2AX139 foci in cycling and dormancy-enriched KG1a cells after treatment with ara-c, DNR, or ETO. Approximately 100 cycling and dormancy-enriched cells were counted and H-scores were estimated for all conditions before and after damage induction. All drugs induced phospho-H2AX139 and formation of foci at both time points in cycling and dormancy-enriched cells compared to untreated cells (Table 3.6.2).

As shown in Figure 3.5.2, treated cells exhibited a significant increase in phospho-H2AX139 foci; 4 hours of ara-c treatment resulted in an H-score of 329 in cycling cells, whereas dormancy-enriched cells scored 280 ($p = 0.0027$, $n = 7$). A similar trend was seen following 4 hours of treatment with ETO, with H-scores of 400 and 345 ($p = 0.0106$, $n = 7$) in cycling and dormant cells, respectively. No significant differences in phospho-H2AX139 foci scores between cycling and dormancy-enriched cells were detected after incubation with DNR (308 and 358, respectively, $p = 0.3620$, $n = 4$) (Figure 3.6.2B). Figure 3.6.2C shows subnuclear foci at and around DSB sites in cycling and dormancy-enriched cells after 24 hours of drug treatment. H-scores were higher in cycling than dormancy-enriched cells (362 and 325, respectively) after ara-c ($p = 0.0201$, $n = 7$) and

(387 and 336, respectively) ETO (p = 0.0048, n = 7) treatment (Figure 3.6.2D). As observed after 4 hours, DNR treatment for 24 hours resulted in no differences in the numbers of phospho-H2AX139 foci between dormancy-enriched and cycling cells (317.3 and 368.8, respectively; p = 0.2533, n = 7).

phospho-H2AX139	**Untreated cycling KG1a**		**Untreated cormancy-enriched KG1a**	
	4 hours	24 hours	4 hours	24 hours
Ara-c	p = 0.0001, n = 7	p = 0.0001, n = 7	p = 0.0367, n = 7	p = 0.0004, n = 7
ETO	p = 0.0001, n = 7	p = 0.0001, n = 7	p = 0.0013, n = 7	p = 0.0001, n = 7
DNR	p = 0.0830 n = 4	p = 0.0396, n = 4	p = 0.0159 n = 4	p = 0.0005, n = 4

Table 3.6.2: P values (p) comparing phospho-H2AX139 foci measured by immunofluorescence staining comparing untreated cycling cells and treated cycling cells or untreated dormancy-enriched and treated dormancy-enriched cells. Treatment was using ara-c, ETO or DNR for 4 and 24 hours.

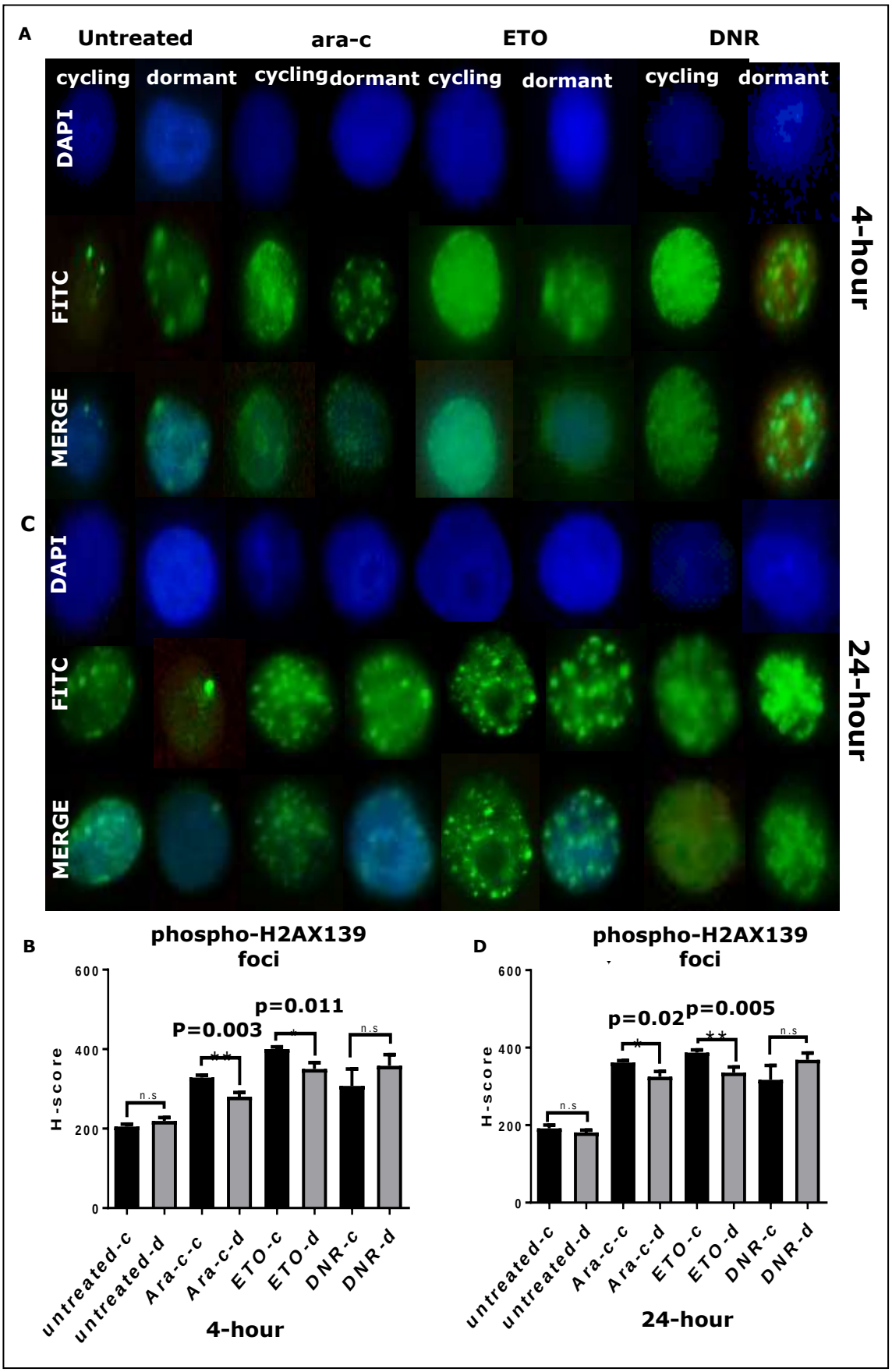
A
Untreated
ara-c
ETO
DNR
cycling
dormant
cycling
dormant
cycling
dormant
cycling
dormant
DAPI
FITC
MERGE
4-hour
C
DAPI
FITC
MERGE
24-hour
B
phospho-H2AX139 foci
H-score
600
400
200
0
p=0.011
P=0.003
n.s
**
*
n.s
untreated-c
untreated-d
Ara-c-c
Ara-c-d
ETO-c
ETO-d
DNR-c
DNR-d
4-hour
D
phospho-H2AX139 foci
H-score
600
400
200
0
p=0.02
p=0.005
n.s
*
**
n.s
untreated-c
untreated-d
Ara-c-c
Ara-c-d
ETO-c
ETO-d
DNR-c
DNR-d
24-hour

Figure 3.6.2.: Immunofluorescence phospho-H2AX139 analysis of cycling KG1a vs. dormancy-enriched KG1a cells after 4 and 24 hours incubation with chemotherapeutic agents. (A) Representative images of indirect detection of phospho-H2AX139 foci following 4 hours treatment. (B) Summary of H-scores calculated from scoring 100 cells. Cycling cells are shown as black bars and dormancy-enriched cells as grey bars. (C) Representative images for indirect detection of phospho-H2AX139 foci following 24 hours of drug treatment in cycling and dormancy-enriched cells. (D) Summary graph of H-scores following 24 hours. Each condition conducted in triplicate, and the data points indicate the mean and SD. * represents a P value of <0.05, ** represents P < 0.01.

3.7 Phosphorylation of Chk2-Thr68 in response to DNA damage in cycling and dormancy-enriched KG1a cells

In addition to pATM and γH2AX, an investigation of the Chk2 checkpoint was conducted. Phosphorylated Chk2-Thr68 levels in response to DNA damage in dormancy-enriched cells were measured by a flow cytometric assay by the fluorescence intensity of Chk2-Thr68 FITC–conjugated antibody after 4- and 24-hour of incubation with the DNA-damaging agents. Figure 3.6 illustrates the fold changes in phosphorylated Chk2 induced by ara-c and ETO in both cycling and dormancy-enriched cells. All treatments induced Chk2 phosphorylation, but there were no significant differences between level of Chk2 phosphorylation in cycling and dormancy-enriched cells after 4 or 24 hours of treatment with either ara-c ($p = 0.2654$, $n = 6$) or ETO ($p = 0.5771$, $n = 6$). All drugs induced significant p-Chk2 at both time points in cycling and dormancy-enriched cells compare to untreated cells (Table 3.7).

Chk2	Untreated Cycling KG1a		Untreated Dormancy-enriched KG1a	
	4 hours	**24 hours**	**4 hours**	**24 hours**
Ara-c	p = 0.0014, n = 5	p = 0.0369, n = 6	p = 0.0289, n = 5	p = 0.0008, n = 6
ETO	p =<0.0001, n = 5	p = 0.0008, n =6	p = <0.0001, n =5	p = 0.0002, n = 6

Table 3.7: P values (p) comparing p-Chk2 levels between untreated cycling and treated cycling cells or untreated dormancy-enriched cells and treated dormancy-enriched cells following ara-c or ETO treatment for 4 and 24 hours.

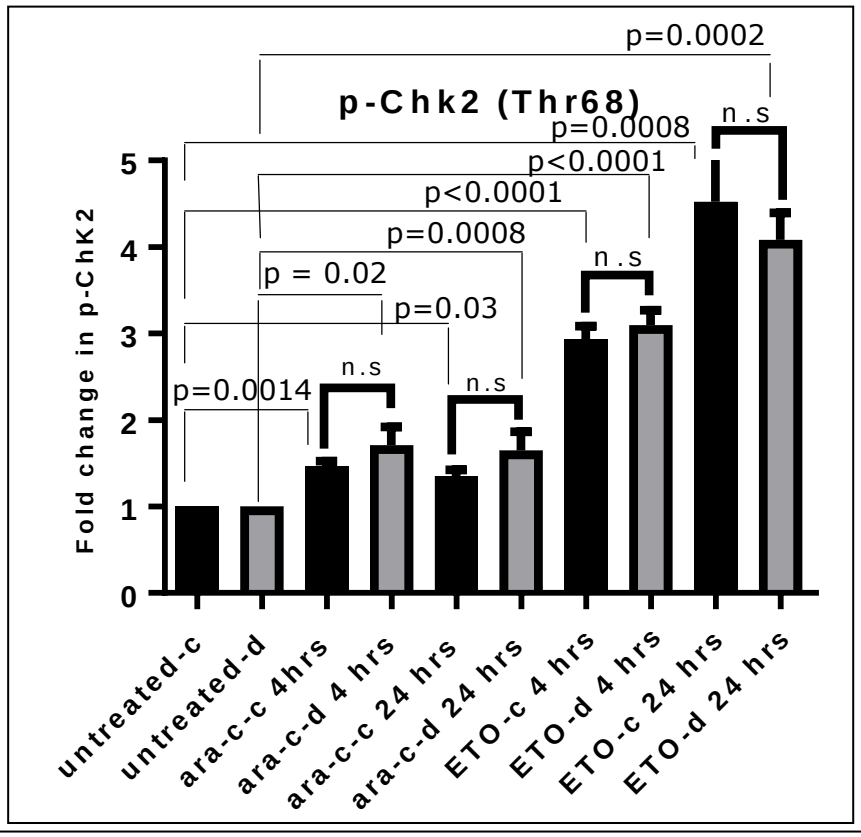

Figure 3.7: Assessment of p-Chk2 levels in cycling and dormancy-enriched KG1a cells following drug treatment. (A) Representative flow cytometric histograms illustrating p-Chk2 in cycling (black bars) and dormancy-enriched KG1a (grey bars) cells with or without drug treatment (B) Summary graphs showing changes in p-Chk2 levels following treatment with 4.1 μM ara-c or 20 μM etoposide (ETO) at 4 hours and 24 hours of treatment. Each condition done in triplicate, and the data points indicate the mean and SD.

3.8 Discussion

DLICs remain an obstacle in improving the efficiency of treatment and avoidance of relapse after induction of remission; this is because of their low prevalence in the BM, difficulty of extracting the cells from primary AML samples, and the precise identification and characterization of DLICs. Thus, establishing an *in vitro* model of a dormancy-enriched leukaemic cell line, mimicking the properties of DLICs, is necessary for investigating DNA damage, and DNA damage response and repair, in this subpopulation. Following detailed literature analysis of the methods used to induce cell-cycle exit in other cancer cells (McCormack, Bruserud *et al.* 2005; Aguirre-Ghiso 2007; Taussig, Miraki-Moud *et al.* 2008; Bockamp, Antunes *et al.* 2009; Saito, Uchida *et al.* 2010; Yoriko, Naoyuki *et al.* 2010; Morrison and Scadden 2014), enrichment of dormancy in an AML cell line to generate an isogeneic model was undertaken in our laboratory. Dormancy enrichment of an AML cell line by serum withdrawal, serum starvation, heparin, L-glutamine, nutrient withdrawal, hypoxia, and mitogen or growth factor withdrawal led to induction of statistically significant levels of apoptosis. Cytokines, such as stem cell factor/steel factor (KitL), TPO, TGFβ1, interleukins 1, 3, 6, 11, the myeloerythroid cytokines GM-CSF, and erythropoietin are known stem-cell stimulators (Zhang, Martino *et al.* 2007; Thorén, Liuba *et al.* 2008; Yamazaki, Iwama *et al.* 2009; de Graaf and Metcalf 2011). TPO plays a role in maintaining the quiescence of HSCs, as is demonstrated by the loss of HSCs in TPO-/- mice *in vivo*, and the increased proportion of quiescent HSCs found after TPO stimulation (de Graaf and Metcalf 2011).

In a preliminary study, we have shown that enrichment of dormancy in the M07e AML cell line in the presence or absence of GM-CSF with TPO showed no evidence of generating dormancy-enriched cell populations when cultured for 7 to 21 days. Nevertheless, TPO enhanced cell survival without inducing a significant level of cell

death; this agreed with previous studies (Borge, Ramsfjell *et al.* 1996; Qian, Buza-Vidas *et al.* 2007; de Graaf and Metcalf 2011). A possible explanation for the different behaviour of M07e may be the fact that individual AML blasts express antigens of more than one lineage, suggesting that the leukaemia-initiating events occur in a primitive progenitor with multi-lineage differentiation potential (Okabe, Kunieda *et al.* 1995; Ehninger, Kramer *et al.* 2014); also TPO may not be required for the initial phase of HSC expansion (Qian, Buza-Vidas *et al.* 2007). In the M07e model, TPO may prolong cell-cycle transit, thereby protecting the steady state of this cell compartment from premature exhaustion. However, the direct effect of TPO, on the formation of cell bursts, has not been demonstrated; this may be caused by the need for accessory cells or other endogenous growth factors, possibly required to optimise the cell culture and mimic the BM environment.

The KG1a-Rapa cell model was already developed in our laboratory and shows a clear dormancy-enriched population with no apoptosis (Pallis, Burrows *et al.* 2013). This model system was selected as the standard dormancy model to compare and contrast the findings from M07e-TPO model, and to evaluate differences between cycling and dormancy-enriched cells; however, establishment of M07e model was challenging. Thus, this chapter describes the use of KG1a-Rapa model to determine the efficacy of chemotherapeutic agents in dormancy-enriched and cycling cells with respect to DNA damage and cellular response to DSBs. This model permitted a detailed assessment of DNA damage and DDRs with respect to standard chemotherapeutic drugs, and a recently developed novel treatment, with the goal of identifying differences between dormancy-enriched and cycling KG1a cells. Baseline damage, which may result from normal cell metabolism and laboratory processing, revealed no differences between dormancy-enriched and cycling KG1a cells based on DNA

strand breaks (assessed using the comet assay) (Figure 3.3.2); this agreed with previous work performed by our group (Seedhouse, Whittall *et al.* 2010; Pallis, Burrows *et al.* 2013). The AML dormancy-enriched KG1a-Rapa cell model was subjected to short-term chemosensitivity assays, to select the optimal concentration of each drug (ara-c, ETO, DNR, and TG02) to damage a sufficient number of cells without inducing death of all the cells; IC_{10}-IC_{20} were consequently determined. To track the an earlier optimal response for chemotherapeutically effective doses, we used 2, 4, 6, and 24 hour time points to study DNA damage and DDR markers induction after ara-c treatment. Ara-c is an S phase specific agent with a short half-life; the S phase of cells, collcted from AML patients, or of the HL-60 myeloid leukemic cells, is as short as 8 to 12 hours with minimal or no any cytotoxic doses of ara-c (Leclerc and Momparler 1984; Herzig, Hines *et al.* 1987; Raza, Preisler *et al.* 1990). In murine tumours, ara-c killes cells within 24 hours following ara-c injection *in vivo* (Pallavicini, Summers *et al.* 1985). The doubling time of KG1a cells is approximately 24 to 27 hours, and the IC_{50} of ara-c in the KG1a cell line was achieved following 48 hours of drug treatment.

The expression of topoisomerase II is cell-cycle-dependent, with the highest levels present in the G2/M cell-cycle phase. ETO is a known inducer of DSBs, which it accomplishes via inhibition of topoisomerase II. KG1a cells have previously shown moderate reduction in transcripts of topoisomerase II after 48 and 72 hours of treatment with anthracyclines, which consequently induce cell death (Morgan, O Onono *et al.* 2011).

The IC_{50} for TG02 has been previously established, causing 50 % of KG1a cell death after 72 hours of 200 nM TG02; death was caused by depletion of mRNA transcripts for survival molecules such as MCL1 (reduced to 23 %) and XIAP (Pallis, Abdul-Aziz *et al.* 2012). The effectiveness of the drugs, in both cycling and dormancy-enriched

cells, is indicated by the presence of a sub-compartment of cells able to escape these DNA-damaging agents and increase resistance to cytotoxic drugs. Additionally, dormancy-enriched cells are not entirely quiescent, which means some of the cells are at G1/G2, and some at the S phase, of the cell-cycle. Our findings have shown an approximate IC_{10}-IC_{20} potency of 4.1 μM ara-c, 100 nM TG02, 1.5 μM DNR, and 20 μM ETO; these results are acceptable, resulting in a statistically significant decrease in the viability of both cycling and dormancy-enriched KG1a cells. The prolonged incubation time was excluded to meet the aims of this study.

We then, optimised methods to determine the differences in damage levels and DDR between dormant cells and cycling cells. Ara-c, ETO, and DNR are used in standard chemotherapy regimens for AML and are known to induce DSBs and apoptosis; these were, therefore, chosen for this study. A fourth drug, the novel multikinase inhibitor, TG02, was also investigated. The 4- and 24-hours time points were selected to identify differences in signalling pathways that may occur after treatment; the ultimate goal was characterising early resistance mechanisms against chemotherapy drugs that may result in physiological and molecular changes in DLICs.

Ara-c is a nucleoside analogue that is incorporated into DNA during the S phase, inhibiting further DNA synthesis. Because DLICs are more commonly in the G0/G1 phases, and are less responsive to ara-c, it follows that more ara-c is incorporated by actively cycling cells than by dormant ones. An assessment of DNA damage, by comet assay, showed that less damage occured in the dormancy-enriched cells than in cycling cells after 4 hours of incubation with ara-c. This is consistent with the chemoresistant nature of quiescent cells (Tothova 2007; Rossi 2008) and the mechanism of action of ara-c discussed above. However, unexpectedly higher levels of DSBs were detected in dormancy-enriched cells after 24 hours of ara-c

treatment. A previous study showed that ara-c uses a different mechanism to eradicate leukemic cells at G0, inhibiting of 40 % of DNA synthesis after 16 hours, and leading to the accumulation of DNA strand breaks that eventually cause apoptosis (de Vries, Falkenburg *et al.* 2006). In addition, ara-c may also inhibit RNA synthesis and/or RNA polymerase, resulting in less incorporation of 3H-uridine that leads to cell killing. This reduction in RNA synthesis synchronizes with the down-regulation of the survival protein Mcl-1 (de Vries, Falkenburg *et al.* 2006).

Antineoplastic anthracyclines, such as DNR, cleave DNA by multiple mechanisms (Burden and Osheroff 1998). Type II topoisomerases are major targets of these enzymes regulate DNA supercoiling by catalysing the winding and unwinding of DNA strands via incisions that break the DNA backbone during replication (Chow and Ross 1987). ETO and DNR are in a different class of drugs; both work by inhibiting topoisomerase II and causing DNA strand breaks, as described in chapter two (Baldwin EL 2005). Interestingly, after 4 hours of treatment with ara-c and ETO, cycling cells showed significantly more DNA damage than did the dormancy-enriched KG1a cells. However, after 24 hours, this trend was reversed, with cycling cells exhibiting less DNA damage than that detected in dormancy-enriched cells. This suggest that cycling cells had already begun the process of resolving DSBs by stimulating DRR pathways. These data also indicate that dormancy-enriched cells accumulate DNA damage during prolonged incubation (up to 24 hours) with chemotherapeutic agents; we hypothesise that the cycling cells showed activation of DNA repair to remove the lesion. These findings support earlier studies showing accumulation of DNA damage in the CD34+ CD38− subset of LSCs (Milyavsky, Gan *et al.* 2010; Rübe, Fricke *et al.* 2011). However, similar levels of DNA damage were observed in both cycling and dormancy-enriched cells, at 4 and 24 hours, after treatment with either DNR or TG02. The mechanisms

underlying DNA damage induced by TG02, are likely multifactorial. TG02 can down-regulate phosphorylation of ERK and STAT5, inhibit transcription through the CDK9-RPIIS2 pathway, enhance sensitivity to BCL-2 targeting agents, delay cell-cycle progression, and stimulate cell death and apoptosis (Goh, Novotny-Diermayr *et al.* 2012; Pallis, Burrows *et al.* 2013). A previous study by our group provided evidence that dephosphorylation of RP2S2 is a common consequence of TG02 treatment in AML cells for 6 to 24 hours, and that this dephosphorylation correlates with the induction of an apoptotic program (Pallis, Burrows *et al.* 2013). Additionally, we previously reported that DNR induces DNA damage after 2 hours of treatment (Jawad, Yu *et al.* 2012). In the current experiments, we have shown that DNA damage is detectable when cells are exposed to DNR for 4 or 24 hours.

DNA DSBs, induced by drugs, have been shown to stimulate DDR pathways (Polo and Jackson 2011). DDR was tested in treated dormancy-enriched cells to evaluate the cellular response compared with that in treated cycling KG1a cells. ATM is the immediate signal transducer that initiates cell-cycle changes after DNA damage is induced by IR (Jazayeri, Falck *et al.* 2006). Assessment of DDR by p-ATM revealed that both dormancy-enriched and cycling cells initially recognized and sensed DNA lesions in a similar manner. Detectable levels of p-ATM were found in cycling and dormancy-enriched KG1a cells following ara-c and ETO treatment, with higher levels observed after ETO treatment. This indicates that p-ATM may recognize a variety of DNA damage types (Guo, Deshpande *et al.* 2010), including DSBs, leading to the activation of cell cycle checkpoints, DNA repair, or apoptosis. An increase in the levels of p-ATM, despite no DSB damage being detected by comet assay, was observed at 4 hours of ara-c treatment in dormancy-enriched cells. Initiation of ATM activation does not always require the direct binding of ATM dimers to DSBs, and minor structural changes in the nucleus may be "sensed"

by ATM dimers (Bakkenist and Kastan 2003; McManus and Hendzel 2005; Boehrer, Ades *et al.* 2009; Suchánková, Kozubek *et al.* 2015); therefore, ATM may recognize damage in these cells, even if it is not detected by comet assay. Interestingly, although TG02 induced DNA damage, as detected by comet assay at both 4- and 24- hour time points, no p-ATM was detected in cells treated with TG02, indicating that TG02 did not induce a canonical DDR signalling pathway. This is the opposite of what was observed with ara-c at 4 hours; ara-c activates ATM with no evidence of damage, whereas TG02 shows damage with no detectable ATM. This implies that TG02 rapidly initiates apoptosis, and that the damage detected may be a consequence of apoptotic cleaved DNA. Thus, we halted the investigations of DDR activation in cells treated with this agent.

In contrast to the similarity in p-ATM results between dormancy-enriched and cycling cells, the levels of phospho-H2AX139 in dormancy-enriched cells, treated with these chemotherapeutic agents, were significantly different compared with those in cycling KG1a cells at both 4- and 24-hour time points. In addition to the flow-cytometric analysis of phospho-H2AX139, immunofluorescence staining indicated distinct foci within the cell nuclei, which strongly suggestes that phospho-H2AX139 was activated in response to the presence of DSBs. Estimating the number of foci by H-scores, acquired using microscopy, confirmed the phospho-H2AX139 data acquired by flow-cytometry (Figure 3.6.2). While these data revealed that dormancy-enriched cells respond to DNA-damaging agents, the levels of phospho-H2AX139 were lower than those in cycling KG1a cells. This was expected at 4 hours, because less DNA damage was detected via the comet assay in dormancy-enriched cells at this time point. More DNA damage was observed in dormancy-enriched cells at 24 hours than in cycling cells, at 24 hours; however, the dormancy-enriched cells showed significantly lower levels of phospho-H2AX139.

Because H2AX is rapidly phosphorylated (between 10 and 20 minutes) after DSB formation, this is not likely the result of time required for phospho-H2AX139 to form (Suchánková, Kozubek *et al.* 2015). Instead, this indicates a difference in responses to damage in dormancy-enriched and cycling cells, which encouraged us to further examine the DDR processes. However, it should be noted that alternative hypotheses exist for these differences in the levels phospho-H2AX139 can be phosphorylated in mitotic cells to form nuclear foci that do not induce a DDR; this may explain increased phospho-H2AX139 levels in cycling cells, compared with those in dormancy-enriched cells, because cells leave the M phase more rapidly than other phases (McManus and Hendzel 2005). Furthermore, studies reveal that phospho-H2AX139 does not always indicate the presence of DSBs; for example, serum starvation can induce the formation of phospho-H2AX139 foci via the p38 MAPK signalling pathway (Lu, Shi *et al.* 2008; Cleaver, Feeney *et al.* 2011).

Phosphorylation of Thr68 is necessary for the efficient activation of Chk2 kinase in response to DNA damage (Ahn, Schwarz *et al.* 2000). Phospho-Chk2 indicated phosphorylation in dormancy-enriched and cycling cells after 4 and 24 hours of incubation with ara-c and ETO; however, no significant difference in phosphorylation levels of these cells was detected. Persistence of pChk2 beyond 24 hours, in both cycling and dormancy-enriched cells may indicate blockade of DNA replication in response to DSBs; this allows for repair, prevents chromosomal instability, and ensures that mutations are not inherited by daughter progeny (Kastan and Bartek 2004; Niida and Nakanishi 2006). To initiate damage sensing and repair repair of downstream DNA, as well as the cell death programs (Neckers and Cossman 1983), Chk2 phosphorylates the mitosis-inducing phosphatase Cdc25C, blocking cells from entry into mitosis and causing G1 arrest (Ahn, Schwarz *et al.* 2000; Niida and Nakanishi 2006). Defective

Chk2, in cancer cells, fails to stop entry into mitosis following irradiation, suggesting the disruption of the G2/M checkpoint (Buscemi, Savio *et al.* 2001). These studies imply that pChk2-T68 plays an essential role in cell cycle regulation, which may explain why both cycling and dormancy-enriched KG1a cells showed similar levels of pChk2-T68 induction. Additionally, pChk2 induction after IR is time-dependent. In one study, maximal levels were noticed between 1 and 3 hours; these levels persisted for up to 10 hours (Buscemi, Savio *et al.* 2001). Another report showed that high levels of pChk2-Thr68, detected at 6 hours after treatment, were sustained for up to 48 hours (Duong, Hong *et al.* 2013).

The comet assay detects damage at the level of individual cells and can be used in cell lines or primary cells (Collins 2004; Olive and Banath 2006); its high level of sensitivity can affect its reproducibility. Several studies have been performed to improve the quality of cell membrane lysis by monitoring the time of lysis. Variations in the temperature of lysis solution have also been studied in order to find the optimal temperature while avoiding extraneous damage (Ersson and Möller 2011; Azqueta, Slyskova *et al.* 2014). Study results differ regarding parameters, used to measure the comet tail; the available software measures tail length, tail moment, or tail intensity. The tail moment measurement was introduced by Olive *et al*. and is defined as the product of tail length and fraction of total DNA in the tail (Olive and Banath 2006). This parameter is most commonly used, thus it was chosen in this study; because the tail moment incorporates a measure of the smallest detectable size of migrating DNA with the comet tail length, and includes the broken or relaxed pieces of DNA that are represented by the intensity of DNA in the tail. The variability in the results of DNA damage has been affirmed in several reports, and stems from the lack of standardised protocol inter-laboratory comparisons. This can be partially resolved

multiple repetition of each experiment; we used this approach to validate our findings and to increase confidence of the results. The number of samples was limited by the size of electrophoresis tank. Therefore, in the future, high-throughput comet approaches will be used to handle a maximal number of samples in one run, to reduce processing time account for the possibility of induction of external damage.

Additionally, KG1a-Rapa model provided a source of dormancy-enriched cells and aimed to mimic *in vivo* criteria of the DLICs in BM niche regulating dormancy, and minimized the difficulties in obtaining these cells from AML patients. KG1a-Rapa model showed largely consistent results and no detrimental effect on KG1a cell line in ordinary culture system. It is relatively constant model for repetition of different experimental conditioning to test different pathways, markers, effects of chemotherapeutic agents and the damage response of DLICs. However; using rapamycin as an external agent to induce the dormancy rather than using the reported intrinsic (e.g. FOXO3a, Fbxw7) and/or extrinsic (e.g. β-catenin) regulatory mediators of dormancy in the BM, is one of few limitations for this model. Taking these data into consideration, it may be worth including more AML cell line model of dormancy and primary AML clinical samples as this will allow broader comparison among diverse cellular responses to external dormancy inducers.

Taken together, these data suggest an accumulation of DNA damage in dormancy-enriched KG1a cells, as assessed by the level of phospho-H2AX139 measured with flow-cytometry and confirmed by immunofluorescence; however the data on p-ATM or p-Chk2 levels, in response to DSB induction, were inclusive. The analysis of upstream biomarkers of DDR suggests a cellular resistance to the tested drugs and differences in the responses of downstream effectors between cycling and dormancy-enriched KG1a; this will be examined in the next chapter.

Chapter 4:

Determination of cell fate after

4.1 Background

A DNA damaging event can corrupt genetic information and threaten the life of a cell. The cellular response to DNA damage results in one of two outcomes: DNA repair and genomic recovery, or, if the damaged DNA cannot be corrected, cells undergo a cell death program, such as apoptosis or permanent cell cycle arrest (d'Adda di Fagagna 2008; Giunta, Belotserkovskaya *et al.* 2010). We have previously shown that dormancy-enriched KG1a cells differ in their response to conventional chemotherapeutic agents with up to 24 hours of exposure compared to that of cycling cells. More damage is detected in dormancy-enriched cells, but there is less phospho-H2AX139, raising the questions as to what is happening? Do the dormancy-enriched cells have a lower efficiency in detecting and repairing damage or is there another explanation? The precise molecular events that determine the outcome of DNA repair and survival or cell death remain incompletely understood.

This chapter explores the hypothesis that sensitivity to chemotherapeutic drugs in dormancy-induced KG1a cells is a result of a unique scenario that determines cell fate and that differs from that when DNA damage is induced in cycling KG1a cells. To establish whether dormancy-induced KG1a cells can resolve DNA damage, we used flow-cytometric and comet assays to detect DDR and apoptotic markers, which were confirmed by immunofluorescence and western blot assays.

4.2 Identification of cell fates after DDR activation

4.2.1 H2AX 142 phosphorylation

In response to DSBs phosphorylation of phospho-H2AX139. phospho-H2AX139 can extend up to several thousand nucleosomes from the actual site of the DSB and may mark the surrounding chromatin for

recruitment of proteins required for DNA damage signalling and repair (Zhang, Lu *et al.* 2012; Turinetto and Giachino 2015). Studies have shown that H2AX142 and other components of damaged chromatin are modified during DDRs (Balajee and Geard 2004; Cook, Ju *et al.* 2009). Under normal conditions, histone H2AX is constitutively phosphorylated at tyrosine (Y) 142. Persistent phosphorylation of H2AX142 after DSBs has been shown to increase apoptosis, whereas a reduction in phosphorylated H2AX142 results in the recruitment of DNA repair factors. Therefore, H2AX142 phosphorylation plays a role in determining cell fates in responses to genotoxic stress (Cook, Ju *et al.* 2009).

4.2.2 Preliminary work on phospho-H2AX142 in dormancy-enriched cells

We examined phosphorylation of H2AX142 after exposure of up to 48 hours to chemotherapeutic drugs to establish an appropriate time point for DDR assessment. The time-course of Tyr-142 histone phosphorylation after continuous treatment with 20 μM ETO of cycling and dormancy-induced KG1a cells is shown in (Figure 4.2.3A). phospho-H2AX142 levels were significantly different in cycling and dormancy-enriched cell populations at 24 hours ($p = 0.0306$, $n = 3$). Lower levels of phospho-H2AX142 were also observed in dormancy-enriched cells compared to cycling KG1a cells at 48 hours ($p = 0.0031$, $n = 3$) (Figure 4.2.3A). Because there was a significant difference between cycling and dormancy-enriched cells at 24 hours in cells treated with ETO, this time point was chosen for further experiments.

4.2.3 Phosphorylation of H2AX142 helps to determine dormancy-enriched cell responses to DNA-damaging agents

We next assessed phospho-H2AX142 in response to DNA damage induced by 4.1 μM ara-c or 20 μM topoisomerase II inhibitor ETO, to determine whether H2AX142 phosphorylation plays a role in

modulating cell fate decisions in dormancy-enriched KG1a cells. The phospho-H2AX142 was detected at 24 hours, but the phosphorylation levels reduced in dormancy-enriched KG1a cells compared with phospho-H2AX142 in cycling cells after ara-c treatment ($p = 0.03$, $n = 7$) (Figure 4.2.3B) and ETO ($p= 0.01$, $n=7$) (Figure 4.2.3B). Additionally, flow cytometric analysis of phosphor-H2AX139 showed contenuing phosphorylation in cycling KG1a cells after 24 hours treatment with ara-c ($p= 0.0182$, $n= 12$), or ETO ($p =0.0273$, $n= 12$) compared with dormancy-enriched KG1a cells (Figure 4.2.3C) as we demonstrated in section 3.6.1 and 3.6.2.

To further confirmation the decrease in the levels of phospho-H2AX-142, western blot assay was performed to measure protein expression. Protein was extracted from cycling and dormancy-enriched KG1a cells, and 50 µg of cell lysate was subjected to SDS-PAGE. A band at approximately 18-KDa band size, correlating with the size of H2AX, was detected by western blot when membranes were probed with a H2AX142 phosphorylation-specific antibody alongside a loading control of 45-KDa β-actin (Figure 4.2.3D, $n = 3$). The densities of bands were determined using ImageJ analysis software and are shown in Figure 4.2.2E ($n = 3$). A decrease in phospho-H2AX142 in dormancy-enriched KG1a cells suggested that these cells are destined for survival ($p = 0.0381$, $n = 3$) (Figure 4.2.3E); this contrasts with the increase in phosphorylation in cycling cells that suggests activation of apoptosis.

Immunofluorescent detection of H2AX142 in cycling and dormancy-enriched KG1a cells was performed to confirm flow cytometric findings. The cells were fixed and stained with FITC-conjugated anti-H2AX142, with green fluorescence indicating the persistence of phospho-H2AX142 in cycling and dormancy-enriched cells. Green fluorescence indicates the overall phosphorylation of H2AX142 in cycling cells compared with dormancy-enriched cells rather than

specific phospho-H2AX139 foci counting. Dormancy-enriched KG1a cells showed a lower level of phospho-H2AX142 compared to cycling cells after ara-c and ETO treatment (Figure 4.2.3F). The switch between cell survival or death is an important one; therefore, downstream effectors of DNA repair and apoptosis markers were explored further.

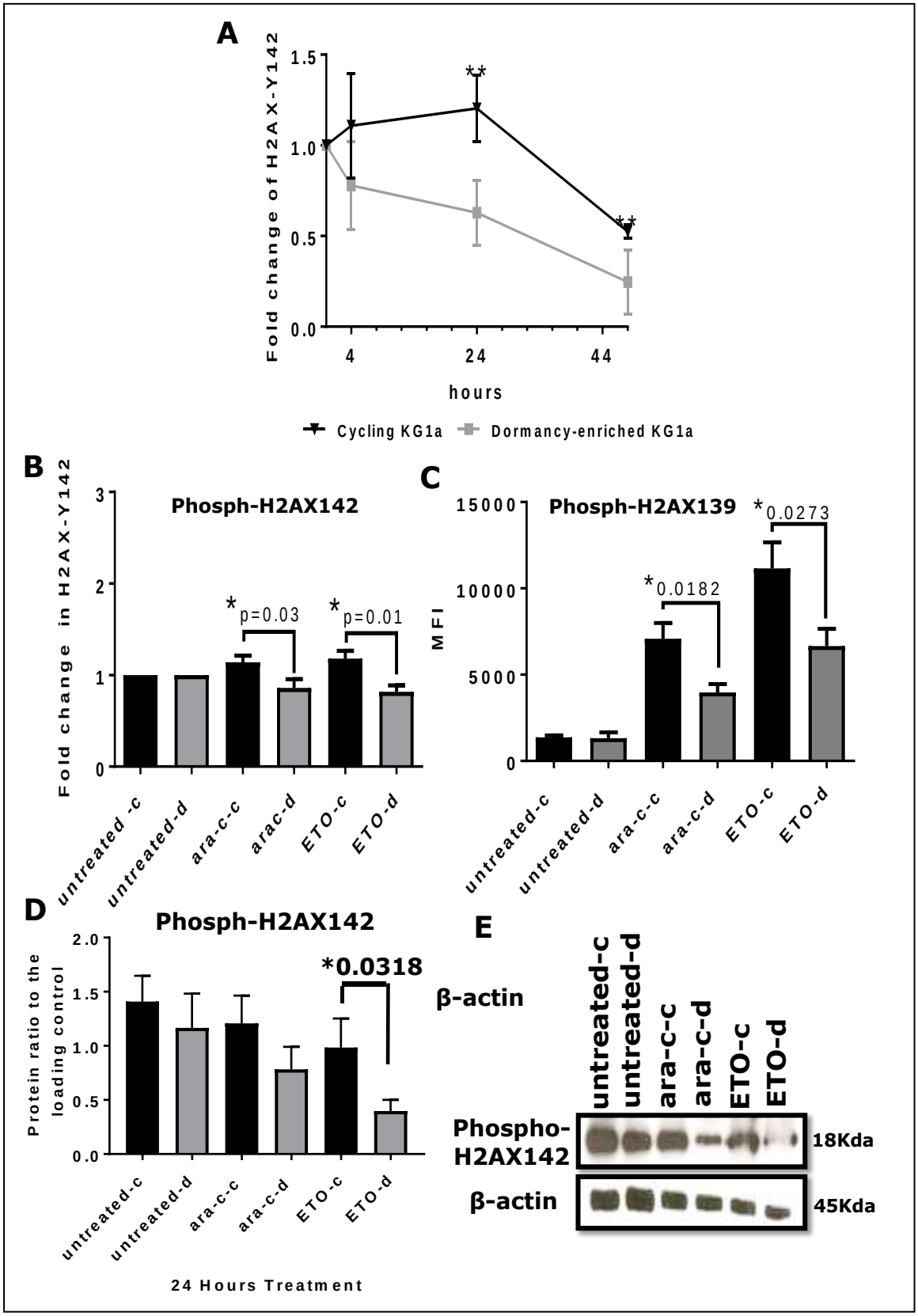
A
Fold change of H2AX-Y142
1.5
1.0
0.5
0.0
4
24
44
hours
**
**
Cycling KG1a
Dormancy-enriched KG1a
B
Fold change in H2AX-Y142
Phosph-H2AX142
3
2
1
0
*p=0.03
*p=0.01
untreated -c
untreated-d
ara-c-c
arac-d
ETO-c
ETO-d
C
MFI
Phosph-H2AX139
15000
10000
5000
0
*0.0182
*0.0273
untreated-c
untreated-d
ara-c-c
ara-c-d
ETO-c
ETO-d
D
Phosph-H2AX142
Protein ratio to the loading control
2.0
1.5
1.0
0.5
0.0
*0.0318
untreated-c
untreated-d
ara-c-c
ara-c-d
ETO-c
ETO-d
24 Hours Treatment
E
β-actin
untreated-c
untreated-d
ara-c-c
ara-c-d
ETO-c
ETO-d
Phospho-H2AX142
18Kda
β-actin
45Kda

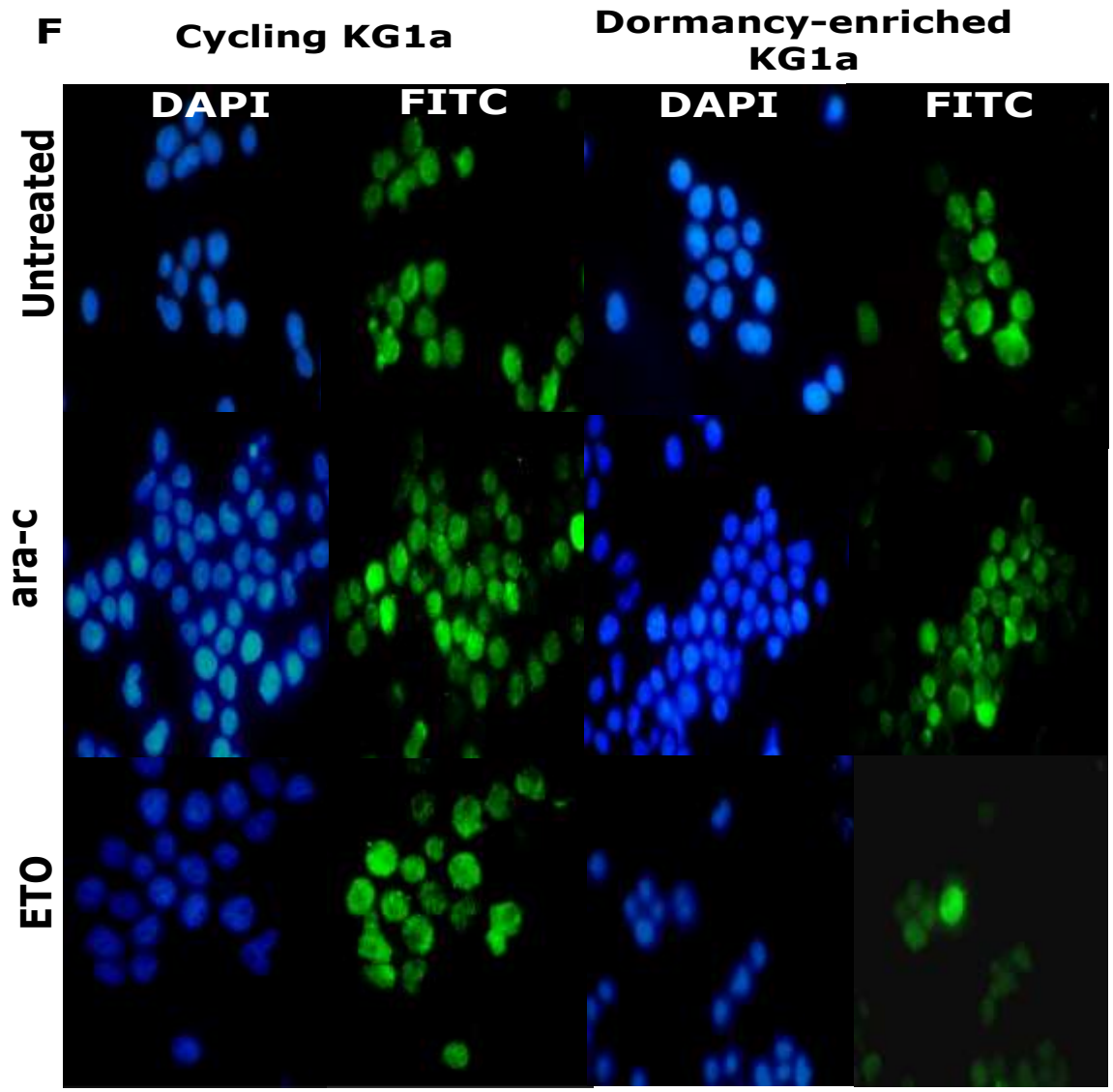

Figure 4.2.3: H2AX-142 phosphorylation plays a role in determining cell fate in cycling and dormancy-enriched KG1a cells in response to DNA-damaging agents. (A) Phospho-H2AX142 were assessed by flow cytometry in cycling cells (black line) and dormancy-enriched cells (grey line) treated with ETO have shown that 24 and 48 hours are significantly phpsphorylated in cycling cells compared with dormancy-enriched cells (n = 3). (B) Fold change of phospho-H2AX142 after DNA damage induction in cycling KG1a (black bars) and dormancy-enriched (grey bars) cells treated with ara-c or ETO for 24 hours (n = 7). (C) Phospho-H2AX139 showed a significant phosphorylation in cycling cells. (D) phospho-H2AX142 protein levels (18 KDa) were detected by western blot, 50 µg of cell lysate was added to an SDS-PAGE gel, with anti-ß-actin used as a loading control (45 KDa) (n = 3). (E) Densitometry of bands was performed using ImageJ software (NIH). (F) Immunofluorescent detection of phospho-H2AX142 in cycling and dormancy-enriched cells. Phospho-H2AX142 was visualized by indirect immunofluorescence using FITC, while the nucleus was stained with DAPI. Green fluorescence indicates the persistence of phospho-H2AX142 in cycling cells compared with dormancy-enriched cells. Mean and SD were calculated, and * represents a P value of <0.05 and ** represents $P < 0.01$.

4.3 Dormancy-enriched KG1a cells show resistance to apoptosis

4.3.1 Cleaved PARP apoptosis marker

The PARP enzyme activates repair and survival machinery and thus helps cells to remain viable. Cleavage of PARP facilitates cellular disassembly and serves as a marker of cells undergoing apoptosis. Cleavage of PARP occurs between Asp214 and Gly215, which separates the PARP amino-terminal DNA-binding domain from the carboxyl-terminal catalytic domain (Krishnakumar and Kraus 2010). To further investigation the consequences of DDR stimulation in cycling and dormancy-enriched cells treated with ara-c or ETO, a flow cytometric apoptosis assay was performed.

In Figure 4.3.1A, shows that there is no apoptosis in dormancy-enriched cells was observed after 4- hours of ara-c or ETO treatment. Figure 4.3.1B shows that 4.9 % of cycling cells were apoptotic compared to 2.8 % of dormancy-enriched cells after 24 hours of incubation with ara-c ($p = 0.0001$, $n = 16$). Apoptosis following ETO treatment was detected in 9.4 % of cycling cells compared to only 3.6 % of dormancy-enriched cells ($p = 0.0001$, $n = 16$). These data show that dormancy-enriched cells are significantly more resistant to apoptosis than cycling cells, which adds credence to the findings on phospho-H2AX142 was presented in section 4.2.

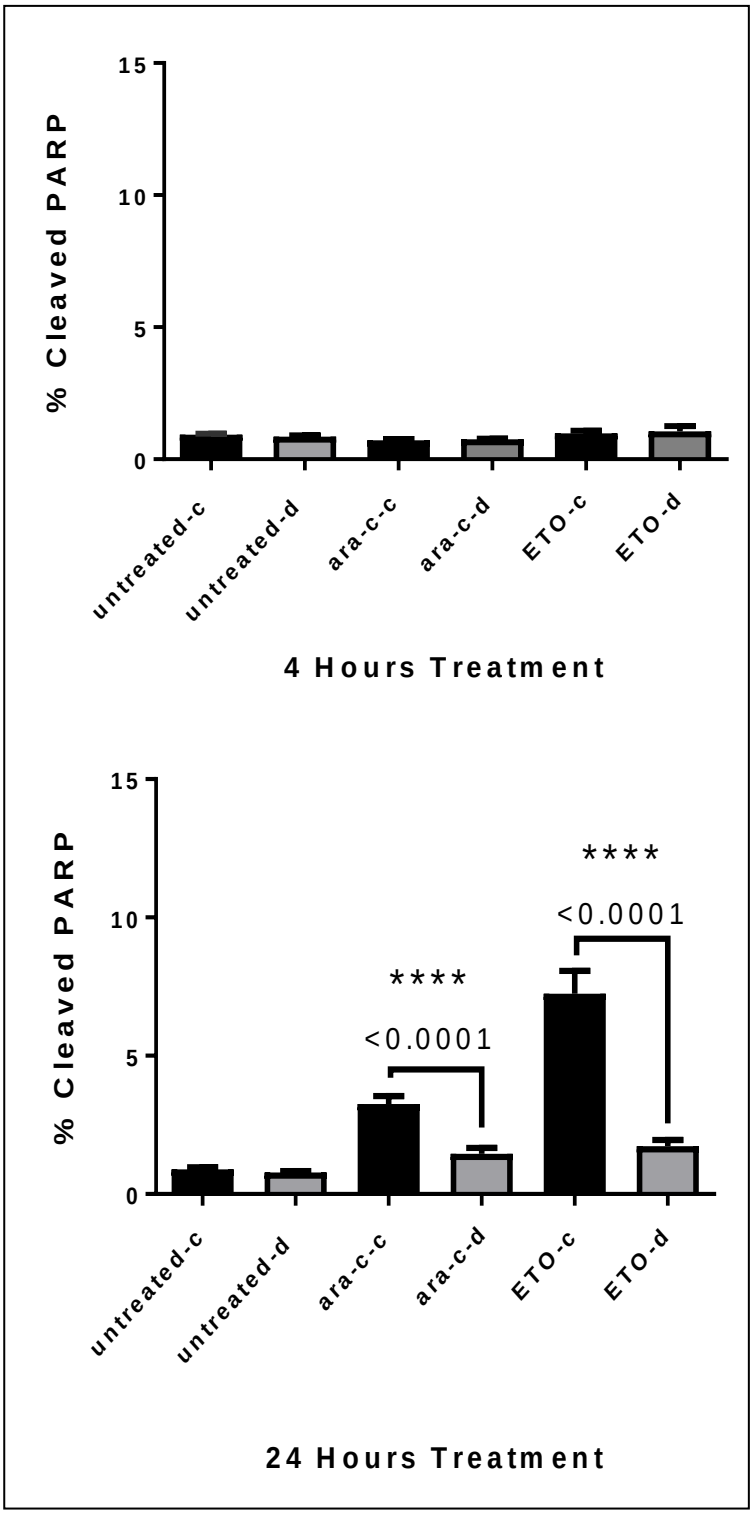

Figure 4.3.1: Dormancy-enriched KG1a cells show greater resistance to apoptosis than cycling KG1a cells after (A) 4-hour n=4, and (B) 24- hours of ara-c and ETO treatment. A cleaved PARP-Asp214 assay was performed as a marker for apoptosis following treatment of cells with 4.1 μM ara-c or 20 μM ETO. Treated cycling KG1a cells (black bars) were compared with treated dormancy-enriched cells (grey bars) n=16. Each condition was conducted in triplicate, mean and SD were calculated, ****P represents a< 0.0001.

4.3.2 Active caspase 3 apoptosis marker

Caspase-3 is a key protease that is activated in the early stages of apoptosis. When DNA damage is irreversible, poly [ADP-ribose] polymerase 1 (PARP1) rapidly cleaves the DNA within minutes of the DNA insult due to effector caspases, this is a hallmark of apoptosis (Salvesen and Dixit 1997; Rosen, Putta *et al.* 2010). Caspase-3 is cleaved, activated by upstream caspases, and is translocated into the nucleus, resulting in nuclear DNA fragmentation and chromatin condensation (Luo, Lu *et al.* 2010). Therefore, we measured the active form of caspase-3 as a biomarker for apoptotic events for further confirmation. Figure 4.3.2 shows that under continuous exposure to ara-c, increasing numbers of cells were positive for active caspase-3 (4.1 %), indicating the progression of apoptosis in the cycling cells population compared to 2.2 % dormant cells ($p = 0.011$, $n = 3$). Additionally, prolonged incubation of dormant cells with ETO emphasizes that dormant cells exert resistance to apoptosis with 1.6 % cells positive for active caspase 3 compared to 3.2 % cycling cells ($p=0.02$, $n=3$). Our data supports above findings affirming c-PARP apoptotic results as presented in section 4.3.1.

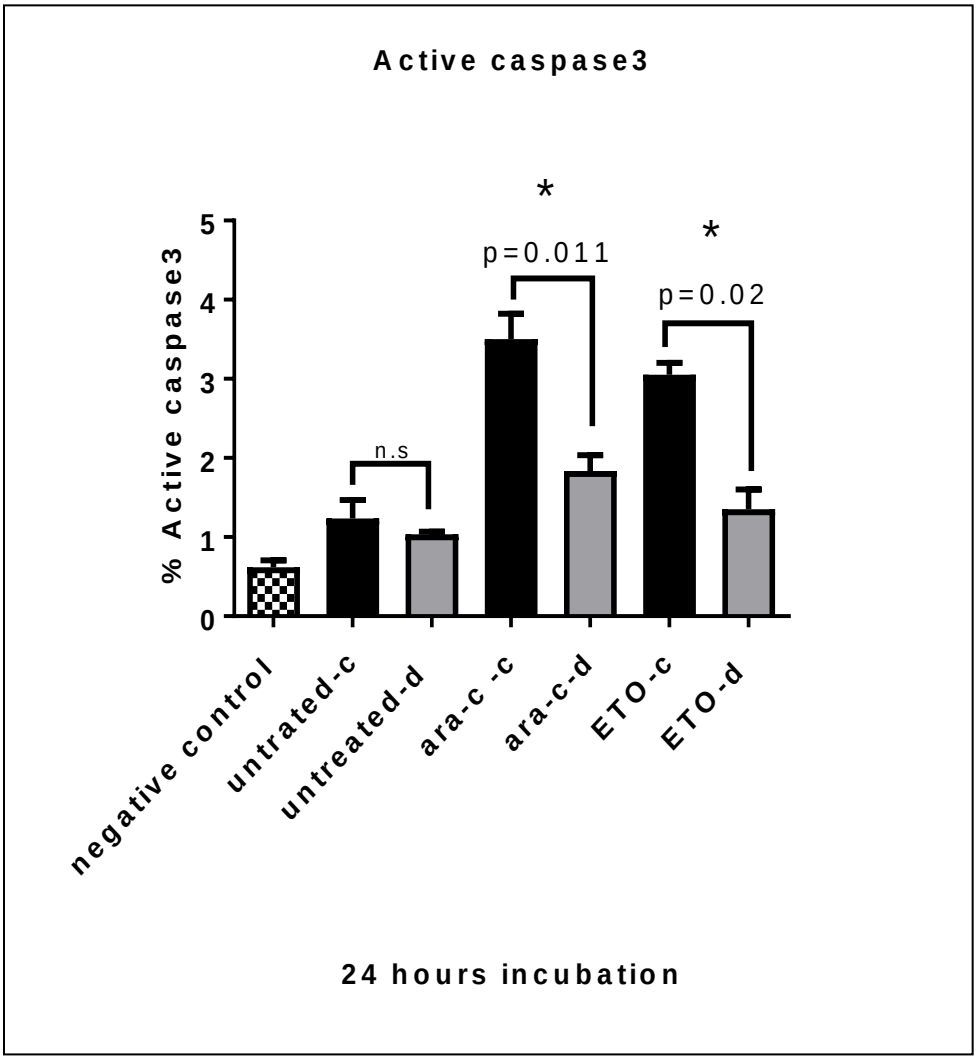

Figure 4.3.2: Dormant cells express a lower percentage of cells expressing active caspase 3. Active caspase 3 assay was performed as a marker for apoptosis following 24 hours treated cells with 1.0 µg/ml ara-c or 20µM ETO. Treated cycling KG1a cells (black bars) were compared to treated cycling cells (grey bars). Each condition was conducted in triplicate, mean and SD were calculated and * represents a P value of <0.05, n.s not significant.

4.4 DNA damage repair activity in response to a DSB-inducing agent

Activation of programmed cell death was confirmed presumably result from continued phosphorylation of H2AX at both Ser139 and Tyr142 residues in cycling cells. However, dormancy-enriched cells showed lower levels of γH2AX-S139 and H2AX-Tyr142. If dormancy-enriched cells do not undergo apoptosis, then they likely trigger DNA repair mechanisms or become senescent. To examine this possibility further, we compared the DNA repair activity in dormancy-enriched and cycling cells.

4.4.1 Assessment of DNA repair by comet assay

Neutral comet assays were used to assess DNA repair as a loss of damage over time in dormancy-enriched and cycling cell populations. The cell lines were treated with ara-c, ETO, and DNR for 24 hours. Following incubation with each drug, the cells were washed twice and resuspended in drug-free medium. Recovery was monitored at two time points (4 and 24 hours) to investigate the DNA repair process. The comet analysis, described in chapter 3, indicated the levels of damage after 24 hours of treatment. The same basal levels of DNA damage were detected in cycling and dormancy-enriched cells. However, at 24 hours, higher levels of DSBs were detected in dormancy-enriched cells than in cycling cells.

During recovery after 4 hours of ara-c treatment, levels of damaged DNA in cycling cells were significantly reduced ($p = 0.0211$, $n = 4$), followed by a further reduction at 24 hours (Figure 4.4.1i, A). However, the decrease in DSBs observed in dormancy-enriched cells did not reach statistical significance until 24 hours of treatment ($p = 0.0414$, $n = 4$) (Figure 4.4.1i, A). Using ETO to induce DSBs in cycling cells resulted in the detection of significant levels of damage in cells after 24 hours of treatment, as described in chapter 3. Cycling

cells showed a significant reduction in DSBs after 4 hours of recovery in drug-free medium ($p = 0.0198$, $n = 3$) (Figure 4.4.1i, B). Recovering dormancy-enriched cells showed low levels of DSBs after 4 hours of incubation in drug-free medium ($p = 0.0016$ and $p = 0.0188$, $n = 3$) (Figure 4.4.1i, B). Additionally, using DNR as a DSB-inducing agent caused extensive damage, as shown by neutral comet assay in cycling cells after 24 hours of treatment. Tracking DNA repair after DNR treatment revealed a more significant reduction in DSBs in cycling cells after 24 hours of recovery ($p = 0.0089$, $n = 4$) compared to that in dormancy-enriched cells (Figure 4.4.1i, C). Additionally, the length of olive tail moments was monitored and used as an indicator for the persistence of damaged or recovered cells compared to ara-c, ETO and DNR treated cells for 24 hours (Figure 4.4.1ii).

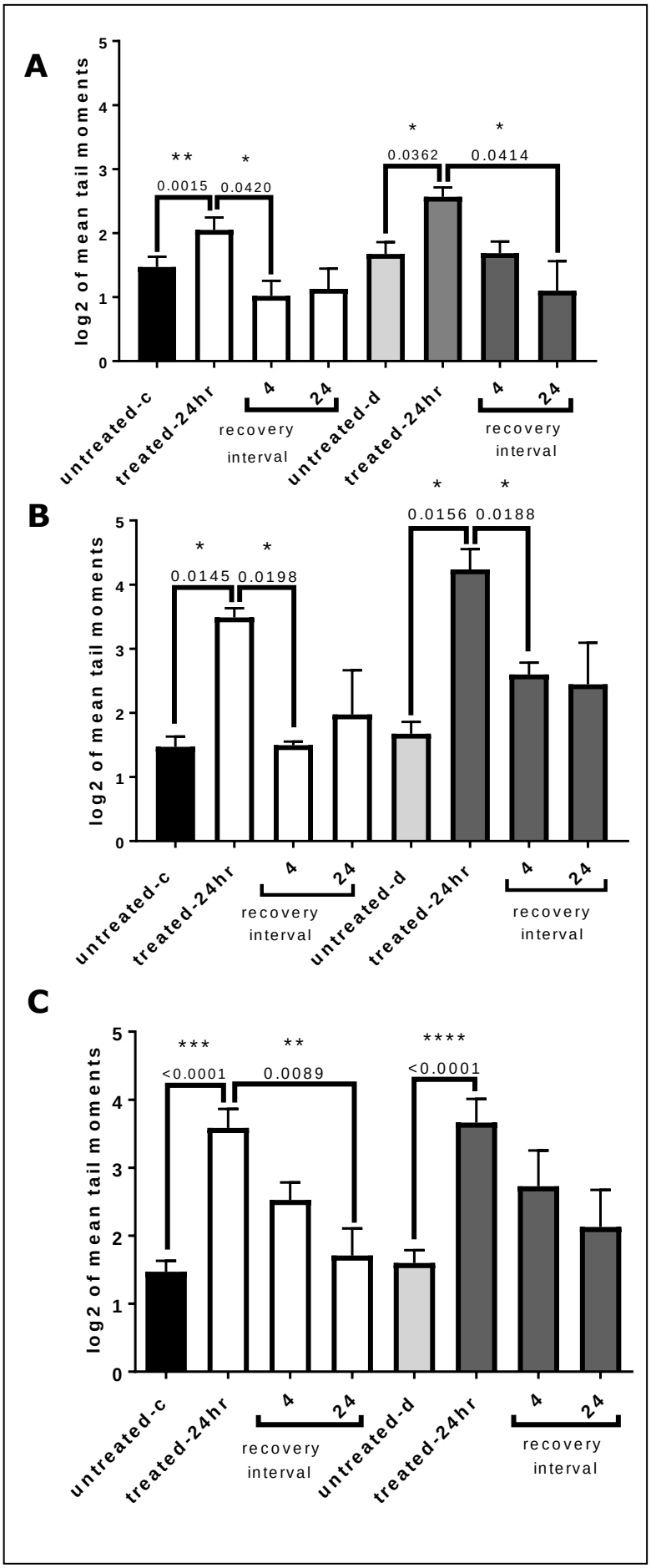
A
log2 of mean tail moments
0
1
2
3
4
5
**
*
0.0015
0.0420
*
*
0.0362
0.0414
untreated-c
treated-24hr
4
24
recovery interval
untreated-d
treated-24hr
4
24
recovery interval
B
log2 of mean tail moments
*
*
0.0145
0.0198
*
*
0.0156
0.0188
untreated-c
treated-24hr
4
24
recovery interval
untreated-d
treated-24hr
4
24
recovery interval
C
log2 of mean tail moments
***
<0.0001
**
0.0089
****
<0.0001
untreated-c
treated-24hr
4
24
recovery interval
untreated-d
treated-24hr
4
24
recovery interval

Figure 4.4.1i: Assessment of DNA damage repair activity by the neutral comet assay. Untreated cycling (black bars) and dormancy-enriched cells (grey) were treated with (A) 4.1 μM ara-c (n = 4), (B) 20 μM ETO (n = 3), or (C) 1.5 μM DNR (n = 4) for 24 hours. Cycling cells (white bars) and dormancy-enriched cells (dark grey) were washed twice and re-cultured in drug-free medium up to 24 hours. 200 cells were scored per condition. Mean and SD were calculated, and * represents a P value of <0.05, ** represent P < 0.01, *** represent P< 0.001 or ********P < 0.0001.

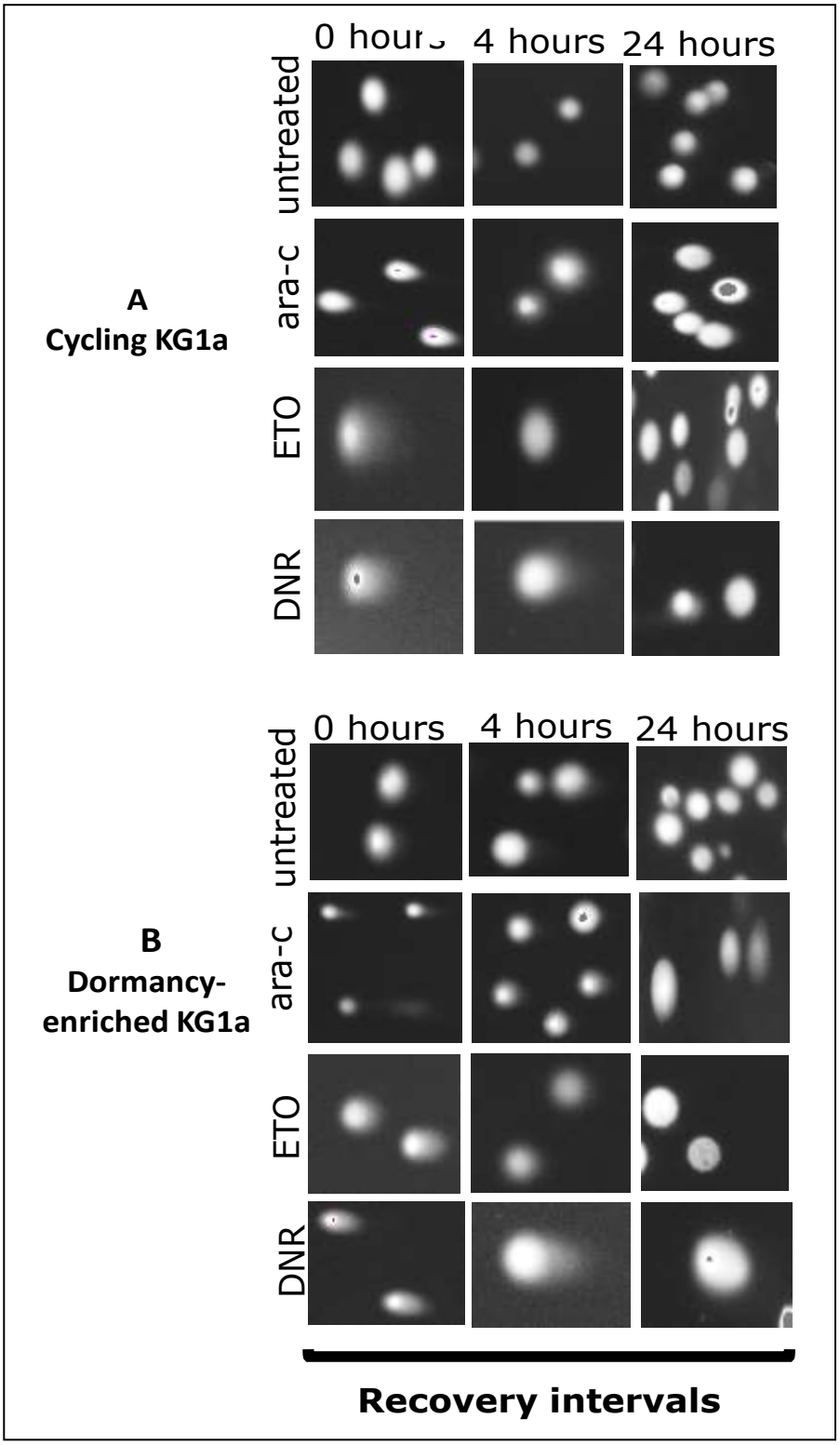

Figure 4.4.1ii: Representative images of comets following 24 hours of treatment in (A) cycling cells and (B) dormancy-enriched cells. Cells were treated with 4.1 μM ara-c, 20 μM etoposide (ETO), or 1.5 μM daunorubicin (DNR). Olive tail moments were scored after 4 and 24 hours of recovery, with 200 cells were scored per condition.

The ability of dormancy-enriched cells to repair DNA damage during recovery in drug-free medium may result from a fraction of the cells being stimulated to escape dormancy and enter into the cell cycle and then, addressing damage with DNA repair mechanisms; alternatively, massively damaged cells may have undergone apoptosis and therefore were not available to be scored. To exclude the second possibility, the rate of apoptotic cells was quantified in both cycling and dormancy-enriched cells during recovery after DNA damage.

The percentage of apoptotic cells was estimated via flow cytometric assay annexin V (in parallel with an assessment of DNA repair activity) in cycling and dormancy-enriched cells, which will be discussed later. During recovery from ara-c in cycling cells, the highest level of apoptotic cells (8.9 %) was measured after 24 hours of recovery. In contrast, dormancy-enriched cells showed a lower level of apoptotic cells (5.3 %) after 24 hours. Approximately 7.7 % apoptotic cycling cells were measured after exposure to 20 μM ETO treatment for 24 hours, implying that the recovery process might result in activation of programmed cell death. A lower level of apoptotic cells (3.2 %) was measured in dormancy-enriched cells after 24 hours of recovery, compared to 1.667 % with no recovery when treated with 20 μM ETO (Figure 4.4.1iii, B). Because fluorescent signals from DNR might overlap with those from flow cytometry fluorochromes, we estimated the percentage of cells that were viable using manual counting with a haemocytometer after Trypan Blue staining. In cycling cells, 77 % were viable at 24 hours after treatment with DNR; this percentage increased after 24 hours of recovery to 93 % viable cells (Figure 4.4.1iii, C). In dormancy-enriched cells, about 83.33% of cells were viable after continuous treatment with DNR for 24 hours; this percentage increased to 92 % after 24 hours of recovery (Figure 4.4.1iii, C).

These data suggest that activation of DNA repair in cycling cells estimated by neutral comet assay, resulted in the loss of some cells via apoptosis, with damaged cells further dying during the recovery intervals. However, dormancy-enriched cells showed efficient triggering of DNA repair activity, based on the lower levels of apoptotic cells detected, indicating recovery and cell survival. The precise mechanism underlying this assumption is investigated in the next sections. Here, we provide the first evidence to support the hypothesis for this chapter, which suggests that dormancy-enriched cells can escape potent chemotherapeutic agents.

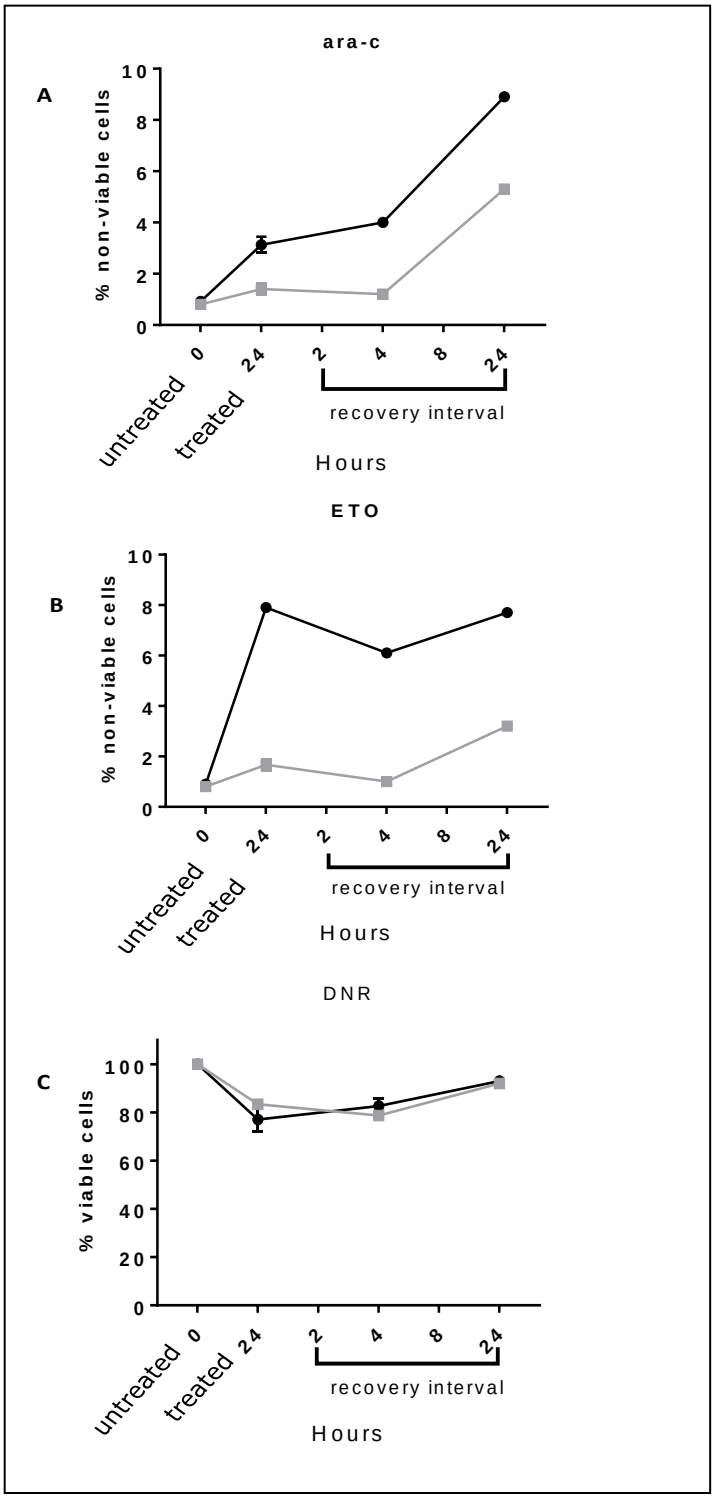

Figure 4.4.1iii: Detection of cell viability during assessment of DNA recovery process. Cycling (black lines) and dormancy-enriched KG1a (grey lines) cells were treated with (A) 4.1 μM ara-c (n = 2), (B) 20 μM ETO (n = 1), or (C) 1.5 μM DNR (n = 2) for 24 hours. Cells were washed twice to remove the drugs and then re-incubated in drug-free medium up to 24 hours. During recovery, the percentage of non-viable cells was assessed by c-PARP flow cytometry assay for ara-c and ETO or manual viable cell count with Trypan Blue for DNR.

4.4.2 Assessment of phospho-H2AX139 by immunofluorescence assay

Preserving genome stability requires DNA DSB repair and this is facilitated by the phosphorylation of multiple histone H2AX molecules that flank break sites. To explore the response of dormancy-enriched cells after treatment with ara-c, ETO, or DNR for 24 hours, followed by recovery in drug-free culture, phospho-H2AX139 antibody was used as a marker of the formation of nuclear foci in response to DSBs (Rogakou 1998; Ewald 2007; Turinetto and Giachino 2015). Figure 4.4.2 presents H-scores determined by visualization of subnuclear foci in 100 cells stained with phospho-H2AX139 antibody by immunofluorescence microscopy. The results showed the extent to which ara-c (A), ETO (B), and (C) DNR triggered DDR, which in turn should activate DNA repair or apoptosis.

In section 3.5.2, we showed that the abundance of phospho-H2AX139 foci was markedly higher in cycling cells after 24 hours of treatment with ara-c, ETO compared to that in dormancy-enriched cells, whilst treatment with DNR resulted in comparable H-scores in dormancy-enriched and cycling cells. When evaluating cells over the recovery period, dormancy-enriched cells showed persistence of phospho-H2AX139 after 24 hours in free-drug medium of ara-c, ETO or DNR compared to cycling cells (Figure 4.4.2 A & B).

In contrast, cycling cells revealed considerable reduction on H.score after 4 hours incubation in ara-c-free medium ($p = 0.0302$, $n = 4$) (Figure 4.4.2A). Additionally, lower H.score was calculated in cycling cells after 24 hours incubation in ETO-free medium ($p = 0.05$, $n = 4$) (Figure 4.4.2B). No differences were scored in both cycling and dormancy-enriched cells over 24 hours of DNR withdrawal (Figure 4.4.2C). This suggested that phospho-H2AX139 foci play a key role in DDR and is required for the assembly of DNA repair proteins, meriting investigation of additional DNA repair markers. This section revealed

that although cycling cells have a higher apoptotic cells, reduction in the number of foci may indicate that also rapid repair process active in the cycling KG1a cells and slower in the dormancy-enriched KG1a cells.

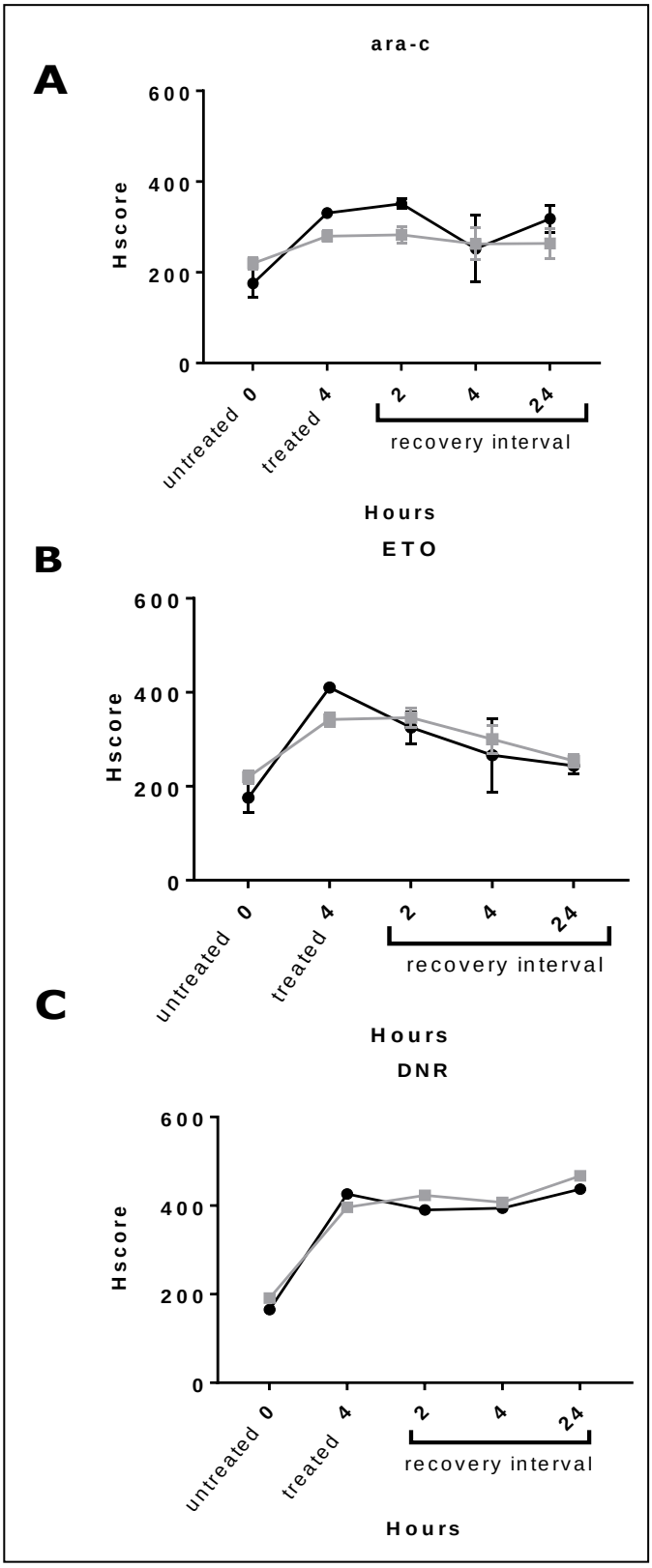

Figure 4.4.2: Immunofluorescence detection of phospho-H2AX139 in cycling KG1a (black lines) and dormancy-enriched KG1a (grey lines) cells after 24 hours of incubation with chemotherapeutic agents followed by 2, 4, or 24 hours of drug-free culture. The graph shows the H-scores calculated from 100 cells for each condition. Detection of phospho-H2AX139 FTIC-conjugated secondary antibody was used to assess DNA repair activity after 24 hours treatment with (A) ara-c, (B) etoposide (ETO), or (C) Daunorubicin (DNR) compared to drug-free culture. Mean and SD were calculated of n=4, independent assays.

4.4.3 DNA repair markers

4.4.3.1 RAD51 protein as a marker of homologous recombination

In order to understand the mechanism underlying DNA repair activation in dormancy-enriched cells, additional DNA repair proteins were investigated. RAD51 protein is a crucial protein in the homologous recombination DSB repair pathway. Distinct RAD51 foci represent sites where the HR process is conducted (Raderschall, Bazarov *et al.* 2002; San Filippo, Sung *et al.* 2008). RAD51 focus formation with DAPI counterstaining was assessed by indirect immunofluorescence in dormancy-enriched cells and cycling cells treated with ara-c or ETO for 4 hours. Figure 4.4.3.1A & B shows representative images of focus formation, with H-scores determined after 4 hours of treatment. Dormancy-enriched cells treated with ETO showed a markedly lower H-score (152) than cycling cells (219) treated with ETO ($p = 0.004$, $n = 3$). ETO invoked considerable damage with the absence of Rad51 foci at 4 hours in dormancy-enriched cells, indicating repair is unlikely to be occurring via the HR pathway. This evidence suggests that the observed differences

between scored RAD51 foci in dormancy-enriched cells reflect HR that is not primarily activated to resolve DSBs, corroborating the findings of previous studies (Mohrin, Bourke *et al.* 2010; Bakr, Oing *et al.* 2015).

Furthermore, to examine the extent to which RAD51 and the HR pathway are important in the resolution of DNA damage in cycling and dormancy-enriched cells, 5 μM B02, a small-molecule inhibitor of RAD51 was used (Huang and Mazin 2014). B02 can enhance the sensitivity of cells to chemotherapeutic agents by disrupting RAD51 binding to DNA. B02 was added to the cell culture and incubated for two hours before cycling and dormancy-enriched KG1a cells were treated with ara-c or ETO and harvested to perform the assay. The rapid effect was observed in a combination of B02 with ara-c or ETO at 4 hours (Figure 4.4.3.1C). Combined treatment with ETO and B02 resulted in a significant increase in apoptosis and reduced cell viability in cycling cells compared to cycling cells treated with ETO alone ($p = 0.03$, $n = 3$). Results of this experiment support our previous finding and demonstrate the importance of Rad51 in the repair of ETO-induced damage in cycling cells, whereas there is no apparent role for Rad51 in the repair of dormancy-enriched cells.

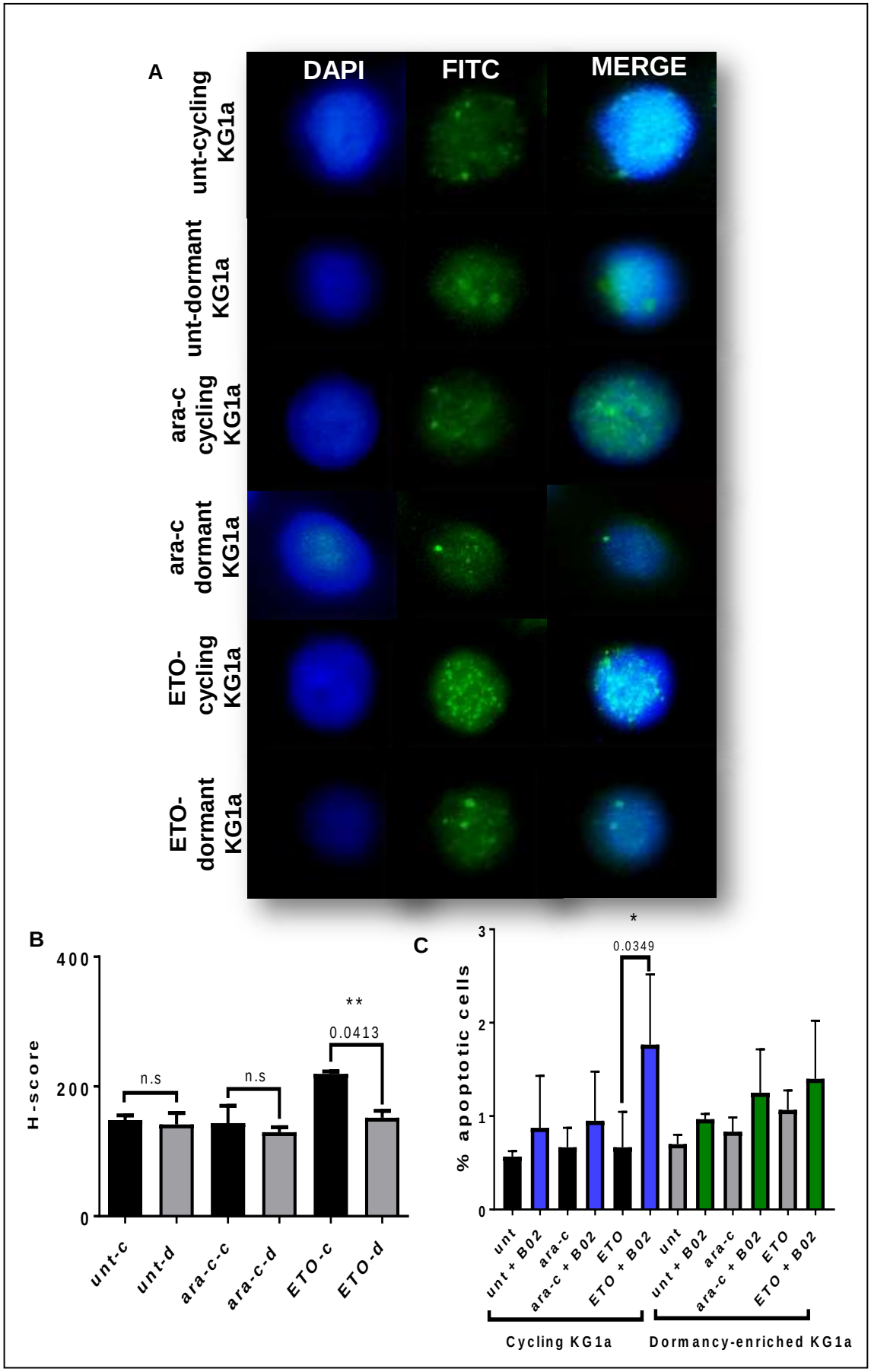
A
DAPI
FITC
MERGE
unt-cycling KG1a
unt-dormant KG1a
ara-c cycling KG1a
ara-c dormant KG1a
ETO-cycling KG1a
ETO-dormant KG1a
B
H-score
400
200
0
n.s
n.s
**
0.0413
unt-c
unt-d
ara-c-c
ara-c-d
ETO-c
ETO-d
C
% apoptotic cells
3
2
1
0
*
0.0349
unt
unt + B02
ara-c
ara-c + B02
ETO
ETO + B02
unt
unt + B02
ara-c
ara-c + B02
ETO
ETO + B02
Cycling KG1a
Dormancy-enriched KG1a

Figure 4.4.3.1: Assessment of the level of RAD51 foci as a marker of homologous recombination in response to DSBs in cycling and dormancy-enriched cells. (A) Representative images of RAD51 focus formation in cycling (black bars) and dormancy-enriched KG1a cells (grey bars) treated with 4.1 μM ara-c and 20 μM etoposide for 4 hours. (B) The H-score for RAD51 foci in (C) cells treated with ara-c, combined ara-c + B02 or ETO, or combined ETO + B02 for 4 hours. Cell viability was assessed via annexin V assay, combined treatment in cycling cells (blue bars), combined treatment in dormancy-enriched cells (green bars). Data represent three independent experiments. Mean and SD were calculated, and * represents a P value of <0.05, ** 0.01, n.s = not significant.

4.4.3.2 Assessment of 53BP1 as a marker of NHEJ

53BP1 protein oligomerizes and is phosphorylated to promote NHEJ and therefore help maintain genome integrity (Zimmermann and de Lange 2014). To further examination how the DSB repair pathway is chosen, we analysed the presence of 53PB1 foci as a marker of NHEJ pathway activity in dormancy-enriched cells. Staining for 53PB1 foci with DAPI counterstaining with assessment by indirect immunofluorescence indicating the activation of NHEJ DNA repair at sites of DNA damage (Figure 4.4.3.2A). Cycling cells and dormancy-enriched cells were treated with ara-c or ETO for 4 hours. Figure 4.4.3.2A shows the formation of a representative focus. A significant elevation in the H-score based on 53BP1 recruitment was observed in dormancy-enriched cells treated for 4 hours with ara-c compared to that in cycling cells ($p = 0.038$, $n = 3$). Similarly, dormancy-enriched cells treated with ETO showed a higher 53BP1 H-score of compare to that in cycling cells ($p = 0.049$, $n = 3$) (Figure 4.4.3.2B). These data imply that there is preferential use of the NHEJ repair pathway in dormancy-enriched cells. Although no detectable damage was seen in response to ara-c at 4 hours, there were a significant number of 53BP

foci. Whether repair induction is very quick or the method for detecting 53BP foci is more sensitive than the comet assay in detecting damage is the subject of further discussion. Taken together, these results demonstrate that dormancy-enriched cells rely on the more error-prone NHEJ mechanism to repair DSBs, and use of this rapid repair mechanism may enhance resistance of these cells to apoptosis (Li and Dalton 2006; Esposito and So 2014).

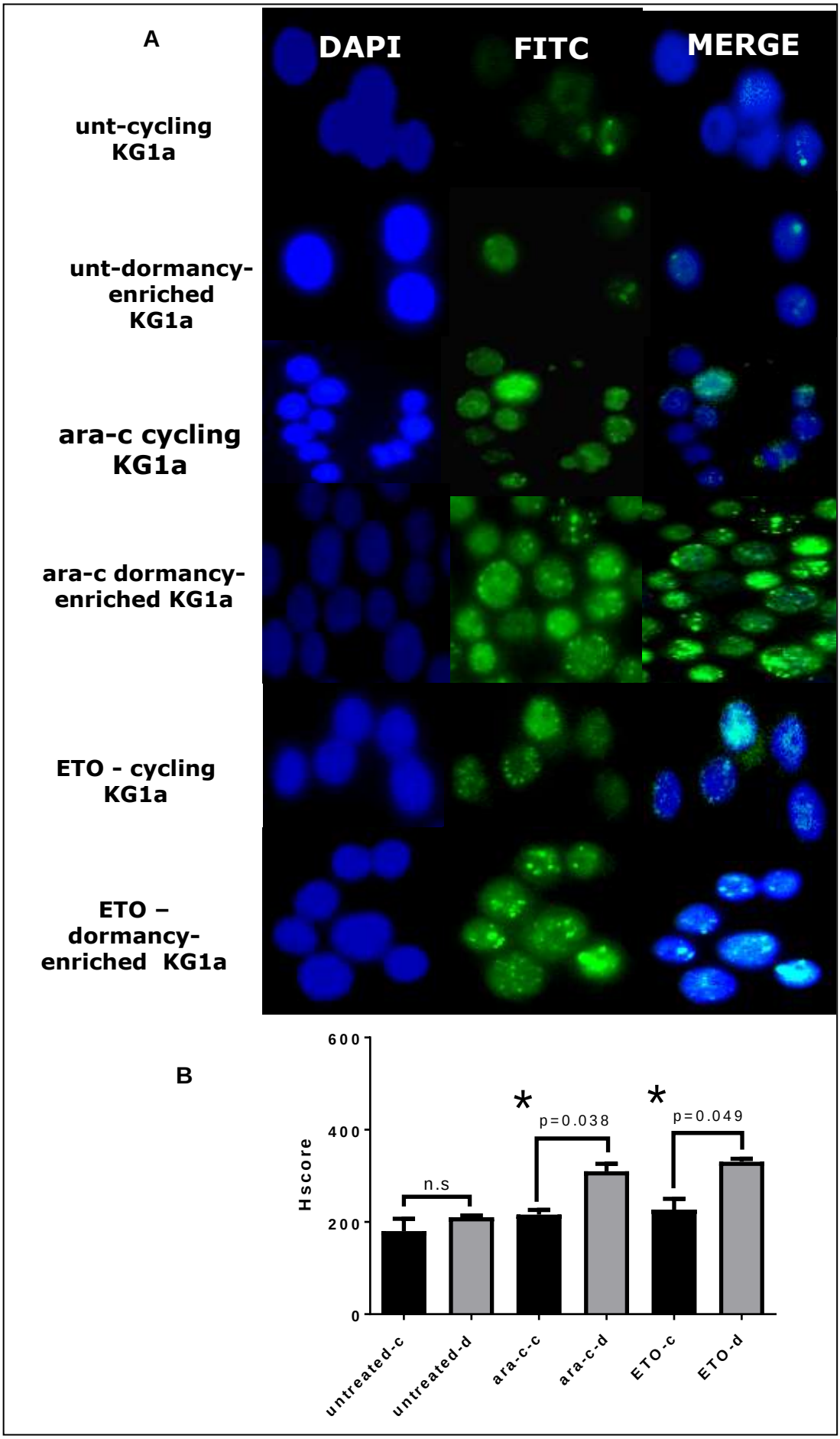
A
DAPI
FITC
MERGE
unt-cycling KG1a
unt-dormancy-enriched KG1a
ara-c cycling KG1a
ara-c dormancy-enriched KG1a
ETO - cycling KG1a
ETO – dormancy-enriched KG1a
B
Hscore
600
400
200
0
n.s
p=0.038
p=0.049
*
*
untreated-c
untreated-d
ara-c-c
ara-c-d
ETO-c
ETO-d

Figure 4.4.3.2: Assessment of the 53BP1 foci as a marker of non-homologous end joining in response to DSBs in cycling and dormancy-enriched cells. (A) Immunofluorescent detection of 53PB1 foci in cycling KG1a and dormancy-enriched KG1a cells treated with 4.1 μM ara-c and 20 μM ETO for 4 hours. (B) H-scores were calculated based on phosphorylated 53BP foci in response to DSBs in both cycling and dormancy-enriched KG1a cells. Mean and SD were calculated of n=3 independent experiments, and * represents a P value of <0.05**,** n.s = not significant.

4.5 Discussion

This chapter focuses on the downstream effectors of the DDR cascade in dormancy-enriched cells compared to cycling cells. Tight orchestration of DNA damage sensors, DNA lesion repair, DNA replication, and cell cycle checkpoint proteins activate checkpoints to arrest cell cycle progression in parallel with DNA repair processes, or, if DNA repair does not occur, the checkpoints can promote senescence or apoptosis (Mandal, Blanpain *et al.* 2011). The ultimate molecular behaviour that determines the path of DNA repair or apoptotic cell death remains incompletely understood in AML. Limited information exists on the damage and repair mechanisms that occur in these cells, resulting in a lack of understanding of how to effectively clear this subpopulation of cells and cure AML. A study of AML samples showed different responses to chemotherapeutic agents between samples, as well as within the same sample (Rosen, Putta *et al.* 2010), and another report demonstrated the role of Chk2 phosphorylation in the DNA damage-induced apoptotic pathway (Tominaga, Morisaki *et al.* 1999; Xu, Tsvetkov *et al.* 2002). Thus, defining the direction of signalling toward repair or death in response to DNA damage was the subject of further investigation in dormancy-enriched cells in our study. The induction of DSBs results in ATM-

dependent phosphorylation of histone H2AX at serine 139 (phospho-H2AX139), a hallmark of DDR. Assessment of phospho-H2AX142 revealed differences in dormancy-enriched and cycling KG1a cell after exposure to ara-c or ETO for 24 hours (Figure 4.2.2). Protein switching between H2AX139 and H2AX142 phospho/dephosphorylation has been observed in a few studies (Cook, Ju *et al.* 2009; Singh, Basnet *et al.* 2012; Jacobs, Misri *et al*. 2016) and therefore we examined phospho-H2AX142 to determine whether it can be used as a marker of cell fate after induction of DSB repair in dormancy-enriched KG1a cells. The decrease in expression of phospho-H2AX142 in dormancy-enriched cells after ara-c or ETO treatment for 24 hours was confirmed by immunoblotting. Additionally, we observed persistence of phospho-H2AX139 foci in cycling KG1a cells. The phosphorylation of H2AX at Ser139, along with phosphorylation at Tyr142, resulted, as expected, in the triggering of apoptosis in cycling cells but not in dormancy-enriched cells. These findings indicate that dormancy-induced KG1a cells are more resistant to apoptosis than cycling KG1a cells (Figure 4.3.2). These observations raise the question of whether dormancy-enriched cells survive because of DNA repair activation via H2AX142.

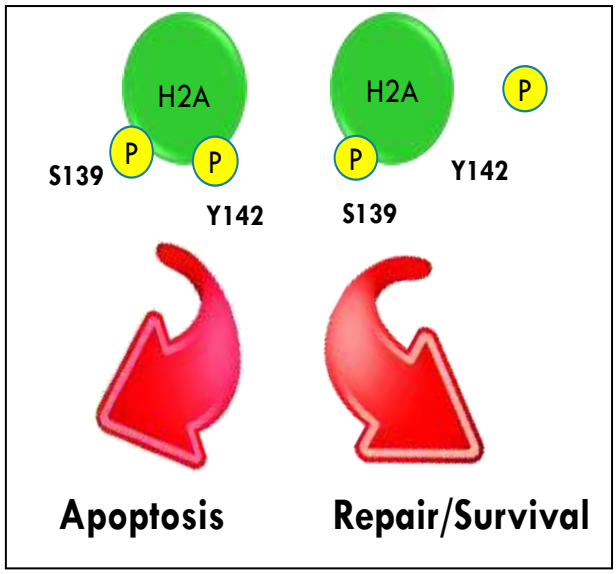

Figure 4.5: Schematic model for H2AX142 phosphorylation in the regulation of apoptosis versus repair response. H2AX142 phosphorylation is involved in determining cell fate with phosphorylated H2AX-Ser139 in dormancy-induced cells. Phosphorylation and dephosphorylation of H2AX142 can indicate whether cells are likely to survive or undergo apoptosis.

Thus, biomarkers of DNA repair stimulation were explored in dormancy-enriched KG1a cells. Standard neutral comet assay of cycling KG1a cells revealed a significant reduction in mean tail moment when the cells were allowed to recover after 4 hours of incubation of cells with ara-c (Figure 4.4.1iA). Although the reduction in mean tail moment was dramatically decreased during recovery in both dormancy-enriched and cycling cells, dormancy-enriched cells showed slower recovery from damaged DNA than that of cycling cells (Figure 4.4.1i A). A significant change in cycling cells was apparent by comet assay at 24 hours of recovery time after DNR treatment, whereas dormancy-enriched cells showed no change during 24 hours

of recovery (Figure 4.4.1i C). Furthermore, differences in cell responses and cell fates may be associated with a difference in cell cycle stages of these cells (Meikrantz and Schlegel 1995; Ma, Kanakousaki *et al.* 2015). Massively damaged cells in the G1/S phase may respond by senescence; however, cells with minor damage in G2/M might exit from the cell cycle (Terasawa, Shinohara *et al.* 2014). We also demonstrated less sensitivity of dormancy-enriched cells compared to that of cycling cells to induction of apoptosis (Figures 4.3.1 and 4.3.2). If a greater percentage of cycling cells were apoptotic during recovery, the reduction in mean tail moment in cycling cells may be because the damaged cells with large tail moments were apoptosing and therefore not available to score. Additionally, earlier studies using a cytotoxicity assay confirmed that immature AML cells were 10–15-fold more resistant to DNR than mature AML cells (Jordan and Guzman 2004; Hauswirth, Florian *et al.* 2007).

Moreover, analysis of phospho-H2AX139 by immunofluorescence staining during recovery showed distinct foci within cell nuclei in both cycling and dormancy-enriched cells. An earlier kinetics study of DNA repair proteins such as phospho-H2AX139, NBS1, BMI1, and 53BP1 in HeLa cells revealed distinct recruitment periods for these proteins to DNA lesions of 2 to 80 minutes after IR (Suchánková, Kozubek *et al*. 2015). H-scores of the number of foci confirmed results of the neutral comet assay of phospho-H2AX139 with less foci scored in cycling cells after 4 hours of treatment with ara-c compared to those in dormancy-enriched cells after the same treatment. However, no significant change was seen in H-scores in dormancy-enriched cells during recovery after ara-c, ETO, or DNR treatment, which might be because of the complexity of chromatin structure disseminating foci assemblies. Rogakau *et al.* reported approximately 2×10^6 base pairs of DNA per DSB are flanked by phospho-H2AX139, indicating that

large amounts of damaged chromatin are in the range of detection by the H2AX assay (Rogakou, Pilch *et al.* 1998).

The HR and NHEJ pathways are responsible for repairing DSBs (Mladenov and Iliakis 2011). Studies have shown that dormant HSCs extracted from mice (Mohrin, Bourke *et al.* 2010) and humans (Rübe, Fricke *et al.* 2011) tend to repair DSBs via the NHEJ repair pathway, which may result in the accumulation of mutations that may then confer radio-resistance and resistance to apoptosis (Igney and Krammer 2002). Therefore, it was valuable to analyse DNA repair markers that might be involved in response to DNA damage to gain a deeper understanding of the molecular mechanism underlying the resistance to chemotherapy of dormancy-enriched cells. Rad51 recombinase is a crucial factor for homologous recombination and DSB repair (Krejci, Altmannova *et al.* 2012; Bakr, Oing *et al.* 2015). Significant increases in RAD51 foci, suggestive of functional repair via the HR repair pathway, were observed in cycling cells 4 hours after treatment with ETO, whereas very few were found in dormancy-enriched cells. This confirms that HR is the preferred repair pathway in proliferating cells, which agrees with previous findings (Deming, Flores *et al*. 2002). The scenario was reversed when we scored 53PB1 foci in dormancy-enriched cells after 4 hours treatment with ara-c or ETO. Dormancy-enriched cells were also able to recover significantly from damage, indicating that the NHEJ repair pathway is an essential mechanism in G0/G1, which agrees with the results of other studies (Mohrin, Bourke *et al.* 2010; Yang, Rudge *et al.* 2013). Evidence that has accumulated over the past decade has defined 53BP1 as a molecular scaffold that recruits DNA repair proteins to sites of DSBs, including the chromatin modulator EXPAND1, which binds to BRCT domains in 53BP1 in a phosphorylation-independent manner, and RAP1-interacting factor 1 (RIF1), which interacts with ATM-residues

at multiple ATM-phosphorylated Ser/Thr-Gln sites in 53BP1, but not in MRE11 (Silverman, Takai *et al.* 2004; Panier and Boulton 2014).

Specific technical issues with immunofluorescence assay of RAD51 foci should be noted. Three different fixation and permeabilization strategies were used to visualize subnuclear foci assembly. In our lab, the standard fixative is 4 % paraformaldehyde, followed by methanol permeabilization for a minimum of 30 minutes (Schnell, Dijk *et al.* 2012), whereas other researchers have studied subcellular localisation using 4 % paraformaldehyde as a fixative and 0.1 % Tween 20 for permeabilization (Schmid, Uittenbogaart *et al.* 1991). However, after several steps to optimise cell type, cell concentration, and intensity, duration, and nature of damage, we found 4 % paraformaldehyde and 0.1 % 100× Triton to be the most efficient preparation to detect RAD51 foci (Bennett, Bewersdorf *et al.* 2009).

Chapter 5: Identification of BTG2 as a Dormancy and

5.1 Background

DNA repair is an essential mechanism for maintaining genetic integrity, correcting lesions and, thus preventing cancer. DNA DSBs are lethal DNA lesions that cause apoptosis of leukemic cells. It is important to understand the mechanisms by which DSBs are sensed and repaired in DLICs; therefore, this chapter describes our endeavours to identify genes, which may be differentially expressed in a dormancy-enriched cell population, in response to genotoxic stress. We conducted quantitative real-time PCR (RT-PCR) and immunofluorescent assays in order to identify candidate genes/proteins. Characteristics of dormancy-enriched cells were also studied using flow cytometry. *BTG2* was one gene identified as a potentially important candidate in promoting dormancy and/or DDR, and the levels of *BTG2* expression in primary samples from patients with AML were examined.

5.2 Analysis of PCR array data and identification of the gene of interest (GOI)

A study conducted in our research group by (Dr. Claire Seedhouse). The 96 well plate for DNA damage signaliing pathway RT^2 profiler PCR Arrays (Qiagen) was used, to detect genes up- or down-regulated by DNA damage, analysing more than 84 genes in addition to the *B2M*, *HPRT1, RPL13A, GAPDH, ACTB* housekeeping genes and assay controls. The profiler plate was used to study expression in dormancy-enriched KG1a cells before and after DNA damage, induced by DNR, and compared to basal and induced gene levels in cycling cells. Six genes out of the 84 DDR genes were shown to be differentially expressed in dormancy-enriched KG1a cells compared with cycling cells, or with DNR for 6 hours compared with untreated cycling or dormancy-enriched KG1a cells (C Seedhouse, unpublished results)

An assessment of basal levels of gene expression, in dormancy-enriched cells, revealed up-regulation of protein 73 (p73), cell death-inducing DFFA-like effector A (CIDEA), poly (rC)-binding protein 4 (PCBP4), B-cell translocation gene 2 (BTG2), ATP transcriptional regulator X-linked (ATRX), and nibrin (NBN), compared with the levels of these proteins in cycling cells. These proteins are known to be involved in multiple biological functions of maintaining cell survival; they are co-factors in DNA damage sensing and repair machinery or apoptosis signalling, such as BTG2, CIDEA and P73. However, three genes were down-regulated two-fold or more, including; *XRCC6BP, GTSE1* and *RAD1.* The down-regulated may have occurred because enrichment of dormancy in these cells lowered the rate of proliferation rate, reflected by *GTSE1*, or because of the absence of DNA damage, in the case of *RAD1* and *XRCC6BP*.

When dormancy-enriched cells were exposed to DNR for 6 hours; the genes *RAD1*, X-ray repair cross-complementing protein 3 (*XRCC3*), fanconi anemia complementation group G (*FANCG*), glycosylphosphatidylinositol anchored molecule-like (*GML*), BTG2, semaphorin 4A (*SEMA4A*), and protein phosphatase 1 regulatory subunit 15A (*PPP1R15A*) were up-regulated two folds or more; the same drug resulted in the up-regulation of *CIDEA* and *p73* in cycling cells. CIDEA was also up-regulated in drug-treated dormancy-enriched cells, but to a lesser extent (less than two-fold), whereas *P73* was actually down-regulated more than two-fold in dormancy-enriched KG1a cells following DNR treatment. Growth arrest and DNA-damage-inducible gamma (*GADD45G*) and *PCBP4* were down-regulated. These down-regulated genes may specifically respond to environmental stresses by mediating the activation of the p38/JNK pathway via MTK1/MEKK4 kinase, or suppressing cell proliferation by inducing apoptosis or cell cycle arrest and DNA repair (Kastan, Zhan *et al.* 1992; Vayssade, Haddada *et al.* 2005). All the genes, showing a two-fold or greater increase, or down-regulation by two-fold or less,

in dormancy-enriched KG1a cells, either at the basal level when compared with cycling cells, or following DNR treatment when compared with untreated cells, are shown in (Table 5.2i) and (Table 5.2ii).

Genes up-regulated in KG1a cells enriched for dormancy Vs cycling KG1a cells			
No.	**Gene symbol**	**Name/Function**	**Fold change**
1	P73	Cell cycle regulation, induction of apoptosis	5.61
2	CIDEA	Cell death activator	2.94
3	PCP4B	purkinje cell protein 4b	2.33
4	**BTG2**	**Transcription regulator - anti-proliferative activity**	**2.19**
5	ATRX	Helicase	2.13
6	**NBN**	**Nibrin – part of DNA damage sensor MRN complex**	**2.01**
7	XRCC6BP	Ku70 binding protein	-2.00
8	GTSE1	G2 And S-Phase Expressed 1	-2.16
9	RAD1	RAD1 checkpoint DNA exonuclease	-2.75

Table 5.2i: Basal-level genes up- or down-regulated in dormancy-enriched KG1a cells compared with cycling KG1a cells. Results were obtained using RT² Profiler PCR Arrays to assess DNA damage signalling, and the fold change is shown. Genes, chosen for further analysis because of their central roles in DDR pathways, are shown in bold.

Genes up- or down-regulated in DNR treated dormancy-enriched KG1a			
No.	**Gene Symbol**	**Gene Name**	**Fold change**
1	ABL1	C-abl oncogene 1, receptor tyrosine kinase	1.2
2	ANKRD17	Ankyrin repeat domain 17	1.06
3	APEX1	APEX nuclease (multifunctional DNA repair enzyme) 1	1.04
4	ATM	Ataxia telangiectasia mutated	1.06
5	ATR	Ataxia telangiectasia and Rad3 related	1.56
6	ATRX	Alpha thalassemia/mental retardation syndrome X-linked	-1.02
7	BRCA1	Breast cancer 1, early onset	1.46
8	**BTG2**	**BTG family, member 2**	**2.01**
9	CCNH	Cyclin H	1.12
10	CDK7	Cyclin-dependent kinase 7	1.07
11	CHEK1	CHK1 checkpoint homolog	1.06
12	CHEK2	CHK2 checkpoint homolog	1.27
13	CIB1	Calcium and integrin binding 1 (calmyrin)	1.08
14	CIDEA	Cell death-inducing DFFA-like effector a	-1.37
15	CRY1	Cryptochrome 1 (photolyase-like)	1.06
16	DDB1	Damage-specific DNA binding protein 1	1.19
17	DDIT3	DNA-damage-inducible transcript 3	1.18
18	DMC1	DMC1 dosage suppressor of mck1 homolog	-1
19	ERCC1	Excision repair cross-complementing rodent repair deficiency, complementation group 1	1.17
20	ERCC2	Excision repair cross-complementing rodent repair deficiency, complementation group 2	1.38
21	EXO1	Exonuclease 1	-1.04
22	**FANCG**	**Fanconi anemia, complementation group G**	**2.42**
23	FEN1	Flap structure-specific endonuclease 1	1.21
24	XRCC6	X-ray repair complementing defective repair in Chinese hamster cells 6	-1.19
25	GADD45A	Growth arrest and DNA-damage-inducible, alpha	-1.18
26	**GADD45G**	**Growth arrest and DNA-damage-inducible, gamma**	**-2.75**
27	**GML**	**Glycosylphosphatidylinositol anchored molecule like protein**	**2.05**

28	GTF2H1	General transcription factor IIH, polypeptide 1	-1
29	GTF2H2	General transcription factor IIH, polypeptide 2	1.03
30	GTSE1	G-2 and S-phase expressed 1	-1.97
31	HUS1	HUS1 checkpoint homolog	-1.08
32	IGHMBP2	Immunoglobulin mu binding protein 2	1.15
33	IHPK3	Inositol hexaphosphate kinase 3	-1.01
34	XRCC6BP1	XRCC6 binding protein 1	1.37
35	LIG1	Ligase I, DNA, ATP-dependent	1.09
36	MAP2K6	Mitogen-activated protein kinase kinase 6	-2.55
37	MAPK12	Mitogen-activated protein kinase 12	1.01
38	MBD4	Methyl-CpG binding domain protein 4	-1.22
39	MLH1	MutL homolog 1, colon cancer, nonpolyposis type 2	1.02
40	MLH3	MutS homolog 3	-1.16
41	MNAT1	CDK-Activating Kinase Assembly Factor 1	1.17
42	MPG	N-methylpurine DNA glycosylase	1.04
43	MRE11A	MRE11A homolog A, double strand break repair nuclease	1.22
44	MSH2	mutS homolog 2	1.15
45	MSH3	mutS homolog 3	-1.08
46	MUTYH	MutY homolog	1.37
47	N4BP2	Nedd4 binding protein 2	1.08
48	NBN	Nibrin	-1.12
49	NTHL1	Nth endonuclease III-like 1	-1.24
50	OGG1	8-oxoguanine DNA glycosylase	1.13
51	**PCBP4**	**Poly(rC) binding protein 4**	**-2.54**
52	PCNA	Proliferating cell nuclear antigen	1.2
53	AIFM1	Apoptosis-inducing factor, mitochondrion-associated 1	-1.25
54	PMS1	PMS1 postmeiotic segregation increased 1	1.37
55	PMS2	PMS2 postmeiotic segregation increased 2	1
56	PMS2L3	Postmeiotic segregation increased 2-like 3	-1.04
57	PNKP	Polynucleotide kinase 3'-phosphatase	1.05
58	PPP1R15A	Protein phosphatase 1, regulatory (inhibitor) subunit 15A	1.59
59	PRKDC	Protein kinase, DNA-activated, catalytic polypeptide	1.2
60	**RAD1**	**RAD1 homolog**	**2.87**
61	RAD17	RAD17 homolog	-1.15
62	RAD18	RAD18 homolog	1.18
63	RAD21	RAD21 homolog	-1.08
64	RAD50	RAD50 homolog	-1.16
65	RAD51	RAD51 homolog (RecA homolog, E. coli)	1.23
66	RAD51L1	RAD51-like 1	1.08

67	RAD9A	RAD9 homolog A	1.16
68	RBBP8	Retinoblastoma binding protein 8	-1.04
69	REV1	REV1 homolog	1.54
70	RPA1	Replication protein A1	1.06
71	SEMA4A	Sema domain, immunoglobulin domain (Ig), transmembrane domain (TM) and short cytoplasmic domain, (semaphorin)	1.31
72	SESN1	Sestrin 1	-1.03
73	SMC1A	Structural maintenance of chromosomes 1A	1.11
74	SUMO1	SMT3 suppressor of mif two 3 homolog 1	-1
75	TP53	Tumor protein p53	1.33
76	**TP73**	**Tumor protein p73**	**-6.98**
77	TREX1	Three prime repair exonuclease 1	1.37
78	UNG	Uracil-DNA glycosylase	-1.05
79	XPA	Xeroderma pigmentosum, complementation group A	-1.01
80	XPC	Xeroderma pigmentosum, complementation group C	1.4
81	XRCC1	X-ray repair complementing defective repair in Chinese hamster cells 1	1.14
82	XRCC2	X-ray repair complementing defective repair in Chinese hamster cells 2	1.06
83	**XRCC3**	**X-ray repair complementing defective repair in Chinese hamster cells 3**	**2.44**
84	ZAK	Sterile alpha motif and leucine zipper containing kinase AZK	1.57
85	B2M	Beta-2-microglobulin	1.11
86	HPRT1	Hypoxanthine phosphoribosyltransferase 1 (Lesch-Nyhan syndrome)	1.14
87	RPL13A	Ribosomal protein L13a	-1.02
88	GAPDH	Glyceraldehyde-3-phosphate dehydrogenase	-1.12
89	ACTB	Actin, beta	-1.09

Table 5.2ii: All genes, up- or down-regulated, in dormancy-enriched KG1a cells following DNR treatment compared with untreated dormancy-enriched KG1a cells. Results were obtained using RT² Profiler PCR Arrays to assess DNA damage signalling; the fold change is shown for five up-regulated genes and three down-regulated genes in dormancy-enriched KG1a cells. Genes in bold were chosen for further analysis because of their central roles in DDR pathways.

5.3 Confirmation of DDR (GOI) expression by RT-PCR

In recent years, there have been several studies on the tightly regulated networks of genes that recognize DNA damage and activate DNA repair via transcriptional up-regulation and post-translational modifications; we aimed to identify a positive regulator and therefore, focused only on the up-regulated genes in this study. Following a literature search, five of these genes were selected for further analysis because of their central roles in the DDR pathways, and their association with the ATM/ATR signalling network and transcriptional target of DDR. These genes were *FANCG* (De Winter, Van Der Weel *et al.* 2000; Xie, De Winter *et al.* 2000; Pulliam-Leath, Ciccone *et al.* 2010; Wang and Gautier 2010), *RAD1* (Bao, Tibbetts *et al.* 2001; Niida and Nakanishi 2006; Esposito and So 2014), *XRCC3* (Tallman, Gilliland *et al.* 2005; Martinez-Marignac, Rodrigue *et al.* 2011), *NBN* (Williams, Williams *et al.* 2007; Hartlerode, Morgan *et al.* 2015), and *BTG2* (Duriez, Moyret-Lalle *et al.* 2004; Choi, Kim *et al.* 2012). Even though it was not up-regulated significantly in the super arrays, we also examined *RAD50* because of its crucial role in coordinating the sensing and detection of DSBs, DNA binding, cell-cycle checkpoint signalling cascades, initiation of DNA DSB end resection, and its function in the MRN complex, which facilitate DSB repair (Cerbinskaite, Mukhopadhyay *et al.* 2012).

Basal levels of *FANCG, RAD1, XRCC3, RAD50, NBN,* and *BTG2* expression were measured in the dormancy-enriched KG1a model to confirm the results of the PCR super array. Figure 5.3 shows that no differences in expression between the cycling and dormancy-enriched cells were found for *RAD50* ($p = 0.5992$, $n = 4$), *FANCG* ($p = 0.2540$), *RAD1* ($p = 0.5731$), *NBN* ($p = 0.8073$), or *XRCC3* ($p = 0.1634$) ($n = 4$). In contrast, *BTG2* was clearly up-regulated in dormancy-enriched cells ($p = 0.0013$) ($n = 8$). Therefore, *BTG2* was explored further, as described in the following sections.

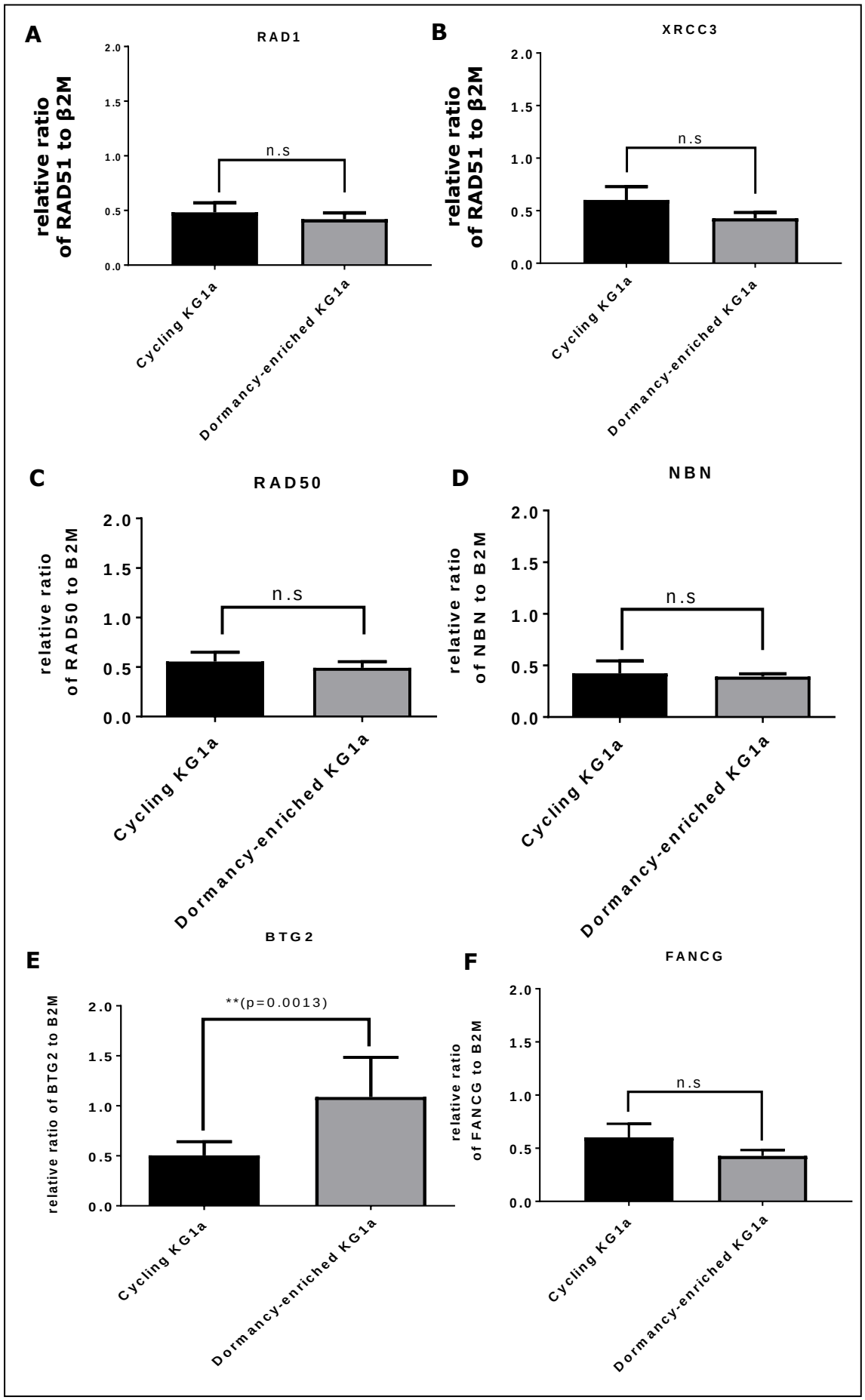
A
RAD1
relative ratio of RAD51 to β2M
2.0
1.5
1.0
0.5
0.0
n.s
Cycling KG1a
Dormancy-enriched KG1a
B
XRCC3
relative ratio of RAD51 to β2M
2.0
1.5
1.0
0.5
0.0
n.s
Cycling KG1a
Dormancy-enriched KG1a
C
RAD50
relative ratio of RAD50 to B2M
2.0
1.5
1.0
0.5
0.0
n.s
Cycling KG1a
Dormancy-enriched KG1a
D
NBN
relative ratio of NBN to B2M
2.0
1.5
1.0
0.5
0.0
n.s
Cycling KG1a
Dormancy-enriched KG1a
E
BTG2
relative ratio of BTG2 to B2M
2.0
1.5
1.0
0.5
0.0
**(p=0.0013)
Cycling KG1a
Dormancy-enriched KG1a
F
FANCG
relative ratio of FANCG to B2M
2.0
1.5
1.0
0.5
0.0
n.s
Cycling KG1a
Dormancy-enriched KG1a

Figure 5.3. Expression of DNA repair genes in dormancy-enriched cells (grey bars) compared with that in cycling cells (black bars). Relative ratios from real-time PCR for (A) *RAD1* (n = 4), (B) *XRCC3* (n = 4), (C) *RAD50* (n = 4), (D) *NBN* (n = 4), (E) *BTG2* (n = 8), and (F) *FANCG* (n = 4) are plotted on the y-axes. *β2M* was used to normalize gene expression. Each condition was assessed in triplicate and data are shown as mean and SD. n.s: not significant. ** P < 0.01.

5.4 BTG2 sequencing

BTG2 is one of 109 recurrently mutated genes were significantly implicated in malignancies due to its multiple functions in cell differentiation, cell cycle control and regulation of apoptosis (Morin, Mendez-Lago *et al*. 2011; Powell, Shao *et al.* 2016). KG1a cells were sequenced to exclude the possibility that it is mutated in these cells. Primers were designed to amplify the BTG2 coding region, and the conditions for PCR amplification were optimised with respect to the annealing temperature and $MgCl_2$ concentration. Figure 5.4i indicates the presence of PCR products at 1.5 mM $MgCl_2$ and an annealing temperature 63°C; therefore, because of the presence of single, tight, bright bands, these conditions were used for amplification prior to sequencing. PCR products were loaded to onto 2 % agarose gels and run with a 1000-bp DNA ladder. As expected, an approximately 472-bp product was found, and contamination was ruled out as no band was seen in the no template control. As shown in Figure 5.4ii, sequencing of BTG2 PCR products, analysed using Genemapper software (Applied Biosystems), confirmed that BTG2 in the KG1a cell line is wild type matched to control sequences in the literature (NCBI reference sequence: NM_006763.2).

.

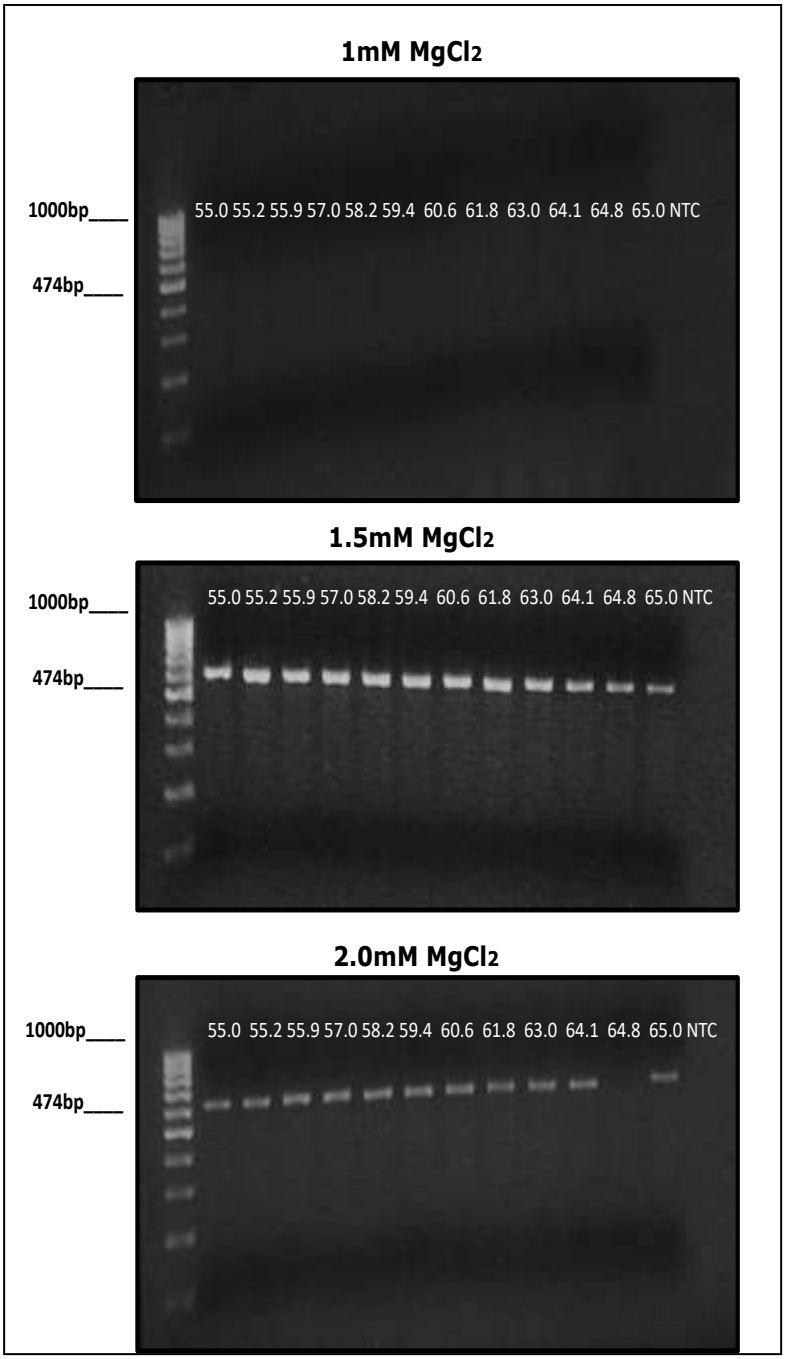

Figure 5.4i: PCR optimization of BTG2 primers. The BTG2 primers were optimized at three different MgCl2 concentrations and a range of annealing conditions. A 1000-bp loading marker was used in the 2 % agarose gel.

A KG1a Forward:

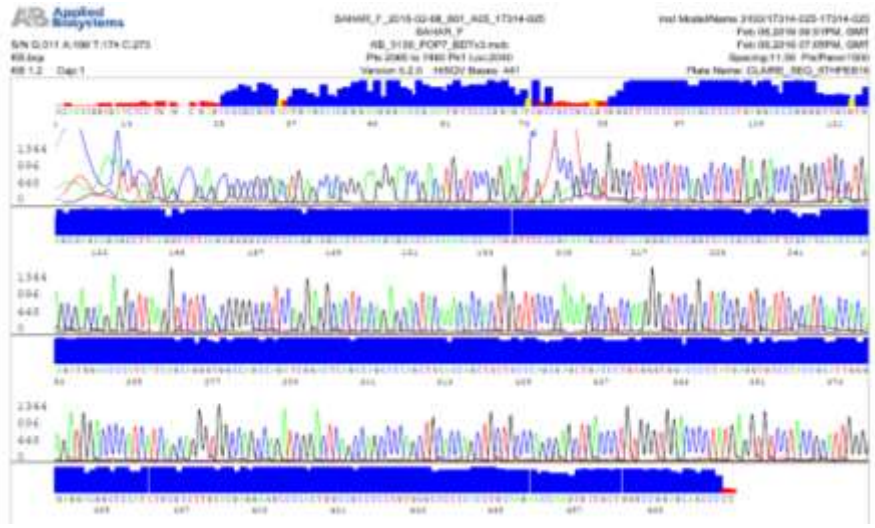

B KG1a Reverse:

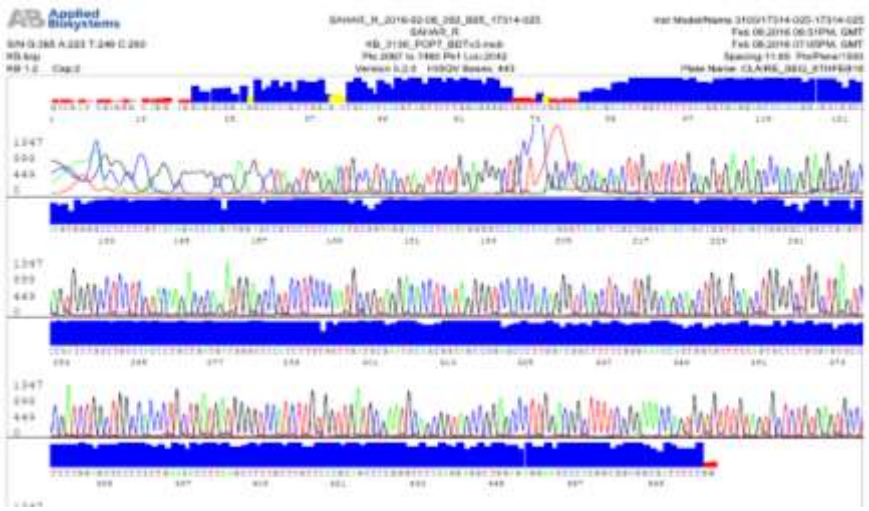

Figure 5.4ii: Electropherograms of wild-type BTG2 sequence in the KG1a AML cell line. (A) Forward primer. (B) Reverse primer.

5.5 Identification of BTG2 as a dormancy marker in AML models

5.5.1 Expression of BTG2 in dormancy-enriched cell models

Studies have shown that BTG2 is expressed during the G0/G1 cell phase, and that levels decline as cells enter the cell cycle (Tirone 2001; Mollerstrom, Kovacs *et al.* 2010; Zhang, Chen *et al.* 2011). Therefore, in this section, we present the hypothesis that *BTG2* is a dormancy marker in AML dormancy-enriched models. Quantitative RT-PCR was used to analyse the expression of *BTG2* transcripts in dormancy-enriched and cycling cells in three AML cell line models: KG1a, TF1a, and M091. The TF1a and M091 cells were enriched for dormancy during a project run by (Dr.Mazin Alasadi), from our group. Because of its involvement in numerous biological processes, including inhibition of proliferation and maintaining HSC quiescence in the BM, TGFβ was chosen to enrich dormancy in AML cells *in vitro* (Yamazaki, Iwama *et al.* 2009) (section 1.6). Cells were exposed to TGFβ for 24 to 72 hours and displayed dormancy features and enriched stemness properties with insignificant induction of apoptosis. The cDNAs for TF1a-TGFβ and M091-TGFβ were kindely donated by (Dr.AL Asadi) from our group, in this study to explore BTG2 as a novel dormancy marker in dormancy-enriched *in vitro* AML models using M091-TGFβ, TF1a-TGFβ, and KG1a-rapamycin. Figure 5.5.1A shows that the levels of *BTG2* expression, in untreated M091 cycling cells, were similar to those in cells that were cultured with TGFβ for 72 hours ($p = 0.4983$, $n = 2$). In contrast, TF1a-enriched dormancy resulted in significant up-regulation of *BTG2,* after 72 hours of exposure to TGFβ, compared with that in untreated cycling TF1a cells (Figure 5.5.1B, $p = 0.0313$, $n = 8$). BTG2 was also induced in KG1a cells, enriched for dormancy by 48 hours of culture with rapamycin (Figure 5.5.1C) ($p = 0.0001$, $n = 8$). In summary, the hypothesis stating that the expression of *BTG2* is associated with dormancy-signature in *in vitro* AML dormancy-models, was rejected.

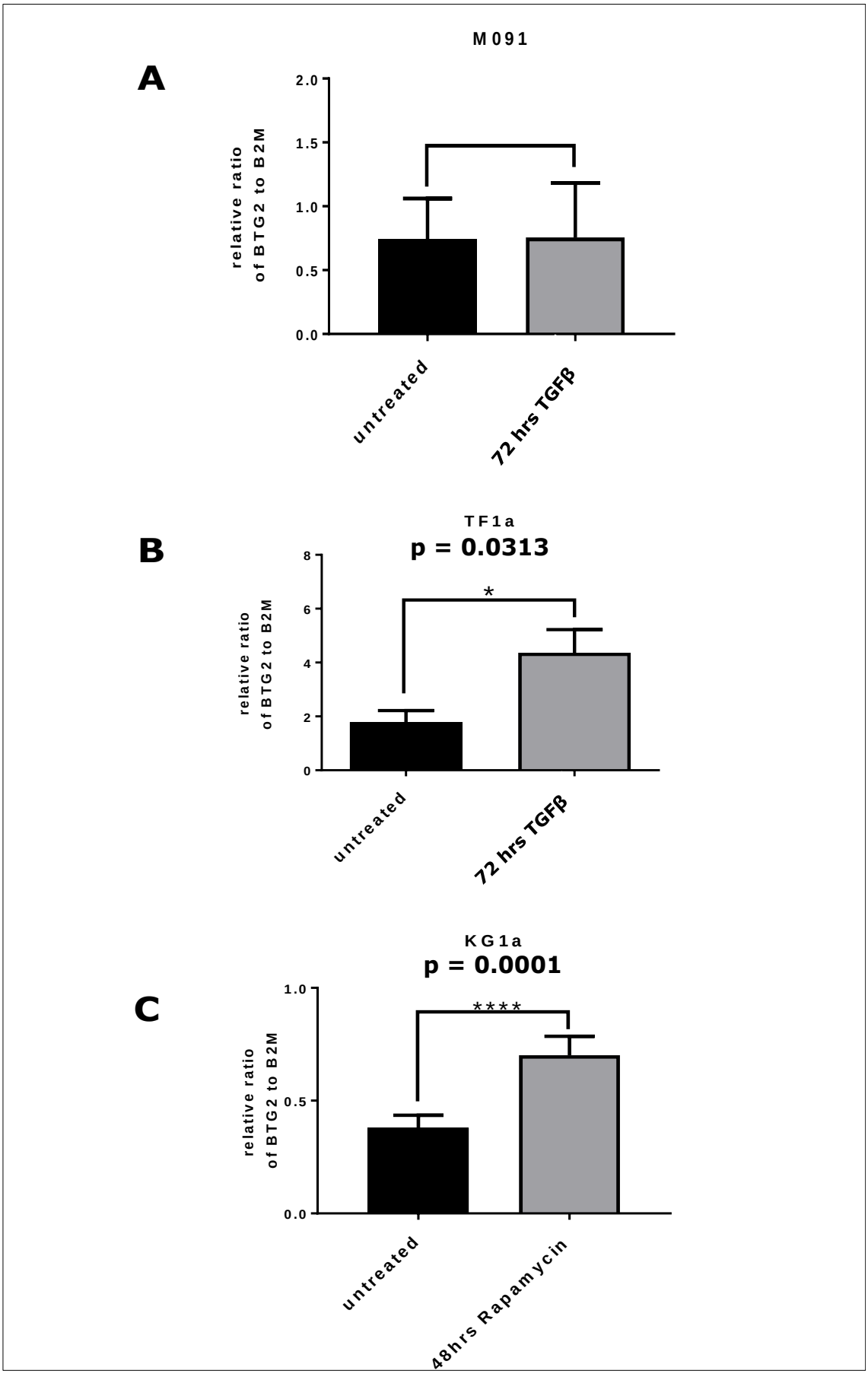
A
M091
relative ratio of BTG2 to B2M
2.0
1.5
1.0
0.5
0.0
untreated
72 hrs TGFβ
B
TF1a
p = 0.0313
*
relative ratio of BTG2 to B2M
8
6
4
2
0
untreated
72 hrs TGFβ
C
KG1a
p = 0.0001
****
relative ratio of BTG2 to B2M
1.0
0.5
0.0
untreated
48hrs Rapamycin

Figure 5.5.1: Identification of BTG2 as a dormancy marker in dormancy-enriched models (grey bars) compared with cycling cells (black bars). (A) Non-significant expression of BTG2 in the M091 cell line after 72 hours of incubation with TGFβ (n = 2). (B) BTG2 was highly expressed in TF1a after exposure to TGFβ for 72 hours (n = 8). (C) Significant expression of BTG2 was detected in KG1a cells, after exposure to rapamycin for 48 hours, compared with that in untreated cycling cells (n = 14). Each experiment was conducted in triplicate and repeated individually; data are shown as mean **±** SD; *P <0.05; ****P <0.0001.

5.5.2 Analysis of *BTG2* expression in primary AML patients' samples

In a previously characterised set of primary AML samples, several molecular and dormancy markers had been studied, including Ki-67. Ki-67 is a nuclear protein expressed during cell proliferation throughout the G1/S and G2/M cell cycle phases (Jaroslav, Martina *et al.* 2005). Variable levels of Ki-67 have been found in primary samples, both when examined in the total blast population (proginitors cells) and when gated on primitive CD34+CD38− cells (unpublished work by Dr Monica Pallis) (Table 5.5.2). Because we were interested in the possibility that *BTG2* might be more highly expressed in dormant rather than in cycling cells. Thus, this experiment aimed to investigate by RT-PCR whether the expression of *BTG2* was inversely proportional to the expression of Ki-67. Table 5.5.2 presents *BTG2* expression levels in the primary cells. A significant positive correlation was found between *BTG2* expression levels and the percentage ki67+ CD34+ CD38− cells (rho = 0.8095, p = 0.0218) (Figure 5.5.2 B), and an insignificant correlation was found between BTG2 expression levels and the percentage of cells that were ki-67+ blasts (rho = 0.326, p = 0.226) (Figure 5.5.2 A). In summary, the hypothesis stating that the expression of *BTG2* is associated with dormancy-signature in primary AML samples, was rejected.

No.	Sample ID	Percentage ki67+ blasts	Percentage ki-67+ CD34+ CD38−	*BTG2* expression
1	668	37	12	**2.67**
2	661	41	NA	**2.18**
3	149223	51	NA	**NA**
4	608	69	27	**1.96**
5	672	37	31	**4.67**
6	665	34	11	**7.75**
7	151701	42	NA	**10.25**
8	151363	7	NA	**4.90**
9	150428	81	94	**11.54**
10	151283	38	42	**4.17**
11	663	41	NA	**5.05**
12	148549	72	78	**9.71**

Table 5.5.2: *BTG2* expression with respect to Ki-67 levels in CD34+CD38− and blasts from patients with AML. Each sample was conducted in triplicate with individual experiment repeat. β2M was used to normalize *BTG2* gene expression.

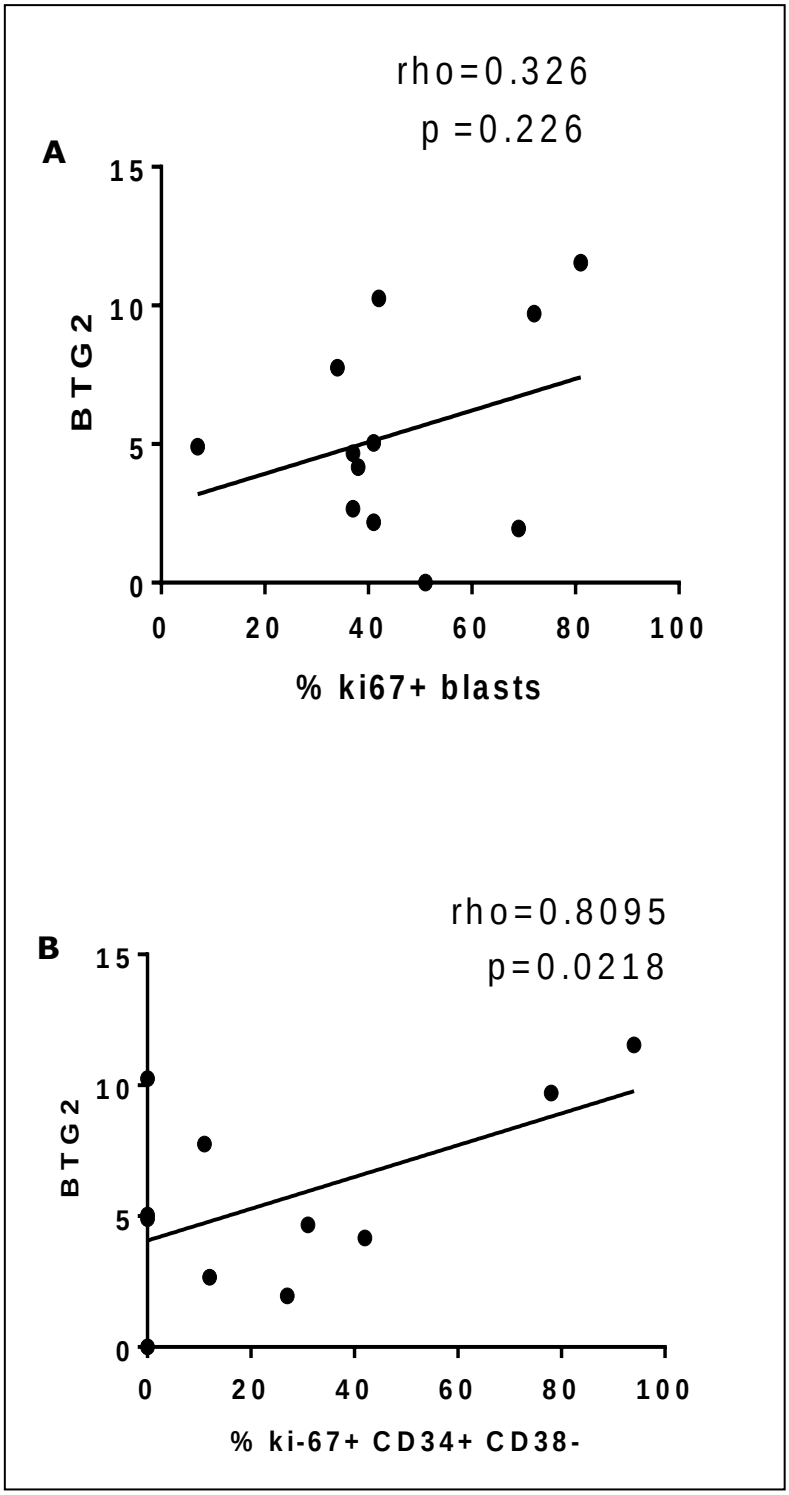

Figure 5.5.2: The correlation between ki-67 proliferation marker and *BTG2* expression. The Spearman's correlation (rho) factor and p values are shown. A correlation was observed between (A) *BTG2* and ki-67 blasts and between (B) *BTG2* and Ki-67+CD34+CD38-) cells.

5.6 Up-regulation of BTG2 in ETO-induced cycling cells and dormancy-enriched cells

Previous work on BTG2 expression is contradictory. It has been shown to be induced during chemotherapy-mediated apoptosis in cancer cells (Lim, Park *et al.* 2008). *BTG2* overexpression has also been shown to increase the radio-sensitivity of breast cancer cells *in vitro* and *in vivo* (Hu, Xing *et al*. 2012) and to halt progression of cells from the G1 to S phase (Montagnoli, Guardavaccaro *et al.* 1996; Gothot, Pyatt *et al.* 1997; Lim, Lee *et al.* 1998). In contrast, another study revealed that up-regulation of *BTG2* contributed to an increase in overall cancer survival and enhanced cell resistance to treatment (Mollerstrom, Kovacs *et al.* 2010).

Figure 5.6A shows that *BTG2* expression increased when cycling cells were treated with ETO for 24 hours ($p = 0.0019$, $n = 8$). To quantify the degree of apoptosis, flow cytometric analysis of c-PARP in treated cycling and dormancy-enriched cells compared to that in untreated control cells was performed in parallel with an RT-PCR assessment of *BTG2* expression. An increase in cleaved PARP was also observed in cycling ($p = 0.0032$, $n = 8$), but not in dormancy enriched cells when treated with ETO for 24 hours indicating that dormancy-enriched cells exhibit a markedly lower DNA damage threshold for ETO-induced *BTG2* expression and apoptosis. (Figure 5.6B). These results were confirmed by an analysis of protein expression for cycling and dormancy-enriched before and after 4 and 24 hours treatment with ETO (Figure 5.6C), and semiquantitivaly estimated by densitometry using Image Lab™ software for total protein normalization on western blots of BTG2 protein expression (Figure 5.6D).

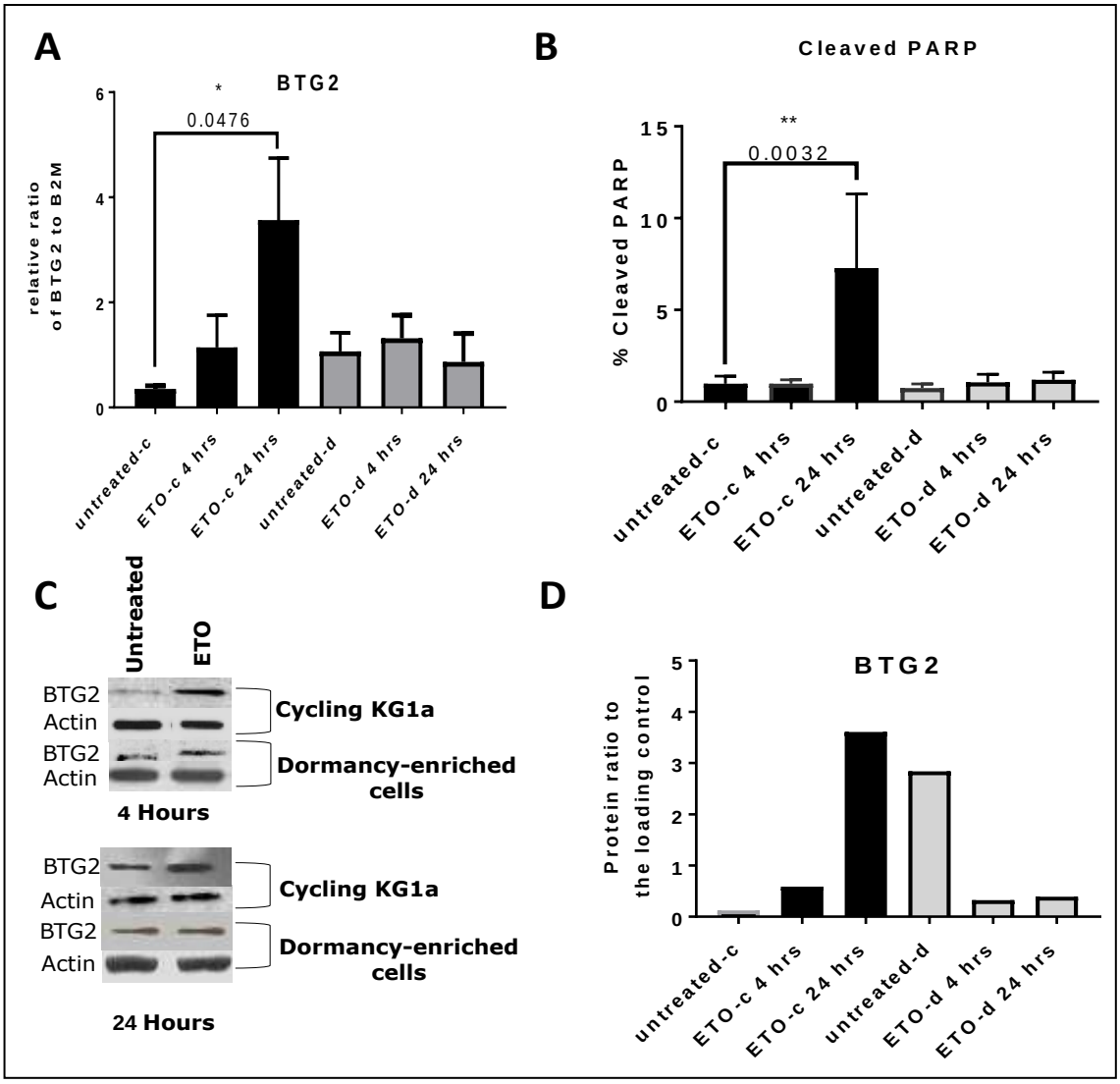

Figure 5.6: Up-regulation of BTG2 in ETO-induced cycling and dormancy enriched cells at 24 hours. (A) RT-PCR analysis for BTG2 expression following 4 and 24 hours of ETO treatment in cycling cells (black bars) and dormancy-enriched cells (grey bars)(n=8). (B) Flow cytometric measurement of c-PARP in cycling and dormancy-induced KG1a cells following ETO treatment. (n=8). (C) Detection of BTG2 at the protein level by western blotting (n=1). (D) Densitometry measurements of BTG2 protein expression (n=1). Each condition was conducted in triplicate with individual experiment repeat. Data represent mean and SD and **P < 0.01.

5.7 Investigation into the regulation of *BTG2* expression via the NF-κB pathway

The genomic structure of BTG2 reveals the presence of six p53-response elements in the promoter and one for NF-κB, implying that NF-κB may be an upstream stimulator of BTG2 expression (Duriez, Falette *et al.* 2002; Shman, Fedasenka *et al.* 2008; Sundaramoorthy, Ryu *et al.* 2013). Additionally, we previously found a 32 % reduction in ROS in dormancy-enriched KG1a cells compared to actively cycling cells (Pallis, Burrows *et al*. 2013). Studies have shown that HSCs have a lower level of basal ROS, known to regulate NF-κB (Myint and Lucie 1992; Zhang, Niu *et al*. 2003; Guzman 2005; Jang 2007). Furthermore, nuclear translocation of NF-κB has been detected in AML cells but not in normal cells (Hehner, Hofmann *et al.* 1999; Pyatt, Stillman *et al.* 1999; Guzman 2005). Because KG1a is a p53 mutated cell line, the hypothesis was that BTG2 expression in cycling and dormancy-enriched KG1a cells is regulated via NF-κB pathway. Therefore, we decided to investigate the relationship between the nuclear translocation of NF-κB (p65) and BTG2 expression to establish whether activation of the ROS-NFκB-BTG2 pathway is likely involved in DDR. Parthenolide (PTH) was used in these experiments as a potent inhibitor of NF-κB activation by binding IκB-kinase (IKK) or directly binding to the p65 subunit of NF-κB.

5.7.1 Preliminary work to determine PTH sensitivity

Dormancy-enriched and cycling cells were treated with different concentrations of PTH for 24 hours to establish an appropriate concentration to use when detecting NF-κB translocation. Figure 5.7.1 shows no differences in cell viability between cycling and dormancy-enriched cells in response to treatment with 1 μM PTH at 24 hours; however, cell viability decreased dramatically with increasing PTH concentrations in cycling cells. Dormancy-enriched KG1a cells showed a lower percentage of viable cells after 24 hours of incubation (86.57

%) compared to that in treated cycling cells (100 % viable) (Figure 5.7.1). Therefore, 1 µM and 10 µM were selected as PTH doses for further experiments to limit its cytotoxic effects.

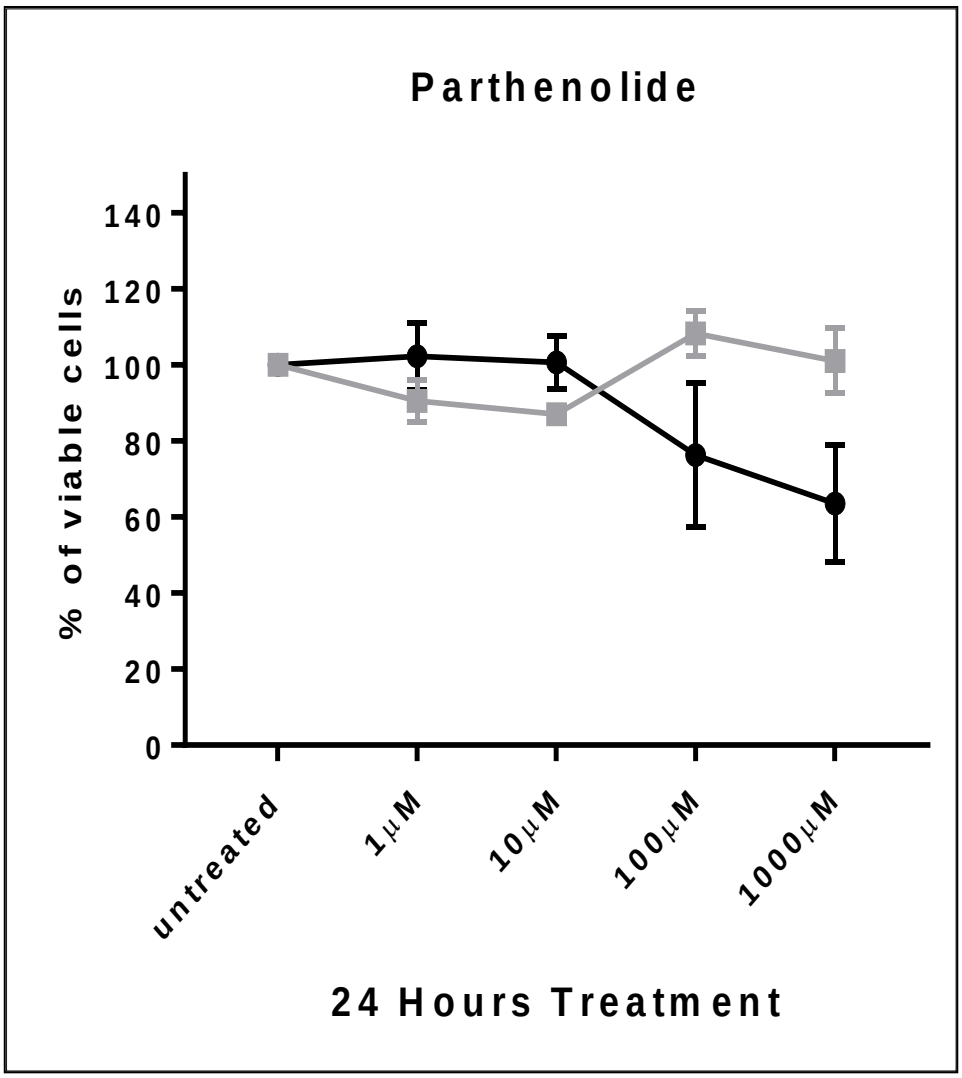

Figure 5.7.1: Cell viability after PTH treatment for 24 hours. Dormancy-enriched cells (grey line) and cycling cells (black line) were treated with PTH at different concentrations, and cell viability was assessed by FSC flow cytometric analysis. Each condition was conducted in triplicate. Data represent mean and SD for n=4 inependent assays.

5.7.2 No evidence that Parthenolide inhibits translocation of NFκB (p65) in cycling and dormancy-enriched KG1a cells

In human AML cells treated with PTH, inhibition of NF-κB activation via PTH binding to IKK has been demonstrated (Hehner, Hofmann *et al.* 1999). This binding inhibits degradation of IκB with the subsequent inhibit translocation of the activated form of NF-κB to the nucleus and NF-κB binding to target DNA (Guzman, Rossi *et al.* 2005; Zahedpanah, Shaiegan *et al.* 2016) and enhances transcription. In this study, cells were treated with 1 μM and 10 μM PTH based on results of a dose-finding experiment (section 5.7.1).

The nuclear localisation of NF-κB (p65) in cycling and dormancy-enriched cells was analysed via indirect immunofluorescence staining. NF-κB (p65) in both untreated cycling and untreated dormancy-enriched cells, accumulated in the cytoplasm (Figure 5.7.2A & B), where it is inactive. Figure 5.7.2A shows nuclear translocation of NF-κB in cycling cells after incubation with 1 μM or 10 μM PTH. In contrast, translocation of NF-κB from the cytoplasm to the nucleus does not appear to occur in dormancy-enriched cells (Figure 5.7.2 B). This may suggest that actively cycling cells can escape the action of PTH result in translocation of NF-κB into the nuclease. However, there is no nuclear translocations of NF-κB were observed in dormancy-enriched cells.

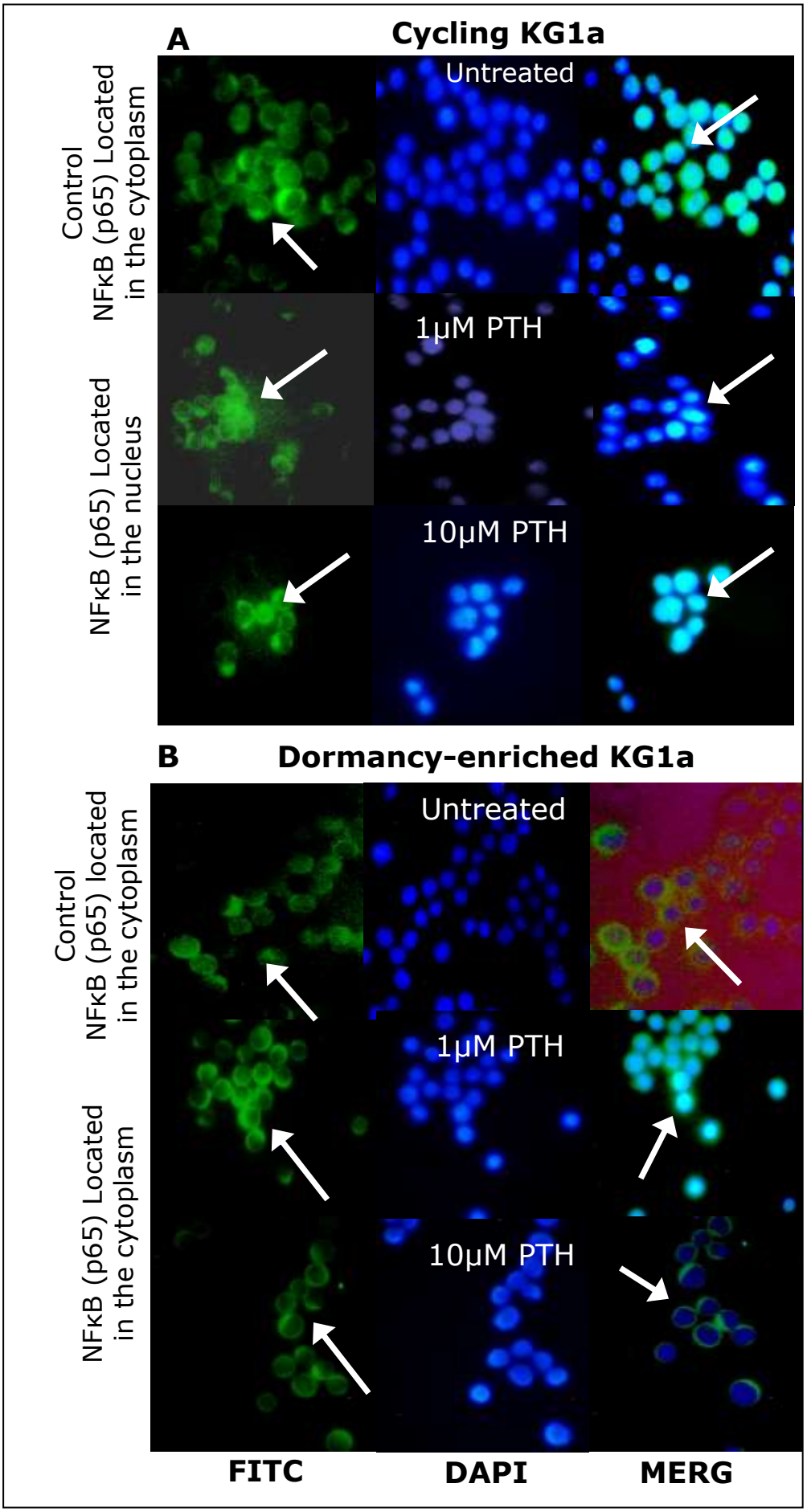
A
Cycling KG1a
Untreated
1μM PTH
10μM PTH
Control NFκB (p65) Located in the cytoplasm
NFκB (p65) Located in the nucleus
B
Dormancy-enriched KG1a
Untreated
1μM PTH
10μM PTH
Control NFκB (p65) located in the cytoplasm
NFκB (p65) Located in the cytoplasm
FITC
DAPI
MERG

Figure 5.7.2: The nuclear localization of NFκB (p65) in cycling and dormancy-enriched KG1a in response to PTH treatment for 24 hours. (A) treated cycling cells show translocation of (p65) compared to untreated cells and (B) accumulation of (p65) in cytoplasm of dormancy-enriched before and after PTH treatment, and these cells treated with 1 μM and 10 μM PTH. Images are representative of two independent experiments, and arrows indicate cytoplasmic and nuclear translocation of NFκB (p65).

5.7.3 Measurement of BTG2 in response to NF-κB inhibition by PTH

BTG2 expression is reported to be down-regulated significantly with low intracellular ROS, and generation of ROS may mediate NF-κB activation resulting in BTG2 transcription (Imran and Lim 2013). This expeirment aiming to investigate wheather the *BTG2* expression after cycling and dormanc-enriched cell treatment with 1 μM and 10 μM of PTH enhances the anti-oxidant defence and provide additional barrier for cells to increase cells resistance for apoptosis. As shown in Figure 5.7.3, expression of *BTG2* eximened by RT-PCR in both cycling and dormancy-enriched KG1a cells showed no significant *BTG2* induction following PTH treatment; however, the error bars are large because of experimental variation. Although this expeirmant conducted twice, but this data indicate that cells may have an alternative pathway to mediate cell survival and escape apoptosis rather that ROS-NF-κB pathway.

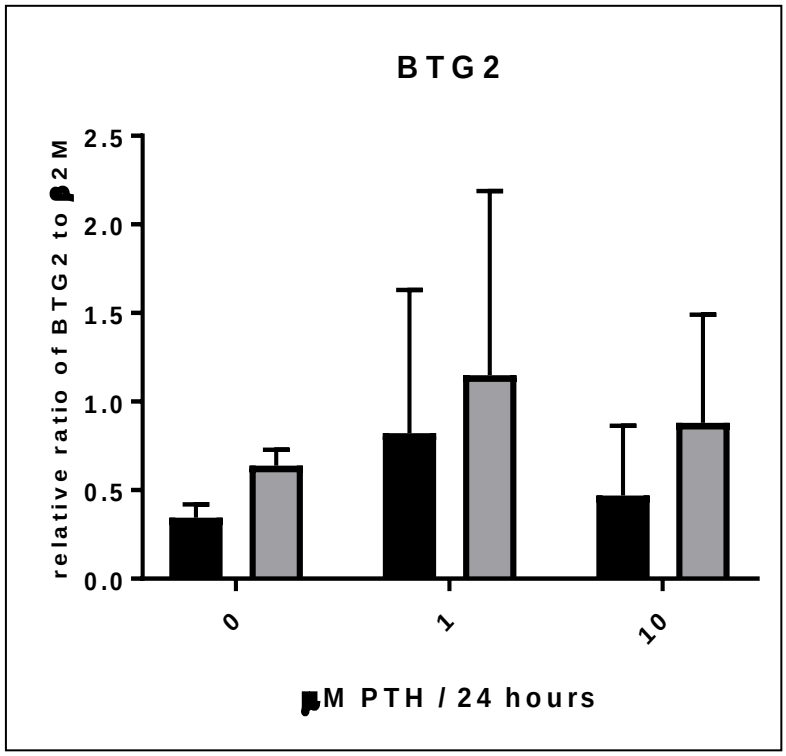

Figure 5.7.3: *BTG2* expression in response to PTH in dormancy-enriched KG1a cells compared to cycling cells. *BTG2* was highly expressed in untreated dormancy-enriched cells (grey bars) compared to cycling cells (black bars), but there were no apparent differences after 24 hours of treatment with 1 μM or 10 μM PTH. β2M was used to normalize *BTG2* gene expression and each condition was conducted in triplicate with individual experiment repeats. Data represent mean and SD for n=2 experiments.

5.8 Discussion

In this chapter, six genes (*FANCG, RAD1, XRCC3, RAD50, NBN*, and *BTG2*) were identified as potentially differentially involved in DNA damage recognition and repair in cycling and dormancy-enriched cells. These genes were chosen from a list of up-regulated genes, as assessed by RT^2 Profiler PCR Arrays, used to examine DNA damage signalling in dormancy-enriched KG1a cells. Previous studies, conducted in our laboratory were inconclusive with respect to the role of down-regulated genes, such as *p73*; this may have stemmed from its involvement in multiple biological processes and signalling pathways (unpublished work). Therefore, assessment of the down-regulated genes was excluded from this study; additionally, their role in promoting stemness was not assessed by these PCR arrays. Further exploration of the literature revealed that the up-regulated genes are involved in DDR pathways and mediate adaptive responses to genotoxic stress. Nevertheless, the assessment of basal expression levels of *FANCG, RAD1, XRCC3, RAD50, NBN*, and *BTG2* by RT-PCR indicated significantly higher expression of *BTG2* only in dormancy-enriched KG1a cells compared with that in cycling KG1a cells. Theses findings may support the usefulness of KG1a-rapamycin model as a robust AML cell line model enriched for dormancy. However, the primary data, obtained using n=1 compared with RT-PCR, is yet unconfirmed, and requires additional primary data and gene expression profiling.

BTG2 expression can be regulated both positively and negatively through different signalling pathway networks (Goss and Chambers 2010; Saito, Uchida *et al.* 2010; Imran and Lim 2013). Down-regulation of BTG2 is mediated by JAK2/STAT3 signalling via indirect regulation by ROS (Quy, Choi *et al.* 2013). The expression of BTG2 is induced by various stimuli such as UV IR (Hu, Xing *et al.* 2012), ROS, and other DNA-damaging agents (Shman, Fedasenka *et al.* 2008). Gene expression profiling has previously identified BTG2 as a

transcriptional cofactor and downstream effector of p53 (Mao, Xiao *et al.* 2015). A number of studies have shown that BTG2 expression is induced through a p53-dependent mechanism and modulates the cell cycle and cellular responses to DNA damage (Cortes, Moyret-Lalle *et al.* 2000; Ryu, Lee *et al.* 2004; Powell, Shao *et al.* 2016). Conversely, BTG2 can be expressed, in a p53-independent manner, in response to DNA damage via posttranslational modifications, including phosphorylation, glycosylation, methylation, ubiquitination, or acetylation (Ryu, Lee *et al.* 2004; Peters and Schwaller 2011; Choi, Kim *et al.* 2012; Duan and Walther 2015).

The p53 mutational status in KG1a cells was determined previously (Banker, Groudine *et al.* 1997) and confirmed in our laboratory by (Dr.Seedhouse). KG1a cells have a 5-base pair insertion in p53. It is unclear how mutations in BTG2 affect the function of the gene products. Mutated *BTG2* disrupts of various cellular processes such as anti-proliferative activity (Doidge, Mittal et al. 2012). In our study, measurements of protein expression, at different time points after drug/inhibitor treatment, were challenging and yielded inconsistent results. Therefore, BTG2 sequencing was performed to rule out the possibility of BTG2 mutations. HL-60 cells, treated with ROS-inducing agents, show BTG2 expression that is up-regulated in a time-dependent manner (Imran and Lim 2013). BTG2 is also rapidly induced in response to genotoxic stress. In addition, the average half-life of BTG2 is less than 1 hour in eukaryotic cells, and BTG2 is easily degraded by the ubiquitin–proteasome system; this may hamper the detection of the protein (Varnum, Reddy *et al.* 1994; Sasajima, Nakagawa *et al.* 2002). However, in this study, the protein expression of BTG2 was detected for up to 24 hours, which differs from previous studies.

BTG2 was also expressed, at a significantly higher level, in the second dormancy-enriched model (TF1a-TGFβ) than in the cycling cell controls, confirming its role as an anti-proliferative gene. In contrast,

there was no difference in the expression of *BTG2* between dormancy-enriched and control M091-TGFβ cells. Of note, KG1a and TF1a cell lines both have a primitive $CD34^{+}38^{-}$ phenotype, unlike the M091 cells used to confirm our assumption on dormancy-enrichment differences with respect to phenotypic features. Additionally, both KG1a-rapamycin and TF1a-TGFβ dormancy models have been established in our laboratory, as robust *in vitro* models, to mimic and explore the properties of DLICs and find future AML treatment strategies. The results on *BTG2* may indicate that biological differences, between primitive and more mature AML cells, have important implications for the molecular signature of dormant cells; these findings may highlight the differences in responses to chemotherapeutic agents. Increased expression of *BTG2*, in both KG1a and TF1a dormancy models implies that BTG2 is associated with the slow rate of proliferation in these cells. Nevertheless, the M091 cells may depend more on other anti-proliferative molecules such as p57 and Kip2 (Borriello, Caldarelli *et al.* 2011).

It is important to note know that enrichment for dormancy *in vitro* can result in acquisition of multiple drug resistance, a $CD34^{+}$ $CD38^{-}$ phenotype, lower levels of ROS, and a weaker expression of Ki-67, ALDH, and CD117, in cellular models of in AML. Our data suggest that each *in vitro* model of AML has specific dormancy characteristics that depend on the origin of the cell line and concentrations of external or internal cytokines or inhibitors that are used at the phenotypic signature and molecular levels (Pallis, Burrows *et al.* 2013). The molecular signature has been studied in KG1a-rapamycin and TF1a-TGFβ dormancy-enriched models in our laboratory, confirming that *BTG2* is expressed at high levels before and after genotoxic stress (unpublished data). The data, obtained using RT^{2} Profiler PCR Arrays to examine DNA damage signalling, showed only genes expressed specifically in response to DNA damaging agents (the anthracyclins ETO or DNR); gene expression profiling for TF1a-TGFβ revealed

insignificant induction in baseline expression of DNA damage-signalling genes. Nevertheless, none of these were triggred after ETO treatment, indicating that each *in vitro* model has a different dormancy feature and/or responses to the genotoxic stress. These differences also demonstrate the heterogeneity of AML and obstacles to control AML relapse.

BTG2 expression was also studied using cDNA extracted from a primary samples obtained from patients with AML. Twelve samples were analysed for *BTG2* as a potential dormancy marker, and the results were compared with the levels of proliferation biomarker Ki-67. The correlation between BTG2 and primitive cells (CD34-CD38+) and more mature (blast) cells with different cytogenetic profiles was positive rather than the expected negative correlation. This may be because primary cells are no longer in their natural environment.

In this work, *BTG2* expression was significantly up-regulated in cycling cells after ETO treatment; this corresponded with the induction of substantial levels of apoptosis in these cells. No change was detected in cell viability or *BTG2* expression in dormancy-enriched cells. These data may indicate that BTG2 is stimulated in a negative feedback mechanism in response to ETO. Increased BTG2 expression leads to reduced transcription of cyclin D1 and activity of CDK4, which are required for cell cycle progression in response to retinoic acid treatment; this induces arrest of cell-cycle (Donato, Suh *et al.* 2007) or apoptosis in response to stress conditions (Tirone 2001; Imran, Park *et al.* 2012).

Furthermore, a pioneering study explored the expression of *BTG2* in response to treatment with doxorubicin or H_2O_2 in the HL-60 leukemic cell line; the results indicated that NF-κB activation modulates BTG2 expression via activity of protein kinase C (PKC) (Imran and Lim 2013). Significant induction of BTG2 after 3 hours of treatment, revealed sensitivity of this response to increased levels of intracellular ROS. Conversely, HL-60 cells, exposed to H_2O_2, failed to induce *BTG2*

expression. When induction of ROS was blocked by N-acetyl-L-cysteine (NAC), a significant reduction in *BTG2* expression was observed, with nuclear translocation of p65 in a Doxo-dependent manner (Imran and Lim 2013). ROS stimulate NF-κB activation, resulting in phosphorylation at Ser-32 and Ser-36 of IκB-α and Ser-19 and Ser-23 of IκB-β, subsequent ubiquitination of β-transducin repeat-containing protein (βTrCP) followed by degradation by the 26S proteasome (Hinz and Scheidereit 2014). Dimerization of NF-κB leads to its translocation into the nucleus, where it may bind to the BTG2 promoter.

In addition, parthenolide (PTH), a sesquiterpene lactone isolated from the herb feverfew (Tanacetum parthenium), is agent used in this study to blocks the activation of NF-κB (Hehner, Hofmann *et al.* 1999)(Figure 5.8). PTH prevente the degradation of IκB-α and IκB-β without interfering with the DNA binding activity of activated NF-κB; this is achieved by inhibition of IkB kinase and/or direct modification of the p65 protein, resulting in stabilization of cytoplasmic IκB-α, which, in turn, inhibits NF-κB translocation. PTH also inhibites of IL-6 induced gene expression by blocking STAT3 phosphorylation on Tyr705 and dimerization required for nuclear translocation (Sobota, Szwed *et al.* 2000).

PTH induces intracellular ROS and subsequent LSC cytotoxicity via extracellular binding events that initiate apoptotic cascades after NF-κB inhibition, proapoptotic p53 activation, and cellular oxidative stress (Guzman, Rossi *et al.* 2005; Baranello, Bauer et al. 2015). Our data revealed cytoplasmic accumulation of NF-Kb (p65) in dormancy-enriched cells after incubation with PTH for 24 hours, which is similar to what was observed in untreated control cells. However, cycling cells have shown nuclear translocation of NF-κB after treatment with PTH. This result is suggests that basal expression of *BTG2* in dormancy-enriched KG1a cells may play a protective role against oxidative stress. Which agrees with several studies (Sundaramoorthy,

Ryu *et al.* 2013; Hinz and Scheidereit 2014). The induction of ROS expression, after 1 hour of treating HL-60 cells with 12-O-tetradecanoylphorbol-13-acetate (TPA), confirmed nuclear translocation of p65 and the recruitment of p65 to BTG2, as determined by chromatin immunoprecipitation (Chip) assay. These results strongly indicate that TPA-induced transcription of BTG2 is regulated via the p53-independent ROS–NF-κB pathway (Imran and Lim 2013), but this did not occur in KG1a cells treated with PTH.

Taken together, these data suggest that inhibition of NF-κB activity, via PTH, does not affect BTG2 expression. Although RT-PCR showed higher expression of BTG2 in dormancy-enriched cells compared with those in cycling cells, the role of BTG2 in dormancy-enriched cells in response to DNA DSBs, is not entirely clear. Cleaved PARP, found in association with upregulated BTG2 in ETO-treated cycling cells (but not in dormancy-enriched cells) suggests that BTG2 upregulation is part of the resistance mechanism. Concurrently, the fact that BTG2 expression did not increase further in dormancy-enriched cells may indicate that ETO did not induce as much damage in cycling cells as indicated by earlier findings in (chapter 3). Accumulated DNA damage was detected in dormancy-enriched cells after 24- hour treatment with ara-c or ETO, with increasing levels of phosphorylated ATM, γH2AX, and Chk2. These data contradict a study, showing that increased expression of BTG2, and down-regulation of Chk2-T68 phosphorylation, accelerates the repair of etoposide-induced DNA damage, as indicated by clearance of phospho-H2AX139 foci in cycling cells (Choi, Kim *et al*. 2012). Additional molecules involved in NF-κB regulation, such as the IKK complex, as well as ROS generation and phosphorylation of ATM, should be examined in dormancy-enriched KG1a cells; the effect of post-translational modification on BTG2 interactions with other DDR molecules should be examined as well.

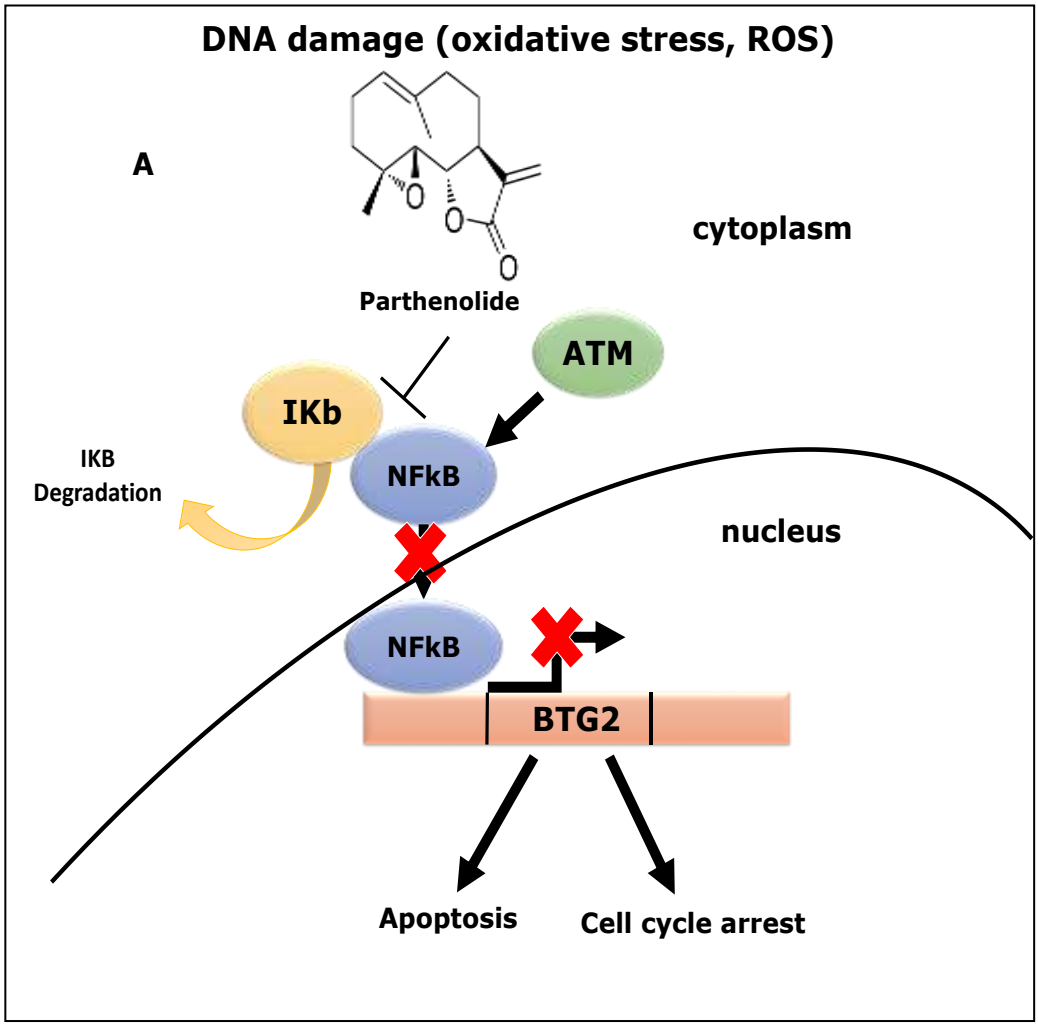

Figure 5.8: Proposed mechanism of action and regulation of BTG2 expression via ROS–NFκB pathway under stress conditions.

Chapter 6: General Discussion and Concluding Remarks

6.1 General discussion

Although 60–70 % of patients with *de novo* AML achieve initial CR, a high proportion of these patients relapse, and eventually die, from the disease (Lai and Kondo 2006; Döhner, Weisdorf *et al.* 2015; Ramos, Mo *et al.* 2015). Relapsed AML is the most common cause of treatment failure among haematological cancers. The relapse is may result from residual leukemic subclones, derived from the founding clone, which may have gained mutations and resistance to therapy and become the dominant aberrant cell clone harboured in the BM niche (Tallman, Gilliland *et al*. 2005; Ding, Ley *et al.* 2012). These cells may be present in tiny numbers and may be undetectable using standard molecular techniques; they are known as dormant leukemic initiating stem cells (DLICs) (Guan and Hogge 2000; Guan, Gerhard *et al.* 2003; Dick 2005; Wilson, Oser *et al.* 2007; Yoriko, Naoyuki *et al.* 2010; Nishioka, Ikezoe *et al.* 2013; Sheng-Dong, Yang *et al.* 2013). Identifying DLICs is a major challenge to eradication; this results from the non-specificity of their cell-surface biomarkers and molecular behaviour. Several studies have investigated the molecular and cellular properties of cancer stem cells to improve targeted therapies; however, only limited research has explored the mechanisms of DDR and repair of DSBs in this primitive and undifferentiated human DLIC population. Thus, we investigated the hypothesis stating that dormancy supress cellular sensitivity to chemotherapeutic drugs and DLICs possess unique strategies for handling DSBs compared with the strategies of cycling leukemic cells (CLCs). The aim of this study was to determine how cells with similar properties to those of DLICs, respond to chemotherapy.

Three main objectives were pursued in this project to understand the behaviour of DLICs compared with that of the more rapidly dividing progenitor cells (the dormancy-enriched cells established in our laboratory). First, using the neutral comet assay, we measured the

amount of DNA damage induced by treating cells with conventional AML chemotherapy drugs (those commonly used to induce DSBs) or an agent being tested in clinical trials (chapter 3). Second, in response to the induced damage, phosphorylation of the main DDR molecules was analysed using flow cytometric and immunofluorescence assays. Third, determining cell fate, and whether these cells stimulate DNA repair mechanisms or undergo apoptosis, was a particular focus of this work (chapters 4 & 5).

Studies on AML rely on the use of AML cell lines, xenografts, primary cell cultures and/or genetically engineered mice (McCormack, Bruserud *et al.* 2005; Kennedy and Barabe 2008; Cook and Pardee 2013; Aroua, Sarry *et al.* 2015). In practice, however, it is difficult to implement a wide range of experimental applications in animal models, or cells isolated from AML patients, because of high costs and ethical issues. Cell lines provide a feasible alternative to, and help overcome, these issues; they are easy to manipulate and characterise at the molecular level. Dormancy-enriched AML cell lines were used in this study to identify critical pathways involved in DLIC resistance to chemotherapy.

HSCs and LSCs reside mainly in the soft, spongy tissue, in hypoxic microenvironments; these conditions maintain and regulate stem cell haematopoiesis in the hollow spaces of bone interior called the bone marrow (BM) (Morrison and Scadden 2014). BM consists of a dense neurovascular network and is enriched for arterioles and capillaries in the endosteum, with large sinusoids located throughout the central bone marrow cavity (Zhang, Niu *et al.* 2003; Wilson, Oser *et al.* 2007). Cellular BM niches contain stromal elements including perivascular mesenchymal stromal cells (MSCs), endothelial cells, differentiated osteoprogenitors and adipocytes, megakaryocytes, macrophages, and osteoclasts. These diverse cell types release signals, soluble factors, and cell surface ligands that control the

different HSCs fates such as mobilization (e.g., VCAM1 and CXCL12), quiescence (TGFβ1, TPO, CXCL4, SCF, CXCL12, and ANGPT1), and differentiation (IL-7, EPO, Notch ligands, FGF1) (Kopp, Avecilla *et al.* 2005; Stier, Ko *et al.* 2005; Sugiyama, Kohara *et al.* 2006; Yoshihara, Arai *et al.* 2007).

To mimic the bone marrow microenvironment surrounding DLICs, we attempted to establish a model *in vitro* culture system of dormancy, which would enable us to study the DNA damage responses following chemotherapeutic treatment. After a detailed analysis of the of methods, used to induce exist of the cell cycle in other cancer cells, enrichment of dormancy in an AML cell line model was undertaken in our laboratory. Unsuccessful trils have made previously by serum withdrawal, serum starvation, nutrient withdrawal, hypoxia and mitogen or growth factor withdrawal all led to induce statistically significant levels of apoptosis with board of AML cells lines.

During this project, it has been shown that the enrichment of dormancy in M07e AML cell line using TPO in presence and absence of GM-CSF was challenging. M07e is GM-CSF-dependent cell line, withdrwal of GM-CSF led to stress the cells and prime apopstosis within 72 hours. Alternatively, culturing M07e with TPO alone has shown cells survive for 14 days, without significant cell duplication. Nevertheless, growing M07e with TPO in presence GM-CSF revealed inconsistence cell proliferation. Attepts to optomize approprtiate concentrations of TPO with different concentrations of GM-CSF failed. A possible explanation for the different behaviour of M07e may be because TPO with M07e needs an additional mixture of factors and cytokines to promote cell quiescence rather than to be used as a single cytokine to enriche dormancy *in vitro.* This is one of the drowbacks and obstecals to enriche dormancy *in vito* culture system. Each AML cell line have special characteristics and grown with or without additional growth factrs. Some cell lines showed sufficient

response to induce dormancy features, others requires at least two or more. Due to time constructions, a standard dormancy model was established previously; KG1a-rapamycin, have been used insteated of M07e-TPO to explore DNA damage responses and repair in dormant cells.

Dormancy-enriched cells with mTOR inhibition showed initial success, which makes this model highly attractive for future preclinical efficacy studies of novel agents. Culturing the KG1a cell line for 2 to 11 days continuously, with an mTOR pathway inhibitor, pushes the cells out of the cell cycle and produces a cell population with features of dormant leukemic cells found in the BM, such as slow-cycling cells with low RNA content and low basal formation of ROS (Pallis, Burrows *et al.* 2013; Pallis, Harvey *et al.* 2016). Halting chemotherapy returns proliferative capacity and the ability to establish colonies; this is similar to DLIC recurrence, which is characterised by chemotherapy resistance in AML patients.

We evaluated the efficiency of ara-c, ETO, and DNR in inducing DNA damage; we also evaluated the sensitivity of cycling and dormancy-enriched KG1a cells to these drugs by establishing to the IC_{10}-$IC_{20,}$ to ensure that a sufficient number of cells were damaged without causing death of all cells. We also evaluated TG02, a novel agent for targeting leukemic cells being tested in clinical trials. Responses to DNA damage, induced by chemotherapy, can generate detectable levels of DNA strand breaks in minutes to hours (Boehrer, Ades *et al*. 2009; Murray, Stiff *et al.* 2012; Pallis, Burrows *et al*. 2013). In our study, two time points, at 4 and 24 hours, were selected to monitor early and late responses to DSBs in the AML cell line. Numerous studies have evaluated the response of DLICs damaged by chemotherapeutics (Maugeri-Saccà, Bartucci *et al.* 2012; Louka, Boutou *et al.* 2015; Chen, Dong *et al.* 2016; Li, Zhou *et al.* 2016); however, we found that examining DSBs first may provide a deeper

understanding of the widely varied responses in DLICs, compared with those in undamaged cells, and/or cells treated with a different DNA damaging agent.

An assessment of DNA damage revealed significantly lower levels of DSBs after 4 hours of treatment with ara-c or ETO in dormancy-enriched KG1a cells compared with those in cycling cells; however, this phenomenon was reversed at the 24-hour time point. Our results showed an increase in damaged DNA in dormancy-enriched cells after 24 hours of ara-c or ETO treatment. This finding may indicate that DNA damage accumulated in dormancy-enriched cells, whereas actively cycling cells were able to stimulate the DDR machinery to trigger apoptosis; this agreed with the results of other studies (Rübe, Fricke *et al.* 2011).

The presence of DSBs rapidly stimulates a DDR cascade via formation of the MRN complex, consisting of Mre11, Rad50, and NBS; this leads to phosphorylation of ATM, followed by activation of downstream damage response proteins (Bakkenist and Kastan 2003; Kastan 2008). In our study, ATM phosphorylation was similar in dormancy-enriched KG1a and cycling cells after 24 hours of treatment with ara-c or ETO. Additionally, flow-cytometric analysis of the levels, of phospho-H2AX139, a hallmark of DDR, showed either the absence, or significantly lower levels of phosphorylation in dormancy-enriched cells compared with those in cycling KG1a cells after ara-c or ETO treatment. The findings on phospho-H2AX139 were confirmed by an assessment of foci by H-scoring. This observation contradicts: (i) studies indicating that DNA-dependent protein kinase (DNA-PK) cooperates with ATM and ATR to phosphorylate proteins involved in the DNA damage checkpoints; and (ii) studies showing that ATM plays a dominant role in H2AX phosphorylation in response to DNA damage (Tanaka, Halicka *et al.* 2007; Callén, Jankovic *et al.* 2009; An, Huang *et al.* 2010; Guo, Deshpande *et al.* 2010). These data may

indicate that pATM and phospho-H2AX139 are not associated with dormancy-enriched KG1a cells; this agrees with studies showing that H2AX is phosphorylated independently of ATM upstream signalling, after IR, *in vivo* (Koike, Mashino *et al.* 2008).

Examining additional downstream DDR markers, such as phosphorylated Chk2-Thr68, again showed the persistence of phospho-Chk2 over 24 hours in both cycling and dormancy-enriched cells. This result suggests that checkpoints slow down DNA replication, to ensure that the DNA breaks are repaired, and to prevent the transfer of defective DNA to progeny cells (Kastan and Bartek 2004; Niida and Nakanishi 2006). The levels of pATM and pChk2 do not appear to correlate with DSB levels in cycling or dormancy-enriched KG1a cells, agreeing with past observations (Boehrer, Ades *et al.* 2009; Halicka, Ozkaynak *et al.* 2009).

Conversely, there has been a growing interest in understanding the mechanisms that regulate chemotherapeutic resistance and fates of DLICs. Accumulating evidence has shown that DSBs induce phosphorylation of H2AX at Ser139 over megabases of chromatin around nucleosomes (Rogakou, Pilch *et al.* 1998; Ali, Zhang *et al.* 2004; Murray, Stiff *et al.* 2012; Jacobs, Misri *et al.* 2016). Additionally, in higher eukaryotes under normal conditions, the Williams–Beuren syndrome transcription factor kinase (WSTF) constitutively phosphorylates H2AX at tyrosine 142 (Cook, Ju *et al.* 2009; Xiao, Li *et al.* 2009). Phosphorylation of novel histone H2AX, at C-terminus of tyrosine 142 (H2AX142), occurs as a result of further post-translational modification (PTM) of H2AX; phosphorylation at this site implicated in the modulation of DDR and cell fates (Cook, Ju *et al.* 2009; Rossetto, Truman *et al.* 2010; Jacobs, Misri *et al.* 2016). With respect to DNA damage, the H2AX142 residue can remain phosphorylated or dephosphorylated by the phosphatases eyes absent homologue 1 (EYA1) and EYA3. Subsequent

dephosphorylation of H2AX142 enhances MDC1 and ATM recruitment to maintain phospho-H2AX139. A regulatory mechanism, controlling H2AX phosphorylation, is mediated by WSTF (Xiao, Li *et al.* 2009). conversely, the loss of WSTF activity leads to defects in Tyr 142 phosphorylation (Lagadinou, Ziros *et al.* 2008). Activation of the WSTF complex is frequently associated with cells in the late S-phase (Culver-Cochran and Chadwick 2012). The fact, that WSTF associates with replicated DNA, provides further evidence that cycling cells are primed for apoptosis more than are dormancy-enriched cells after induction of DNA damage. Recent work, published by Jacobs *et al.,* revealed that normal stem cells are highly radiosensitive because of an epigenetic influence. Increased histone-3 lysine-56 acetylation (H3K56ac) dephosphorylates H2AX142, with increased expression of phospho-H2AX139, after DSBs and cells exhibit reduced ATM activation; results in decreased DNA repair and increased apoptosis (Jacobs, Misri *et al.* 2016). Failure to dephosphorylate H2AX142 blocks the DDR cascade and apoptosis occurs via activation of JNK in stem cells (Cook, Ju *et al.* 2009; Jacobs, Misri *et al.* 2016). H2AX139 phosphorylation, in irradiated stem cells, is delayed for up to 6 hours, *in vivo* and *in vitro* (Jacobs, Misri *et al.* 2016). These findings contradict our study, in which the levels of H2AX142 appeared lower in dormancy-enriched KG1a cells, while phospho-H2AX139 showed persistent expression after 24 hours of ara-c or ETO treatment. Cycling cells, contain large amounts of phospho-H2AX142 and high levels of phospho-H2AX139, which induces apoptosis. Using c-PARP assessment, fewer apoptotic cells were detected in dormancy-enriched KG1a compared with the number in cyling KG1a cells, after 24 hours of treatment with ara-c or ETO. Dormancy-enriched KG1a cells also showed a greater tendency to survive, as assessed using the apoptotic marker active caspase 3. This approach may help to explain the mechanism underlying DLIC escape of apoptosis and resistance to chemotherapy (Jacobs, Misri *et al.* 2016).

Zhang *et al.* suggested that regulation of apoptosis, in Bcr-Abl-positive K562 cells, is induced through the caspase-3/Mst1 pathway, which is required for H2AX139 and H2AX142 phosphorylation (Zhang, Lu *et al.* 2012). Others have suggested that mediator of DNA damage checkpoint protein 1 (MDC1) is involved in determining cell survival fate (Stewart, Wang *et al.* 2003; Jacobs, Misri *et al.* 2016). MDC1, a major mediator of phospho-H2AX139, recognises DSBs, and H2AX142 is crucial for establishing the MDC1/phospho-H2AX139 complex. This complex is required for recruitment of 53BP1, phospho-ATM, and other DNA repair proteins (Stewart, Wang *et al.* 2003). Hence, impaired interactions between MDC1 and γH2AX block the accumulation of other DDR factors at sites of DNA damage. The work outlined in this thesis suggests that dormancy-enriched KG1a cells can escape apoptosis, even when DSBs are present and DDR pathways are activated.

I aimed to investigate the DNA repair capacity of dormancy-enriched cells. After treatment with genotoxic drugs, ara-c and ETO, the cells were allowed to recover by drug withdrawal. Dormancy-enriched cells were able to resolve damage within 4 to 24 hours, whereas cycling cells showed resolution of damage at 4 hours. After incubation with DNR, dormancy-enriched KG1a cells significantly trended toward resolving damage after 24 hours in a drug-free medium, compared with significant levels of repair activation in cycling cells; this agreed with other studies (Jawad, Yu *et al.* 2012). H-scores indicated that more phospho-H2AX139 foci remained in dormancy-enriched KG1a cells, compared with those in cycling cells, after ara-c, ETO, or DNR withdrawal. Residual phospho-H2AX139 foci may not indicate the persistence of DSBs (Banáth, MacPhail *et al.* 2004; Banáth, Bañuelos *et al.* 2009); however, they may represent re-joined DSBs with unrestored chromatin structure, or the accumulation of a cluster of DNA repair proteins, such as RAD51 and 53PB1, at the site of

damage, leading to a delay in the dissociation process (Lee and Chowdhury 2011; Zimmermann and de Lange 2014). The mechanism, underlying dephosphorylation of the H2AX complex, is not completely understood. Stucki *et al.* suggested that MDC1 controls H2AX139 phosphorylation by two synergistic mechanisms (Stucki, Clapperton *et al.* 2005). First, MDC1 may protect phospho-H2AX139 from dephosphorylation by physically inhibiting access of phosphatases to the phospho-H2AX139 site. Alternatively, MDC1 may mediate H2AX139 phosphorylation by maintaining ATM and DNA-PK in active forms in regions of damaged chromatin (Stucki, Clapperton *et al.* 2005).

I also analysed various DNA repair markers to precisely evaluate the ability of dormancy-enriched cells to resolve DSBs. RAD51 foci formation was assessed because RAD51 is a key enzyme involved in DSB repair by HR. RAD51 foci can be detected at 2 hours after IR, but their number peaks at 6–10 hours in HeLa cells (Bakr, Oing *et al.* 2015). Our results revealed significant RAD51 foci in cycling cells after 4 hours of treatment with ETO, implying that cycling cells respond rapidly to repair DNA breaks via HR. No RAD51 foci were observed in dormancy-enriched KG1a cells. Additionally, inhibition of RAD51 foci formation by B02 (RAD51 inhibitor) revealed a significant percentage of apoptotic cycling cells, indicating that RAD51 plays a crucial role in maintaining genome integrity in these cells. The mechanism underlying RAD51 foci formation after DSB induction, may be controlled by RAD51 paralogues, including RAD51B, RAD51C, RAD51D, XRCC2, and XRCC3, with breast cancer 2 (BRCA2) accumulating within foci in a highly ordered manner (Yilmaz, Valdez *et al*. 2006). Others have suggested that RAD51 localisation is regulated by urokinase-type plasminogen activator receptor (PLAUR) (Narayanaswamy, Tkachuk *et al.* 2016).

For confirmation, 53PB1 was examined as a marker of NHEJ. Studies have shown that NHEJ is prominent at early stages of the cell cycle (Zimmermann and de Lange 2014; Feng, Li *et al.* 2015). Others have suggested that damage accumulates in quiescent stem cells, and that repair is triggered when they must enter the cell cycle (Beerman, Seita *et al.* 2014). This notion agrees with our finding of an increased in the number of 53PB1 foci in dormancy-enriched cells after treatment with ara-c or ETO for 4 hours. These observations suggest that dormancy-enriched KG1a cells may be more resistant to chemotherapy because of their NHEJ repair capacity; this ability to recover injured DSBs remains active throughout the cell cycle. In contrast, cycling cells mainly depend on HR during the S, G2, and/or M phases of the cell cycle (Wunderlich, Mizukawa *et al.* 2013). Our study revealed that 53BP1 foci are rapidly visualised at 4 hours, which is consistent with recruitment of H2AX in response to DSBs. This result agrees with the previous finding, indicating that 53BP1 foci are not only implicated in repair, but may also be involved in checkpoint control; the mechanism, however, is still unknown (Anderson, Henderson *et al.* 2001). In contrast, 53BP1 foci are persistent in non-proliferating cells for up to 48 hours. Unlike in proliferating cells, the number of 53BP1 foci decreased more rapidly within 24 hours after IR (Marková, Schultz *et al*. 2007; Williams, Williams *et al.* 2007). This finding indicates that foci formation and disappearance depend on the time elapsed after treatment with DNA damaging agents, the duration of treatment, and the cell cycle. These findings disagree with those of a recent study, showing that the absence of, or deficiency in, p53, in human and mouse cells, results in impaired 53BP1 foci recruitment after IR (Cuella-Martin, Oliveira *et al.* 2016; Moureau, Luessing *et al.* 2016).

Overall, approximately 130 genes, associated with DNA repair in the human genome, were identified. These genes have various functions

and are involved in numerous pathways associated with the recognition of DNA lesions, and control of damaged DNA, during DNA replication; these genes, thereby, are direct or indirect regulators of the cell cycle for DNA repair or apoptosis (Ronen and Glickman 2001; Wood, Mitchell et al. 2001). In mammalian cells, regulation of DNA repair machinery occurs at many stages, including transcriptional and post-transcriptional (RNA processing, RNA stability, translation, and protein stability) levels. In recent years, studies have focused on transcriptionally up-regulated DNA repair; therefore, in this study, I examined genes up-regulated in the dormancy-enriched KG1a cell model. Analysis of 91 DDR genes, using a PCR super array, showed increased expression of six genes: *FANCG, RAD1, XRCC3, RAD50*, *NBN*, and *BTG2. BTG2* was found to have two-fold or higher expression in dormancy-enriched cells compared to cycling cells. Further validation of super array data confirmed that only *BTG2* was up-regulated. This result supports the role of BTG2 as an anti-proliferative gene (Kim, Ryu *et al.* 2008; Winkler 2010). Similarly, a second dormancy-enriched model, the TF1a-TGFβ model, revealed that *BTG2* expression was induced two-fold more than that in actively cycling TF1a cells. These findings suggest that *BTG2* is a promising marker for *in vitro* models of dormancy. A number of studies have revealed the role of *BTG2* in p53-dependent and p53-independent, as well as other, biological functions in response to genotoxic stress (Cortes, Moyret-Lalle *et al.* 2000; Tirone 2001; Hu, Xing *et al.* 2012).
In this study, dormancy-enriched cells, treated with ETO for 24 hours, showed no difference in *BTG2* expression compared with that in untreated dormancy-enriched cells. In contrast, treated cycling cells showed a three-fold increase compared with that in untreated cycling cells. The levels of c-PARP confirmed that a significant percentage of cycling cells was apoptotic. This observation indicates that up-regulation of *BTG2* occurs, in response to stress, in different signal transduction pathways (Kim, Ryu *et al.* 2008; Shman, Fedasenka *et*

al. 2008; Mollerstrom, Kovacs *et al.* 2010; Quy, Choi *et al.* 2013). The mechanisms, underlying the up-regulation of *BTG2,* downregulate cyclin D1, leading to a pause in the cell cycle (Guardavaccaro, Corrente *et al.* 2000) or induction of apoptosis after a damaging event (Shman, Fedasenka *et al.* 2008). BTG2 is a member of the Tob/BTG anti-proliferative family (Winkler 2010). Tob expression may participate in cell fate decisions in response to DNA damage (Suzuki, Tsuzuku *et al.* 2012). Suzuki *et al.* reported that inhibition of DNA damage-induced apoptosis is regulated via cell division cycle 7 (Cdc7) stabilisation of Tob (Suzuki, Tsuzuku *et al.* 2012). Cdc7 interacts with Tob and controls the stability of BTG2, whereas depletion of Cdc7 stimulates cell death (Ito, Ishii *et al.* 2012). These data indicate that cells deal with DNA damage not only by cell cycle arrest, but also via pro-survival signalling mediated by the Cdc7-Tob pathway (Guo, Romero *et al*. 2005).

Oxidative stress induces ROS and activates the NF-κB pathway (Pyatt, Stillman *et al.* 1999). NF-κB can be activated via canonical and/or alternative pathway signals such as TNF and cytokines. In response to the accumulation of ROS, IκBα is phosphorylated at Ser32 and Ser36, along with ubiquitination at Lys21 and Lys22, followed by degradation in the proteasome; these changes result in the translocation of NF-κB (p65) into the nucleus, where it can interact with the BTG2 promoter. This is the canonical pathway. An alternative pathway involves NF-κB activation by IκBα phosphorylation at tyrosine residues without degradation IkBα (Takada, Mukhopadhyay *et al.* 2003). To understand the regulatory mechanism, underlying the p53-independent involvement of BTG2 in the chemotherapeutic resistance of dormancy-enriched cells, cells were screened for NF-κB (p65) translocation after exposure to PTH, which upregulates ROS and inhibits NF-κb translocation. NF-κB activity is aberrantly increased in primitive human leukemia cells compared with that in normal primitive bone marrow cells (Guzman,

Neering *et al.* 2001; Kagoya, Yoshimi *et al.* 2014). Unexpectedly, cytoplasmic NF-κB (p65) localisation was detected in both untreated cycling cells and dormancy-enriched KG1a cells. Upon induction of DNA damage, persistence of cytoplasmic localisation of NF-κB (p65) in dormancy-enriched KG1a cells, was notable compated with nuclear localisation in cycling cells. This observation indicates that dormancy-enriched cells may be able to attenuate the effects of PTH-induced oxidative stress because of high basal BTG2 expression, or that ROS levels were under the threshold for activation of NF-κB. Therefore, we next measured the levels of BTG2 in response to oxidative stress. RT-PCR assays of BTG2 expression, in dormancy-enriched and cycling cells, showed no difference after inhibiting of NF-κB translocation via PTH. This result was unexpected and showed no definitive difference between the two populations.

An analysis of BTG2 expression was performed using samples from patients with AML. The samples were analysed to assess whether the levels of the proliferation marker Ki-67 decreased proportionally with up-regulation of *BTG2*. A correlation was found between Ki-67 levels and *BTG2* levels in the $CD34^{+}CD38^{-}$ cell compartment (rho = 0.8095, p = 0.0218); however, there was no correlation between Ki-67 and *BTG2* in progenitor cells, confirming that BTG2 is involved in multiple signalling pathways and mediates other biological functions depending on cellular context.

Taken together, these results identify crucial differences in the responses of dormancy-enriched cells to DNA damage as compared with the responses of cycling cells. These findings may also apply to DLICs. Despite DLICs sharing similarities with actively dividing leukemic stem cells in terms of cellular and molecular characteristics, this study indicates that dormancy-enriched KG1a cells can escape conventional chemotherapy via H2AX142 phosphorylation-dephosphorylation. Understanding the molecular mechanisms, behind DDR and key molecules, regulating this process will contribute to the

development of rational targeted therapies for AML. Inhibition of upstream kinases (ATR and ATM) in DDR may efficiently target AML cells (Morgado-Palacin, Day et al. 2016; Ma, Li et al. 2017). In this study, I demonstrated significant induction of DNA repair markers in the NHEJ pathway in dormancy-enriched cells. NHEJ is the prominent DSB repair mechanism in quiescent HSCs (Mohrin, Bourke *et al.* 2010).

6.2 Research limitations and future directions

These findings need to be replicated in other AML-dormancy models. Attempts to establish a new dormancy AML model in M07e cells, using TPO in the absence and presence of GM-CSF, were unsuccessful. The major challenges were determining the appropriate environment for cells growth, maintaining survival and health in long term culture, and controlling proliefration rates to enrich for dormancy. Using various cytokine concentrations, to produce sets of cell population in different phases of the cell cycle, is not usually successful strategy for enriched dormancy; however, previous trials, using a single agent, showed satisfactory features of dormancy *in vitro*. The current model was established in our labratory using a single and/or synergized factors. This indicates that cell behaviours are heterogeneous from one cell line to another, and may be present within the same cell line. Because of these variations, some experiments showed inconsistent data or disagreeing with previous findings by other studies using primary cells.

Advances in HSC culturing methods have increased the use of *in vitro* models. This approach has several major advantages compared with *in vivo* systems. In *in vitro* models, manipulation and testing are relatively easy, reflect the *in vivo* environmental for short- and long-term cell culture, and allow for identification of drug interactions, cell characterisation, determination of behaviours, or prediction of drug toxicity in HSCs. In contrast, establishing a standard dormancy model DLICs *in vitro* is necessary; targeting these cells *in vivo* is difficult

because of their quiescent status, low prevalence, and difficult isolation from the BM. The current *in vitro* AML dormancy model, used in this study, is based on cells enriched for dormancy for a certain period, leading to induction of some features of quiescent cells in BM. Nonetheless, not providing the true environment for stem cells is one drawback of an *in vitro* AML stem-cell model. LSCs are regulated by a tight network of molecules, in a hypoxic niche, maintaining and differentiating cells when stimulated by external stress. Concurrently, exposing cells to multiple dormancy-inducing factors, and inappropriate handling in cell culture, may lead to cell sensitisation, causing cells to become unstable for assays of DNA damage and DDR. In contrast to two-dimensional culture, three-dimensional (3D) cell culture systems are increasingly used to evaluate cellular responses to anticancer drugs. A 3D system can offer a simple, rapid, and cost-effective tool that eliminates the need for animal models. Additionally, 3D culture systems enable monitoring of cell morphology and behaviour, and multiple layers enhance the access of drugs to all cells in the scaffold (Rimann and Graf-Hausner 2012; Edmondson, Broglie *et al.* 2014). Mimicking the functional BM niche for quiescent HSCs in a 3D model *in vitro* has been achieved (Sharma, Limaye *et al.* 2012).

DDR signalling pathways are complex networks, which include numerous protein components working in dependent and independent manner, to coordinate the processes of sensing DNA damage, damage repaire, cell-cycle arrest, and programmed cell death. There is much overlap between DDR mechanisms; these were not explored because of the specific objectives pursued in this study and time constraints. However, this is may explaine the non-significant results such as those in sections (3.5.1) and (3.7). Furthermore, the regulation of BTG2 via NF-κB in dormancy-enriched cells is controversial. Further work is required to validate BTG2 as a dormancy marker in AML. Interaction of BTG2 with other DDR

markers, including ATM, 53BP1, PRMT1, NEMO, IKK complex, and check-point molecules, should be investigated. A larger set of primary samples, from patients with AML, is needed to explore BTG2 expression in response to stress. Further research should also examine Cdc7 phosphorylation in the Tob/BTG2 protein family and its proposed ability to determine cell fate in DLICs (Suzuki, Tsuzuku *et al*. 2012).

Examining phosphorylated H2AX142 in other dormancy models, using a single or synergistic dose of chemotherapeutic agents, would be informative. Identifying signalling pathways that use H2AX142 phosphorylation, or other physiologically relevant phosphorylation events regulated by the WICH chromatin remodelling complex, will also be of interest in future studies. Specifically, it would be informative to examine the epigenetic modification of histones, which are critical for recognition and repair of DSBs (Ramos, Mo *et al.* 2015; Jacobs, Misri *et al.* 2016). Evaluation of curcumine (an anti-leukemic drug), as a growth stimulant and H3K56 acetylation inhibitor, is needed to determine its effect on DDR and survival in the dormancy models (Choi, Kim *et al.* 2008; Ramos, Mo *et al.* 2015).

6.2 Concluding remarks

In conclusion, activation of the DDR cascade, via phosphorylation of a series of checkpoints and effectors, is complex and time dependent; dormancy featurs advantageous in terms of evading targeted chemotherapy. Consequently, a relapse can occur. This study showed that dormancy-enriched KG1a cells acquire resistance to chemotherapy via molecular differences in responses to genotoxic stress. We have provided evidence that small amounts of H2AX, phosphorylated at 142, may play a crucial role in determining KG1a cell fate and enhancing dormancy-enriched cell survival after 24 hours of exposure to a chemotherapeutic agents. Immunofluorescence analysis of H2AX139 confirmed that persistence

of H2AX139 was associated with a significant reduction in H2AX142 levels in dormancy-enriched KG1a cells after 24 hours of ETO or ara-c treatment compared with the levels of H2AX142 in cycling KG1a cells. Dephosphorylation of H2AX142, in conjunction with highly phosphorylated H2AX139, a hallmark of DDR, provides a cell with an opportunity to overcome genotoxic stress and promote NHEJ through 53BP1 foci; this phenomenon may be associated with other DSB repair markers in dormancy-enriched cells. The neutral comet assay confirmed activation of DNA repair by the absence of comet tails after drug withdrawal in dormancy-enriched and cycling KG1a cells. Our data suggest that inhibition of H2AX142 via dephosphorylation may be used as a new approach in dormant leukemic cells to improve disease outcome. Inducing DSBs by the chemotherapeutic dose along with inhibition of 53BP1 or other components of NHEJ may trigger DLIC apoptosis and eradicate these cells permanently.

Bibliography

Aguirre-Ghiso, J. (2007). "Models, mechanisms and clinical evidence for cancer dormancy." Nat Rev Cancer **7**(11): 834 - 846.

Ahn, J.-Y., J. K. Schwarz, *et al.* (2000). "Threonine 68 Phosphorylation by Ataxia Telangiectasia Mutated Is Required for Efficient Activation of Chk2 in Response to Ionizing Radiation." Cancer Research **60**(21): 5934-5936.

Ali, A., J. Zhang, *et al.* (2004). "Requirement of protein phosphatase 5 in DNA-damage-induced ATM activation." Genes & Development **18**(3): 249-254.

An, J., Y.-C. Huang, *et al.* (2010). "DNA-PKcs plays a dominant role in the regulation of H2AX phosphorylation in response to DNA damage and cell cycle progression." BMC Molecular Biology **11**: 18-18.

Anderson, L., C. Henderson, *et al.* (2001). "Phosphorylation and Rapid Relocalization of 53BP1 to Nuclear Foci upon DNA Damage." Molecular and Cellular Biology **21**(5): 1719-1729.

Andoh, T. and R. Ishida (1998). "Catalytic inhibitors of DNA topoisomerase II." Biochimica et Biophysica Acta (BBA) - Gene Structure and Expression **1400**(1): 155-171.

Arinobu, Y., S.-i. Mizuno, *et al.* (2007). "Reciprocal Activation of GATA-1 and PU.1 Marks Initial Specification of Hematopoietic Stem Cells into Myeloerythroid and Myelolymphoid Lineages." Cell Stem Cell **1**(4): 416-427.

Aroua, N., J.-E. Sarry, *et al.* (2015). "In Vivo Response to Cytarabine Chemotherapy Uncovers the Role of the Oxidative and Energetic Metabolism in the Chemoresistance of Human Primary AML Stem Cells." Blood **126**(23): 4269-4269.

Azqueta, A., K. B. Gutzkow, *et al.* (2011). "Towards a more reliable comet assay: Optimising agarose concentration, unwinding time and electrophoresis conditions." Mutation Research/Genetic Toxicology and Environmental Mutagenesis **724**(1–2): 41-45.

Azqueta, A., J. Slyskova, *et al.* (2014). "Comet assay to measure DNA repair: approach and applications." Frontiers in Genetics **5**: 288.

Baer, M., C. Stewart, *et al.* (2001). "High frequency of immunophenotype changes in acute myeloid leukemia at relapse: implications for residual disease detection (Cancer and Leukemia Group B Study 8361)." Blood **97**: 3574 - 3580.

Bakkenist, C. J. and M. B. Kastan (2003). "DNA damage activates ATM through intermolecular autophosphorylation and dimer dissociation." Nature **421**(6922): 499-506.

Bakr, A., C. Oing, *et al.* (2015). "Involvement of ATM in homologous recombination after end resection and RAD51 nucleofilament formation." Nucleic Acids Research.

Balajee, A. S. and C. R. Geard (2004). "Replication protein A and γ-H2AX foci assembly is triggered by cellular response to DNA double-strand breaks." Experimental Cell Research **300**(2): 320-334.

Baldwin EL, O. N. (2005). "Etoposide, topoisomerase II and cancer." Current Medical Chemistry: Anticancer Agents **5**(4): 363-372.

Banáth, J. P., C. A. Bañuelos, *et al.* (2009). "Explanation for excessive DNA single-strand breaks and endogenous repair foci in pluripotent mouse embryonic stem cells." Experimental Cell Research **315**(8): 1505-1520.

Banáth, J. P., S. H. MacPhail, *et al.* (2004). "Radiation Sensitivity, H2AX Phosphorylation, and Kinetics of Repair of DNA Strand Breaks in Irradiated Cervical Cancer Cell Lines." Cancer Research **64**(19): 7144-7149.

Banáth, J. P. and P. L. Olive (2003). "Expression of Phosphorylated Histone H2AX as a Surrogate of Cell Killing by Drugs That Create DNA Double-Strand Breaks." Cancer Research **63**(15): 4347-4350.

Banker, D. E., M. Groudine, *et al.* (1997). "Measurement of Spontaneous and Therapeutic Agent-Induced Apoptosis With BCL-2 Protein Expression in Acute Myeloid Leukemia." Blood **89**(1): 243-255.

Bao, S., R. S. Tibbetts, *et al.* (2001). "ATR/ATM-mediated phosphorylation of human Rad17 is required for genotoxic stress responses." Nature **411**(6840): 969.

Baranello, M. P., L. Bauer, *et al.* (2015). "Micelle Delivery of Parthenolide to Acute Myeloid Leukemia Cells." Cellular and Molecular Bioengineering **8**(3): 455-470.

Bartkova, J., Z. Horejsi, *et al.* (2005). "DNA damage response as a candidate anti-cancer barrier in early human tumorigenesis." Nature **434**(7035): 864-870.

Beerman, I., J. Seita, *et al.* (2014). "Quiescent Hematopoietic Stem Cells Accumulate DNA Damage during Aging that Is Repaired upon Entry into Cell Cycle." Cell Stem Cell **15**(1): 37-50.

Benjamin, D., M. Colombi, *et al.* (2011). "Rapamycin passes the torch: a new generation of mTOR inhibitors." Nat Rev Drug Discov **10**(11): 868-880.

Bennett, B. T., J. Bewersdorf, *et al.* (2009). "Immunofluorescence imaging of DNA damage response proteins: Optimizing protocols for super-resolution microscopy." Methods **48**(1): 63-71.

Bennett, J. M., D. Catovsky, *et al.* (1976). "Proposals for the Classification of the Acute Leukaemias French-American-British (FAB) Co-operative Group." British Journal of Haematology **33**(4): 451-458.

Bernasconi, P. (2008). "Molecular pathways in myelodysplastic syndromes and acute myeloid leukemia: relationships and distinctions–a review." British Journal of Haematology **142**(5): 695-708.

Besaratinia, A., T. W. Synold, *et al.* (2005). "DNA lesions induced by UV A1 and B radiation in human cells: Comparative analyses in the overall genome and in the p53 tumor suppressor gene." Proceedings of the National Academy of Sciences of the United States of America **102**(29): 10058-10063.

Bianco, P. (2011). "Bone and the hematopoietic niche: a tale of two stem cells." Blood **117**(20): 5281-5288.

Bianco, T., B. J. Farmer, *et al.* (2001). "Loss of red cell A, B, and H antigens is frequent in myeloid malignancies." Blood **97**(11): 3633-3639.

Blagosklonny, M. (2006). "Cell senescence: hypertrophic arrest beyond the restriction point." J Cell Physiol **209**(3): 592 - 597.

Bockamp, E., C. Antunes, *et al.* (2009). "In vivo fate mapping with SCL regulatory elements identifies progenitors for primitive and definitive hematopoiesis in mice." Mechanisms of Development **126**(10): 863-872.

Bodó, A., É. Bakos, *et al.* (2003). "The role of multidrug transporters in drug availability, metabolism and toxicity." Toxicology Letters **140–141**(0): 133-143.

Boehrer, S., L. Ades, *et al.* (2009). "Suppression of the DNA damage response in acute myeloid leukemia versus myelodysplastic syndrome." Oncogene **28**(22): 2205-2218.

Bonnet, D. and J. E. Dick (1997). "Human acute myeloid leukemia is organized as a hierarchy that originates from a primitive hematopoietic cell." Nature medicine **3**(7): 730-737.

Borge, O., V. Ramsfjell, *et al.* (1996). "Thrombopoietin, but not erythropoietin promotes viability and inhibits apoptosis of multipotent murine hematopoietic progenitor cells in vitro." Blood **88**(8): 2859-2870.

Borriello, A., I. Caldarelli, *et al*. (2011). "p57 Kip2 is a downstream effector of BCR–ABL kinase inhibitors in chronic myelogenous leukemia cells." Carcinogenesis **32**(1): 10-18.

Bothmer, A., Davide F. Robbiani, *et al.* (2011). "Regulation of DNA End Joining, Resection, and Immunoglobulin Class Switch Recombination by 53BP1." Molecular Cell **42**(3): 319-329.

Brecqueville, M., J. Rey, *et al.* (2012). "Mutation analysis of ASXL1, CBL, DNMT3A, IDH1, IDH2, JAK2, MPL, NF1, SF3B1, SUZ12, and TET2 in myeloproliferative neoplasms." Genes Chromosomes Cancer **51**: 743 - 755.

Brown, J. A. L., J. K. Eykelenboom, *et al.* (2012). "Co-mutation of histone H2AX S139A with Y142A rescues Y142A-induced ionising radiation sensitivity." FEBS Open Bio **2**: 313-317.

Buccisano, F., L. Maurillo, *et al.* (2012). "Prognostic and therapeutic implications of minimal residual disease detection in acute myeloid leukemia." Blood **119**(2): 332-341.

Buis, J., Y. Wu, *et al*. (2008). "Mre11 nuclease activity has essential roles in DNA repair and genomic stability distinct from ATM activation." Cell **135**(1): 85-96.

Burden, D. A. and N. Osheroff (1998). "Mechanism of action of eukaryotic topoisomerase II and drugs targeted to the enzyme." Biochimica et Biophysica Acta (BBA) - Gene Structure and Expression **1400**(1–3): 139-154.

Burnett, A., M. Wetzler, *et al*. (2011). "Therapeutic Advances in Acute Myeloid Leukemia." Journal of Clinical Oncology **29**(5): 487-494.

Burnett, A. K., N. H. Russell, *et al.* (2010). "European development of clofarabine as treatment for older patients with acute myeloid leukemia considered unsuitable for intensive chemotherapy." J Clin Oncol **28**(14): 2389-2395.

Buscemi, G., C. Savio, *et al.* (2001). "Chk2 Activation Dependence on Nbs1 after DNA Damage." Molecular and Cellular Biology **21**(15): 5214-5222.

Cahill, D. and J. P. Carney (2007). "Dimerization of the Rad50 protein is independent of the conserved hook domain." Mutagenesis **22**(4): 269-274.

Callén, E., M. Jankovic, *et al*. (2009). "Essential Role for DNA-PKcs in DNA Double-Strand Break Repair and Apoptosis in ATM-Deficient Lymphocytes." Molecular Cell **34**(3): 285-297.

Carracedo, A., L. Ma, *et al.* (2008). "Inhibition of mTORC1 leads to MAPK pathway activation through a PI3K-dependent feedback loop in human cancer." The Journal of Clinical Investigation **118**(9): 3065-3074.

Carter, B. Z., D. Mak, *et al.* (2005). "Simultaneous Inhibition of Mcl-1 and XIAP To Induce Apoptosis in AML Cells." Blood **106**(11): 1520-1520.

Cerbinskaite, A., A. Mukhopadhyay, *et al.* (2012). "Defective homologous recombination in human cancers." Cancer Treatment Reviews **38**(2): 89-100.

Challen, G., D. Sun, *et al.* (2012). "Dnmt3a is essential for hematopoietic stem cell differentiation." Nat Genet **44**: 23 - 31.

Chambard, J.-C., R. Lefloch, *et al.* (2007). "ERK implication in cell cycle regulation." Biochimica et Biophysica Acta (BBA) - Molecular Cell Research **1773**(8): 1299-1310.

Chan, D. and A. Giaccia (2011). "Harnessing synthetic lethal interactions in anticancer drug discovery." Nat Rev Drug Discov **10**: 351 - 364.

Chang, C.-C., Mandar T. Naik, *et al.* (2011). "Structural and Functional Roles of Daxx SIM Phosphorylation in SUMO Paralog-Selective Binding and Apoptosis Modulation." Molecular Cell **42**(1): 62-74.

Chao, M. P., J. Seita, *et al.* (2008). "Establishment of a Normal Hematopoietic and Leukemia Stem Cell Hierarchy." Cold Spring Harbor Symposia on Quantitative Biology **73**: 439-449.

Chapman, J. R., Martin R. G. Taylor, *et al.* (2012). "Playing the End Game: DNA Double-Strand Break Repair Pathway Choice." Molecular cell **47**(4): 497-510.

Chen, C., Y. Liu, *et al*. (2008). "TSC-mTOR maintains quiescence and function of hematopoietic stem cells by repressing mitochondrial biogenesis and reactive oxygen species." J Exp Med **205**(10): 2397 - 2408.

Chen, W., J. Dong, *et al.* (2016). "Cancer Stem Cell Quiescence and Plasticity as Major Challenges in Cancer Therapy." Stem Cells International **2016**: 1740936.

Cheng, T., N. Rodrigues, *et al.* (2000). "Hematopoietic Stem Cell Quiescence Maintained by p21cip1/waf1." Science **287**(5459): 1804-1808.

Cho, J.-W., J. J. Kim, *et al*. (2004). "Identification of B-cell translocation gene 1 as a biomarker for monitoring the remission of acute myeloid leukemia." PROTEOMICS **4**(11): 3456-3463.

Choi, B., C. Kim, *et al.* (2008). "Curcumin down-regulates the multidrug-resistance mdr1b gene by inhibiting the PI3K/Akt/NF kappa B pathway." Cancer Lett **259**: 111 - 118.

Choi, K.-S., J. Y. Kim, *et al.* (2012). "TIS21/BTG2/PC3 accelerates the repair of DNA double strand breaks by enhancing Mre11 methylation and blocking damage signal transfer to the Chk2T68–p53S20 pathway." DNA Repair **11**(12): 965-975.

Chow, K. C. and W. E. Ross (1987). "Topoisomerase-specific drug sensitivity in relation to cell cycle progression." Molecular and Cellular Biology **7**(9): 3119-3123.

Chrzanowska, K. H., H. Gregorek, *et al*. (2012). "Nijmegen breakage syndrome (NBS)." Orphanet Journal of Rare Diseases **7**: 13-13.

Cleaver, J. E., L. Feeney, *et al.* (2011). "Phosphorylated H2Ax is not an unambiguous marker for DNA double-strand breaks." Cell Cycle **10**(19): 3223-3224.

Collins, A. (2004). "The comet assay for DNA damage and repair." Molecular Biotechnology **26**(3): 249-261.

Cook, G. J. and T. S. Pardee (2013). "Animal Models of Leukemia: Any closer to the real thing?" Cancer metastasis reviews **32**(0): 63-76.

Cook, P. J., B. G. Ju, *et al.* (2009). "Tyrosine Dephosphorylation of H2AX Modulates Apoptosis and Survival Decisions." Nature **458**(7238): 591-596.

Copley, M. R. and C. J. Eaves (2013). "Developmental changes in hematopoietic stem cell properties." Experimental & Molecular Medicine **45**(11): e55.

Cordeiro-Spinetti, E., R. S. Taichman, *et al.* (2015). "The bone marrow endosteal niche: how far from the surface?" Journal of cellular biochemistry **116**(1): 6-11.

Cortes, J., S. O'Brien, *et al.* (2004). "Discontinuation of imatinib therapy after achieving a molecular response." Blood **104**(7): 2204-2205.

Cortes, U., C. Moyret-Lalle, *et al.* (2000). "BTG gene expression in the p53-dependent and -independent cellular response to DNA damage." Mol Carcinog **27**: 57 - 64.

Cortes, U., C. Moyret-Lalle, *et al.* (2000). "BTG gene expression in the p53-dependent and -independent cellular response to DNA damage." Molecular Carcinogenesis **27**(2): 57-64.

Crisan, M., S. Yap, *et al.* (2008). "A Perivascular Origin for Mesenchymal Stem Cells in Multiple Human Organs." Cell Stem Cell **3**(3): 301-313.

Cuella-Martin, R., C. Oliveira, *et al.* (2016). "53BP1 Integrates DNA Repair and p53-Dependent Cell Fate Decisions via Distinct Mechanisms." Molecular Cell **64**(1): 51-64.

Cully, M. and J. Downward (2012). Assessing Cell Size and Cell Cycle Regulation in Cells with Altered TOR Activity. mTOR. T. Weichhart, Humana Press. **821:** 227-237.

Culver-Cochran, A. E. and B. P. Chadwick (2012). "The WSTF-ISWI Chromatin Remodeling Complex Transiently Associates with the Human Inactive X Chromosome during Late S-Phase Prior to BRCA1 and γ-H2AX." PLoS ONE **7**(11): e50023.

Curtin, N. J. (2012). "DNA repair dysregulation from cancer driver to therapeutic target." Nat Rev Cancer **12**(12): 801-817.

d'Adda di Fagagna, F. (2008). "Living on a break: cellular senescence as a DNA-damage response." Nat Rev Cancer **8**(7): 512-522.

Dahlmann, H. A., V. G. Vaidyanathan, *et al.* (2009). "Investigating the Biochemical Impact of DNA Damage with Structure-Based Probes: Abasic Sites, Photodimers, Alkylation Adducts, and Oxidative Lesions." Biochemistry **48**(40): 9347-9359.

Dalle-Donne, I., R. Rossi, *et al.* (2006). "Biomarkers of Oxidative Damage in Human Disease." Clinical Chemistry **52**(4): 601-623.

Davis, A. J. and D. J. Chen (2013). "DNA double strand break repair via non-homologous end-joining." Translational cancer research **2**(3): 130-143.

de Graaf, C. A. and D. Metcalf (2011). "Thrombopoietin and hematopoietic stem cells." Cell Cycle **10**(10): 1582-1589.

De La Luz Sierra, M., P. Gasperini, *et al.* (2007). "Transcription factor Gfi-1 induced by G-CSF is a negative regulator of CXCR4 in myeloid cells." Blood **110**(7): 2276-2285.

De Vos, M., V. Schreiber, *et al.* (2012). "The diverse roles and clinical relevance of PARPs in DNA damage repair: Current state of the art." Biochemical Pharmacology **84**(2): 137-146.

de Vries, J., J. Falkenburg, *et al.* (2006). "The mechanisms of Ara-C-induced apoptosis of resting B-chronic lymphocytic leukemia cells." Haematologica **91**(7): 912-919.

De Winter, J. P., L. Van Der Weel, *et al.* (2000). "The Fanconi anemia protein FANCF forms a nuclear complex with FANCA, FANCC and FANCG." Human Molecular Genetics **9**(18): 2665-2674.

Deans, A. J. and S. C. West (2011). "DNA interstrand crosslink repair and cancer." Nature reviews. Cancer **11**(7): 467-480.

Deming, P. B., K. G. Flores, *et al.* (2002). "ATR Enforces the Topoisomerase II-dependent G2 Checkpoint through Inhibition of Plk1 Kinase." Journal of Biological Chemistry **277**(39): 36832-36838.

Di Marco, A., F. Arcamone, *et al.* (1975). Daunomycin (Daunorubicin) and Adriamycin and Structural Analogues: Biological Activity and Mechanism of Action. Mechanism of Action of Antimicrobial and Antitumor Agents. J. Corcoran, F. Hahn, J. F. Snell and K. L. Arora, Springer Berlin Heidelberg. **3:** 101-128.

Dick, J. E. (2005). "Acute Myeloid Leukemia Stem Cells." Annals of the New York Academy of Sciences **1044**(1): 1-5.

Difilippantonio, M. J., J. Zhu, *et al.* (2000). "DNA repair protein Ku80 suppresses chromosomal aberrations and malignant transformation." Nature **404**(6777): 510-514.

Ding, L., T. Ley, *et al.* (2012). "Clonal evolution in relapsed acute myeloid leukaemia revealed by whole-genome sequencing." Nature **481**: 506 - 510.

Dinkelmann, M., E. Spehalski, *et al.* (2009). "Multiple functions of MRN in end-joining pathways during isotype class switching." Nature structural & molecular biology **16**(8): 808-813.

Döhner, H., E. H. Estey, *et al.* (2010). "Diagnosis and management of acute myeloid leukemia in adults: recommendations from an international expert panel, on behalf of the European LeukemiaNet." Blood **115**(3): 453-474.

Döhner, H., D. J. Weisdorf, *et al.* (2015). "Acute Myeloid Leukemia." New England Journal of Medicine **373**(12): 1136-1152.

Doidge, R., S. Mittal, *et al.* (2012). "The Anti-Proliferative Activity of BTG/TOB Proteins Is Mediated via the Caf1a (CNOT7) and Caf1b (CNOT8) Deadenylase Subunits of the Ccr4-Not Complex." PLoS ONE **7**(12): e51331.

Dolbeare, F. (1995). "Bromodeoxyuridine: a diagnostic tool in biology and medicine, Part II: Oncology, chemotherapy and carcinogenesis." The Histochemical Journal **27**(12): 923-964.

Dombret , H., C. Chastang , *et al.* (1995). "A Controlled Study of Recombinant Human Granulocyte Colony-Stimulating Factor in Elderly Patients after Treatment for Acute Myelogenous Leukemia." New England Journal of Medicine **332**(25): 1678-1683.

Donato, L. J., J. H. Suh, *et al.* (2007). "Suppression of Mammary Carcinoma Cell Growth by Retinoic Acid: the Cell Cycle Control Gene Btg2 Is a Direct Target for Retinoic Acid Receptor Signaling." Cancer Research **67**(2): 609-615.

Drake, A. C., M. Khoury, *et al.* (2011). "Human CD34+ CD133+ Hematopoietic Stem Cells Cultured with Growth Factors Including Angptl5 Efficiently Engraft Adult NOD-SCID Il2rγ (NSG) Mice." PLoS ONE **6**(4): e18382.

Duan, G. and D. Walther (2015). "The Roles of Post-translational Modifications in the Context of Protein Interaction Networks." PLoS Computational Biology **11**(2): e1004049.

Duchayne, E., C. Demur, *et al.* (1999). "Diagnosis of Acute Basophilic Leukemia." Leukemia & Lymphoma **32**(3-4): 269-278.

Duong, H.-Q., Y. B. Hong, *et al.* (2013). "Inhibition of checkpoint kinase 2 (CHK2) enhances sensitivity of pancreatic adenocarcinoma cells to gemcitabine." Journal of Cellular and Molecular Medicine **17**(10): 1261-1270.

Duriez, C., N. Falette, *et al.* (2002). "The human BTG2/TIS21/PC3 gene: genomic structure, transcriptional regulation and evaluation as a candidate tumor suppressor gene." Gene **282**(1–2): 207-214.

Duriez, C., C. Moyret-Lalle, *et al.* (2004). "BTG2, its family and its tutor." Bull Cancer **91**: E242 - 253.

Edmondson, R., J. J. Broglie, *et al.* (2014). "Three-Dimensional Cell Culture Systems and Their Applications in Drug Discovery and Cell-Based Biosensors." Assay and Drug Development Technologies **12**(4): 207-218.

Ehninger, A., M. Kramer, *et al.* (2014). "Distribution and levels of cell surface expression of CD33 and CD123 in acute myeloid leukemia." Blood Cancer Journal **4**: e218.

Ehninger, A. and A. Trumpp (2011). "The bone marrow stem cell niche grows up: mesenchymal stem cells and macrophages move in." The Journal of Experimental Medicine **208**(3): 421-428.

Ersson, C. and L. Moller (2011). "The effects on DNA migration of altering parameters in the comet assay protocol such as agarose density, electrophoresis conditions and durations of the enzyme or the alkaline treatments." Mutagenesis **26**(6): 689-695.

Escobar, P. A., M. T. Smith, *et al.* (2007). "Leukaemia-specific chromosome damage detected by comet with fluorescence in situ hybridization (comet-FISH)." Mutagenesis **22**(5): 321-327.

Esposito, M. and C. So (2014). "DNA damage accumulation and repair defects in acute myeloid leukemia: implications for pathogenesis, disease progression, and chemotherapy resistance." Chromosoma **123**(6): 545-561.

Essers, M. A. G. and A. Trumpp (2010). "Targeting leukemic stem cells by breaking their dormancy." Molecular oncology **4**(5): 443-450.

Estcourt, L. J. and B. J. Bain (2013). WHO Classification of Leukemia. Brenner's Encyclopedia of Genetics (Second Edition). M. Editors-in-Chief: Stanley and H. Kelly. San Diego, Academic Press**:** 329-336.

Estey, E. and H. Dohner (2006). "Acute myeloid leukaemia." Lancet **368**(9550): 1894 - 1907.

Ewald, B. S., D. Plunkett, W. (2007). "H2AX phosphorylation marks gemcitabine-induced stalled replication forks and their collapse upon S-phase checkpoint abrogation." Molecular Cancer Therapeutics **6**(4): 1239-1248.

Ezzeddine, N., T.-C. Chang, *et al.* (2007). "Human TOB, an antiproliferative transcription factor, is a poly (A)-binding protein-dependent positive regulator of cytoplasmic mRNA deadenylation." Molecular and cellular biology **27**(22): 7791-7801.

Faderl, S., S. Verstovsek, *et al.* (2006). "Clofarabine and cytarabine combination as induction therapy for acute myeloid leukemia (AML) in patients 50 years of age or older." Blood **108**(1): 45-51.

Fattah, K. R., B. L. Ruis, *et al.* (2008). "Mutations to Ku Reveal Differences in Human Somatic Cell Lines." DNA repair **7**(5): 762-774.

Fedor, Y., J. Vignard, *et al.* (2013). "From single-strand breaks to double-strand breaks during S-phase: a new mode of action of the Escherichia coliCytolethal Distending Toxin." Cellular Microbiology **15**(1): 1-15.

Feng, L., N. Li, *et al.* (2015). "Cell cycle-dependent inhibition of 53BP1 signaling by BRCA1." Cell Discovery **1**: 15019.

Ferguson, D. O., J. M. Sekiguchi, *et al.* (2000). "The nonhomologous end-joining pathway of DNA repair is required for genomic stability and the suppression of translocations." Proceedings of the National Academy of Sciences of the United States of America **97**(12): 6630-6633.

Fernandez, H. F., Z. Sun, *et al.* (2009). "Anthracycline Dose Intensification in Acute Myeloid Leukemia." The New England journal of medicine **361**(13): 1249-1259.

Ferrara, F., S. Palmieri, *et al.* (2004). "Prognostic factors and therapeutic options for relapsed or refractory acute myeloid leukemia." Haematologica **89**(8): 998-1008.

Figueroa, M., O. Abdel-Wahab, *et al.* (2010). "Leukemic IDH1 and IDH2 mutations result in a hypermethylation phenotype, disrupt TET2 function, and impair hematopoietic differentiation." Cancer Cell **18**: 553 - 567.

Figueroa, M. E., S. Lugthart, *et al.* (2010). "DNA Methylation Signatures Identify Biologically Distinct Subtypes in Acute Myeloid Leukemia." Cancer Cell **17**(1): 13-27.

Frankenberg-Schwager, M., A. Gebauer, *et al.* (2009). "Single-Strand Annealing, Conservative Homologous Recombination, Nonhomologous DNA End Joining, and the Cell Cycle-Dependent Repair of DNA Double-Strand Breaks Induced by Sparsely or Densely Ionizing Radiation." Radiation Research **171**(3): 265-273.

Fresco, J. R. and O. Amosova (2017). "Site-Specific Self-Catalyzed DNA Depurination: A Biological Mechanism That Leads to Mutations and Creates Sequence Diversity." Annual Review of Biochemistry **86**(1): 461-484.

Friedberg, E. C. (2003). "DNA damage and repair." Nature **421**(6921): 436-440.

Fukuda, S. and L. M. Pelus (2001). "Regulation of the inhibitor-of-apoptosis family member survivin in normal cord blood and bone marrow CD34⁺ cells by hematopoietic growth factors: implication of survivin expression in normal hematopoiesis." Blood **98**(7): 2091-2100.

Gal, H., N. Amariglio, *et al.* (2006). "Gene expression profiles of AML derived stem cells; similarity to hematopoietic stem cells." Leukemia **20**(12): 2147-2154.

Garg, M., Y. Nagata, *et al.* (2015). "Profiling of somatic mutations in acute myeloid leukemia with *FLT3*-ITD at diagnosis and relapse." Blood **126**(22): 2491-2501.

Gavande, N. S., P. S. VanderVere-Carozza, *et al.* (2016). "DNA repair targeted therapy: The past or future of cancer treatment?" Pharmacology & Therapeutics **160**: 65-83.

Geller, R., M. Zahurak, *et al.* (1990). "Prognostic importance of immunophenotyping in adults with acute myelocytic leukaemia: the significance of the stem-cell glycoprotein CD34 (My10)." Br J Haematol **76**: 340 - 347.

Gewirtz, D. (1999). "A critical evaluation of the mechanisms of action proposed for the antitumor effects of the anthracycline antibiotics adriamycin and daunorubicin." Biochemical Pharmacology **57**(7): 727-741.

Ghanem, H., E. Jabbour, *et al.* (2010). "Clofarabine in leukemia." Expert Review of Hematology **3**(1): 15-22.

Gilliland, D. G., C. T. Jordan, *et al.* (2004). "The Molecular Basis of Leukemia." ASH Education Program Book **2004**(1): 80-97.

Giunta, S., R. Belotserkovskaya, *et al.* (2010). "DNA damage signaling in response to double-strand breaks during mitosis." The Journal of Cell Biology **190**(2): 197-207.

Goh, K., V. Novotny-Diermayr, *et al.* (2012). "TG02, a novel oral multi-kinase inhibitor of CDKs, JAK2 and FLT3 with potent anti-leukemic properties." Leukemia **26**(2): 236 - 243.

Gorgoulis, V. G., L.-V. F. Vassiliou, *et al.* (2005). "Activation ov the DNA damage checkpoint and genomic instability in human precancerous lesions." Nature **434**(7035): 907.

Görlach, A., K. Bertram, *et al.* (2015). "Calcium and ROS: A mutual interplay." Redox Biology **6**: 260-271.

Goss, P. and A. Chambers (2010). "Does tumour dormancy offer a therapeutic target?" Nat Rev Cancer **10**(12): 871 - 877.

Gothot, A., R. Pyatt, *et al.* (1997). "Functional heterogeneity of human CD34(+) cells isolated in subcompartments of the G0/G1 phase of the cell cycle." Blood **90**(11): 4384 - 4393.

Grawunder, U., M. Wilm, *et al.* (1997). "Activity of DNA ligase IV stimulated by complex formation with XRCC4 protein in mammalian cells." Nature **388**(6641): 492-495.

Grimwade, D., R. K. Hills, *et al.* (2010). "Refinement of cytogenetic classification in acute myeloid leukemia: determination of prognostic significance of rare recurring chromosomal abnormalities among 5876 younger adult patients treated in the United Kingdom Medical Research Council trials." Blood **116**(3): 354-365.

Guan, Y., B. Gerhard, *et al.* (2003). "Detection, Isolation and Stimulation of Quiescent Primitive Leukemic Progenitor Cells from Patients with Acute Myeloid Leukemia (AML)." Blood **101**: 3142 - 3149.

Guan, Y. and D. Hogge (2000). "Proliferative status of primitive hematopoietic progenitors from patients with acute myelogenous leukemia (AML)." Leukemia **14**(12): 2135.

Guardavaccaro, D., G. Corrente, *et al*. (2000). "Arrest of G1-S progression by the p53-inducible gene PC3 is Rb dependent and relies on the inhibition of cyclin D1 transcription." Molecular and cellular biology **20**(5): 1797-1815.

Guo, B., J. Romero, *et al.* (2005). "High levels of Cdc7 and Dbf4 proteins can arrest cell-cycle progression." European Journal of Cell Biology **84**(12): 927-938.

Guo, Z., R. Deshpande, *et al.* (2010). "ATM activation in the presence of oxidative stress." Cell Cycle **9**(24): 4805-4811.

Guzman, M. L., S. J. Neering, *et al.* (2001). "Nuclear factor-κB is constitutively activated in primitive human acute myelogenous leukemia cells." Blood **98**(8): 2301-2307.

Guzman, M. L., R. M. Rossi, *et al.* (2005). "The sesquiterpene lactone parthenolide induces apoptosis of human acute myelogenous leukemia stem and progenitor cells." Blood **105**(11): 4163-4169.

Guzman, M. L., D. Upchurch, *et al.* (2001). "Expression of tumor-suppressor genes interferon regulatory factor 1 and death-associated protein kinase in primitive acute myelogenous leukemia cells." Blood **97**(7): 2177-2179.

Guzman, M. L. R., R.M. Karnischky, L. Li, X. Peterson, D.R. Howard, D.S. Jordan, C.T. (2005). "The sesquiterpene lactone parthenolide induces apoptosis of human acute myelogenous leukemia stem and progenitor cells." Blood **105**(11): 4163-4169.

Halicka, H. D., F. Ozkaynak, *et al.* (2009). "DNA damage response as a biomarker in treatment of leukemias." Cell Cycle **8**(11): 1720-1724.

Hande, K. R. (2008). "Topoisomerase II inhibitors." Update on Cancer Therapeutics **3**(1): 13-26.

Hao, S. and D. Baltimore (2009). "The stability of mRNA influences the temporal order of the induction of genes encoding inflammatory molecules." Nature immunology **10**.

Hartlerode, A. J., M. J. Morgan, *et al.* (2015). "Recruitment and activation of the ATM kinase in the absence of DNA-damage sensors." Nat Struct Mol Biol **advance online publication**.

Hauswirth, A., S. Florian, *et al.* (2007). "Expression of the target receptor CD33 in CD34+/CD38-/CD123+ AML stem cells." Eur J Clin Invest **37**(1): 73 - 82.

Hehner, S. P., T. G. Hofmann, *et al.* (1999). "The Antiinflammatory Sesquiterpene Lactone Parthenolide Inhibits NF-κB by Targeting the IκB Kinase Complex." The Journal of Immunology **163**(10): 5617-5623.

Heikkinen, K., S.-M. Karppinen, *et al.* (2003). "Mutation screening of Mre11 complex genes: indication of RAD50 involvement in breast and ovarian cancer susceptibility." Journal of Medical Genetics **40**(12): e131-e131.

Heil, G., D. Hoelzer, *et al.* (1997). "A Randomized, Double-Blind, Placebo-Controlled, Phase III Study of Filgrastim in Remission Induction and Consolidation Therapy for Adults With De Novo Acute Myeloid Leukemia." Blood **90**(12): 4710-4718.

Hermitte, F., P. Brunet de la Grange, *et al.* (2006). "Very Low O2 Concentration (0.1%) Favors G0 Return of Dividing CD34+ Cells." STEM CELLS **24**(1): 65-73.

Herzig, R. H., J. D. Hines, *et al*. (1987). "Cerebellar toxicity with high-dose cytosine arabinoside." Journal of Clinical Oncology **5**(6): 927-932.

Heyer, W.-D., K. T. Ehmsen, *et al.* (2010). "Regulation of homologous recombination in eukaryotes." Annual review of genetics **44**: 113-139.

Hill, R. and P. W. Lee (2010). "The DNA-dependent protein kinase (DNA-PK): More than just a case of making ends meet?" Cell Cycle **9**(17): 3460-3469.

Hinz, M. and C. Scheidereit (2014). "The IκB kinase complex in NF-κB regulation and beyond." EMBO Reports **15**(1): 46-61.

Hope, K. J., L. Jin, *et al.* (2004). "Acute myeloid leukemia originates from a hierarchy of leukemic stem cell classes that differ in self-renewal capacity." Nat Immunol **5**(7): 738-743.

Horiuchi, M., K. Takeuchi, *et al.* (2009). "Structural Basis for the Antiproliferative Activity of the Tob-hCaf1 Complex." The Journal of Biological Chemistry **284**(19): 13244-13255.

Horton, S. J. and B. J. P. Huntly (2012). "Recent advances in acute myeloid leukemia stem cell biology." Haematologica **97**(7): 966-974.

Hoshii, T., S. Matsuda, *et al.* (2014). "Pleiotropic roles of mTOR complexes in haemato-lymphopoiesis and leukemogenesis." The Journal of Biochemistry **156**(2): 73-83.

Hoshii, T., Y. Tadokoro, *et al.* (2012). "mTORC1 is essential for leukemia propagation but not stem cell self-renewal." J Clin Invest **122**(6): 2114 - 2129.

Hsu, P. P., S. A. Kang, *et al*. (2011). "The mTOR-Regulated Phosphoproteome Reveals a Mechanism of mTORC1-Mediated Inhibition of Growth Factor Signaling." Science **332**(6035): 1317-1322.

Hu, X., L. Xing, *et al.* (2012). "BTG2 Overexpression Increases the Radiosensitivity of Breast Cancer Cells In Vitro and In Vivo." Oncology Research Featuring Preclinical and Clinical Cancer Therapeutics **20**(10): 457-465.

Huang da, W., B. T. Sherman, *et al.* (2009). "Systematic and integrative analysis of large gene lists using DAVID bioinformatics resources." Nature protocols **4**.

Huang, F. and A. V. Mazin (2014). "A Small Molecule Inhibitor of Human RAD51 Potentiates Breast Cancer Cell Killing by Therapeutic Agents in Mouse Xenografts." PLoS ONE **9**(6): e100993.

Hung, C.-M., L. Garcia-Haro, *et al.* (2012). "mTOR-Dependent Cell Survival Mechanisms." Cold Spring Harbor Perspectives in Biology **4**(12): a008771.

Igney, F. H. and P. H. Krammer (2002). "Death and anti-death: tumour resistance to apoptosis." Nat Rev Cancer **2**(4): 277-288.

Imran, M. and I. K. Lim (2013). "Regulation of Btg2/TIS21/PC3 expression via reactive oxygen species–protein kinase C–NFκB pathway under stress conditions." Cellular Signalling **25**(12): 2400-2412.

Imran, M., T. J. Park, *et al.* (2012). "TIS21/BTG2/PC3 enhances downregulation of c-Myc during differentiation of HL-60 cells by activating Erk1/2 and inhibiting Akt in response to all-trans-retinoic acid." European Journal of Cancer **48**(15): 2474-2485.

Ito, S., A. Ishii, *et al.* (2012). "Mechanism of cancer cell death induced by depletion of an essential replication regulator." PLoS ONE **7**(5): e36372.

Jackson, A. L. and L. A. Loeb (2001). "The contribution of endogenous sources of DNA damage to the multiple mutations in cancer." Mutation Research/Fundamental and Molecular Mechanisms of Mutagenesis **477**(1–2): 7-21.

Jackson, N., B. S. Menon, *et al.* (1999). "Why is acute leukemia more common in males? A possible sex-determined risk linked to the ABO blood group genes." Annals of Hematology **78**(5): 233-236.

Jackson, S. P. and J. Bartek (2009). "The DNA-damage response in human biology and disease." Nature **461**(7267): 1071-1078.

Jacobs, K. M., S. Misri, *et al.* (2016). "Unique Epigenetic Influence of H2AX Phosphorylation and H3K56 Acetylation On Normal Stem Cell Radioresponses." Molecular Biology of the Cell.

Jain, D. (2000). "Cardiotoxicity of doxorubicin and other anthracycline derivatives." Journal of Nuclear Cardiology **7**(1): 53-62.

Jan, M. and R. Majeti (2013). "Clonal evolution of acute leukemia genomes." Oncogene **32**(2): 135-140.

Jang, Y.-Y. S., S.J. (2007). "A low level of reactive oxygen species selects for primitive hematopoietic stem cells that may reside in in the low-oxygenic niche." Blood **110**(8): 3056-3063.

Jankowska, A. and H. Szpurka (2012). "Mutational determinants of epigenetic instability in myeloid malignancies." Semin Oncol **39**: 80 - 96.

Jaroslav, P., H. Martina, *et al.* (2005). "Expression of cyclins D1, D2 and D3 and Ki-67 in human leukemia." Leukemia & Lymphoma **46**(11): 1605-1612.

Jawad, M., C. Seedhouse, *et al.* (2010). "Analysis of factors that affect in vitro chemosensitivity of leukaemic stem and progenitor cells to gemtuzumab ozogamicin (Mylotarg) in acute myeloid leukaemia." Leukemia **24**: 74 - 80.

Jawad, M., N. Yu, *et al.* (2012). "Targeting of CD34+CD38- cells using Gemtuzumab ozogamicin (Mylotarg) in combination with tipifarnib (Zarnestra) in acute Myeloid Leukaemia." BMC Cancer **12**(1): 431.

Jazayeri, A., J. Falck, *et al.* (2006). "ATM- and cell cycle-dependent regulation of ATR in response to DNA double-strand breaks." Nat Cell Biol **8**(1): 37-45.

Jerez, A., Y. Sugimoto, *et al.* (2012). "Loss of heterozygosity in 7q myeloid disorders: clinical associations and genomic pathogenesis." Blood **119**(25): 6109-6117.

Jin, L., K. J. Hope, *et al.* (2006). "Targeting of CD44 eradicates human acute myeloid leukemic stem cells." Nat Med **12**(10): 1167-1174.

Jordan, C. T. and M. L. Guzman (2004). "Mechanisms controlling pathogenesis and survival of leukemic stem cells." Oncogene **23**(43): 7178-7187.

Kagoya, Y., A. Yoshimi, *et al.* (2014). "Positive feedback between NF-κB and TNF-α promotes leukemia-initiating cell capacity." The Journal of Clinical Investigation **124**(2): 528-542.

Kantarjian, H. M., S. Jeha, *et al.* (2007). "Clofarabine: Past, present, and future." Leukemia & Lymphoma **48**(10): 1922-1930.

Kastan, M. B. (2008). "DNA Damage Responses: Mechanisms and Roles in Human Disease: 2007 G.H.A. Clowes Memorial Award Lecture." Molecular Cancer Research **6**(4): 517-524.

Kastan, M. B. and J. Bartek (2004). "Cell-cycle checkpoints and cancer." Nature **432**(7015): 316-323.

Kastan, M. B., Q. Zhan, *et al.* (1992). "A mammalian cell cycle checkpoint pathway utilizing p53 and GADD45 is defective in ataxia-telangiectasia." Cell **71**(4): 587-597.

Kennedy, J. A. and F. Barabe (2008). "Investigating human leukemogenesis: from cell lines to in vivo models of human leukemia." Leukemia **22**(11): 2029-2040.

Kim, B. C., M. S. Ryu, *et al.* (2008). "TIS21/BTG2 Negatively Regulates Estradiol-Stimulated Expansion of Hematopoietic Stem Cells by Derepressing Akt Phosphorylation and Inhibiting mTOR Signal Transduction." STEM CELLS **26**(9): 2339-2348.

Kim, J. K., Y. Jung, *et al.* (2013). "TBK1 Regulates Prostate Cancer Dormancy through mTOR Inhibition." Neoplasia (New York, N.Y.) **15**(9): 1064-1074.

Koike, M., M. Mashino, *et al.* (2008). "Histone H2AX Phosphorylation Independent of ATM after X-irradiation in Mouse Liver and Kidney in situ." Journal of Radiation Research **49**(4): 445-449.

Kopp, H., S. Avecilla, *et al.* (2005). "The bone marrow vascular niche: home of HSC differentiation and mobilization." Physiology **20**: 349 - 356.

Krejci, L., V. Altmannova, *et al.* (2012). "Homologous recombination and its regulation." Nucleic Acids Research.

Krenzlin, H., I. Demuth, *et al.* (2012). "DNA Damage in Nijmegen Breakage Syndrome Cells Leads to PARP Hyperactivation and Increased Oxidative Stress." PLoS Genetics **8**(3): e1002557.

Krishnakumar, R. and W. L. Kraus (2010). "The PARP Side of the Nucleus: Molecular Actions, Physiological Outcomes, and Clinical Targets." Molecular Cell **39**(1): 8-24.

Kunisaki, Y., I. Bruns, *et al*. (2013). "Arteriolar niches maintain haematopoietic stem cell quiescence." Nature **502**(7473): 637-643.

Kunkel, T. A. (2004). "DNA Replication Fidelity." Journal of Biological Chemistry **279**(17): 16895-16898.

Kurimasa, A., S. Kumano, *et al.* (1999). "Requirement for the Kinase Activity of Human DNA-Dependent Protein Kinase Catalytic Subunit in DNA Strand Break Rejoining." Molecular and Cellular Biology **19**(5): 3877-3884.

Lagadinou, E., P. Ziros, *et al.* (2008). "c-Jun N-terminal kinase activation failure is a new mechanism of anthracycline resistance in acute myeloid leukemia." Leukemia **22**: 1899 - 1908.

Lai, A. Y. and M. Kondo (2006). "Asymmetrical lymphoid and myeloid lineage commitment in multipotent hematopoietic progenitors." The Journal of Experimental Medicine **203**(8): 1867-1873.

Lamarche, B. J., N. I. Orazio, *et al.* (2010). "The MRN complex in Double-Strand Break Repair and Telomere Maintenance." FEBS letters **584**(17): 3682-3695.

Langelier, M.-F., A. A. Riccio, *et al.* (2014). "PARP-2 and PARP-3 are selectively activated by 5' phosphorylated DNA breaks through an allosteric regulatory mechanism shared with PARP-1." Nucleic acids research **42**(12): 7762-7775.

Leclerc, J.-M. and R. Momparler (1984). Effect of the interval between exposures to cytarabine on its cytotoxic action on HL-60 myeloid leukemic cells.

Lee, D.-H. and D. Chowdhury (2011). "What Goes On Must Come Off: phosphatases gate-crash the DNA damage response." Trends in Biochemical Sciences **36**(11): 569-577.

Lee, J. and W. G. Dunphy (2013). "The Mre11-Rad50-Nbs1 (MRN) complex has a specific role in the activation of Chk1 in response to stalled replication forks." Molecular Biology of the Cell **24**(9): 1343-1353.

Lee, V. Y., D. S. McClintock, *et al.* (2002). "Hypoxia Sensitizes Cells to Nitric Oxide-induced Apoptosis." Journal of Biological Chemistry **277**(18): 16067-16074.

Leung, M., D. Rosen, *et al.* (2011). "Poly(ADP-ribose) polymerase-1 inhibition: preclinical and clinical development of synthetic lethality." Mol Med **17**(7-8): 854-862.

Lewinsohn, M., A. L. Brown, *et al.* (2016). "Novel germ line DDX41 mutations define families with a lower age of MDS/AML onset and lymphoid malignancies." Blood **127**(8): 1017-1023.

Ley, T., L. Ding, *et al.* (2010). "DNMT3A mutations in acute myeloid leukemia." N Engl J Med **363**: 2424 - 2433.

Li, T., Z.-W. Zhou, *et al.* (2016). "DNA Damage Response in Hematopoietic Stem Cell Ageing." Genomics, Proteomics & Bioinformatics **14**(3): 147-154.

Li, X. and W.-D. Heyer (2008). "Homologous recombination in DNA repair and DNA damage tolerance." Cell Res **18**(1): 99-113.

Li, Z. and W. Dalton (2006). "Tumor microenvironment and drug resistance in hematologic malignancies." Blood Rev **20**(6): 333 - 342.

Liao, W., M. A. McNutt, *et al.* (2009). "The comet assay: a sensitive method for detecting DNA damage in individual cells." Methods **48**(1): 46-53.

Lim, I., M. Lee, *et al*. (1998). "Induction of growth inhibition of 293 cells by downregulation of the cyclin E and cyclin-dependent kinase 4 proteins due to overexpression of TIS21." Mol Carcinog **23**: 25 - 35.

Lim, Y.-B., T. J. Park, *et al.* (2008). "B Cell Translocation Gene 2 Enhances Susceptibility of HeLa Cells to Doxorubicin-induced Oxidative Damage." Journal of Biological Chemistry **283**(48): 33110-33118.

Lin, W. J., J. D. Gary, *et al.* (1996). "The mammalian immediate-early TIS21 protein and the leukemia-associated BTG1 protein interact with a protein-arginine N-methyltransferase." Journal of Biological Chemistry **271**(25): 15034-15044.

Lindahl, T. (1993). "Instability and decay of the primary structure of DNA." Nature **362**(6422): 709-715.

Logue, S. E., M. Elgendy, *et al.* (2009). "Expression, purification and use of recombinant annexin V for the detection of apoptotic cells." Nat. Protocols **4**(9): 1383-1395.

Lord, C. J. and A. Ashworth (2012). "The DNA damage response and cancer therapy." Nature **481**(7381): 287-294.

Louka, M., E. Boutou, *et al.* (2015). DNA Damage Response/Repair in Cancer Stem Cells — Potential vs. Controversies.

Louria-Hayon, I. (2014). "Signal, Transduction, and the Hematopoietic Stem Cell." Rambam Maimonides Medical Journal **5**(4): e0033.

Löwenberg , B., G. J. Ossenkoppele , *et al.* (2009). "High-Dose Daunorubicin in Older Patients with Acute Myeloid Leukemia." New England Journal of Medicine **361**(13): 1235-1248.

Löwenberg , B., T. Pabst , *et al.* (2011). "Cytarabine Dose for Acute Myeloid Leukemia." New England Journal of Medicine **364**(11): 1027-1036.

Löwenberg , B., W. van Putten , *et al.* (2003). "Effect of Priming with Granulocyte Colony-Stimulating Factor on the Outcome of Chemotherapy for Acute Myeloid Leukemia." New England Journal of Medicine **349**(8): 743-752.

Lu, C., Y. Shi, *et al.* (2008). "Serum starvation induces H2AX phosphorylation to regulate apoptosis via p38 MAPK pathway." FEBS Letters **582**(18): 2703-2708.

Luo, G., M. S. Yao, *et al.* (1999). "Disruption of mRad50 causes embryonic stem cell lethality, abnormal embryonic development, and sensitivity to ionizing radiation." Proceedings of the National Academy of Sciences of the United States of America **96**(13): 7376-7381.

Luo, M., Z. Lu, *et al.* (2010). "Nuclear entry of active caspase-3 is facilitated by its p3-recognition-based specific cleavage activity." Cell Res **20**(2): 211-222.

Ma, J., X. Li, *et al.* (2017). "Mechanisms responsible for the synergistic antileukemic interactions between ATR inhibition and cytarabine in acute myeloid leukemia cells." Scientific Reports **7**: 41950.

Ma, Y., K. Kanakousaki, *et al.* (2015). "How the cell cycle impacts chromatin architecture and influences cell fate." Frontiers in Genetics **6**: 19.

Mahaney, B. L., K. Meek, *et al.* (2009). "Repair of ionizing radiation-induced DNA double-strand breaks by non-homologous end-joining." Biochem J **417**(3): 639-650.

Mandal, P. K., C. Blanpain, *et al.* (2011). "DNA damage response in adult stem cells: pathways and consequences." Nat Rev Mol Cell Biol **12**(3): 198-202.

Manz, M. G. and S. Boettcher (2014). "Emergency granulopoiesis." Nat Rev Immunol **14**(5): 302-314.

Mao, B., H. E. Xiao, *et al.* (2015). "MicroRNA-21 regulates the expression of BTG2 in HepG2 liver cancer cells." Molecular Medicine Reports **12**(4): 4917-4924.

Marková, E., N. Schultz, *et al*. (2007). "Kinetics and dose-response of residual 53BP1/γ-H2AX foci: Co-localization, relationship with DSB repair and clonogenic survival." International Journal of Radiation Biology **83**(5): 319-329.

Martinez-Marignac, V. L., A. Rodrigue, *et al*. (2011). "The Effect of a DNA Repair Gene on Cellular Invasiveness: Xrcc3 Over-Expression in Breast Cancer Cells." PLoS ONE **6**(1): e16394.

Martinez, J. S., C. von Nicolai, *et al.* (2016). "BRCA2 regulates DMC1-mediated recombination through the BRC repeats." Proceedings of the National Academy of Sciences of the United States of America **113**(13): 3515-3520.

Maugeri-Saccà, M., M. Bartucci, *et al.* (2012). "DNA Damage Repair Pathways in Cancer Stem Cells." Molecular Cancer Therapeutics **11**(8): 1627-1636.

Mawad, R. and E. Estey (2012). "Acute Myeloid Leukemia with Normal Cytogenetics." Current Oncology Reports **14**(5): 359-368.

McCormack, E., O. Bruserud, *et al*. (2005). "Animal models of acute myelogenous leukaemia - development, application and future perspectives." Leukemia **19**: 687 - 706.

McManus, K. J. and M. J. Hendzel (2005). "ATM-dependent DNA Damage-independent Mitotic Phosphorylation of H2AX in Normally Growing Mammalian Cells." Molecular Biology of the Cell **16**(10): 5013-5025.

Meek, D. W. (2004). "The p53 response to DNA damage." DNA repair **3**(8): 1049-1056.

Meikrantz, W. and R. Schlegel (1995). "Apoptosis and the cell cycle." Journal of Cellular Biochemistry **58**(2): 160-174.

Milyavsky, M., O. Gan, *et al.* (2010). "A distinctive DNA damage response in human hematopoietic stem cells reveals an apoptosis-independent role for p53 in self-renewal." Cell Stem Cell **7**(2): 186 - 197.

Mladenov, E. and G. Iliakis (2011). "Induction and repair of DNA double strand breaks: The increasing spectrum of non-homologous end joining pathways." Mutation Research/Fundamental and Molecular Mechanisms of Mutagenesis **711**(1–2): 61-72.

Mohrin, M., E. Bourke, *et al.* (2010). "Hematopoietic stem cell quiescence promotes error prone DNA repair and mutagenesis." Cell stem cell **7**(2): 174-185.

Moignard, V., I. C. Macaulay, *et al.* (2013). "Characterization of transcriptional networks in blood stem and progenitor cells using high-throughput single-cell gene expression analysis." Nat Cell Biol **15**(4): 363-372.

Mollerstrom, E., A. Kovacs, *et al.* (2010). "Up-regulation of cell cycle arrest protein BTG2 correlates with increased overall survival in breast cancer, as detected by immunohistochemistry using tissue microarray." BMC Cancer **10**(1): 296.

Montagnoli, A., D. Guardavaccaro, *et al.* (1996). "Overexpression of the nerve growth factor-inducible PC3 immediate early gene is associated with growth inhibition." Cell Growth Differ **7**: 1327 - 1336.

Mony, U., M. Jawad, *et al.* (2008). "Resistance to FLT3 inhibition in an in vitro model of primary AML cells with a stem cell phenotype in a defined microenvironment." Leukemia **22**(7): 1395 - 1401.

Moon, A. F., M. Garcia-Diaz, *et al.* (2007). "Structural insight into the substrate specificity of DNA Polymerase [mu]." Nat Struct Mol Biol **14**(1): 45-53.

Morgado-Palacin, I., A. Day, *et al.* (2016). "Targeting the kinase activities of ATR and ATM exhibits antitumoral activity in mouse models of MLL rearranged AML." Science Signaling **9**(445): ra91-ra91.

Morgan, M., F. O Onono, *et al.* (2011). Modulation of anthracycline-induced cytotoxicity by targeting the prenylated proteome in myeloid leukemia cells.

Morin, R. D., M. Mendez-Lago, *et al.* (2011). "Frequent mutation of histone-modifying genes in non-Hodgkin lymphoma." Nature **476**(7360): 298-303.

Morrison, S. J. and D. T. Scadden (2014). "The bone marrow niche for haematopoietic stem cells." Nature **505**(7483): 327-334.

Moureau, S., J. Luessing, *et al.* (2016). "A role for the p53 tumour suppressor in regulating the balance between homologous recombination and non-homologous end joining." Open Biology **6**(9): 160225.

Mrozek, K. (2008). "Cytogenetic, molecular genetic, and clinical characteristics of acute myeloid leukemia with a complex karyotype." Semin Oncol **35**(4): 365 - 377.

Murray, J. M., T. Stiff, *et al.* (2012). "DNA double-strand break repair within heterochromatic regions." Biochem Soc Trans **40**(1): 173-178.

Myint, H. and N. Lucie (1992). "The prognostic significance of the CD34 antigen in acute myeloid leukaemia." Leuk Lymphoma **7**: 425 - 429.

Nakamura-Ishizu, A. and T. Suda (2013). "Hematopoietic stem cell niche: An interplay among a repertoire of multiple functional niches." Biochimica et Biophysica Acta (BBA) - General Subjects **1830**(2): 2404-2409.

Nakamura, J. and J. A. Swenberg (1999). "Endogenous apurinic/apyrimidinic sites in genomic DNA of mammalian tissues." Cancer Research **59**(11): 2522-2526.

Narayanaswamy, P. B., S. Tkachuk, *et al.* (2016). "CHK1 and RAD51 activation after DNA damage is regulated via urokinase receptor/TLR4 signaling." Cell Death & Disease **7**(9): e2383.

Nardi, V. and R. P. Hasserjian (2016). "Genetic Testing in Acute Myeloid Leukemia and Myelodysplastic Syndromes." Surgical Pathology Clinics **9**(1): 143-163.

Neckers, L. and J. Cossman (1983). "Transferrin receptor induction in mitogen-stimulated human T lymphocytes is required for DNA synthesis and cell division and is regulated by interleukin 2." Proc Natl Acad Sci U S A **80**(11): 3494 - 3498.

Nickson, C. M. and J. L. Parsons (2014). "Monitoring regulation of DNA repair activities of cultured cells in-gel using the comet assay." Frontiers in genetics **5**.

Niida, H. and M. Nakanishi (2006). "DNA damage checkpoints in mammals." Mutagenesis **21**(1): 3-9.

Nishioka, C., T. Ikezoe, *et al.* (2013). "CD34+/CD38− acute myelogenous leukemia cells aberrantly express CD82 which regulates adhesion and survival of leukemia stem cells." International Journal of Cancer **132**(9): 2006-2019.

Nitiss, J. L. (2009). "Targeting DNA topoisomerase II in cancer chemotherapy." Nature reviews. Cancer **9**(5): 338-350.

Nomdedeu, M., M. C. Lara-Castillo, *et al.* (2015). "Treatment with G-CSF reduces acute myeloid leukemia blast viability in the presence of bone marrow stroma." Cancer Cell International **15**: 122.

O'Donnell, M. R., C. N. Abboud, *et al.* (2012). "Acute Myeloid Leukemia." Journal of the National Comprehensive Cancer Network **10**(8): 984-1021.

Octavia, Y., C. G. Tocchetti, *et al.* (2012). "Doxorubicin-induced cardiomyopathy: From molecular mechanisms to therapeutic strategies." Journal of Molecular and Cellular Cardiology **52**(6): 1213-1225.

Ohta, K., A. Nicolas, *et al.* (1998). "Mutations in the MRE11, RAD50, XRS2, and MRE2 genes alter chromatin configuration at meiotic DNA double-stranded break sites in premeiotic and meiotic cells." Proceedings of the National Academy of Sciences of the United States of America **95**(2): 646-651.

Okabe, M., Y. Kunieda, *et al*. (1995). "Megakaryocytic differentiation of a leukemic cell line, MC3, by phorbol ester: Induction of glycoprotein IIb/IIIa and effects on expression of IL-6, IL-6 receptor, mpl and GATA genes." Leukemia Research **19**(12): 933-943.

Olive, P. L. and J. P. Banath (2006). "The comet assay: a method to measure DNA damage in individual cells." Nat Protoc **1**(1): 23-29.

Osmulski, P. A. and M. Gaczynska (2013). "Rapamycin Allosterically Inhibits the Proteasome." Molecular Pharmacology **84**(1): 104-113.

Otsuki, Y., Z. Li, *et al.* (2003). "Apoptotic detection methods — from morphology to gene." Progress in Histochemistry and Cytochemistry **38**(3): 275-339.

Pabst, T., E. Vellenga, *et al.* (2012). "Favorable effect of priming with granulocyte colony-stimulating factor in remission induction of acute myeloid leukemia restricted to dose escalation of cytarabine." Blood **119**(23): 5367-5373.

Pallavicini, M. G., L. J. Summers, *et al.* (1985). "Cytokinetic properties of asynchronous and cytosine arabinoside perturbed murine tumors measured by simultaneous bromodeoxyuridine/DNA analyses." Cytometry **6**(6): 602-610.

Pallis, M., A. Abdul-Aziz, *et al.* (2012). "The multi-kinase inhibitor TG02 overcomes signalling activation by survival factors to deplete MCL1 and XIAP and induce cell death in primary acute myeloid leukaemia cells." Br J Haematol **159**(2): 191 - 203.

Pallis, M., F. Burrows, *et al.* (2013). "Efficacy of RNA polymerase II inhibitors in targeting dormant leukaemia cells." BMC Pharmacology and Toxicology **14**(1): 32.

Pallis, M., T. Harvey, *et al*. (2016). "Phenotypically Dormant and Immature Leukaemia Cells Display Increased Ribosomal Protein S6 Phosphorylation." PLOS ONE **11**(3): e0151480.

Pallis, M., J. Syan, *et al.* (1999). "Flow cytometric chemosensitivity analysis of blasts from patients with acute myeloblastic leukemia and myelodysplastic syndromes: the use of 7AAD with antibodies to CD45 or CD34." Cytometry **37**(4): 308-313.

Pallisgaard, N., N. Clausen, *et al.* (1999). "Rapid and sensitive minimal residual disease detection in acute leukemia by quantitative real-time RT-PCR exemplified by t(12;21) TEL-AML1 fusion transcript." Genes, Chromosomes and Cancer **26**(4): 355-365.

Panier, S. and S. J. Boulton (2014). "Double-strand break repair: 53BP1 comes into focus." Nat Rev Mol Cell Biol **15**(1): 7-18.

Pardo, B., B. Gómez-González, *et al.* (2009). "DNA Repair in Mammalian Cells." Cellular and Molecular Life Sciences **66**(6): 1039-1056.

Pelicci, P. G. (2012). "Normal and leukemic stem cells." Leukemia **1**(S2): S54-S55.

Peng, G. and S.-Y. Lin (2011). "Exploiting the homologous recombination DNA repair network for targeted cancer therapy." World Journal of Clinical Oncology **2**(2): 73-79.

Peters, A. and J. Schwaller (2011). "Epigenetic mechanisms in acute myeloid leukemia." Prog Drug Res **67**: 197 - 219.

Pietras, E. M., M. R. Warr, *et al.* (2011). "Cell cycle regulation in hematopoietic stem cells." The Journal of Cell Biology **195**(5): 709-720.

Polo, S. E. and S. P. Jackson (2011). "Dynamics of DNA damage response proteins at DNA breaks: a focus on protein modifications." Genes & Development **25**(5): 409-433.

Powell, E., J. Shao, *et al*. (2016). "p53 deficiency linked to B cell translocation gene 2 (BTG2) loss enhances metastatic potential by promoting tumor growth in primary and metastatic sites in patient-derived xenograft (PDX) models of triple-negative breast cancer." Breast Cancer Research : BCR **18**: 13.

Price, N. E., K. M. Johnson, *et al.* (2014). "Interstrand DNA–DNA Cross-Link Formation Between Adenine Residues and Abasic Sites in Duplex DNA." Journal of the American Chemical Society **136**(9): 3483-3490.

Pulliam-Leath, A. C., S. L. Ciccone, *et al.* (2010). "Genetic disruption of both Fancc and Fancg in mice recapitulates the hematopoietic manifestations of Fanconi anemia." Blood **116**(16): 2915-2920.

Pyatt, D. W., W. S. Stillman, *et al*. (1999). "An Essential Role for NF-κB in Human CD34+Bone Marrow Cell Survival." Blood **93**(10): 3302-3308.

Qian, H., N. Buza-Vidas, *et al*. (2007). "Critical role of thrombopoietin in maintaining adult quiescent hematopoietic stem cells." Cell stem cell **1**(6): 671-684.

Quy, L. N., Y. W. Choi, *et al.* (2013). "TIS21/BTG2/PC3 inhibits interleukin-6 expression via downregulation of STAT3 pathway." Cellular Signalling **25**(12): 2391-2399.

Raderschall, E., A. Bazarov, *et al.* (2002). "Formation of higher-order nuclear Rad51 structures is functionally linked to p21 expression and protection from DNA damage-induced apoptosis." Journal of Cell Science **115**(1): 153-164.

RAI, R., G. PENG, *et al*. (2007). "DNA Damage Response: The Players, the Network and the Role in Tumor Suppression." Cancer Genomics - Proteomics **4**(2): 99-106.

Ramos, N. R., C. C. Mo, *et al.* (2015). "Current Approaches in the Treatment of Relapsed and Refractory Acute Myeloid Leukemia." Journal of Clinical Medicine **4**(4): 665-695.

Rastogi, R., Z. Jiang, *et al*. (2013). "Rapamycin Induces Mitogen-activated Protein (MAP) Kinase Phosphatase-1 (MKP-1) Expression through Activation of Protein Kinase B and Mitogen-activated Protein Kinase Kinase Pathways." Journal of Biological Chemistry **288**(47): 33966-33977.

Raza, A., H. Preisler, *et al.* (1990). "Direct relationship between remission duration in acute myeloid leukemia and cell cycle kinetics: a leukemia intergroup study." Blood **76**(11): 2191-2197.

Reagan, M. R. and C. J. Rosen (2016). "Navigating the bone marrow niche: translational insights and cancer-driven dysfunction." Nat Rev Rheumatol **12**(3): 154-168.

Récher, C., O. Beyne-Rauzy, *et al*. (2005). Antileukemic activity of rapamycin in acute myeloid leukemia.

Relling, M. V., J. M. Boyett, *et al.* (2003). "Granulocyte colony-stimulating factor and the risk of secondary myeloid malignancy after etoposide treatment." Blood **101**(10): 3862-3867.

Rimann, M. and U. Graf-Hausner (2012). "Synthetic 3D multicellular systems for drug development." Current Opinion in Biotechnology **23**(5): 803-809.

Rogakou, E. P., D. R. Pilch, *et al.* (1998). "DNA Double-stranded Breaks Induce Histone H2AX Phosphorylation on Serine 139." Journal of Biological Chemistry **273**(10): 5858-5868.

Ronen, A. and B. W. Glickman (2001). "Human DNA repair genes." Environmental and Molecular Mutagenesis **37**(3): 241-283.

Rooney, S., J. Sekiguchi, *et al*. (2002). "Leaky Scid Phenotype Associated with Defective V(D)J Coding End Processing in Artemis-Deficient Mice." Molecular Cell **10**(6): 1379-1390.

Rosen, D. B., S. Putta, *et al.* (2010). "Distinct Patterns of DNA Damage Response and Apoptosis Correlate with Jak/Stat and PI3Kinase Response Profiles in Human Acute Myelogenous Leukemia." PLoS ONE **5**(8): e12405.

Rossetto, D., A. W. Truman, *et al.* (2010). "Epigenetic modifications in double-strand break DNA damage signaling and repair." Clinical Cancer Research **16**(18): 4543-4552.

Rossi, D. J., D. Bryder, *et al*. (2007). "Deficiencies in DNA damage repair limit the function of haematopoietic stem cells with age." Nature **447**(7145): 725-729.

Rossi, D. J., J. Seita, *et al*. (2007). "Hematopoietic Stem Cell Quiescence Attenuates DNA Damage Response and Permits DNA Damage Accumulation During Aging." Cell Cycle **6**(19): 2371-2376.

Rossi, D. J. J. C. H. W. I. L. (2008). "Stem Cells and the Pathways to Aging and Cancer." Cell **132**(4): 681-696.

Rowe, J. M. (2009). "Optimal induction and post-remission therapy for AML in first remission." ASH Education Program Book **2009**(1): 396-405.

Rübe, C. E., A. Fricke, *et al*. (2011). "Accumulation of DNA Damage in Hematopoietic Stem and Progenitor Cells during Human Aging." PLoS ONE **6**(3): e17487.

Ryu, M. S., M. S. Lee, *et al.* (2004). "TIS21/BTG2/PC3 is expressed through PKC-δ pathway and inhibits binding of cyclin B1-Cdc2 and its activity, independent of p53 expression." Experimental Cell Research **299**(1): 159-170.

Saito, Y., H. Kitamura, *et al.* (2010). "Identification of Therapeutic Targets for Quiescent, Chemotherapy-Resistant Human Leukemia Stem Cells." Science Translational Medicine **2**(17): 17ra19.

Saito, Y., N. Uchida, *et al*. (2010). "Induction of cell cycle entry eliminates human leukemia stem cells in a mouse model of AML." Nat Biotechnol **28**(3): 275 - 280.

Salvesen, G. S. and V. M. Dixit (1997). "Caspases: Intracellular Signaling by Proteolysis." Cell **91**(4): 443-446.

San Filippo, J., P. Sung, *et al.* (2008). "Mechanism of eukaryotic homologous recombination." Annu. Rev. Biochem. **77**: 229-257.

Sasajima, H., K. Nakagawa, *et al.* (2002). "Antiproliferative proteins of the BTG/Tob family are degraded by the ubiquitin-proteasome system." European Journal of Biochemistry **269**(14): 3596-3604.

Schmid, I., C. H. Uittenbogaart, *et al*. (1991). "A gentle fixation and permeabilization method for combined cell surface and intracellular staining with improved precision in DNA quantification." Cytometry **12**(3): 279-285.

Schmitt-Graeff, A. H., R. Nitschke, et al. (2015). "The Hematopoietic Niche in Myeloproliferative Neoplasms." Mediators of Inflammation **2015**: 347270.

Schnell, U., F. Dijk, *et al.* (2012). "Immunolabeling artifacts and the need for live-cell imaging." Nat Meth **9**(2): 152-158.

Scholz, G., C. Jandus, *et al.* (2016). "Modulation of mTOR Signalling Triggers the Formation of Stem Cell-like Memory T Cells." EBioMedicine **4**: 50-61.

Seedhouse, C., M. Grundy, *et al.* (2009). "Impaired S-phase arrest in acute myeloid leukemia cells with a FLT3 internal tandem duplication treated with clofarabine." Clin Cancer Res **15**(23): 7291 - 7298.

Seedhouse, C., A. Whittall, *et al.* (2010). "An Immortalised Leukaemia Cell Line Models the Quiescence of Leukaemic Stem Cells and Shows Impaired Double Strand Break Repair Following Daunorubicin Treatment." Blood **116**(21): 3989-3989.

Seita, J. and I. L. Weissman (2010). "Hematopoietic Stem Cell: Self-renewal versus Differentiation." Wiley interdisciplinary reviews. Systems biology and medicine **2**(6): 640-653.

Shah, A., T. M. L. Andersson, *et al.* (2013). "Survival and cure of acute myeloid leukaemia in England, 1971-2006: a population–based study." British Journal of Haematology **162**(4): 509-516.

Shaheen, M., C. Allen, *et al*. (2011). "Synthetic lethality: exploiting the addiction of cancer to DNA repair." Blood **117**(23): 6074-6082.

Shalem, O., O. Dahan, *et al*. (2008). "Transient transcriptional responses to stress are generated by opposing effects of mRNA production and degradation." Molecular systems biology **4**.

Shang, S., C. Seedhouse, *et al*. (2008). "Low dose rapamycin does not modulate p-glycoprotein function in acute myeloid leukaemia." Leuk Res **32**(5): 836 - 837.

Shaposhnikov, S. A., V. B. Salenko, *et al*. (2008). "Single-cell gel electrophoresis (the comet assay): Loops or fragments?" ELECTROPHORESIS **29**(14): 3005-3012.

Sharma, M. B., L. S. Limaye, *et al*. (2012). "Mimicking the functional hematopoietic stem cell niche in vitro: recapitulation of marrow physiology by hydrogel-based three-dimensional cultures of mesenchymal stromal cells." Haematologica **97**(5): 651-660.

Shaul, Y. D. and R. Seger (2007). "The MEK/ERK cascade: From signaling specificity to diverse functions." Biochimica et Biophysica Acta (BBA) - Molecular Cell Research **1773**(8): 1213-1226.

She, M., X. Niu, *et al.* (2012). "Resistance of leukemic stem-like cells in AML cell line KG1a to natural killer cell-mediated cytotoxicity." Cancer letters **318**(2): 173-179.

Sheng-Dong, H., Y. Yang, *et al.* (2013). "Tumor Cells Positive and Negative for the Common Cancer Stem Cell Markers Are Capable of Initiating Tumor Growth and Generating Both Progenies." PLoS ONE **8**(1).

Shibata, A., S. Conrad, *et al.* (2011). "Factors determining DNA double-strand break repair pathway choice in G2 phase." EMBO J **30**(6): 1079-1092.

Shibata, A., D. Moiani, *et al.* (2014). "DNA double-strand break repair pathway choice is directed by distinct MRE11 nuclease activities." Molecular cell **53**(1): 7-18.

Shman, T., U. Fedasenka, *et al.* (2008). "CD34+ leukemic subpopulation predominantly displays lower spontaneous apoptosis and has higher expression levels of Bcl-2 and MDR1 genes than CD34- cells in childhood AML." Ann Hematol **87**: 353 - 360.

Silverman, J., H. Takai, *et al*. (2004). "Human Rif1, ortholog of a yeast telomeric protein, is regulated by ATM and 53BP1 and functions in the S-phase checkpoint." Genes & Development **18**(17): 2108-2119.

Singh, N., H. Basnet, *et al*. (2012). "Dual recognition of phosphoserine and phosphotyrosine in histone variant H2A.X by DNA damage response protein MCPH1." Proceedings of the National Academy of Sciences of the United States of America **109**(36): 14381-14386.

Sobota, R., M. Szwed, *et al.* (2000). "Parthenolide inhibits activation of signal transducers and activators of transcription (STATs) induced by cytokines of the IL-6 family." Biochemical and biophysical research communications **267**(1): 329-333.

Souza, L. M. (1986). "Recombinant human granulocyte colony-stimulating factor: effects on normal and leukemic myeloid cells." Science **232**: 61-66.

Sparks, C. A. and D. A. Guertin (2010). "Targeting mTOR: prospects for mTOR complex 2 inhibitors in cancer therapy." Oncogene **29**(26): 3733-3744.

Spivak, G. (2010). The Comet-FISH Assay for the Analysis of DNA Damage and Repair. Fluorescence in situ Hybridization (FISH). J. M. Bridger and E. V. Volpi, Humana Press. **659:** 129-145.

Spivak, G., R. A. Cox, *et al.* (2009). "New applications of the Comet assay: Comet-FISH and transcription-coupled DNA repair." Mutat Res **681**(1): 44-50.

Staib, P., B. Lathan, *et al.* (1998). "Cytosine arabinoside, etoposide and aclarubicin (AVA) for the treatment of acute myeloid leukemia (AML) in elderly patients." Annals of Oncology **9**(2): 221-223.

Steinbach, J. P., H. Wolburg, *et al.* (2003). "Hypoxia-induced cell death in human malignant glioma cells: energy deprivation promotes decoupling of mitochondrial cytochrome c release from caspase processing and necrotic cell death." Cell Death Differ **10**(7): 823-832.

Steinbach, J. P., H. Wolburg, *et al.* (2005). "Hypoxia sensitizes human malignant glioma cells towards CD95L-induced cell death." Journal of neurochemistry **92**(6): 1340-1349.

Stewart, G. S., B. Wang, *et al.* (2003). "MDC1 is a mediator of the mammalian DNA damage checkpoint." Nature **421**(6926): 961-966.

Stier, S., Y. Ko, *et al.* (2005). "Osteopontin is a hematopoietic stem cell niche component that negatively regulates stem cell pool size." The Journal of Experimental Medicine **201**(11): 1781-1791.

Strober, W. (2001). Trypan Blue Exclusion Test of Cell Viability. Current Protocols in Immunology, John Wiley & Sons, Inc.

Stucki, M., J. A. Clapperton, *et al.* (2005). "MDC1 Directly Binds Phosphorylated Histone H2AX to Regulate Cellular Responses to DNA Double-Strand Breaks." Cell **123**(7): 1213-1226.

Suchánková, J., S. Kozubek, *et al.* (2015). "Distinct kinetics of DNA repair protein accumulation at DNA lesions and cell cycle-dependent formation of γH2AX- and NBS1-positive repair foci." Biology of the Cell **107**(12): 440-454.

Sugiyama, T., H. Kohara, *et al.* (2006). "Maintenance of the hematopoietic stem cell pool by CXCL12-CXCR4 chemokine signaling in bone marrow stromal cell niches." Immunity **25**(6): 977-988.

Sundaramoorthy, S., M. S. Ryu, *et al.* (2013). "B-cell translocation gene 2 mediates crosstalk between PI3K/Akt1 and NFκB pathways which enhances transcription of MnSOD by accelerating IκBα degradation in normal and cancer cells." Cell Communication and Signaling **11**(1): 69.

Suzuki, T., J. Tsuzuku, *et al.* (2012). "Inhibition of DNA Damage-induced Apoptosis through Cdc7-mediated Stabilization of Tob." The Journal of Biological Chemistry **287**(48): 40256-40265.

Takada, Y., A. Mukhopadhyay, *et al.* (2003). "Hydrogen Peroxide Activates NF-κB through Tyrosine Phosphorylation of IκBα and Serine Phosphorylation of p65: EVIDENCE FOR THE INVOLVEMENT OF IκBα KINASE AND Syk PROTEIN-TYROSINE KINASE." Journal of Biological Chemistry **278**(26): 24233-24241.

Takahashi, S. (2011). "Current findings for recurring mutations in acute myeloid leukemia." J Hematol Oncol **4**: 36.

Takata, M., M. S. Sasaki, *et al.* (1998). "Homologous recombination and non-homologous end-joining pathways of DNA double-strand break repair have overlapping roles in the maintenance of chromosomal integrity in vertebrate cells." EMBO J **17**(18): 5497-5508.

Talhaoui, I., V. Shafirovich, *et al.* (2015). "Oxidatively Generated Guanine(C8)-Thymine(N3) Intrastrand Cross-links in Double-stranded DNA Are Repaired by Base Excision Repair Pathways." The Journal of Biological Chemistry **290**(23): 14610-14617.

Tallman, M., D. Gilliland, *et al.* (2005). "Drug therapy for acute myeloid leukemia." Blood **106**: 1154 - 1163.

Tamm, I., S. M. Kornblau, *et al*. (2000). "Expression and Prognostic Significance of IAP-Family Genes in Human Cancers and Myeloid Leukemias." Clinical Cancer Research **6**(5): 1796-1803.

Tamm, I., S. Richter, *et al.* (2004). "High Expression Levels of X-Linked Inhibitor of Apoptosis Protein and Survivin Correlate with Poor Overall Survival in Childhood stronge de Novo strong Acute Myeloid Leukemia." Clinical Cancer Research **10**(11): 3737-3744.

Tanaka, T., H. D. Halicka, *et al.* (2007). "Induction of ATM Activation, Histone H2AX Phosphorylation and Apoptosis by Etoposide: Relation to Cell Cycle Phase." Cell Cycle **6**(3): 371-376.

Taussig, D. C., F. Miraki-Moud, *et al.* (2008). "Anti-CD38 antibody–mediated clearance of human repopulating cells masks the heterogeneity of leukemia-initiating cells." Blood **112**(3): 568-575.

Tavasolian, F., E. Abdollahi, *et al.* (2014). "Relationship between ABO blood group and Acute Lymphoblastic Leukemia." Iranian Journal of Pediatric Hematology and Oncology **4**(1): 1-4.

Tefferi, A. and L. Letendre (2012). "Going Beyond 7 + 3 Regimens in the Treatment of Adult Acute Myeloid Leukemia." Journal of Clinical Oncology **30**(20): 2425-2428.

Terasawa, M., A. Shinohara, *et al*. (2014). "Canonical Non-Homologous End Joining in Mitosis Induces Genome Instability and Is Suppressed by M-phase-Specific Phosphorylation of XRCC4." PLOS Genetics **10**(8): e1004563.

Thomas, L. W., C. Lam, *et al.* (2010). "Mcl-1; the molecular regulation of protein function." FEBS Letters **584**(14): 2981-2989.

Thorén, L. A., K. Liuba, *et al*. (2008). "Kit Regulates Maintenance of Quiescent Hematopoietic Stem Cells." The Journal of Immunology **180**(4): 2045-2053.

Tice, R. R., E. Agurell, *et al.* (2000). "Single cell gel/comet assay: guidelines for in vitro and in vivo genetic toxicology testing." Environmental and molecular mutagenesis **35**(3): 206-221.

Tirone, F. (2001). "The gene PC3TIS21/BTG2, prototype member of the PC3/BTG/TOB family: Regulator in control of cell growth, differentiation, and DNA repair?" Journal of Cellular Physiology **187**(2): 155-165.

Tomecki, R., K. Drazkowska, *et al*. (2014). "Multiple myeloma-associated hDIS3 mutations cause perturbations in cellular RNA metabolism and suggest hDIS3 PIN domain as a potential drug target." Nucleic Acids Research **42**(2): 1270-1290.

Tomimatsu, N., C. G. T. Tahimic, *et al*. (2007). "Ku70/80 Modulates ATM and ATR Signaling Pathways in Response to DNA Double Strand Breaks." Journal of Biological Chemistry **282**(14): 10138-10145.

Tominaga, K., H. Morisaki, *et al*. (1999). "Role of Human Cds1 (Chk2) Kinase in DNA Damage Checkpoint and Its Regulation by p53." Journal of Biological Chemistry **274**(44): 31463-31467.

Tothova, Z. K., Ramya Huntly, *et al.* (2007). "FoxOs are critical mediators of hematopoietic stem cell resistance to physiologic oxidative stress." Cell **128**(2): 325-339.

Tretyakova, N. Y., A. Groehler, *et al.* (2015). "DNA-Protein Cross-links: Formation, Structural Identities, and Biological Outcomes." Accounts of chemical research **48**(6): 1631-1644.

Tsubouchi, H. and H. Ogawa (1998). "A Novel mre11 Mutation Impairs Processing of Double-Strand Breaks of DNA during Both Mitosis and Meiosis." Molecular and Cellular Biology **18**(1): 260-268.

Tu, W.-Z., B. Li, *et al*. (2013). "γH2AX foci formation in the absence of DNA damage: Mitotic H2AX phosphorylation is mediated by the DNA-PKcs/CHK2 pathway." FEBS Letters **587**(21): 3437-3443.

Turinetto, V. and C. Giachino (2015). "Multiple facets of histone variant H2AX: a DNA double-strand-break marker with several biological functions." Nucleic Acids Research **43**(5): 2489-2498.

Tzachanis, D., G. J. Freeman, *et al*. (2001). "Tob is a negative regulator of activation that is expressed in anergic and quiescent T cells." Nat Immunol **2**(12): 1174-1182.

van der Linden, E., H. Sanchez, *et al*. (2009). "RAD50 and NBS1 form a stable complex functional in DNA binding and tethering." Nucleic Acids Research **37**(5): 1580-1588.

van Rhenen, A., G. A. M. S. van Dongen, *et al.* (2007). "The novel AML stem cell–associated antigen CLL-1 aids in discrimination between normal and leukemic stem cells." Blood **110**(7): 2659-2666.

Varnum, B. C., S. T. Reddy, *et al*. (1994). "Synthesis, degradation, and subcellular localization of proteins encoded by the primary response genes TIS7/PC4 and TIS21/PC3." Journal of Cellular Physiology **158**(1): 205-213.

Vayssade, M., H. Haddada, *et al.* (2005). "P73 functionally replaces p53 in Adriamycin-treated, p53-deficient breast cancer cells." International Journal of Cancer **116**(6): 860-869.

Viale, A. and P. G. Pelicci (2009). "Awaking stem cells from dormancy: growing old and fighting cancer." EMBO Molecular Medicine **1**(2): 88-91.

Walter, R. B., M. Othus, *et al.* (2013). "Significance of FAB subclassification of "acute myeloid leukemia, NOS" in the 2008 WHO classification: analysis of 5848 newly diagnosed patients." Blood **121**(13): 2424-2431.

Wang, L. C. and J. Gautier (2010). "The Fanconi anemia pathway and ICL repair: implications for cancer therapy." Critical reviews in biochemistry and molecular biology **45**(5): 424-439.

Wang, L. D. and A. J. Wagers (2011). "Dynamic niches in the origination and differentiation of haematopoietic stem cells." Nature reviews. Molecular cell biology **12**(10): 643-655.

Wang, X., N. Hawk, *et al.* (2008). "Overcoming mTOR inhibition-induced paradoxical activation of survival signaling pathways enhances mTOR inhibitors' anticancer efficacy." Cancer biology & therapy **7**(12): 1952-1958.

Welch, John S., Timothy J. Ley, *et al.* (2012). "The Origin and Evolution of Mutations in Acute Myeloid Leukemia." Cell **150**(2): 264-278.

Williams, R. S., J. S. Williams, *et al.* (2007). "Mre11–Rad50–Nbs1 is a keystone complex connecting DNA repair machinery, double-strand break signaling, and the chromatin template" Biochemistry and Cell Biology **85**(4): 509-520.

Willmore, E., N. Sunter, *et al.* (2005). "Sensitisation of leukaemia cells to the DNA Topoisomerase II inhibitor, ICRF-193 via inhibition of DNA-dependent protein kinase." AACR Meeting Abstracts **2005**(1): 562-b-.

Wilson, A., E. Laurenti, *et al.* (2009). "Balancing dormant and self-renewing hematopoietic stem cells." Current Opinion in Genetics & Development **19**(5): 461-468.

Wilson, A., G. M. Oser, *et al.* (2007). "Dormant and Self-Renewing Hematopoietic Stem Cells and Their Niches." Annals of the New York Academy of Sciences **1106**(1): 64-75.

Wilson, A. and A. Trumpp (2006). "Bone-marrow haematopoietic-stem-cell niches." Nat Rev Immunol **6**(2): 93-106.

Winkler, G. S. (2010). "The mammalian anti-proliferative BTG/Tob protein family." Journal of Cellular Physiology **222**(1): 66-72.

Winkler, G. S. (2010). "The mammalian anti-proliferative BTG/Tob protein family." Journal of cellular physiology **222**(1): 66-72.

Wojewódzka, M., I. Buraczewska, *et al*. (2002). "A modified neutral comet assay: elimination of lysis at high temperature and validation of the assay with anti-single-stranded DNA

antibody." Mutation Research/Genetic Toxicology and Environmental Mutagenesis **518**(1): 9-20.

Wolff, S. N., R. H. Herzig, *et al*. (1989). "High-dose cytarabine and daunorubicin as consolidation therapy for acute myeloid leukemia in first remission: long-term follow-up and results." Journal of Clinical Oncology **7**(9): 1260-1267.

Wood, R. D., M. Mitchell, *et al*. (2001). "Human DNA Repair Genes." Science **291**(5507): 1284-1289.

Woodbine, L., H. Brunton, *et al.* (2011). "Endogenously induced DNA double strand breaks arise in heterochromatic DNA regions and require ataxia telangiectasia mutated and Artemis for their repair." Nucleic Acids Research **39**(16): 6986-6997.

Woolthuis, C. M. and C. Y. Park (2016). "Hematopoietic stem/progenitor cell commitment to the megakaryocyte lineage." Blood **127**(10): 1242-1248.

Wunderlich, M., B. Mizukawa, *et al.* (2013). AML cells are differentially sensitive to chemotherapy treatment in a human xenograft model.

Xiao, A., H. Li, *et al.* (2009). "WSTF regulates the function of H2A. X via a novel tyrosine kinase activity." Nature **457**(7225): 57.

Xiao, Y., P. Zou, *et al.* (2012). "Lower phosphorylation of p38 MAPK blocks the oxidative stress-induced senescence in myeloid leukemic CD34+CD38− cells." Journal of Huazhong University of Science and Technology [Medical Sciences] **32**(3): 328-333.

Xie, C., H. Edwards, *et al.* (2012). "Valproic acid synergistically enhances the cytotoxicity of clofarabine in pediatric acute myeloid leukemia cells." Pediatric Blood & Cancer **59**(7): 1245-1251.

Xie, Y., J. P. De Winter, *et al.* (2000). "Aberrant Fanconi anaemia protein profiles in acute myeloid leukaemia cells." British Journal of Haematology **111**(4): 1057-1064.

Xu, X., L. M. Tsvetkov, *et al*. (2002). "Chk2 Activation and Phosphorylation-Dependent Oligomerization." Molecular and Cellular Biology **22**(12): 4419-4432.

Yahata, T., Y. Muguruma, *et al*. (2008). "Quiescent Human Hematopoietic Stem Cells in the Bone Marrow Niches Organize the Hierarchical Structure of Hematopoiesis." STEM CELLS **26**(12): 3228-3236.

Yamazaki, S., A. Iwama, *et al.* (2009). "TGF-beta as a candidate bone marrow niche signal to induce hematopoietic stem cell hibernation." Blood **113**.

Yan, H., J. Qin, *et al.* (2009). Cancer Stem Cells: Potential Mediators of Therapeutic Resistance and Novel Targets of Anti-cancer Treatments. Pharmaceutical Perspectives of Cancer Therapeutics. Y. Lu and R. I. Mahato, Springer US**:** 559-579.

Yan, X., J. Xu, *et al*. (2011). "Exome sequencing identifies somatic mutations of DNA methyltransferase gene DNMT3A in acute monocytic leukemia." Nat Genet **43**: 309 - 315.

Yang, H., D. G. Rudge, *et al.* (2013). "mTOR kinase structure, mechanism and regulation." Nature **497**(7448): 217-223.

Yang, X., M. Morita, *et al*. (2008). "Crystal structures of human BTG2 and mouse TIS21 involved in suppression of CAF1 deadenylase activity." Nucleic Acids Research **36**(21): 6872-6881.

Yilmaz, O., R. Valdez, *et al.* (2006). "Pten dependence distinguishes haematopoietic stem cells from leukaemia-initiating cells." Nature **441**(7092): 475 - 482.

Yoriko, S., U. Naoyuki, *et al.* (2010). "Induction of cell cycle entry eliminates human leukemia stem cells in a mouse model of AML." Nature Biotechnology **28**(3): 275-280.

Yoshihara, H., F. Arai, *et al.* (2007). "Thrombopoietin/MPL Signaling Regulates Hematopoietic Stem Cell Quiescence and Interaction with the Osteoblastic Niche." Cell Stem Cell **1**(6): 685-697.

Yu, S., G. Shen, *et al.* (2008). "Curcumin inhibits Akt/mammalian target of rapamycin signaling through protein phosphatase-dependent mechanism." Mol Cancer Ther **7**: 2609 - 2620.

Yusuf, I. and D. A. Fruman (2003). "Regulation of quiescence in lymphocytes." Trends in immunology **24**(7): 380-386.

Zahedpanah, M., M. Shaiegan, *et al.* (2016). "Parthenolide Induces Apoptosis in Committed Progenitor AML Cell line U937 via Reduction in Osteopontin." Reports of Biochemistry & Molecular Biology **4**(2): 82-88.

Zhang, J., S. H. Lu, *et al*. (2004). "Platelet factor 4 enhances the adhesion of normal and leukemic hematopoietic stem/progenitor cells to endothelial cells." Leukemia Research **28**(6): 631-638.

Zhang, J., C. Niu, *et al*. (2003). "Identification of the haematopoietic stem cell niche and control of the niche size." Nature **425**(6960): 836-841.

Zhang, Y.-j., C.-r. Lu, *et al.* (2012). "Imatinib induces H2AX phosphorylation and apoptosis in chronic myelogenous leukemia cells in vitro via caspase-3/Mst1 pathway." Acta Pharmacologica Sinica **33**(4): 551-557.

Zhang, Z., C. Chen, *et al.* (2011). "Aberrant Expression of the p53-Inducible Antiproliferative Gene BTG2 in Hepatocellular Carcinoma is Associated with Overexpression of the Cell Cycle-Related Proteins." Cell Biochemistry and Biophysics **61**(1): 83-91.

Zhang, Z., A. Martino, *et al*. (2007). "Identification of expression patterns of IL-2-responsive genes in the murine T cell line CTLL-2." J Interferon Cytokine Res **27**.

Zhao, W., S. Vaithiyalingam, *et al.* (2015). "Promotion of BRCA2-dependent Homologous Recombination by DSS1 via RPA Targeting and DNA Mimicry." Molecular cell **59**(2): 176-187.

Zhenchuk, A., K. Lotfi, *et al.* (2009). "Mechanisms of anti-cancer action and pharmacology of clofarabine." Biochemical Pharmacology **78**(11): 1351-1359.

Zimmermann, M. and T. de Lange (2014). "53BP1: Pro Choice in DNA Repair." Trends in cell biology **24**(2): 108-117.

Zorov, D. B., M. Juhaszova, *et al.* (2014). "Mitochondrial Reactive Oxygen Species (ROS) and ROS-Induced ROS Release." Physiological Reviews **94**(3): 909-950.